

Multilevel Optimisation of Aerospace and Lightweight Structures Incorporating Postbuckling Effects

by

Shuang QU

**Thesis submitted to the
Cardiff University in candidature
for the degree of
Doctor of Philosophy**

April 2011



**Cardiff School of Engineering
Cardiff University
Wales, UK.**

UMI Number: U585469

All rights reserved

INFORMATION TO ALL USERS

The quality of this reproduction is dependent upon the quality of the copy submitted.

In the unlikely event that the author did not send a complete manuscript and there are missing pages, these will be noted. Also, if material had to be removed, a note will indicate the deletion.



UMI U585469

Published by ProQuest LLC 2013. Copyright in the Dissertation held by the Author.
Microform Edition © ProQuest LLC.

All rights reserved. This work is protected against
unauthorized copying under Title 17, United States Code.



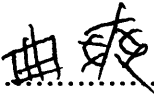
ProQuest LLC
789 East Eisenhower Parkway
P.O. Box 1346
Ann Arbor, MI 48106-1346

子曰：“知之者不如好之者

好之者不如乐之者”

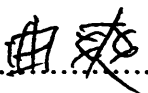
DECLARATION

This work has not previously been accepted in substance for any degree and is not being concurrently submitted in candidature for any degree.

Signed .....(candidate) Date 25/05/2011

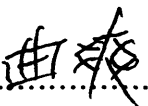
STATEMENT 1

This thesis is being submitted in partial fulfilment of the requirements for the degree of PhD.

Signed .....(candidate) Date 25/05/2011


STATEMENT 2

This thesis is the result of my own independent work/investigations, except where otherwise stated. Other sources are acknowledged by explicit references.

Signed .....(candidate) Date 25/05/2011

STATEMENT 3

I hereby give consent for my thesis, if accepted, to be available for photocopying and for inter-library loan, and for the title and summary to be made available to outside organisations.

Signed .....(candidate) Date 25/05/2011

ACKNOWLEDGEMENTS

This thesis would not have been possible without the support and help from many people, to only some of whom I would like to address my appreciation:

First of all, I would like to express my sincere gratitude to my supervisors Professor David Kennedy and Dr. Carol Featherston, for their consistent support, guidance and encouragement throughout my PhD study.

I am also grateful to all the staff of Cardiff University for their direct and indirect teaching and help during these eight years of my university education.

Special thanks should go to my friends Robert Carvell and Jianyu Lai, who kindly gave me valuable advice on English writing skills, and my flatmates Weitong Liu, Xinxin Wang and Ringo Chan, who have offered me warm support during my life in the UK.

Last but not least, I am deeply indebted to my beloved family for their loving considerations and great confidence in me, especially my parents who have been assisting, supporting and caring for me all of my life.

SUMMARY

The optimisation of aerospace structures is a very complex problem, due to the hundreds of design variables a multidisciplinary optimisation may contain, so that multilevel optimisation is required. This thesis presents the recent developments to the multilevel optimisation software VICONOPT MLO, which is a multilevel optimisation interface between the well established analysis and design software packages VICONOPT and MSC/NASTRAN. The software developed is called VICONOPT MLOP (Multilevel Optimisation with Postbuckling), and allows for postbuckling behaviour, using analysis based on the Wittrick-Williams algorithm. The objective of this research is to enable a more detailed insight into the multilevel optimisation and postbuckling behaviour of a complex structure.

In VICONOPT MLOP optimisation problems, individual panels of the structural model are allowed to buckle before the design load is reached. These panels continue to carry load with differing levels of reduced stiffness. VICONOPT MLOP creates new MSC/NASTRAN data files based on this reduced stiffness data and iterates through *analysis cycles* to converge on an appropriate load re-distribution. Once load convergence has been obtained with an appropriate criterion, the converged load distribution is used as a starting point in the optimisation of the constituent panels, i.e. a new *design cycle* is started, in which the updated ply thicknesses for each panel are calculated by VICONOPT and returned to MSC/NASTRAN through VICONOPT MLOP. Further finite element analysis of the whole structure is then carried out to determine the new stress distributions in each panel. The whole process is repeated until a mass convergence criterion is met.

A detailed overview of the functionality of VICONOPT MLOP is presented in the thesis. A case study is conducted into the multilevel optimisation of a composite aircraft wing, to demonstrate the capabilities of VICONOPT MLOP and identify areas for future studies. The results of the case study show substantial mass savings, proving the software's capabilities when dealing with such problems. The time taken for this multilevel optimisation also proves the efficiency of the software.

CONTENTS

<u>SECTION</u>	<u>PAGE</u>
Declaration, Statement 1, Statement 2 and Statement 3	i
Acknowledgements	ii
Summary	iii
Contents	iv
List of Figures and Tables	viii
Notation	xiv
<u>CHAPTER 1</u>	
<u>Introduction</u>	
1.1 General Background	1
1.2 Scope of Thesis	3
1.3 Review of Previous Work	5
1.3.1 Review of Postbuckling	5
1.3.2 Review of VICONOPT	7
1.3.3 Review of Optimisation	8
1.3.4 Previous Work on Multilevel Optimisation	10
1.3.5 Previous Work on Optimisation Including Postbuckling Effects	11
<u>CHAPTER 2</u>	
<u>Theoretical Background</u>	
2.1 General Methods of Analysis	14
2.1.1 The Finite Element Method	14
2.1.2 The Finite Strip Method	16
2.2 Buckling and Postbuckling	16
2.2.1 Buckling	16
2.2.2 Postbuckling	17
2.3 Optimisation	21

2.3.1 General	21
2.3.2 Methodology	22
2.3.2.1 The Method of Feasible Directions	23
2.3.3 Multilevel Optimisation	25
<u>CHAPTER 3</u>	
<u>VICONOPT and VICONOPT MLO</u>	
3.1 Introduction	27
3.2 VICONOPT	28
3.2.1 General Theoretical Background	28
3.2.1.1 The Exact Strip Method and The Wittrick-Williams Algorithm	29
3.2.1.2 VIPASA and VICON	31
3.2.2 VICONOPT Design Optimisation	34
3.2.3 VICONOPT Postbuckling Analysis	37
3.3 VICONOPT MLO	40
3.3.1 Introduction	40
3.3.2 MSC/NASTRAN Model Translation	42
3.3.2.1 Node Numbering for VICONOPT	43
3.3.3 Load Transfer between NASTRAN and VICONOPT	44
<u>CHAPTER 4</u>	
<u>VICONOPT MLOP (Multilevel Optimisation with Postbuckling): Theory</u>	
4.1 Introduction	52
4.2 Strain Increment Calculation	54
4.3 Reduced Stiffness Ratio	55
4.4 Plates with Negative Reduced Stiffness	57
4.5 Load Convergence	65
4.6 Mass Convergence	66
4.7 Convergence Acceleration	68

CHAPTER 5**Multilevel Optimisation Procedure of VICONOPT MLOP**

5.1 Introduction	70
5.2 Postbuckling Model Building Process	72
5.2.1 General	72
5.2.2 MSC/NASTRAN Model Translation	73
5.2.3 Assembly of Geometric Models	74
5.2.4 Panel Parameter Specification	76
5.2.4.1 Boundary Conditions	77
5.2.4.2 Stress and Strain Constraints	80
5.2.4.3 Buckling Parameters	81
5.2.4.4 Postbuckling Parameters	84
5.2.4.5 VICONOPT Output Requests	86
5.2.5 Design Variables	89
5.2.5.1 Continuous Design Variables	90
5.2.5.2 Equivalencing of Plates in VICONOPT MLOP	91
5.2.6 Assigning Load Cases in VICONOPT MLOP	92
5.2.7 Format of VICONOPT Plate Description	93
5.2.8 Generation of VICONOPT Input Files	94
5.2.9 Viewing VICONOPT Input Files	95
5.2.10 Save Optimisation	96
5.2.11 Multilevel Optimisation Parameters and Execution	99
5.3 Multilevel Postbuckling Optimisation Process	102
5.3.1 General	102
5.3.2 VICONOPT Postbuckling Analysis	105
5.3.2.1 VICONOPT Process Control File	105
5.3.2.2 VICONOPT Postbuckling Analysis Results File	107
5.3.3 VICONOPT Design	107
5.3.4 MSC/NASTRAN Model Updating	110
5.3.5 VICONOPT MLOP Output File	111
5.4 Conclusion	113

CHAPTER 6**Multilevel Optimisation of a Composite Aircraft Wing Incorporating Postbuckling Effects**

6.1 Introduction and Problem Description	115
6.2 Initial Design	118
6.3 Numerical Results	120
6.4 Extended Research	134
6.4.1 Convergence Criteria	134
6.4.2 Convergence Acceleration	137
6.4.3 Computational Efficiency	138
6.5 Conclusion	141

CHAPTER 7**Conclusion and Recommendations for Future Work**

7.1 Conclusions	142
7.2 Future Study and Development	144
7.2.1 Further Research Area Expansion	144
7.2.2 Further Manual Input Simplification	145
7.2.3 Further VICONOPT MLO Data File Development	147

Appendix A – Mass changes in individual panels	150
---	------------

Appendix B – Changes of ply thicknesses	154
--	------------

Appendix C – Redistribution of axial loads and bending moments in each panel	170
---	------------

REFERENCES	189
-------------------	------------

LIST OF FIGURES AND TABLES

<u>Figure No.</u>	<u>Description</u>	<u>Page</u>
1.1	The engineering design process including aircraft design.	1
1.2	The Airbus modern commercial aircraft.	2
1.3	Multilevel nature of the optimisation procedure for an aircraft wing [Fischer (2002b)].	11
2.1	Finite Element Method [Mohsin <i>et al.</i> (2008)].	14
2.2	Finite Element and Finite Strip.	16
2.3	(a) Stable, (b) neutral and (c) unstable equilibriums [Kennedy (2006a)].	17
2.4	Concept of effective width [Kennedy (2006b)].	18
2.5	Effective Young's modulus.	19
2.6	Buckling modes, (a) the overall mode, (b) the tripping/torsional mode and (c) the local mode [Powell (1997)].	20
2.7	Move in design space between two iterations [Fischer (2002)].	23
2.8	Usable and feasible direction [Fischer (2002)].	24
2.9	Effect of push-off factors θ on direction S^r .	25
3.1	Typical sections which VICONOPT can analyze.	28
3.2	Component plate showing in-plane loading.	29
3.3	Simply supported end conditions in VIPASA analysis.	32
3.4	Illustration of an infinitely long plate assembly with point supports [Φ], (a) plan view (b) isometric view.	33
3.5	Panel design strategy showing the continuous design phase.	35
3.6	Postbuckling of a stiffened panel. (a) Panel cross-section. (b) Contour and isometric plots of buckling mode. (c) Normalised stress-strain plots at various locations in the skin and stiffeners.	38
3.7	Calculation of effective stiffness for a postbuckled plate.	39
3.8	Multilevel framework for optimum design using VICONOPT MLO.	41

3.9	Typical MSC/NASTRAN Property Card.	42
3.10	Node numbering of a wing-box.	43
3.11	QUAD4 element and coordinate system definition.	45
3.12	Force convention for plate elements.	45
3.13	Moment convention for plate elements.	46
3.14	Stress convention for plate elements.	46
3.15	Typical element stress distributions.	47
4.1	Multi-level framework for postbuckling design.	53
4.2	Calculation of strain increment.	55
4.3	Plot of load against end shortening for a panel.	55
4.4	Plot of load against end shortening for a plate.	57
4.5	Load against end shortening for a plate with negative stiffness ratio.	58
4.6	Schematic load distributions across a panel.	58
4.7	Theoretical calculation for a plate with negative stiffness ratio.	60
4.8	Load convergence acceleration, (a) oscillating convergence ($0 < \kappa < 1$) and (b) one-sided convergence ($\kappa > 1$).	68
5.1	A typical window with 'Default Values' options.	71
5.2	VICONOPT MLOP main window.	73
5.3	VICONOPT MLOP—MLOP Process & Procedure.	74
5.4	'Assemble VICONOPT Optimisation Model' window.	75
5.5	'Parameters' window.	77
5.6	'Boundary Conditions' window.	78
5.7	'Longitudinal Line Supports' window.	78
5.8	'Point Supports' window.	79
5.9	Point support generation example: 4-point supports across a plate.	80
5.10	'Allowable Stress & Strain' window.	81
5.11	'Buckling Parameters' window.	82
5.12	'Postbuckling Methods' window.	84
5.13	'Latest Newton Method' window.	85

5.14	'Output Request' window.	87
5.15	'Reset Data' window.	88
5.16	'VICONOPT Design Variables' window.	89
5.17	'Continuous Optimisation' window.	90
5.18	'Equivalencing of Plates' window.	92
5.19	'Load Cases' window.	93
5.20	'VICONOPT Plate Description Format' window.	94
5.21	Display the VICONOPT input files.	95
5.22	'Save' window.	96
5.23	VICONOPT MLO Save File: .MLO1.	98
5.24	'Multilevel Optimisation Control Deck' window.	100
5.25	'MLO Parameters' window.	101
5.26	Procedure for optimising a multilevel postbuckling model in VICONOPT MLOP.	104
5.27	VICONOPT Process Control File: Input.dat.	105
5.28	VICONOPT analysis/design window.	106
5.29	VICONOPT Postbuckling Analysis Results File: .u14.	107
5.30	VICONOPT design Results File: .u11.	108
5.31	VICONOPT .res file.	109
5.32	Typical MSC/NASTRAN Material Card.	110
5.33	VICONOPT MLO Output File: .clog.	112
6.1	Panels T1 to T6 on the top of the wing and adapter.	115
6.2	Panels B1 to B6 at the bottom of the wing, spars and ribs.	116
6.3	Typical wing panel (skin plates and stringers).	116
6.4	Load case: Twist.	117
6.5	Component plates of the wing (excluding spar and rib plates).	117
6.6	Total mass changes during the multilevel optimisation process.	121
6.7	Mass changes in panels T5 & T6.	122
6.8	Mass changes in panels B5 & B6.	122
6.9	Mass changes in panels S4, S5 & S6.	122
6.10	Changes of ply thicknesses (T6), (a) skin, (b) flange and (c) web.	124
6.11	Changes of ply thicknesses (B6), (a) skin, (b) flange and (c) web.	125

6.12	Changes of ply thicknesses (S5).	126
6.13	Redistribution of axial loads in panels (a) T5 and (b) T6.	127
6.14	Redistribution of axial loads in panels (a) B5 and (b) B6.	128
6.15	Redistribution of axial loads in panels S5.	129
6.16	Redistribution of bending moments in panels T6.	130
6.17	Redistribution of bending moments in panels B6.	130
6.18	Redistribution of bending moments in panels S5.	131
6.19	Redistribution of bending moments in panel S5 (using different scale of Figure 6.18).	131
6.20	Longitudinal stress contours for the initial designs, (a) top skin (b) spars (c) bottom skin (N/mm^2).	132
6.21	Longitudinal stress contours for the final designs, (a) top skin (b) spars and (c) bottom skin (N/mm^2).	133
6.22	The total mass convergence through out the optimisation.	135
6.23	Load convergence with and without convergence acceleration.	138
7.1	Group input — MSC/PATRAN.	146
7.2	Table input format — WinDes [Micro Drainage (2011)].	147
7.3	Typical MSC/NASTRAN input file.	148
7.4	Results diagram — WinDes [Micro Drainage (2011)].	149
A.1	Mass changes in panels T1 & T2.	151
A.2	Mass changes in panels T3 & T4.	151
A.3	Mass changes in panels T5 & T6.	151
A.4	Mass changes in panels B1 & B2.	152
A.5	Mass changes in panels B3 & B4.	152
A.6	Mass changes in panels B5 & B6.	152
A.7	Mass changes in panels S1, S2 & S3.	153
A.8	Mass changes in panels S4, S5 & S6.	153
A.9	Mass changes in panels S7, S8 & S9.	153
B.1	Changes of ply thicknesses (T1), (a) skin, (b) flange and (c) web.	155
B.2	Changes of ply thicknesses (T2), (a) skin, (b) flange and (c) web.	156

B.3	Changes of ply thicknesses (T3), (a) skin, (b) flange and (c) web.	157
B.4	Changes of ply thicknesses (T4), (a) skin, (b) flange and (c) web.	158
B.5	Changes of ply thicknesses (T5), (a) skin, (b) flange and (c) web.	159
B.6	Changes of ply thicknesses (T6), (a) skin, (b) flange and (c) web.	160
B.7	Changes of ply thicknesses (B1), (a) skin, (b) flange and (c) web.	161
B.8	Changes of ply thicknesses (B2), (a) skin, (b) flange and (c) web.	162
B.9	Changes of ply thicknesses (B3), (a) skin, (b) flange and (c) web.	163
B.10	Changes of ply thicknesses (B4), (a) skin, (b) flange and (c) web.	164
B.11	Changes of ply thicknesses (B5), (a) skin, (b) flange and (c) web.	165
B.12	Changes of ply thicknesses (B6), (a) skin, (b) flange and (c) web.	166
B.13	Changes of ply thicknesses (S1).	167
B.14	Changes of ply thicknesses (S2).	167
B.15	Changes of ply thicknesses (S3).	167
B.16	Changes of ply thicknesses (S4).	168
B.17	Changes of ply thicknesses (S5).	168
B.18	Changes of ply thicknesses (S6).	168
B.19	Changes of ply thicknesses (S7).	169
B.20	Changes of ply thicknesses (S8).	169
B.21	Changes of ply thicknesses (S9).	169
C.1	Redistribution of axial loads in panels (a) T1 and (b) T2.	171
C.2	Redistribution of axial loads in panels (a) T3 and (b) T4.	172
C.3	Redistribution of axial loads in panels (a) T5 and (b) T6.	173
C.4	Redistribution of axial loads in panels (a) B1 and (b) B2.	174
C.5	Redistribution of axial loads in panels (a) B3 and (b) B4.	175
C.6	Redistribution of axial loads in panels (a) B5 and (b) B6.	176
C.7	Redistribution of axial loads in panels (a) S1, (b) S2 and (c) S3.	177
C.8	Redistribution of axial loads in panels (a) S4, (b) S5 and (c) S6.	178
C.9	Redistribution of axial loads in panels (a) S7, (b) S8 and (c) S9.	179
C.10	Redistribution of bending moments in panels (a) T1 and (b) T2.	180
C.11	Redistribution of bending moments in panels (a) T3 and (b) T4.	181
C.12	Redistribution of bending moments in panels (a) T5 and (b) T6.	182
C.13	Redistribution of bending moments in panels (a) B1 and (b) B2.	183

C.14	Redistribution of bending moments in panels (a) B3 and (b) B4.	184
C.15	Redistribution of bending moments in panels (a) B5 and (b) B6.	185
C.16	Redistribution of bending moments in panels (a) S1, (b) S2 and (c) S3.	186
C.17	Redistribution of bending moments in panels (a) S4, (b) S5 and (c) S6.	187
C.18	Redistribution of bending moments in panels (a) S7, (b) S8 and (c) S9.	188

<u>Table No.</u>	<u>Description</u>	<u>Page</u>
4.1	The variables of a simple panel.	63
5.1	Differences between VICONOPT MLO and VICONOPT MLOP.	114
6.1	Material properties of high strength carbon-epoxy.	118
6.2	Initial ply thicknesses, upper and lower bounds (all in <i>mm</i>).	119
6.3	Mass of designs obtained by two different version of VICONOPT MLO. Percentage changes are relative to the initial design.	123
6.4	The individual mass convergence for each top panel.	136
6.5	The individual mass convergence for each bottom panel.	136
6.6	The individual mass convergence for each spar panel.	137
6.7	Parameters of the example for efficiency calculation.	140
6.8	Time taken for different optimisation techniques.	140

NOTATION

a	analysis cycle number
b	width of a plate
b_e	effective width of a plate
b_{el}	width of an element
\mathbf{D}	vector of global displacements
d	design cycle number
E	Young's modulus
E_1, E_2, E_3	elastic moduli of an orthotropic material
F	the eigenparameter
$f_1(y)$	function to allow simply supported boundary conditions in VIPASA type analyses
$F(x)$	objective function
\hat{F}	objective function value of the optimum combinatorial partial enumeration design determined by the sequential rounding technique
F_{el}^L	local axial force per unit length in an element
FX_{el}^L, FY_{el}^L	local axial and transverse forces per unit length in an element
FX_{panel}	panel's total longitudinal load
FXY_{el}	shear force acting on each element
FXY_{plate}	shear force for the component plates in the panel
FY_{plate}	transverse stress resultants for the component plates in the panel
FX_{el}^G	axial forces per unit width in the global x direction
G_1, G_2, G_3, G_4	grid points of a QUAD4 element in MSC/NASTRAN
G_{12}, G_{23}, G_{31}	shear moduli of an orthotropic material
$G_i(x)$	equality constraints on the objective function
g_{ix}, g_{iy}, g_{iz}	global coordinates of grid points $G_1, G_2, G_3, G_4, i = (1, \dots, 4)$

$H_j(x)$	inequality constraints on the objective function
i, j, k	base vectors of the local element coordinate system
i_0, j_0, k_0	unit base vectors of the local element coordinate system
$i_{0x}, i_{0y}, j_{0x}, j_{0y}$	components of i_0 and j_0 in the x and y directions
J	number of eigenvalues lying between zero and a trial value
J_0	value of J when the components of the displacement vector corresponding to \mathbf{K} are clamped
J_m	number of eigenvalues lying between zero and a trial value for a constituent member of a structure with its ends clamped
\mathbf{K}	global stiffness matrix for the overall structure
\mathbf{K}_m	member stiffness matrices
\mathbf{K}^Δ	upper triangular matrix obtained by applying a conventional Gauss elimination to stiffness matrix \mathbf{K}
L	interval at which buckling mode repeats in VICON type analyses
ℓ	panel length
ℓ_{el}	length of an element
M_0	total initial mass for the whole structure
M_d	total current mass for the whole structure in design cycle d
M_{el}^L	local bending moment acting on an element
MX_{el}^L, MY_{el}^L	local bending moments per unit length in an element
MY_{panel}	panel's total bending moment
m	number of constituent members in a structure
$m_{s,0}$	initial mass for panel s
$m_{s,d}$	current mass for panel s in design cycle d
N_d, N_a	number of design/analysis cycles taken in a multilevel optimisation
N_{elx}	total number of elements along the length of the panel
N_{elp}	total number of elements per plate

N_L, N_T, N_S	in-plane longitudinal, transverse and shear stress resultants
N_p	number of panels contained in a model
p	predicted load from an analysis cycle
\bar{p}	expected converged resultant load
p^*	load at start of an analysis cycle
P_{cr}	critical buckling load
P_{crx}, P_x	critical buckling load and applied design load for plate x
$P_{designx}$	design load for each plate x
P_{compx}	assumed compressive load for each plate x
P_{tenx}	assumed tensile load for each plate x
P'_{compx}	applied compressive load calculated by MSC/NASTRAN
P'_{tenx}	applied tensile load calculated by MSC/NASTRAN
$p_{s,0}^*$	initial load for panel s in a design cycle
$p_{s,a}^*$	current load for panel s in analysis cycle a of a design cycle
q_a	number of currently active constraints
$s\{\mathbf{K}\}$	sign count of \mathbf{K} , calculated as the number of negative elements on the leading diagonal of the upper triangular matrix \mathbf{K}^Δ
\mathbf{S}^r	move direction vector
s	panel number
t	thickness
t_{Ms}, t_{Mb}, t_{Mp}	time taken for MSC/NASTRAN to complete a static, a finite element buckling analysis and a finite element postbuckling analysis
t_{Vd}, t_{Va}	time taken for VICONOPT to complete a buckling design and a postbuckling analysis
T_{FE}, T'_{FE}	time taken for MSC/NASTRAN to complete a buckling and postbuckling optimisation

T_{MLO}, T'_{MLO}	time taken for VICONOPT MLOP to complete a buckling and postbuckling optimisation
u, v, w	perturbation displacements of a member in the x, y and z direction
v_1, v_2	diagonal vectors used to determine the local coordinate system of an element
X	factor which equals $\frac{P_{cr}}{\beta\gamma}$
x	plate number
z_t, z_b	distance between the top and bottom surfaces of a shell element and the element's profile axis
α	average postbuckling to prebuckling stiffness ratio for the panel
α_x	postbuckling to prebuckling stiffness ratio for plate x
β	value of the panel's critical buckling load relative to the design load
γ	overall reduced stiffness ratio for the panel (estimated at the design load)
γ_x	reduced stiffness ratio for plate x
γ_{comp_x}	effective non-negative reduced stiffness ratio for plate x
γ_{tens_x}	effective tensile reduced stiffness ration for plate x , which is always equal to 1.
δ^*	extra pre-buckling stiffness
ϵ_{inc}	strain increment
ϵ_{design}	strain at design load
ϵ_{cr}	strain at the critical buckling load p_{cr}
ζ	distance of movement
η	convergence criterion
κ	ratio between the required step and the predicted step in the load convergence acceleration

λ	half-wavelength of buckling response
λ_1, λ_2, r	buckling parameters required for ratio-specification in VIPASA models
ξ	parameter in VICON affecting the coupling of half-wavelengths λ
ξ_1, ξ_2, ξ_{inc}	buckling parameters required for VICON models
ρ	density
σ, σ'	stress values
$\sigma_1, \sigma_2, \sigma_3$	principal direct stresses in an orthotropic material
σ_{ax}	constant axial stress in a shell element
σ_{cr}	critical buckling stress
σ_t, σ_b	maximum stress at the top and bottom surfaces of an element
$\sigma_{flex}^t, \sigma_{flex}^b$	bending stress at the top and bottom of an element
$\sigma_{xyel}^t, \sigma_{xyel}^b$	shear stresses in the top and bottom surfaces of an element
σ_y	yield stress
$\tau_{12}, \tau_{23}, \tau_{31}$	principal shear stresses in an orthotropic material
φ	time required for all the VICONOPT MLOP processes in each design and analysis cycle
ψ	rotation amplitude

Chapter 1

Introduction

1.1 GENERAL BACKGROUND

An aircraft is one of most complex manmade flying systems, and as such requires strict and meticulous design and manufacture. Aircraft design and manufacturing is always responding to the most recent scientific and technological developments.

Design of an aircraft is a complex task. A successful design may take more than a decade to complete. As for most engineering designs, the design process takes place in three stages, conceptual design, preliminary design and detailed design as shown in Figure 1.1.

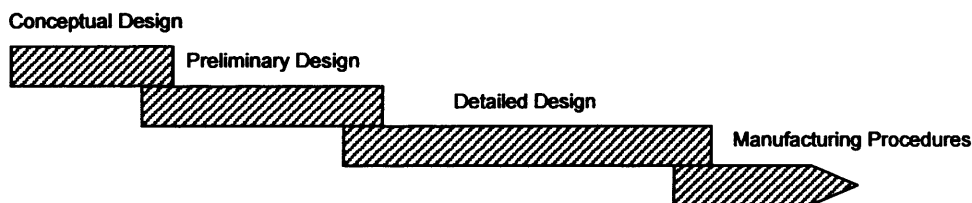


Figure 1.1 The conceptual design period including aircraft design.

In the concept design period, the overall design concept will be defined and one or more possible candidate designs selected for the next step. The aim of the preliminary design stage is to investigate the best complete design concept for the whole aircraft based on multidisciplinary considerations. This requires development and analysis of the selected draft design. Large numbers of design cases are tested and analysed during this period. In modern aircraft design, computer software is commonly used to carry out this analysis, so increasing efficiency, reducing human workload and therefore saving money. In the final stage, the detailed design stage, the design of

each component of the aircraft is completed. Detailed drawings of the whole structure and its components are prepared for manufacture. Detailed design therefore is also called manufacturing or engineering design.



Figure 1.2 The Airbus modern commercial aircraft.

Structural design is one of the major parts of aircraft design. One of the most important objectives of aircraft structural design is minimising weight. In recent years, the overall configuration of commercial aircraft has been almost standardized without major differences between aircraft (Figure 1.2). Modern design increasingly utilises high performance materials, such as carbon-fibre reinforced composites. When combined with efficient analysis and optimisation tools, these can lead to significantly increased stiffness, strength and reliability, while reducing the weight of structural components and systems.

The optimisation of aerospace structures is a very complex problem, due to the hundreds of design variables a multidisciplinary optimisation may contain, so that multilevel optimisation is required. The research presented in this thesis is based on the development of the software VICONOPT MLO which is a multilevel optimisation interface between the well established analysis and design software packages VICONOPT (Williams *et al.*, 1991) and MSC/NASTRAN (MSC/Software, 1999a).

The software developed is called VICONOPT MLOP which in comparison to its previous version not only takes postbuckling effects into account but also provides improved design convergence and manual and computational input/output data systems. The work, in particular the wing geometry for the case study described in Chapter 6 is based on recommendations made by GARTEUR (Group for Aeronautical Research and Technology in Europe) (GARTEUR, 1997a-c).

1.2 SCOPE OF THESIS

This thesis presents the recent developments to the multilevel optimisation software VICONOPT MLO, which allow for postbuckling behaviour, using analysis based on the Wittrick-Williams algorithm. The software developed is VICONOPT MLOP. A case study is conducted into the multilevel optimisation of a composite aircraft wing, to demonstrate the capabilities of VICONOPT MLOP and identify areas for future studies.

The thesis has been structured into seven chapters. Following the introduction and the literature review in this chapter, Chapter 2 describes the theoretical background of the research, which includes the general analysis method, buckling and postbuckling behaviour and optimisation. An introduction to the optimisation procedures used by VICONOPT is also presented in this chapter.

Chapter 3 describes some of the main features of VICONOPT and VICONOPT MLO. The general theoretical background of VICONOPT is presented first, followed by an introduction of the two types of analysis possible, VIPASA and VICON. A brief overview of VICONOPT design and postbuckling analysis features is also included. Concerning VICONOPT MLO, an introduction is given followed by the key underlying theory and concepts.

Chapter 4 presents the theory underlying VICONOPT MLOP. An introduction to the design philosophy required to incorporate postbuckling reserve into the design of complex structures is given at the beginning of this chapter, followed by a description of the detailed theories developed for the software.

Chapter 5 introduces the postbuckling optimisation procedures of VICONOPT MLOP. The main procedures for setting up a multilevel postbuckling optimisation problem and the process carried out by the software are outlined.

Chapter 6 presents a case study of a composite aircraft wing which was carried out to prove the capabilities of VICONOPT MLOP as a tool for multilevel optimisation. A series of results from the case study are provided and discussed.

Finally, Chapter 7 concludes the work carried out to date and gives detailed recommendations for future work.

The postbuckling optimisation procedures of VICONOPT MLOP have been published in two conference papers, Qu *et al.* (2008, 2009). Qu *et al.* (2009) also contains details of the case study with the first stage results. More detailed results of the case study can be found in Qu *et al.* (2010). A journal paper Qu *et al.* (2011) which including full details of theory and the case study results has recently been accepted for publication.

When reading this thesis, it is very important to note the following definitions.

1. **Plate:** A single piece of thin-walled structure. Usually the smallest construction unit of the whole structure.
2. **Panel:** A component which while forming part of the whole structure, may contain one or more plates. In the software described in this thesis, the user is allowed to define the content of a panel under some restrictions.
3. **CONMIN cycles:** The cycles carried out by the programming optimiser CONMIN in VICONOPT.
4. **Sizing cycles:** The cycles carried out by VICONOPT to define the new design.
5. **Analysis cycles:** The cycles in VICONOPT MLOP, which involve postbuckling analysis only with no design taking place. These cycles provide updated

information on reduced stiffness after each cycle. The geometry of the model is kept the same.

6. Design cycles: The cycles in both VICONOPT MLO and VCIONOPT MLOP during which design is carried out and the geometry of the model (the thickness of each plate) is changed. In VICONOPT MLOP, a design cycle contains a number of analysis cycles.

All these cycles mentioned above will be explained in more detail in Chapters 3 and 4.

1.3 REVIEW OF PREVIOUS WORK

1.3.1 Review of Postbuckling

The review presented here is concerned with the postbuckling of plates, sections and stiffened panels which is considered relevant to the research described in this thesis. During the last 60 years, a number of ways of determining the buckling behaviour of plates have been devised. With increases in computational power, many of these methods can be solved using computational calculations where human hand calculation is infeasible. The Finite Element Method (FEM) is one of the most widely used methods. Other related methods include the Finite Strip Method and the 'Exact' Strip Method. Further details of these methods will be given in Chapter 2.

There are many books and survey papers in the literature which provide a good overview of issues relating to the analysis of plates in both the buckling and postbuckling regimes. A good overview of the buckling and postbuckling behaviour of plates is given by Turvey and Marshall (1995) and Hutchinson and Koiter (1970). A useful historical review regarding the development of the theory of postbuckling behaviour is given by Gioncu (1994).

Even though the buckling behaviour of thin walled structures, e.g. plates and shells, is well understood, the prediction of postbuckling behaviour of these structures still

provides many opportunities for improved understanding and has therefore been the focus of much academic research recently.

Wagner (1931) was one of the first to investigate the postbuckling problem, looking specifically at the shear buckling behaviour of plates. He established the experimental capacities of such field theory, to explain the capacity of a plate to carry shear loads well into the post-buckling region.

The postbuckling analysis of plates in compression was first investigated by Von Karman (1932). He developed the concept of effective width, which models the redistribution of initially uniform stresses within the plate, once buckling has occurred, enabling plates to take loads which considerably exceed their critical buckling loads. In the 1940's, numbers of authors presented their research on this new field, such as Koiter (1967) and Von Karman and Tsien (1941). Experimental observations of postbuckled plates have been used to develop theories and methods for analytical work.

Extensive research has been carried out regarding the local postbuckling of plates which was first investigated by Graves-Smith and Sridharan (1978). This research gives a solution to the postbuckling analysis of stiffened panels. The finite strip method was used to investigate the local postbuckling of plates by Dawe *et al.* (1993). An introduction to postbuckling analysis for a wide range of geometries and analytical solution methods is given by Powell (1997).

Recently, more and more research work has been done, in order to bring the postbuckling range into the industrial design guidelines. The GARTEUR (Group for Aeronautical Research and Technology in Europe) which was involved in collaborative research of multilevel optimisation of aircraft wing design during the 1990s published a final technical report AG-25 (van Houten and Zdunek, 2004) on the buckling postbuckling and collapse research work on aerospace structures and gave recommendations based on three benchmark tests carried out by Airbus France, SAAB and DLR separately. A POSICOSS (Improved POstbuckling SIMulation for Design of Fibre COmposite Stiffened Fuelage Structures) project was carried out based on the GARTEUR recommendations to provide an improved, fast and reliable

approach for postbuckling analysis and design of fibre composite stiffened panels and design guidelines based on experimental data (Zimmermann and Rolfes, 2006). The COCOMAT (Improved MATERIAL Exploitation at Safe Design of COMposite Airframe Structures by Accurate Simulation of COLLapse) project followed up the POSICOSS project by simulating future design scenario on real aircraft structures, and improving the experimental data based design guidelines (Degenhardt *et al.*, 2006).

1.3.2 Review of VICONOPT

VICONOPT (VIPASA with CONstraints and OPTimisation) is a FORTRAN 77 computer program with approximately 50000 lines of coding which incorporates the earlier programs VIPASA (Vibration and Instability of Plate Assemblies including Shear and Anisotropy) (Wittrick and Williams, 1974) and VICON (Anderson *et al.*, 1976). It covers prismatic assemblies of anisotropic plates which can carry any combination of longitudinally invariant in-plane stresses (Powell, 1997). An introduction to the software and its underlying theory will be provided in Chapter 3.

VICONOPT was first presented by Butler and Williams (1990) and Williams *et al.* (1990). In 1993 a further release (Williams *et al.*, 1993) provided a considerably more sophisticated buckling analysis capability and also included material strength constraints, bending and pressure loading, approximations for curved and tapered members and allowance for the effects of transverse shear deformation. Finally, in the spring of 1996 a new release was made available (Williams *et al.*, 1996) which included new features such as multilevel substructuring with constraints and a preliminary form of the local postbuckling analysis described in this thesis, as well as cost optimisation, simultaneous analysis and/or design of multiple structures, the ability to study wave propagation along the plate assembly and the ability to attach three-dimensional supporting frames.

The design capability of VICONOPT is based on the gradient based optimiser CONMIN (Vanderplaats, 1973). CONMIN is based on the method of feasible directions developed by Vanderplaats and Moses (1973). In the research presented in

this thesis, VICONOPT (including CONMIN) is essentially used as a ‘black-box’ style module. For completeness a brief introduction to the method of feasible directions will be presented in Chapter 2.

More recently, VICONOPT was extended to enable postbuckling analysis (Powell *et al.*, 1998). The method is based on a geometrically non-linear analysis for perfect or imperfect longitudinally compressed prismatic plate assemblies. Beyond the critical buckling load, the ratio of postbuckling to prebuckling axial stiffness is found by an iterative procedure, which establishes the relationship between the applied load and the longitudinal end shortening strain. The stabilizing effect of transverse tension, developed in the central portion of the plate when its longitudinal edges remain straight, has also been incorporated into the analysis to improve its overall accuracy. Another method for postbuckling analysis, given by Anderson and Kennedy (2008), is based on Newton iterations to give accurate convergence on the critical buckling load and associated mode. The work presented in this thesis is based on this method, therefore more information on this method will be given in Chapter 3. Currently, this method is under further development by Che *et al.* (2010), in order to improve the accuracy of mode shapes and stress distributions in the postbuckling analysis. A good review regarding the recent developments of VICONOPT incorporating postbuckling behaviour is given by Kennedy *et al.* (2007).

1.3.3 Review of Optimisation

Optimisation techniques are used in a whole range of disciplines e.g. mathematics, computer and natural sciences, economics etc. Various optimisation methods have evolved over the years, some of which are better suited for structural engineering applications than others. There are two main types of optimisation problems: unconstrained and constrained. A good introduction to both of these types of problems and the methods used is given by Cooper and Steinberg (1970) and Haftka and Gurdal (1991). Arora (1997) gives a good introduction to the structural optimisation of a number of design models in different engineering areas.

One of the most commonly used methods for both unconstrained and constrained problems is stochastic optimisation. Some of the well-established stochastic methods are Dynamic Relaxation (Day, 1965), Simulated Annealing (Aarts and Korst, 1989), Tabu Search (Glover, 1989, 1990), Genetic Algorithms (Goldberg, 1989), Differential Evolution (Storn and Price, 1997), Particle Swarm Optimisation (Eberhart and Kennedy, 1995) and so on.

For unconstrained optimisation problems, direct search and gradient based methods can be used. Some of the best known direct search methods are the Pattern Search Method (Hooke and Jeeves, 1961), Nelder-Mead's Sequential Simplex Method (Nelder and Mead, 1965), Random Search Methods (Rao, 1984; Vanderplaats, 1984), and Powell's Conjugate Directions Method (Powell, 1964). Some of the most widely used gradient based methods are the Method of Steepest Descent (Kirsch, 1993), Fletcher-Reeves' Conjugate Gradient Method (Fletcher and Reeves, 1964), the Newton Method (Kirsch, 1993), and the Variable Metric Method (Davidon, 1959; Fletcher and Powell, 1963). Some of these methods can also be used to solve constrained optimisation problems (Parkinson and Hutchinson, 1972).

In the field of engineering, most of the optimisation design problems are constrained optimisation problems. Among the numerous methods developed to solve constrained optimisation problems are Linear Programming and Nonlinear Programming techniques. Linear Programming is perhaps the widest and most general optimisation method. A detailed introduction to the method has been provided by Dantzig (1963), Gass (1969) and Hadley (1962).

Although Linear Programming is the widest used optimisation method, most real life optimisation problems are nonlinear. A detailed introduction to constrained optimisation has been provided by Leunberger (1984) and Gill *et al.* (1981). Two of the most common Nonlinear Programming methods are the Feasible Directions Method and Sequential Linear Programming (Griffith and Stewart, 1961; Kirsch, 1993). Gradient Methods can also solve Nonlinear Programming problems when some local linear assumptions are made.

1.3.4 Previous Work on Multilevel Optimisation

In the 1970s, a multilevel approach was used in the design of wing and fuselage structures (Giles, 1971; Sobieszczanski and Leondorf, 1972). Further work investigated the use of techniques such as multilevel decomposition (Sobieszczanski-Sobieski *et al.*, 1983), generalized multilevel optimisation (Sobieszczanski-Sobieski *et al.*, 1987), and response surface methodology (Ragon *et al.*, 1997).

In Europe, the GARTEUR (Group for Aeronautical Research and Technology in Europe) mentioned previously was involved in collaborative research of multilevel optimisation of aircraft wing design. This group defined a two level optimisation framework operating either at an overall system level or a more detailed panel level. A summary of the work, results and recommendations of the GARTEUR Action Group has been published in a three volume report (GARTEUR, 1997a,b,c). More recently, the GARTEUR group presented a report (Arendsen, 2001) on Multi-disciplinary wing optimisation which gives the results of their research on six different aspect wings in an overall optimum including structure, aero-elastic and aero-dynamics.

At Cardiff University, VICONOPT MLO (Fischer, 2002) has been developed as a multilevel optimisation interface between the well-established analysis and design software package VICONOPT (Williams *et al.*, 1991) and MSC/NASTRAN (MSC/Software, 1999). VICONOPT MLO is a 150MB Visual C++ program, which aims to provide an efficient solution for the optimisation of typical aerospace structures, such as aircraft wings. The software was first established by Fischer *et al.* (2002a,b), and the development of this software to incorporate postbuckling effects is presented in this thesis.

In addition to providing an interface for multilevel optimisation, VICONOPT MLO can be used as a pre-processor for VICONOPT, avoiding the need for text input files to be generated manually. Models can be assembled, analysed and optimised much more quickly and efficiently. These can be generated in two ways, being built either directly using VICONOPT MLO or assembled from MSC/NASTRAN data.

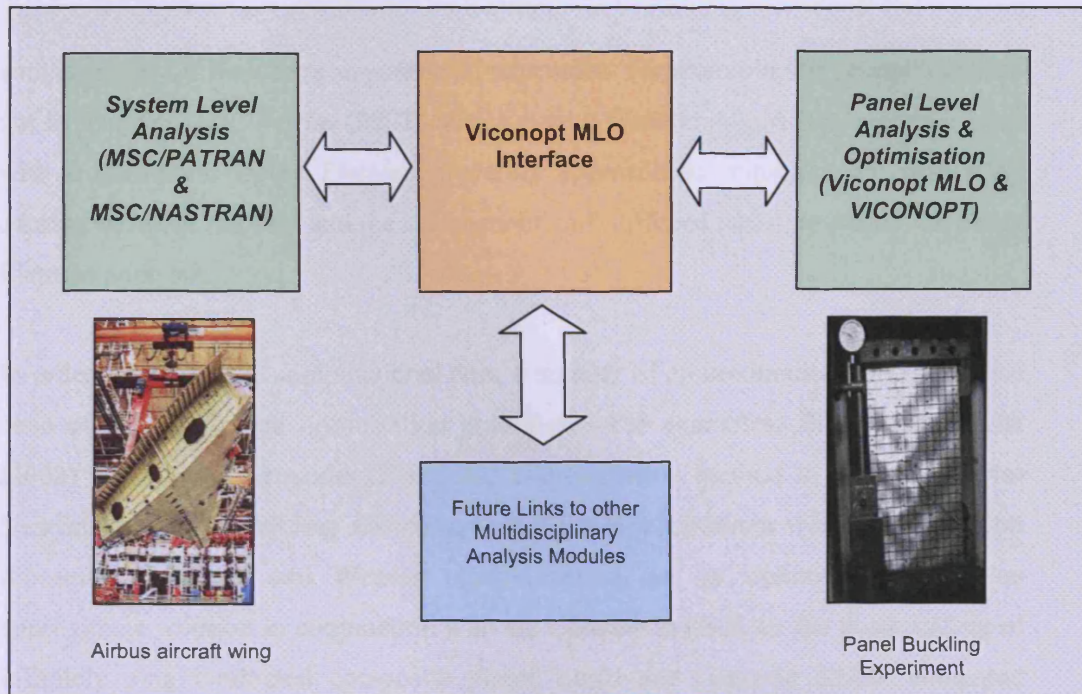


Figure 1.3 Multilevel nature of the optimisation procedure for an aircraft wing (Fischer *et al.*, 2002b).

The multilevel optimisation process is of an iterative nature, and based on the interaction between the models at the MSC/NASTRAN and VICONOPT levels. Corresponding to the GARTEUR definitions, these two levels are referred to as system level and panel level, respectively as shown in Figure 1.3.

1.3.5 Previous Work on Optimisation Including Postbuckling Effects

Most recently, attention has been paid to the optimisation of composite panels/plates considering postbuckling behaviour. During the last decade, the most commonly used method for optimisation considering postbuckling is Genetic Algorithms. A number of researches (Faggiani and Falzon, 2007; Sun *et al.*, 2010; Wu *et al.*, 2010) were carried out to underline their advantages, which include their ability to directly consider integer variables such as the number and the orientation of the layers of the skin and stiffeners, as well as the number of stiffeners (Lanzi and Giavotto, 2006). However, Genetic Algorithms are population based methods which require large numbers of evaluations of the objective functions and constraints before reaching

convergence, i.e. they are computational expensive. For example, the research carried out by Faggiani and Falzon (2007), which used a Genetic Algorithm in combination with a multilevel Finite Element modeling approach to minimise the debonding damage between the skin and the stiffeners of an I-stiffened panel, required 720 Finite Element analyses.

In order to reduce the computational cost, a number of approximation strategies have been evaluated for the optimisation procedures. For examples, Bisagni and Lanzi (2002) used neural networks as a global approximation method to incorporate pre-buckling stiffness, buckling and collapse loads into a minimum weight optimisation procedure. Diaconu and Weaver (2005) carried out an optimisation using an approximate solution in conjunction with the Galerkin method for the postbuckling of infinitely long laminated composite plates. Lanzi and Giavotto (2006) compared Neural Networks with two other global approximation methods i.e. Radial Basis Functions and Kriging approximation, in combination with a multi-objective Genetic Algorithm for the optimisation of a composite stiffened panel, in order to obtain a good compromise between minimal mass and maximal buckling or collapse load. The number of stiffeners and their dimensions, as well as the lay-ups which are used to describe the stacking sequences of the skin and stiffeners, were used as design variables. Wu *et al.* (2010) carried out an optimisation of a composite advanced grid-stiffened cylinder using an adaptive approximation-based optimisation procedure. The number, thickness and height of stiffeners were used as design variables. Irisarri *et al.* (2011) investigated a multi-objective optimisation methodology for composite stiffened panels to maximise an objective function defined in terms of the approximations of the critical buckling load and ultimate collapse or failure loads, by optimising the stacking sequences of the skin and the stiffeners of the panel.

Instead of looking into approximation strategies to reduce computational cost, a very limited number of researches focus on the development of new optimisation methods to design structures incorporating postbuckling. Fares *et al.* (2005, 2006) presented an integrated approach to solve a non-linear multi-objective optimisation problem for composite laminated plates, in order to minimise the postbuckling dynamic response and maximise the buckling load. The layer thicknesses and fibre orientations were taken as design variables. Lillico *et al.* (2000) performed a minimum weight

optimisation using VICONOPT to take into account the buckling and maximum strength considerations. The results obtained by VICONOPT were then verified using ABAQUS (ABAQUS, 1998). Liu *et al.* (2006) evaluated a bilevel optimisation strategy using VICONOPT by the design of a relatively short Z stiffened panel and a long wing cover panel.

In order to ensure that postbuckling optimisation results are close to real life scenarios, researches need to be carried out on more realistic and complex structures, i.e. comprising more than just a single plate or panel as described above. In this case, it is important to note that any changes made to a component plate/panel also affect the load carrying capacity elsewhere in the structure, and therefore a multilevel optimisation process is needed to iterate on an optimum design of the whole structure. The research presented in this thesis aims to develop a recently devised multilevel optimisation method (Fischer *et al.*, 2002a, b), which is based on an iterative approach using VICONOPT to obtain minimum mass designs for each component panel in conjunction with Finite Element static analysis of the whole structure, subjected to loads which cause parts of the structure to exhibit postbuckling behaviour. In this thesis, an indication is given of the computational benefits of the proposed method compared with a single level optimisation using only Finite Element analysis. It is shown that the use of VICONOPT gives computational savings over Finite Element analysis, demonstrating the efficiency of the new multilevel optimisation method when dealing with complex structures, such as an aircraft wing.

Chapter 2

Theoretical Background

2.1 GENERAL METHODS OF ANALYSIS

2.1.1 The Finite Element Method

Over the last 60 years numerous ways of determining the buckling and postbuckling behaviour of plates and plate assemblies have been developed. Nowadays, the Finite Element Method (FEM) is the most commonly used numerical method. Although an apparently complex technique, the fundamental principles are relatively straightforward.

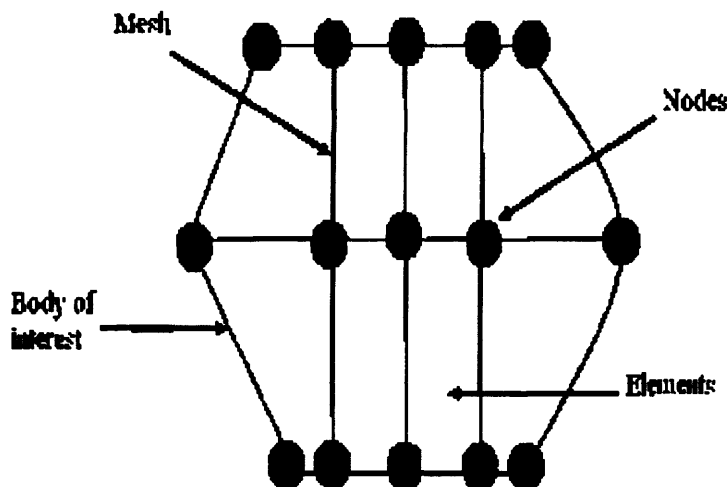


Figure 2.1 Finite Element Method (Mohsin *et al.*, 2008).

As shown in Figure 2.1, the FEM solves problems by dividing large complex structures into a collection of discrete portions which are known as finite elements. These finite elements are joined together by shared nodes to create a mesh to cover the whole structure. For example, in stress analysis of a structure, instead of calculating the stress for the whole structure directly, FEM determines the displacements of each node first. The stresses and strains of each element can then be calculated as functions of the displacements. Some boundary conditions can be applied to avoid unlimited rigid body motion.

The accuracy of the method depends upon the complexity of the model and is not 'exact'. The finite element method does however give good results for a large number of problems including those with transverse shear deformation (Rock and Hinton, 1976) and a better accuracy can be achieved by using a finer mesh. However, the problem that does exist with the finite element method is that it is computationally expensive in comparison with other techniques, especially for structures having regular geometric plans and simple boundary conditions, e.g. aircraft wings and fuselages, bridge decks and ship hulls where a number of simpler alternative schemes are possible.

For more introduction to the finite element method in general, the reader is referred to Henwood and Bonet (1996), and Zienkiewicz (2000).

NASTRAN (NAsa STRuctural ANalysis) is one of the best known and widely used commercially available finite element structural analysis computer programs, and was originally developed for NASA in the late 1960s by The MacNeal-Schwendler Corporation (MSC). Written primarily in FORTRAN it contains over one million lines of code. NASTRAN is compatible with a large variety of computers and operating systems ranging from small workstations to the largest supercomputers. Presently, the NASTRAN source code is integrated in a number of different software packages, which are distributed by a range of companies (MSC/Software, 1999a). More valuable references about MSC/NASTRAN can be found at <http://www.mscsoftware.com>.

2.1.2 The Finite Strip Method

The finite strip method represents a modification of the finite element method, and was introduced initially in the solution of static plate bending problems by Cheung (1968). Structures are divided into a number of strips, each having a constant thickness and width (Figure 2.2). A simple displacement function is required along the length of the strip, e.g. sinusoidal variation.

In comparison with the finite element method, the advantage of the finite strip method is that the order and bandwidth of the matrix to be solved are considerably reduced, thus making it more computationally efficient. However, the finite element method is still the best choice, when dealing with irregular structures which can not be easily divided into strips.

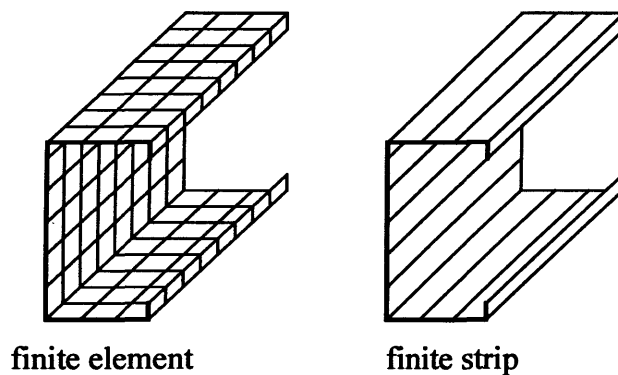


Figure 2.2 Finite Element and Finite Strip

2.2 BUCKLING AND POSTBUCKLING

2.2.1 Buckling

When a structure is carrying compressive loads, it may develop relatively large displacements under certain critical loading conditions, and then it is said to buckle at these critical loads (Case *et al.*, 1997).

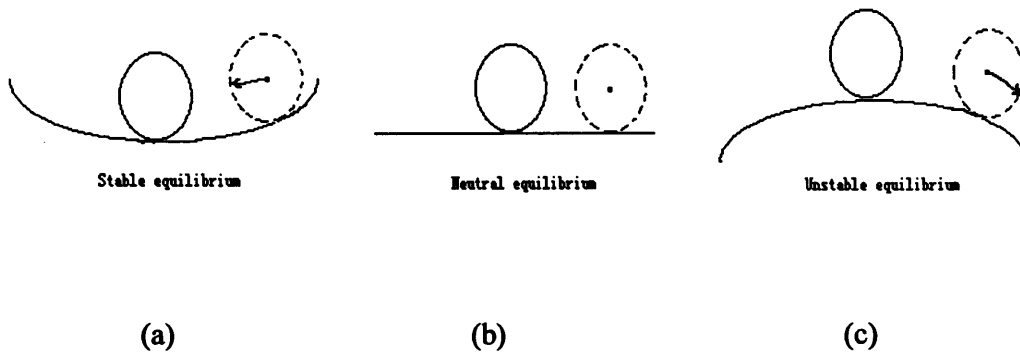


Figure 2.3 (a) Stable, (b) neutral and (c) unstable equilibrium (Kennedy, 2006a).

If the compressive loads are small, there are no lateral displacements, and the structure is in stable equilibrium. If the loads are increased which cause large lateral displacements, the structure is in unstable equilibrium. The point at which the lateral displacements first occur is called neutral equilibrium. The compressive load at this point is called the critical buckling load (Figure 2.3).

2.2.2 Postbuckling

When the structure has become unstable, it can often still carry loads far in excess of the critical buckling loads of its component plates before overall collapse occurs, a phenomenon known as postbuckling (Von Karman, 1932).

Although the buckling behaviour of thin walled structures such as plates and shells under a number of commonly experienced loading conditions is well understood, postbuckling behaviour has only fairly recently been given increased consideration. The postbuckling behaviour of plates in compression was first investigated by Von Karman (1932). He developed the concept of effective width, which models the redistribution of initially uniform stresses within a plate, once buckling has occurred as shown in Figure 2.4.

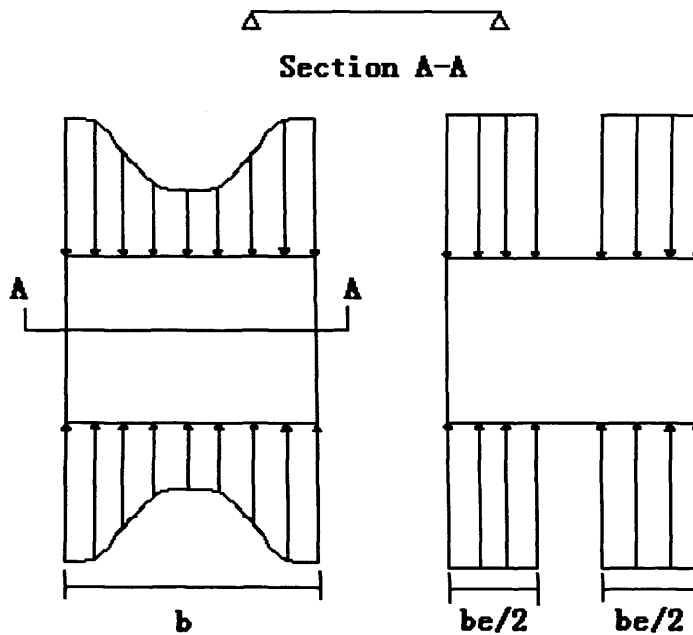


Figure 2.4 Concept of effective width (Kennedy, 2006b).

Following the buckling of a flat plate under compression, its central region deforms and barely participates in carrying any further loading. The edge regions near the supports however, remain almost straight and can continue to resist increasing loads. This leads to a non-uniform stress distribution across the width of the plate. Von Karman considered the edges of such a plate to act together as a single plate of width b_e to carry the stresses applied. The ultimate stress distribution in a simply supported plate of width b could then be replaced by a simplified distribution in which the central portion of the plate is ignored. The remaining effective width b_e carries all the load, with failure occurring when the critical buckling stress σ_{cr} of this notional plate reaches the yield stress σ_y (Figure 2.4). Instead of considering the effective width of the plate, other related geometric properties of plate can also be made effective, e.g. cross-sectional areas.

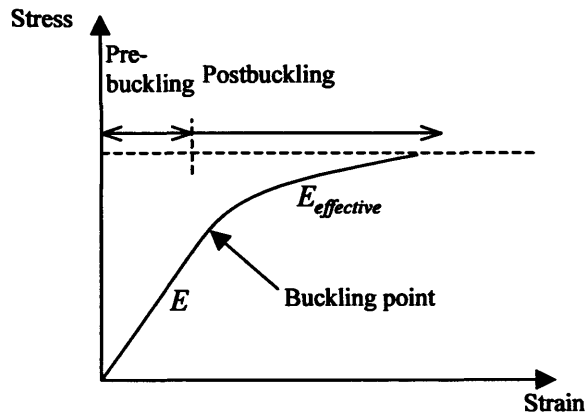


Figure 2.5 Effective Young's modulus

Alternatively, since the stiffness of a structure is very much governed by the Young's modulus, values of the Young's modulus E in the postbuckling region can also be made effective. As shown in Figure 2.5, before the initial buckling point is reached Hooke's law applies, and therefore the gradient of the stress-strain curve is defined by Young's modulus. After the initial buckling point, the stress-strain gradient is reduced to give an effective value of Young's modulus and the stress-strain relationship is no longer linear. The ultimate failure criterion is reached when the material finally starts to yield.

The mode shape of the structure gives a valuable insight into the postbuckling behaviour of a plate in an aerospace panel. In stiffened panel buckling problems it is important to find out whether the buckling mode is overall, torsional or local, as shown in Figure 2.6.

Figure 2.6(a) shows an overall mode in which the whole panel deflects laterally with a long wavelength, and with the stiffeners bending. Figure 2.6(b) shows a torsional mode in which the parts of the panel between the stiffeners buckle with an intermediate wavelength, and the stiffeners themselves have torsional deformations. Figure 2.6(c) shows a local mode in which the junctions between the stiffeners and panel skins remain essentially straight; but each plate of the panel deforms.

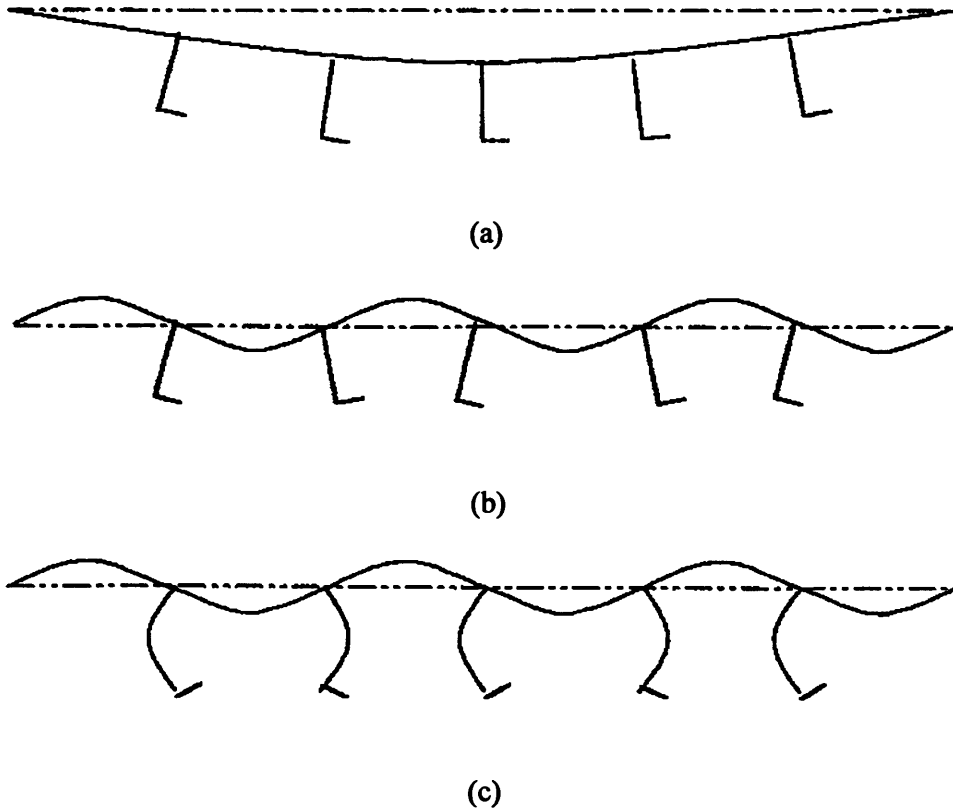


Figure 2.6 Buckling modes, (a) the overall mode, (b) the tripping/torsional mode and (c) the local mode (Powell, 1997).

If the buckling mode of the structure is a local mode, an additional load may be carried after initial buckling due to the postbuckling reserve of strength as described above. If the buckling mode of the structure is an overall mode, the postbuckling reserve of strength may have very limited effect. Local geometric imperfections can also affect postbuckling behaviour, increasing or decreasing the load-carrying capabilities predicted by a buckling/post-buckling analysis (Powell *et al.*, 1998).

2.3 OPTIMISATION

2.3.1 General

Structural optimisation can be defined as the rational finding of a structural design that is the best of all possible designs for a chosen objective and a given set of geometrical and behavioural constraints (Altair Engineering, 2000). There are many different types of structural optimisation techniques, which can be generally classified in terms of topology optimisation, shape optimisation, sizing optimisation and material optimisation. In this section, a general introduction will be given on structural optimisation and the optimisation techniques used for the research described in this thesis.

Topology optimisation is concerned with the topology for the structure. This optimisation selects the number of members and voids, e.g. holes, within the structure to generate a conceptual design within a given design space (Sigmund, 2000). Shape optimisation is concerned with the geometric shape of the designed structure. The optimisation starts with an initial topological design and the best suitable geometric shape of the structure or its components is extracted based on the design loading and boundary conditions. Sizing optimisation is concerned with the dimensions of the designed structure, e.g. the length, width and thickness. If the structure is assembled from a number of components, the dimensions of each component need to be optimised based on the design loading and boundary conditions. For a modern aircraft, composite materials are widely used. Therefore, the thicknesses and orientations of each of the individual plies also need to be optimised. However, in most practical industrial problems, the individual ply thicknesses are fixed, and therefore instead of the geometry of an individual ply, the number of plies may be considered as a design variable. Material optimisation is concerned with the material of the structure. The structure is given an initial design material at the beginning and the most suitable material is then determined at the end by improving the initial design material or determining a new material.

2.3.2 Methodology

Optimisation is a very old and important research topic in engineering, computer science and related fields. Optimisation is a process which is used to find the best solution for a problem from a range of options. This selection usually aims to find the minimum or maximum of a real function. In mathematical form, this can be described as, minimise or maximise a function $F(x)$, where $x = \{x_1, x_2, \dots, x_n\}$, subject to equalities $G_i(x) = 0 \quad i = (1, 2, \dots, p)$, or inequalities $H_j(x) \leq 0 \quad j = (1, 2, \dots, q)$ that the x has to satisfy within $x_l \leq x \leq x_u$ where x_u and x_l represent upper and lower bounds on the design variables.

In structural optimisation, the objective function often represents the mass or overall cost of the structure. Design variables can be used to express geometric dimensions of the structure, parameters defining its topology or shape, or material properties. When both equality and inequality constraints are satisfied, a design is feasible, i.e. within the design space of possible solutions. The inequality constraints typically represent buckling, vibration or material strength constraints, while the equality constraints reflect equilibrium and compatibility requirements by linking two or more variables to one another. Furthermore, constraints are often specified for overall stiffnesses, deflections and general geometric requirements.

Various optimisation methods have evolved over the years, some of which are better suited to structural engineering applications than others. For unconstrained problems, generally direct search and gradient-based methods can be distinguished. The direct search methods require only objective function evaluations, and there is no need to determine any derivatives. For this reason, they are sometimes referred to as non-gradient methods or zero-order methods. Gradient-based methods are usually more efficient than direct search methods. Some of the most widely used gradient based methods are the first order methods (using first derivatives of the objective functions and constraints) and second order methods (using first and second derivatives). Some of these procedures can also be used for the solution of constrained optimisation problems.

Numerous methods have been developed to solve constrained optimisation problems. Generally, these methods can be categorized as indirect and direct. Indirect methods convert the constrained optimisation problem into an equivalent unconstrained problem, while direct methods attempt to solve the constrained optimisation problem as it is. Examples of indirect methods include Penalty Function Methods and the Augmented Lagrange Multiplier Method (Courant, 1943; Carroll, 1961; Fiacco and McCormick, 1968). Direct Methods include the Method of Feasible Directions, Dual Methods, and Reduced Gradient Methods (Vanderplaats, 1984).

2.3.2.1 The Method of Feasible Directions

The method of feasible directions is selected for the multilevel optimisation which is described in the following chapters. This is one of the gradient based methods which can deal with a series of problems with both inequality and equality constraint functions. This method is used in VICONOPT in the form of the optimizer CONMIN (Vanderplaats, 1973), which assumes the constraints are locally linear, so it is used in conjunction with a “stabilisation” procedure using the Wittrick -Williams algorithm.

In accordance with the mathematical meaning of optimisation problems described above, the optimisation problem is given in terms of an objective function $F(x)$, and equality and inequality constraint functions $G_i(x)$ and $H_j(x)$. As shown in Figure 2.7, the objective function can be improved by the new design within the variables. The new design x^{r+1} is obtained from the previous design x^r by

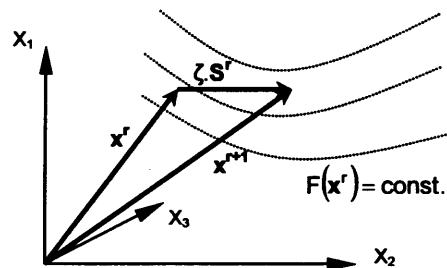


Figure 2.7 Move in design space between two iterations (Fischer, 2002).

$$x^{r+1} = x^r + \zeta \cdot S^r \quad (2.1)$$

where S^r is a move direction vector and ζ is the distance of movement.

S^r has to point in a direction which is both a usable direction, to ensure the value of the objective function is decreased, and a feasible direction to ensure no constraints are reached, as shown in Figure 2.8.

For a usable direction, S^r has to satisfy the following condition,

$$\nabla F(x^r) \cdot S^r \leq 0 \quad (2.2)$$

where $\nabla F(x^r)$ is the Nabla differential of the objective function $F(x)$ with respect to the current design variables x^r .

For a feasible direction, S^r has to satisfy the following,

$$\nabla H_i(x^r) \cdot S^r \leq 0 \quad i = (1, 2, \dots, q_a) \quad (2.3)$$

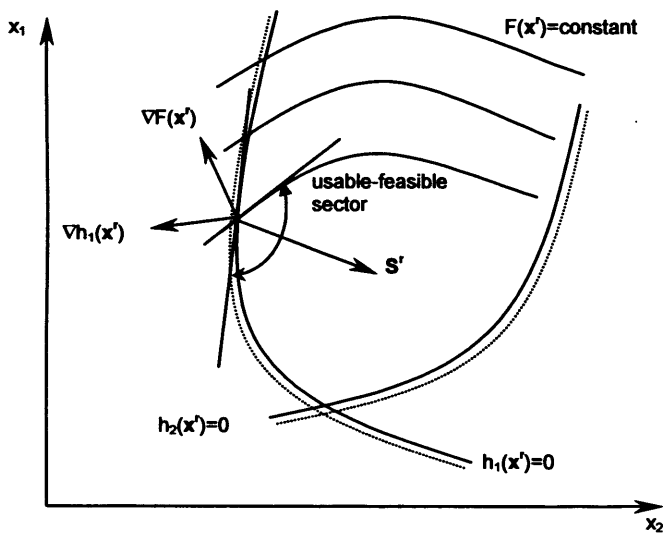


Figure 2.8 Usable and feasible direction (Fischer, 2002).

where $\nabla H_i(x^r)$ is the normalised analytic gradient of the constraint function $H_i(x^r)$ which satisfies $H_i(x^r) = 0$, and q_a is the number of currently active constraints.

The move direction vector S^r is determined by a push-off factor θ which moves the design away from the active constraints. A geometrical interpretation of θ is shown in Figure 2.9. A greater push-off factor θ will push the direction vector S^r more rapidly into the feasible region, though perhaps at the expense of improving the objective function less rapidly. For most cases $\theta = 1$ will provide acceptable and efficient results (Moses and Onoda, 1969; Fox, 1971).

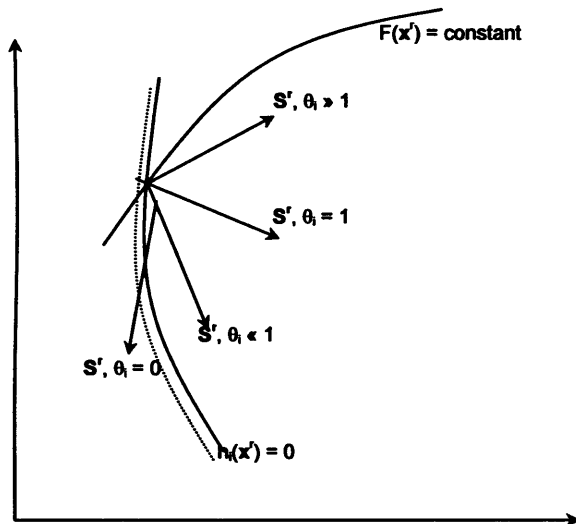


Figure 2.9 Effect of push-off factors θ on direction S^r .

2.3.3 Multilevel Optimisation

In many optimisation problems, the designer is faced with the dilemma of how to simulate the problem at hand using a number of different models. Some models may be quite elaborate in their representation of the problem and hence tend to be computationally expensive. Other models may be far less elaborate and hence computationally cheaper. The computationally cheap models tend to be less accurate than the expensive ones. The designer uses his/her experience and understanding of

the problem domain to switch between different models. She/he goes through a number of iterations until a satisfactory design is found. Designs created in such a fashion are not necessarily optimal and they could be improved upon, given more design iterations and an adequate search technique. It is hence important to develop techniques that make maximal use of the many models available within a limited computational budget. Conducting a search in such an environment where there are multiple models for evaluation of fitness is what is meant by the term Multilevel Optimisation (MLO). Suitable methods for conducting MLO may be sought using algorithms and techniques gleaned from natural processes, such as Evolutionary Algorithms, Artificial Neural Networks and Iterative Methods. Good introductions to these methods are given by Fogel (1994), Gurney (1997) and Kelley (1999), separately.

The method used in the research described in this thesis is an Iterative Method. The term 'iterative method' refers to a wide range of techniques that use successive approximations to obtain more accurate solutions to a linear system at each step (Barrett *et al.*, 1994).

Chapter 3

VICONOPT and VICONOPT MLO

3.1 INTRODUCTION

This chapter provides an introduction to VICONOPT and Viconopt MLO, and presents the underlying principles of the multilevel optimization procedure adopted.

VICONOPT (VIPASA with CONstraints and OPTimisation) is a FORTRAN program which incorporates two earlier programs, VIPASA (Vibration and Instability of Plate Assemblies including Shear and Anisotropy) (Wittrick and Williams, 1974) and VICON (Vipasa with CONstraints) (Anderson *et al.*, 1983).

VICONOPT (Williams *et al.*, 1991; Kennedy *et al.*, 2007) is an exact strip software providing a powerful tool for preliminary aircraft design which performs initial buckling, postbuckling and free vibration analyses of prismatic assemblies of isotropic and anisotropic plates, which can carry any combination of longitudinally invariant in-plane stresses.

VICONOPT MLO (Fischer *et al.*, 2002a,b; Fischer, 2002) has been developed as a windows interface between VICONOPT (Williams *et al.*, 1991; Kennedy *et al.*, 2007) and the well established analysis package MSC/NASTRAN (MSC/Software, 1999a). This software provides an easy-to-use, fast and flexible integrated analysis and design environment, and allows the structural optimization of typical aerospace structures, such as composite aircraft wings, to be carried out as a multilevel activity.

3.2 VICONOPT

3.2.1 General Theoretical Background

VICONOPT is a powerful structural analysis and design program which covers the buckling, postbuckling and free vibration analysis of prismatic assemblies of isotropic or anisotropic thin plates, and provides an efficient design tool in structural optimisation. VICONOPT can analyse many different structural cross-sections, including those in Figure 3.1, which can carry any combination of longitudinal, transverse, in-plane shear and bending loads. It calculates critical buckling loads, undamped natural frequencies and corresponding mode shapes. A typical component plate and its in-plane loading are shown in Figure 3.2. The underlying theory and capabilities of VICONOPT will now be described.

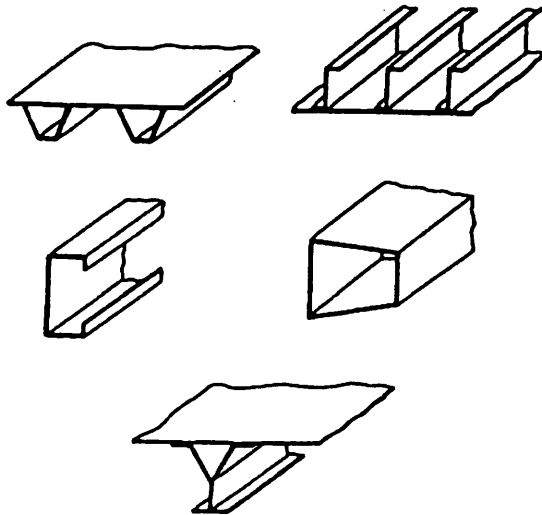


Figure 3.1 Typical sections which VICONOPT can analyze.

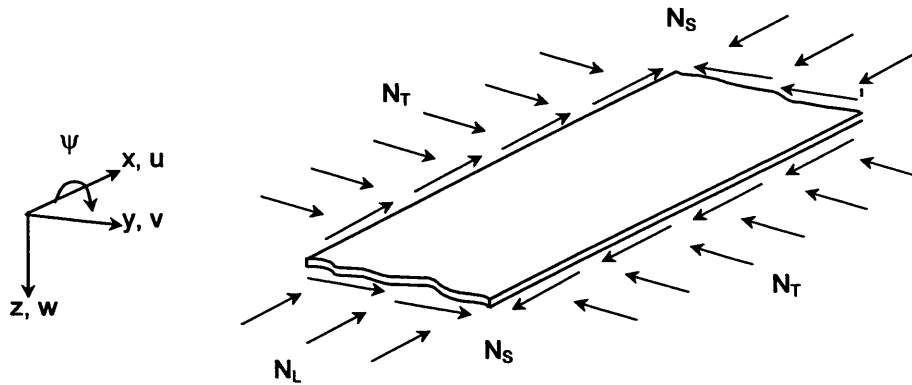


Figure 3.2 Component plate showing in-plane loading.

3.2.1.1 The Exact Strip Method and The Wittrick-Williams Algorithm

The ‘exact’ strip method provides an alternative approach to the finite element and finite strip methods. This method is based on analytical solutions to the partial differential equations which govern the in-plane and out-of-plane deformations of the component plates (Kennedy *et al.*, 2007), reducing them to ordinary differential equations which are solved analytically whenever possible.

The global stiffness matrix \mathbf{K} of the overall structure is first assembled from the member stiffness matrices \mathbf{K}_m . The eigenvalues can then be obtained by solving

$$\mathbf{KD} = \mathbf{0} \quad (3.1)$$

where \mathbf{D} is the displacement amplitude vector.

The advantage of this method is that no subdivision into elements or strips is necessary to achieve the required accuracy, and thus the overall stiffness matrix is reduced to half the size at most (Powell, 1997). A disadvantage of this method over the finite strip method is that the elements of \mathbf{K} are transcendental functions of the eigenparameter F (which represents the load factor or frequency) and are thus highly non-linear (Plank and Wittrick, 1974; Cheung, 1976; Dawe, 1977). Standard linear eigenvalue routines cannot therefore be used to extract the buckling loads or natural

frequencies of vibration. In order to solve this problem an iterative technique has to be adopted to find the values of F at which Equation 3.1 is satisfied, which has led to the development of the Wittrick-Williams algorithm.

The Wittrick-Williams algorithm (Wittrick and Williams, 1971; Wittrick and Williams, 1973) is based on the calculation of the number of critical load factors or natural frequencies, commonly referred to as J , which lie between zero and any trial value of F . Any change in J between two trial values is equal to the number of eigenvalues lying between these trial values.

The general form of the Wittrick-Williams algorithm is.

$$J = J_0 + s\{\mathbf{K}\} \quad (3.2)$$

where $s\{\mathbf{K}\}$ states the number of negative leading diagonal elements of the upper triangular matrix \mathbf{K}^Δ which can be found from \mathbf{K} by the usual form of Gauss elimination, and J_0 is the value that J would have if all freedoms corresponding to \mathbf{K} were fully restrained. J_0 can be obtained from

$$J_0 = \sum_m J_m \quad (3.3)$$

where the summation is over all members m of the structure (e.g. plates in the panel), and J_m is the number of eigenvalues of each member exceeded by the trial value of F when the member ends are clamped.

For computational efficiency, the algorithm allows the use of substructures (Powell, 1997). A substructure's contribution to J_m is computed by prior application of Equation 3.2 to the substructure, where \mathbf{K} is the stiffness matrix when all points of attachment to the parent structure are clamped (Wittrick and Williams, 1973).

With J known for each trial value of F , convergence on all required eigenvalues is easy, for example by bisection or by simple linear or parabolic interpolation on the determinant of \mathbf{K} .

3.2.1.2 VIPASA and VICON

VIPASA (Vibration and Instability of Plate Assemblies including Shear and Anisotropy) is a computer program developed in 1974 at the University of Birmingham (Wittrick and Willams, 1974), and enhanced at the NASA Langley Research Center (Anderson *et al.*, 1976). The main advantage of VIPASA over finite strip and finite element methods is its speed, due to it being based upon the exact strip method described in Section 3.2.1.1 above. Compared to finite element programs, e.g. STAGS (Structural Analysis of General Shells) (Almroth, 1978), VIPASA has proved to be 1000 times faster when finding the eigenvalues of a stiffened panel (Butler and Williams, 1992).

In a VIPASA analysis the mode shape is assumed to vary sinusoidally in the longitudinal direction, with displacements u , v , w and ψ as shown in Figure 3.2 and with half-wavelength λ . The out-of-plane buckling displacement is given by

$$w = f_1(y) \sin\left(\frac{\pi x}{\lambda}\right) \quad (3.4)$$

where f_1 is a function of y , to allow simply supported end conditions. Similar expressions are assumed for the in-plane displacements u and v , providing a series of straight nodal lines perpendicular to the longitudinal axis spaced at longitudinal intervals of half-wavelength λ as shown in Figure 3.3.

As shown in Figure 3.3, simply supported end conditions are satisfied when the nodal lines are straight and perpendicular to the longitudinal direction (i.e. x -axis), all the plates are orthotropic and carry no shear loads, and the half-wavelength λ divides into the panel length ℓ exactly. There are then no phase differences between the sinusoidal variations of w along the longitudinal lines at the edges, so that the

solutions obtained are exact for plate assemblies of finite length ℓ . Edge boundary conditions, e.g. rigid, elastic, pinned or sliding edge supports, can be defined explicitly by using continuous longitudinal line supports to constrain any combination of the four degrees of freedom (u, v, w, ψ) at the nodes, i.e. the longitudinal lines representing the edges.

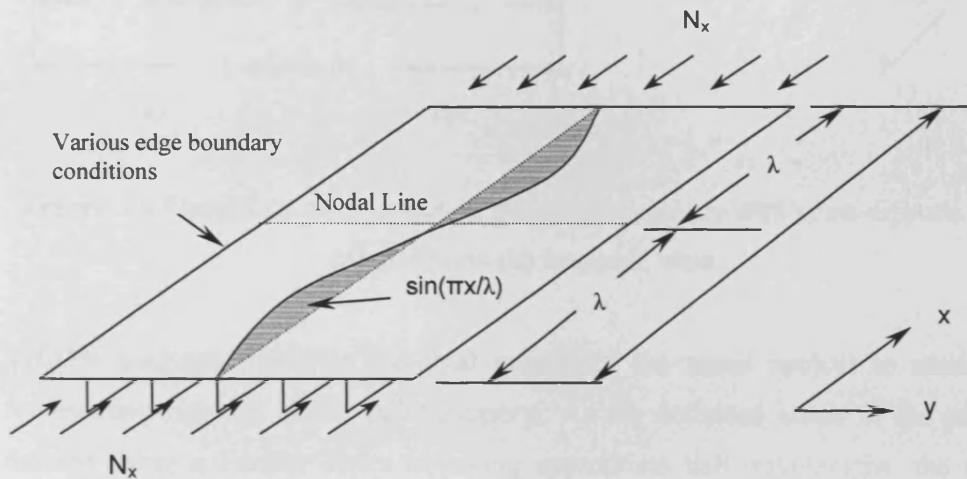


Figure 3.3 Simply supported end conditions in VIPASA analysis.

VIPASA provides exact solutions when the assumptions described above are met, but otherwise the results are conservative for panels which are loaded in shear or have anisotropic material properties, because the nodal lines are no longer straight but skewed. As the half-wavelength λ approaches the length of the panel ℓ , VIPASA will provide increasingly conservative buckling loads and natural frequencies.

VICON (VIPASA with CONstraints) was developed at Cardiff University (Anderson *et al.*, 1983; Williams and Anderson, 1983) to overcome the conservative nature of a VIPASA analysis for shear loaded and anisotropic plates. VICON (Anderson *et al.*, 1983) couples the VIPASA stiffness matrices for different wavelength responses through the use of Lagrangian Multipliers and retains the complete generality and capability of VIPASA, being based upon the same assumptions, loading, plate stiffness matrices, etc. Compared to the finite element program STAGS, VICON has proved to be 150 times quicker (Butler and Williams, 1992).

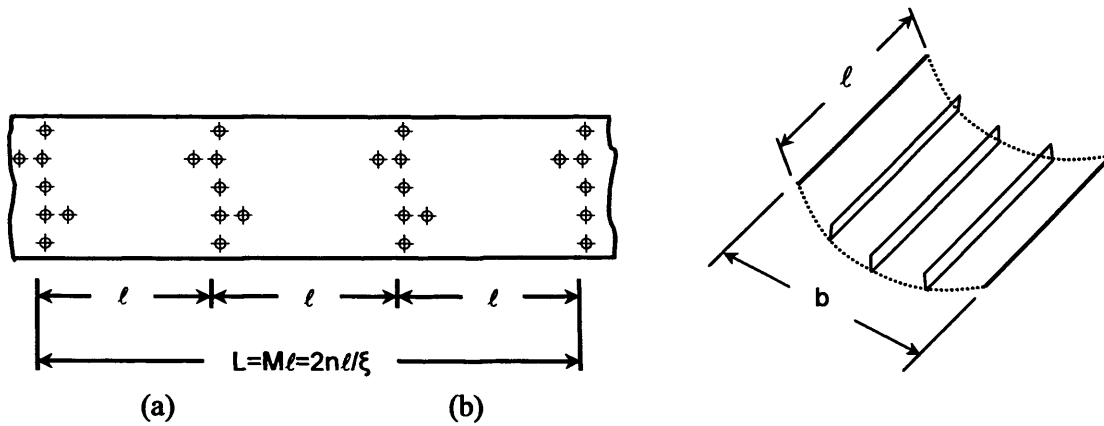


Figure 3.4 Illustration of an infinitely long plate assembly with point supports [\oplus],
(a) plan view (b) isometric view.

VICON analyses minimise the total energy of the panel subject to constraints representing rigid or elastic point supports. As the deflected shape of the panel is defined using a Fourier series involving appropriate half-wavelengths, the results correspond to an infinitely long panel with constraints repeating at intervals of ℓ . The mode of buckling or vibration repeats n times over a interval $L = M\ell$, where M and n are integers, as shown in Figure 3.4. The infinitely long plate assembly gives the advantage of modelling the continuity over several bays of a typical aerospace structure, e.g. an aircraft wing.

In order to provide the best results, an infinite series of half-wavelengths should ideally be used. However, in order to ensure an acceptable computational solution time, a finite series of half-wavelengths λ_i are used at the expense of some loss of accuracy. Therefore, it is important to choose the λ_i to provide satisfactory results. The choice of λ_i is governed by (Anderson *et al.*, 1983)

$$\lambda_i = \frac{\ell}{(\xi + 2i)} \quad (i = 0, \pm 1, \pm 2, \dots, \pm q) \quad (3.5)$$

where ℓ is the length of one bay of the structure, q is a integer chosen by the user and ξ is a parameter given by $\xi = \frac{2n}{M}$ ($0 \leq \xi \leq 1$). When choosing ξ and q , it must be ensured that the lowest buckling load can be identified for all values of ξ that are likely to be critical for the design problem. As the mode repeats n times over M lengthwise bays of length ℓ , L can be represented by

$$L = \frac{2n\ell}{\xi} \quad (3.6)$$

The buckling load factors and natural frequencies of vibration calculated by VICON are obtained in a similar way to those using VIPASA analyses, with appropriate extensions to the Wittrick-Williams algorithm (Williams and Anderson, 1983). A full derivation of the governing equations and extended stiffness matrix based on Lagrangian multipliers has been provided by Anderson and Williams (Anderson *et al.*, 1983; Williams and Anderson, 1983).

3.2.2 VICONOPT Design Optimisation

VICONOPT has a number of design capabilities, including continuous optimisation (Kennedy *et al.*, 1999), discrete optimisation (Kennedy *et al.*, 1999), discontinuous cost functions (Kennedy *et al.*, 1999) and vibration constraints (O'Leary, 2000; O'Leary *et al.*, 2001; Kennedy *et al.*, 2005). This section describes the well proven continuous optimisation features. In a VICONOPT design problem, a range of different design variables (e.g. plate widths and ply thicknesses) are optimised subject to buckling, strength, stiffness and geometric constraints, in order to obtain the minimum mass.

The continuous design phase (CDP) in VICONOPT is based on the sizing strategy of steps 1-9 in Figure 3.5 (Kennedy *et al.*, 2007).

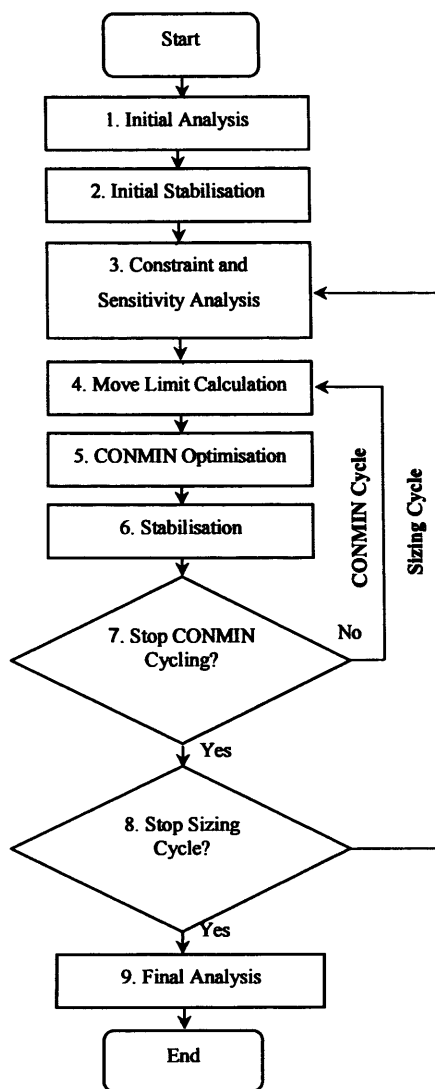


Figure. 3.5 Panel design strategy showing the continuous design phase.

In the CDP, a range of different design variables can be specified, including plate widths, breadths, layer thicknesses and ply orientations. Design variables also can be controlled or linked to each other, in order to meet practical requirements or to reduce the computation time. The two main optimisation objectives are total mass minimization and cost reduction.

At the beginning of the design, an initial analysis (step 1) is carried out to determine the critical buckling load, followed by an initial stabilization (step 2) (Butler and Williams, 1992). Some of the design variables (i.e. layer thicknesses) are then

factored uniformly to achieve a just stable configuration. This process is repeated after each use of the mathematical programming optimiser CONMIN (step 6) (Vanderplaats and Moses, 1973) during the subsequent iterative procedure, which consists of a number of sizing cycles.

At the beginning of each sizing cycle, a constraint and sensitivity analysis is carried out (Step 3) to determine the buckling load factors for the structure. The buckling constraints which are critical, or close to critical, for the current design are then calculated on the basis of the load factors. Their sensitivities (i.e. derivatives with respect to the design variables) are found by an efficient finite difference approach (Butler and Williams, 1992).

The second step of the sizing cycle is a move limit calculation (Step 4), which is also the start of the CONMIN cycle. In this step, appropriate lower and upper design variable limits are determined.

In the CONMIN optimisation (Step 5), VICONOPT linearises the non-linear constraints obtained from the previous step using a first order Taylor series expansion. An iterative procedure based on the method of feasible directions (Section 2.3.2.1) is also contained in this step. In accordance with the move limits determined in step 4, changes are made to the design variables to minimise the objective function.

After the CONMIN optimisation stage, a stabilization stage, which is similar to the initial stabilization stage, is carried out (Step 6) to verify the feasibility of the new design. By doing this, the design is adjusted to be just stable before the next CONMIN cycle. Therefore, the design convergence can be accelerated.

Once convergence has been obtained for all the CONMIN and sizing cycles (Steps 7 and 8), a final VICONOPT analysis (Step 9) is carried out to verify the buckling results.

A subsequent discrete design phase (DDP) has been added to handle problems where some or all of the design variables are required to take discrete values (Kennedy *et al.*, 1999). This requirement is not considered in the present work.

3.2.3 VICONOPT Postbuckling Analysis

VICONOPT has been extended to enable postbuckling analysis (Powell *et al.*, 1998; Anderson and Kennedy, 2008) of prismatic panels. The method is based on a geometrically non-linear analysis with optional allowance for initial imperfections, and is currently restricted to the VIPASA form of analysis.

After critical buckling has occurred, additional load is carried under a regime in which the stiffness of the panel is reduced by differing amounts due to the re-distribution of stress among and within the component plates (Anderson, 1997). The ratio of postbuckling to prebuckling axial stiffness is found by an iterative procedure, which establishes the relationship between the applied longitudinal load and the longitudinal end shortening strain, while ensuring consistency of the stress distribution, postbuckling mode shape and amplitude. The stabilising effect of transverse tension, developed in the central portion of the plate when its longitudinal edges remain straight, has been incorporated empirically into the analysis to improve the overall accuracy (Powell *et al.*, 1998). There are two methods which can be used to perform postbuckling analysis in VICONOPT.

The first of these methods (Powell *et al.*, 1998) is based on the Wittrick-Williams algorithm. At the start of each new cycle, the mode amplitude is incremented by a certain amount, and an iterative procedure is performed to find the critical buckling load, the longitudinal strain, the postbuckling mode shape and the stress distribution within the structure. A disadvantage of this method is the difficulty in converging when analysing a problem with regularly spaced stiffeners, due to the limited numerical accuracy of the mode shapes, interaction between similar local modes and mode jumping (Watson and Kennedy, 2004).

The second method uses a Newton-based iteration scheme (Anderson and Kennedy, 2008). Instead of using the Wittrick-Williams algorithm, this method uses Newton iterations to give accurate convergence on the critical buckling load and associated mode. At the start of each new cycle, the longitudinal and/or shear strain is incremented by a certain amount. Then, the total applied load, the stress distribution

across the structure and the postbuckling mode shape and amplitude can be determined. The research described in this thesis is based on this method.

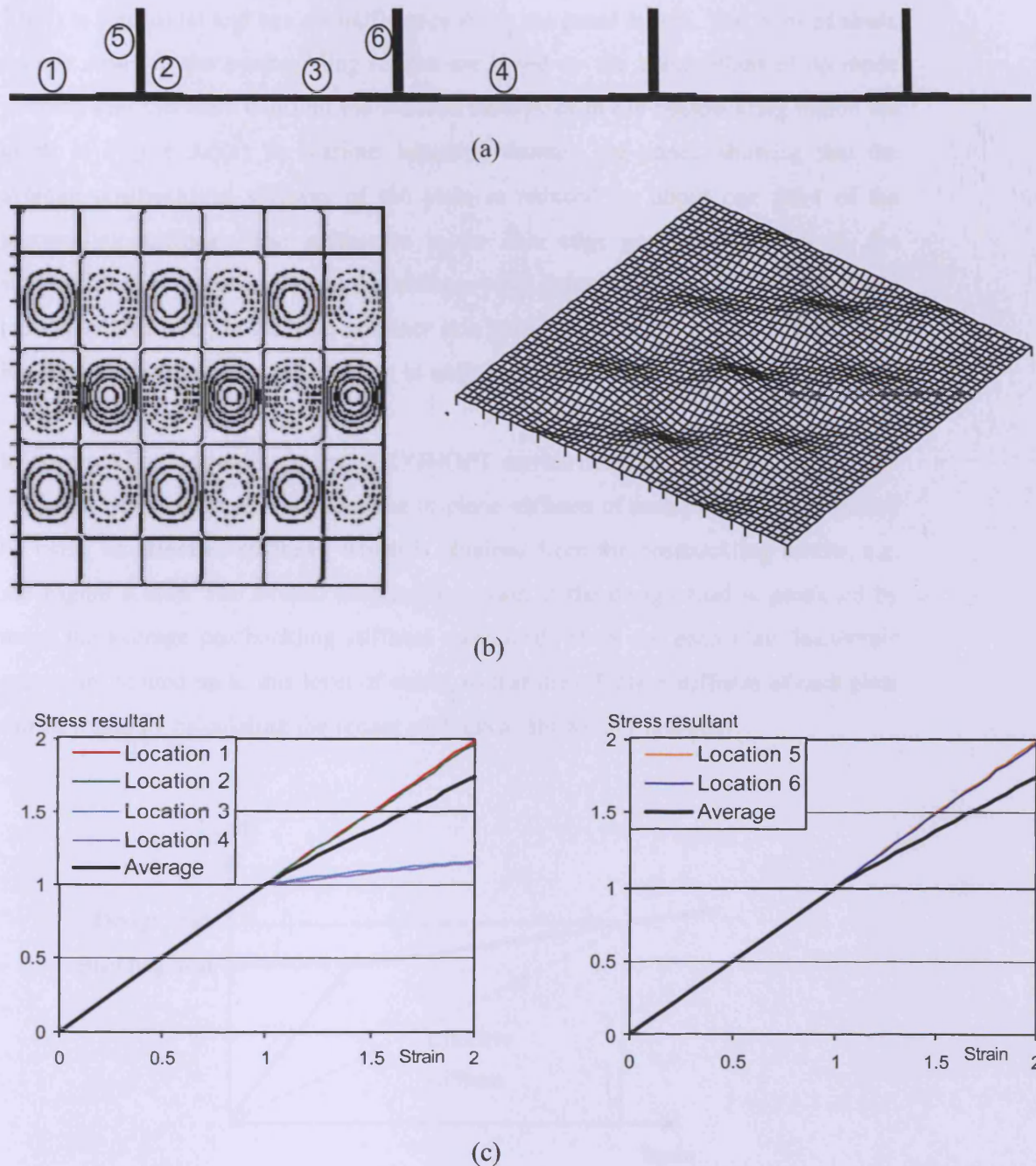


Figure 3.6 Postbuckling of a stiffened panel. (a) Panel cross-section. (b) Contour and isometric plots of buckling mode. (c) Normalised stress-strain plots at various locations in the skin and stiffeners.

A typical example is shown in Figure 3.6 (Kennedy and Featherston, 2010). A simply supported square panel with four longitudinal stiffeners (Figure 3.6(a)) is loaded in longitudinal compression. The local mode shape of initial buckling shown in Figure 3.6(b) is sinusoidal and has six half waves along the panel length. The plots of stress against strain in the postbuckling regime are based on the assumptions of no mode jumping and therefore constant but reduced stiffnesses in the postbuckling region are given in Figure 3.6(c) for various locations through the panel, showing that the average postbuckling stiffness of the plate is reduced by about one third of the prebuckling stiffness. The stiffnesses in the skin edge portions (location 1), the stiffener flanges (location 2) and the stiffener webs (locations 5 and 6) have negligible reduction. However, in the inter-stiffener skin portions (locations 3 and 4) where there is a large deflection, a large reduction in stiffness has occurred.

In postbuckling optimum design, VICONOPT carries out a postbuckling analysis on the panel before each sizing cycle. The in-plane stiffness of each plate is then adjusted by using an effective stiffness, which is obtained from the postbuckling results, e.g. see Figure 3.6(c). The overall longitudinal strain at the design load is predicted by using the average postbuckling stiffness calculated. Then, for each plate load/strain curves are plotted up to this level of strain, so that the effective stiffness of each plate can be found by calculating the secant stiffness as shown in Figure 3.7.

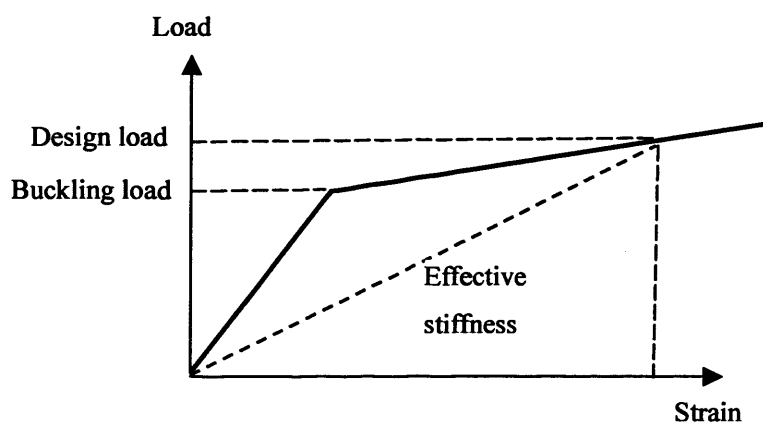


Figure 3.7 Calculation of effective stiffness for a postbuckled plate.

3.3 VICONOPT MLO

3.3.1 Introduction

VICONOPT MLO (Fischer *et al.*, 2002a,b; Fischer, 2002) is a Visual C++ program providing a multilevel optimisation interface between VICONOPT and the finite element software MSC/NASTRAN (MSC/Software, 1999a) (Figure 3.8), which aims to provide an efficient solution for the optimisation of complex aerospace structures, such as aircraft wings.

Viconopt MLO not only provides an interface for multilevel optimisation, but can also be used as a pre-processor for VICONOPT, avoiding the need for text input files to be generated manually, and allowing models to be assembled, analyzed and optimized much more quickly and efficiently. These can be generated in two ways, being built either directly using VICONOPT MLO or assembled from MSC/NASTRAN data.

During a multilevel optimisation, finite element models are created using MSC/PATRAN (MSC/Software, 1999b) and a static analysis is performed by MSC/NASTRAN, at an overall or system level, e.g. for the whole wing. VICONOPT MLO then uses the resultant MSC/NASTRAN data (i.e. geometry, material properties, stress distributions, etc.) together with design variables and appropriate bounds defined by the user, to create VICONOPT input files for each of the structure's constituent panels at panel level, e.g. the skin panels and spars. VICONOPT analyses and optimises each of the panels by minimising the mass subject to initial buckling constraints. Updated finite element model data, including ply thicknesses, are calculated and returned to MSC/NASTRAN by VICONOPT MLO. Further finite element analysis of the whole structure (system level) is carried out with the updated geometry to determine the new stress distributions in each panel. Each panel is now re-optimised. The process is repeated until a convergence criterion based on the overall mass of the structure is met. This criterion may either be specified by the user or taken as the default option of 1% of the overall mass changes; further details will be given in the next Chapter. Figure 3.8 illustrates this part of the multilevel

optimisation framework which will be referred to as the design cycle in the rest of this thesis.

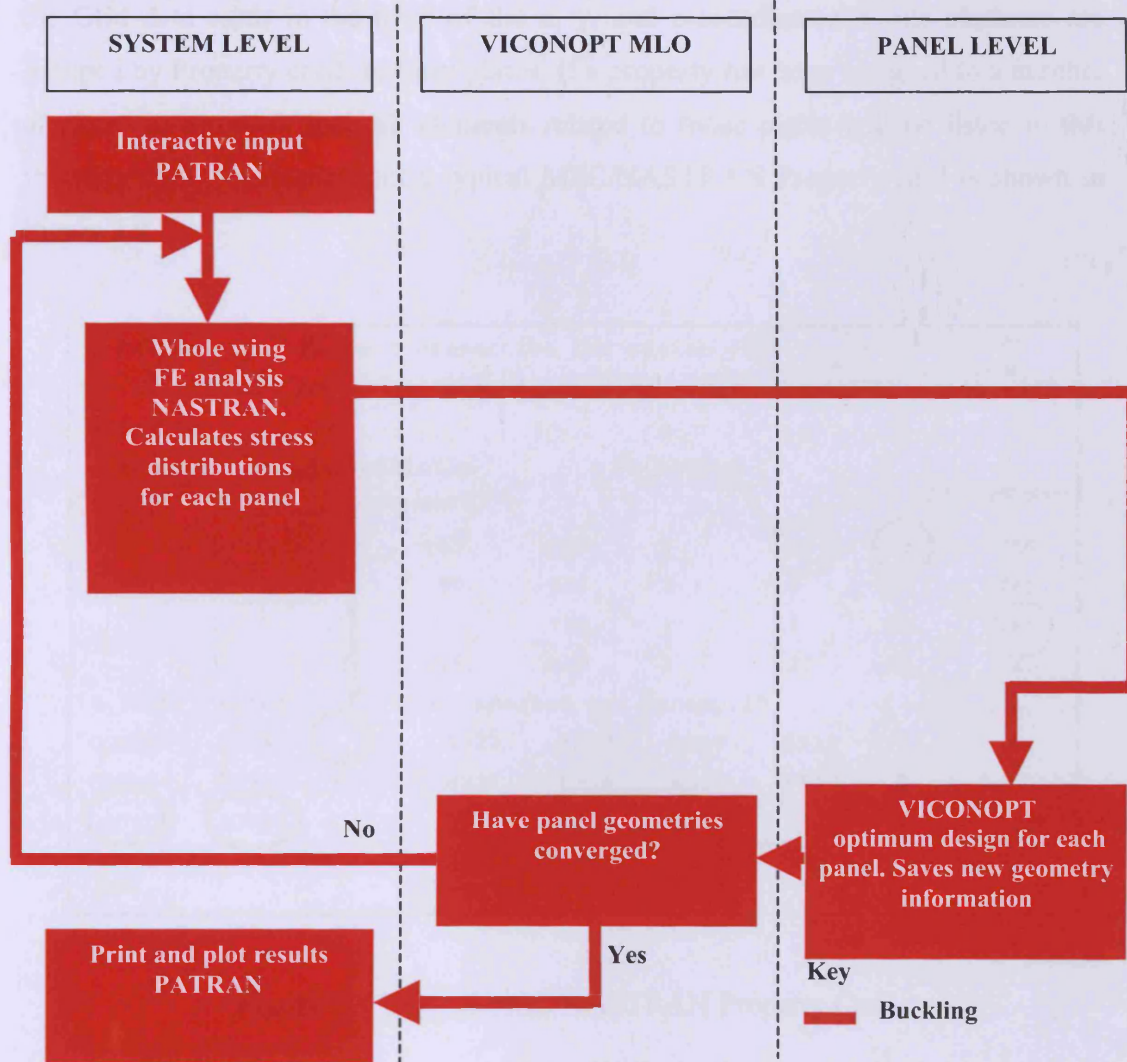


Figure 3.8 Multilevel framework for optimum design using VICONOPT MLO.

3.3.2 MSC/NASTRAN Model Translation

MSC/NASTRAN stores all the model's geometric and material property information in a .bdf file. The location of each finite element's nodes are given within this file in the Grid data cards in the form of the x, y, and z-coordinates. Finite elements are grouped by Property cards to form plates. If a property has been assigned to a number of plates in a model, then all elements related to those plates will be listed in this Property card. An example of a typical MSC/NASTRAN Property card is shown in Figure 3.9.

```

$ Elements and Element Properties for region : skin1_1
$ Composite Property Record created from P3/PATRAN composite
material
$ record : CompositeSkinTip
PCOMP 1
      1 .25 -45. YES 1 .25 45. YES
      1 .5 90. YES 1 .5 0. YES
      1 .5 0. YES 1 .5 90. YES
      1 .25 45. YES 1 .25 -45. YES
$ Pset: "skin1_1" will be imported as: "pcomp.1"
CQUAD4 20392 1 8323 8322 8509 8512 0
CQUAD4 20393 1 8322 8316 8507 8509 0
CQUAD4 20707 1 8316 8312 8505 8507 0 [...]
  
```

Figure 3.9 Typical MSC/NASTRAN Property Card

In the Property cards, material properties, ply orientation and thicknesses are stored in multi-dimensional arrays which allow each entry to be clearly related to a specific layer within a specific plate of a specific panel.

When VICONOPT MLO transfers the finite element model to VICONOPT, each of the panel geometries is determined on the basis of the x, y, and z-coordinates of the nodes within each of the component plates. VICONOPT MLO first calculates the length and breadth of each plate using the maximum and minimum coordinates found within the plate. It then selects all the nodes which are found at the edges of each plate

from the finite element model and gives each of them a unique reference number. Finally all the nodes are re-numbered and those nodes which lie on the boundaries of adjacent plates are equivalenced. More details on node numbering are given below.

When updating the finite element model at system level after a completed panel level optimisation, the modified design variables can easily be included in the MSC/NASTRAN model, by simply replacing the relevant entries for each property card in the previous model.

3.3.2.1 Node Numbering For VICONOPT

As described above, once the overall panel geometry has been extracted from the finite element model, the nodes at the edges of each VICONOPT component plate are assigned a unique number. If the user specifies extra point supports (as described in Section 3.2.1.2) on the plates, more nodes will be added to subdivide those plates. On the other hand, some nodes will be deleted, due to the equivalencing process described above. It is therefore important to re-number all the nodes before entering the VICONOPT optimisation stage. This re-numbering work is done automatically by VICONOPT MLO when it generates new VICONOPT input files.

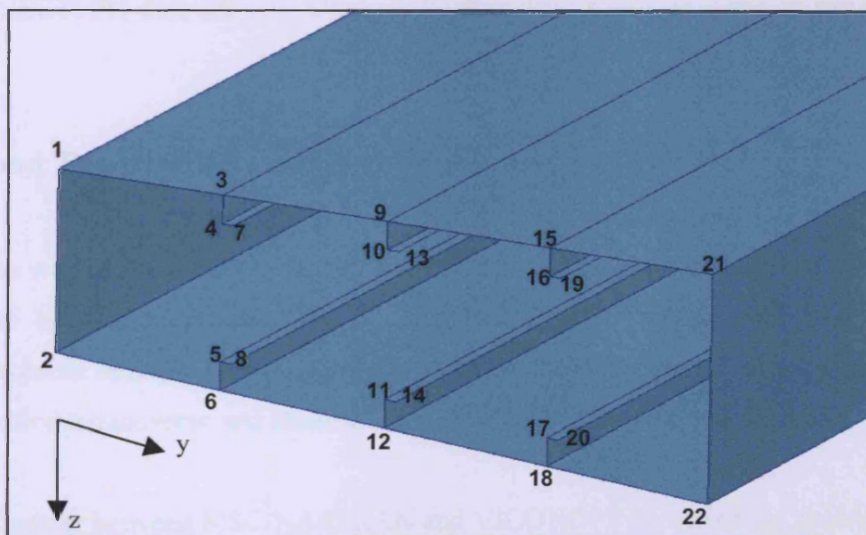


Figure 3.10 Node numbering of a wing-box.

VICONOPT MLO re-numbers the nodes of each component panel according to their increasing global y and z-coordinates (Fischer *et al.*, 2002a), i.e. if the nodes have the same y-coordinates, but different z-coordinates, the one with the lower z-coordinate is given preference over the node with the higher z-coordinate. An example of the final node numbering of a wing-box is shown in Figure 3.10.

This node re-numbering increases the efficiency of the VICONOPT analyses and optimisations by reducing the maximum bandwidth of the overall stiffness matrix. After node re-numbering, VICONOPT MLO generates the VICONOPT input files with these new node numbers. VICONOPT allows the geometries of the models to be defined using two different formats (William *et al.*, 1991). The first uses CONNECTION data groups to assemble models and stores the information on the width of each component plate in the PLATE data groups. ALIGNMENT data groups are then used to specify the rotations and offsets of the plates. Alternatively, COORDINATE data groups are used based on the global coordinates of each of the nodes. The widths of each component plate are calculated automatically by VICONOPT during the optimisation stage.

VICONOPT MLO previously only allowed the COORDINATE data groups to be used, but in the currently developed version of VICONOPT MLO, the ALIGNMENT and CONNECTION data are also allowed. Further details will be given in the next chapter.

3.3.3 Load Transfer between NASTRAN and VICONOPT

In the same way as the model geometry transfer, load transfer is an important part of model data conversion process. During load transfer, the overall axial load and bending moment need to be calculated for each of the VICONOPT panel models, together with the transverse and shear loads in their individual component plates.

The load transfer between MSC/NASTRAN and VICONOPT is carried out according to the type of elements used for the finite element model at system level (Fischer *et al.*, 2002a). There are many types of shell elements available in MSC/NASTRAN. Each

contains specific element properties which can affect the load distribution calculation. In MSC/NASTRAN, element resultant stresses are defined according to their individual local coordinate system. Therefore, VICONOPT MLO needs to transform these results into a global context for the overall structure.

In previous work and the work presented in this thesis, QUAD4 elements (MSC/Software, 1999a) have been used. However, the transfer procedures could be readily adapted for other types of element. QUAD4 elements are quadrilateral elements with a total of four nodes, one at each corner as shown in Figure 3.11. The nodes $G_1 - G_4$ are each assigned a unique number and coordinates automatically according to the model's global coordinate system when generating a model using MSC/PATRAN. Figures 3.12 to 3.14 show the QUAD4 element force, moment and stress conventions separately.

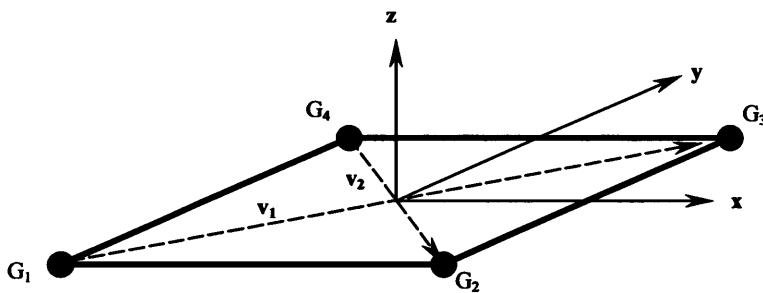


Figure 3.11 QUAD4 element and coordinate system definition.

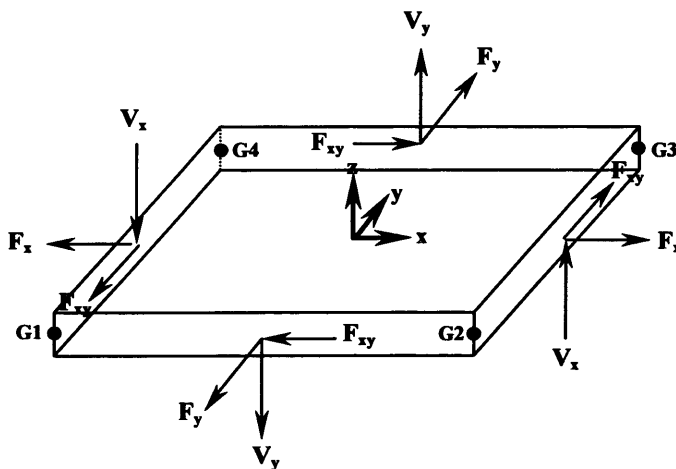


Figure 3.12 Force convention for plate elements.

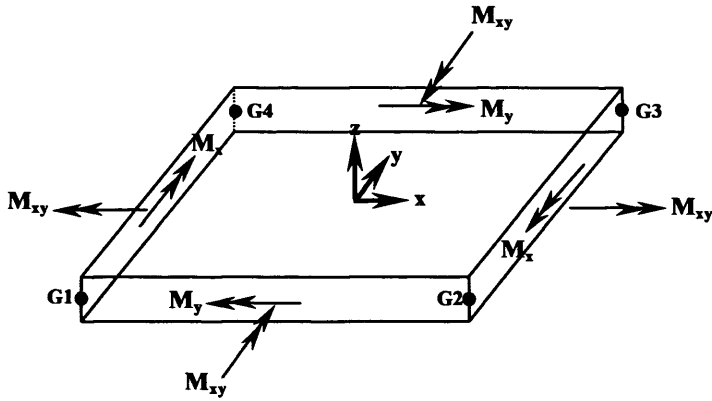


Figure 3.13 Moment convention for plate elements.

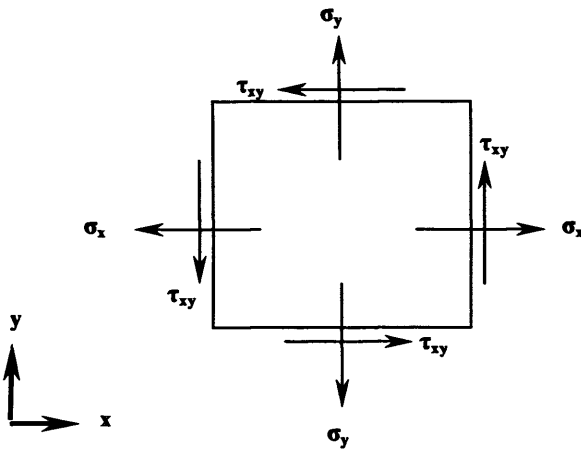


Figure 3.14 Stress convention for plate elements.

The locations of the nodes of the element shown in Figure 3.11 can be expressed in vector notation as

$$G_1 = \begin{Bmatrix} g_{1x} \\ g_{1y} \\ g_{1z} \end{Bmatrix}, G_2 = \begin{Bmatrix} g_{2x} \\ g_{2y} \\ g_{2z} \end{Bmatrix}, G_3 = \begin{Bmatrix} g_{3x} \\ g_{3y} \\ g_{3z} \end{Bmatrix}, G_4 = \begin{Bmatrix} g_{4x} \\ g_{4y} \\ g_{4z} \end{Bmatrix} \quad (3.7)$$

Diagonal vectors v_1 and v_2 can be written in terms of G_1, G_2, G_3 and G_4 .

$$v_1 = G_3 - G_1, \quad v_2 = G_2 - G_4 \quad (3.8)$$

Vectors i , j and k in the local x , y and z directions can then be written in terms of v_1 and v_2

$$i = v_1 + v_2, \quad j = v_1 - v_2, \quad k = i \times j \quad (3.9)$$

and their unit vectors i_0 , j_0 and k_0 can be shown as

$$i_0 = \frac{i}{|i|}, \quad j_0 = \frac{j}{|j|}, \quad k_0 = \frac{k}{|k|} \quad (3.10)$$

The axial component of the element stress σ_{ax} can be easily determined by calculating the stress at the profile axis, as shown in Figure 3.15.

Where the element has balanced material on either side of this axis, then σ_{ax} can be written as

$$\sigma_{ax} = \left(\frac{\sigma_b - \sigma_t}{z_t + z_b} \right) z_t + \sigma_t \quad (3.11)$$

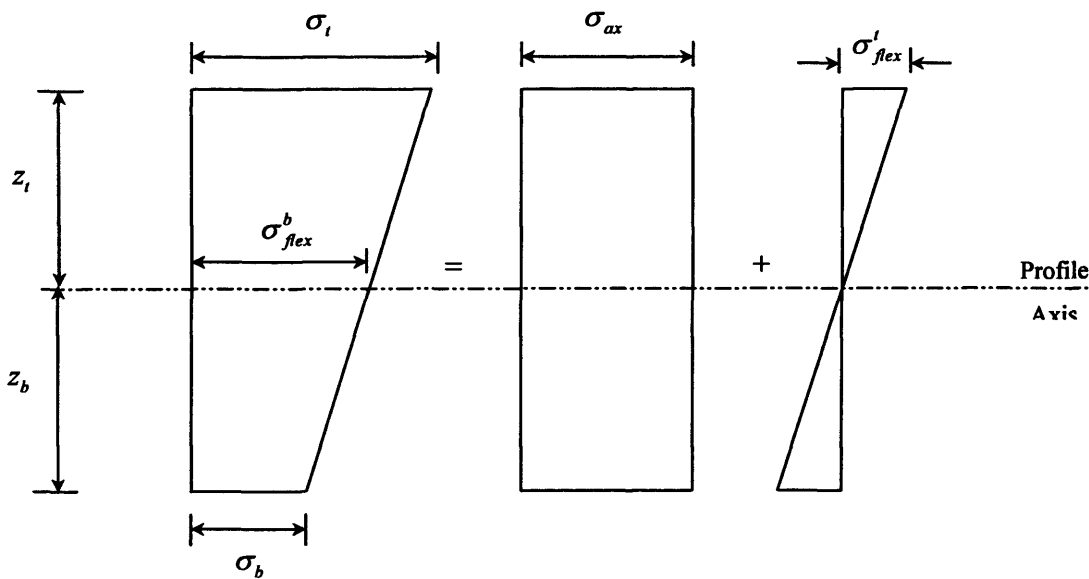


Figure 3.15 Typical element stress distributions.

where σ_t is the stress in the top surface of the element, σ_b is the stress on the bottom surface of the element, z_t is the distance between the top surface and the profile axis and z_b is the distance between the bottom surface and the profile axis. σ_t and σ_b are determined by MSC/NASTRAN as part of the results.

If the bending is about the mid-surface, i.e. $z_t = z_b$, then Equation 3.12 can be rearranged to give

$$\sigma_{ax} = \frac{\sigma_b + \sigma_t}{2} \quad (3.12)$$

Once the value of σ_{ax} is calculated, the axial force per unit width can be approximated as

$$F_{el}^L = \sigma_{ax} t \quad (3.13)$$

where t is the thickness of the element. The values of the bending stresses at the top and bottom surfaces of the element, σ_{flex}^t and σ_{flex}^b , can be calculated as

$$\sigma_{flex}^t = \sigma_t - \sigma_{ax}, \quad \sigma_{flex}^b = \sigma_b - \sigma_{ax} \quad (3.14)$$

The bending moment per unit length acting on the element can be calculated as

$$M_{el}^L = \frac{\sigma_{flex}^t z_t^2 + \sigma_{flex}^b z_b^2}{3} \quad (3.15)$$

If $z_t = z_b$, Equation 3.16 can be rearranged to give

$$M_{el}^L = \frac{\sigma_{flex} t^2}{6} \quad (3.16)$$

From Equation 3.14, the axial forces per unit width in the local x direction FX_{el}^L and in the local y direction FY_{el}^L , and the bending moments per unit length in the local x direction MX_{el}^L and in the local y direction MY_{el}^L can be calculated.

As described at beginning of this section, the type of element used in this research is QUAD4 which is a rectangular element. The total forces $FX_{el}^L|_{total}$ and $FY_{el}^L|_{total}$ and bending moments $MX_{el}^L|_{total}$ and $MY_{el}^L|_{total}$ acting on each of these elements can be calculated as

$$\left. \begin{aligned} FX_{el}^L|_{total} &= FX_{el}^L \ell_{el}, & FY_{el}^L|_{total} &= FY_{el}^L b_{el} \\ MX_{el}^L|_{total} &= MX_{el}^L \ell_{el}, & MY_{el}^L|_{total} &= MY_{el}^L b_{el} \end{aligned} \right\} \quad (3.17)$$

where ℓ_{el} is the length of the element and b_{el} is the width of the element where

$$\ell_{el} = |G_2 - G_1|, \quad b_{el} = |G_4 - G_1| \quad (3.18)$$

The total axial forces acting on the element in the global system $FX_{el}^G|_{total}$ and $FY_{el}^G|_{total}$ and the total bending moments acting on the element in the global system $MX_{el}^G|_{total}$ and $MY_{el}^G|_{total}$ can be calculated as

$$\left. \begin{aligned} FX_{el}^G|_{total} &= |i_{0x}| FX_{el}^L|_{total} + |j_{0x}| FY_{el}^L|_{total} \\ FY_{el}^G|_{total} &= |i_{0y}| FX_{el}^L|_{total} + |j_{0y}| FY_{el}^L|_{total} \\ MX_{el}^G|_{total} &= |i_{0x}| MX_{el}^L|_{total} + |j_{0x}| MY_{el}^L|_{total} \\ MY_{el}^G|_{total} &= |i_{0y}| MX_{el}^L|_{total} + |j_{0y}| MY_{el}^L|_{total} \end{aligned} \right\} \quad (3.19)$$

where i_{0x} , i_{0y} , j_{0x} and j_{0y} are the components of i_0 and j_0 in the x and y directions separately. Absolute values are used for the components of i_0 and j_0 , due to the signs of the element forces not being consistent with the coordinate system, but simply reflecting whether an element goes into compression or into tension as shown in Figures 3.12 and 3.13. Therefore, the base vector may cause unwanted sign changes when transforming data from one coordinate system into the other.

The panel's total longitudinal load FX_{panel} and bending moment MY_{panel} which are used for the VICONOPT optimisation can be calculated as

$$FX_{panel} = \frac{\sum_{panel} FX_{el}^G \Big|_{total}}{N_{elx}}, \quad MY_{panel} = \frac{\sum_{panel} MY_{el}^G \Big|_{total}}{N_{elx}} \quad (3.20)$$

where N_{elx} is the total number of elements along the length of the panel.

Besides the calculation of the longitudinal load and the bending moment, the shear forces acting on the panel's component plates are also determined by VICONOPT MLO. The shear force acting on each element FXY_{el} can be calculated as

$$FXY_{el} = \left(\frac{\sigma_{xy_{el}}^t + \sigma_{xy_{el}}^b}{2} \right) \times t \quad (3.21)$$

where $\sigma_{xy_{el}}^t$ is the shear stress on the top surface of the element and $\sigma_{xy_{el}}^b$ is the shear stress on the bottom surface of the element.

The shear and transverse stress resultants for the component plates (FXY_{plate} and FY_{plate}) in the panel are then given by

$$FXY_{plate} = \frac{\sum FXY_{el}}{N_{elp}}, \quad FY_{plate} = \frac{\sum FY_{el}^G}{N_{elp}} \quad (3.22)$$

where N_{elp} is the total number of elements per plate and the axial forces per unit width in the global x direction are $FX_{el}^G = |i_{0x}| \times FX_{el}^L + |j_{0x}| \times FY_{el}^L$.

The calculation of the stress resultants described above assumes that all elements have the same length. Otherwise, a weighted average needs to be determined.

If more than one load case is defined in the MSC/NASTRAN model, the Change Set facility of VICONOPT can be used to run the problem consecutively with very concise additions to the data of the default loading problem, and a set of Reset data may also be involved to give different variables to each load case (Williams *et al.*, 1996).

The load transfer process described in this section needs to be repeated every time a new multilevel optimisation cycle is entered, as shown in Figure 3.9. After the VICONOPT optimisation, the design changes carried out by VICONOPT also affect the load carrying capacity of the overall structure at the system level, i.e. stress redistributions will occur.

Chapter 4

VICONOPT MLOP (Multilevel Optimisation with Postbuckling): Theory

4.1 INTRODUCTION

This chapter introduces the newly developed version of VICONOPT MLO, VICONOPT MLOP (Multilevel Optimisation with Postbuckling) which allows individual panels to buckle before the design load is reached (Qu *et al.*, 2008). These panels continue to carry load with differing levels of reduced stiffness (Anderson and Kennedy, 2008). VICONOPT MLOP creates new MSC/NASTRAN data files based on this reduced stiffness data and iterates to converge on an appropriate load redistribution. Once obtained, this load distribution is used as a starting point in the optimisation of the constituent panels as previously described in Section 3.3.1. The extended multilevel optimisation framework flowchart of Figure 3.9 is shown in Figure 4.1. The blue lines show the new developed optimisation process which links VICONOPT and MSC/NASTRAN data files (shown in boxes) to include the postbuckling effect. All the new theories investigated for the development are described in this chapter. The new optimisation process will be introduced briefly in the following paragraphs and described in detail in Chapter 5.

The new part of the optimisation process, starting with the NASTRAN results and following the blue lines, is referred to as the analysis cycle. The sequence of analysis cycles culminating in convergence of the stress distributions, together with the following VICONOPT design runs and the subsequent finite element analysis for the new geometry, is called the design cycle. The rest of this chapter describes the developments made to the analysis and design procedures.

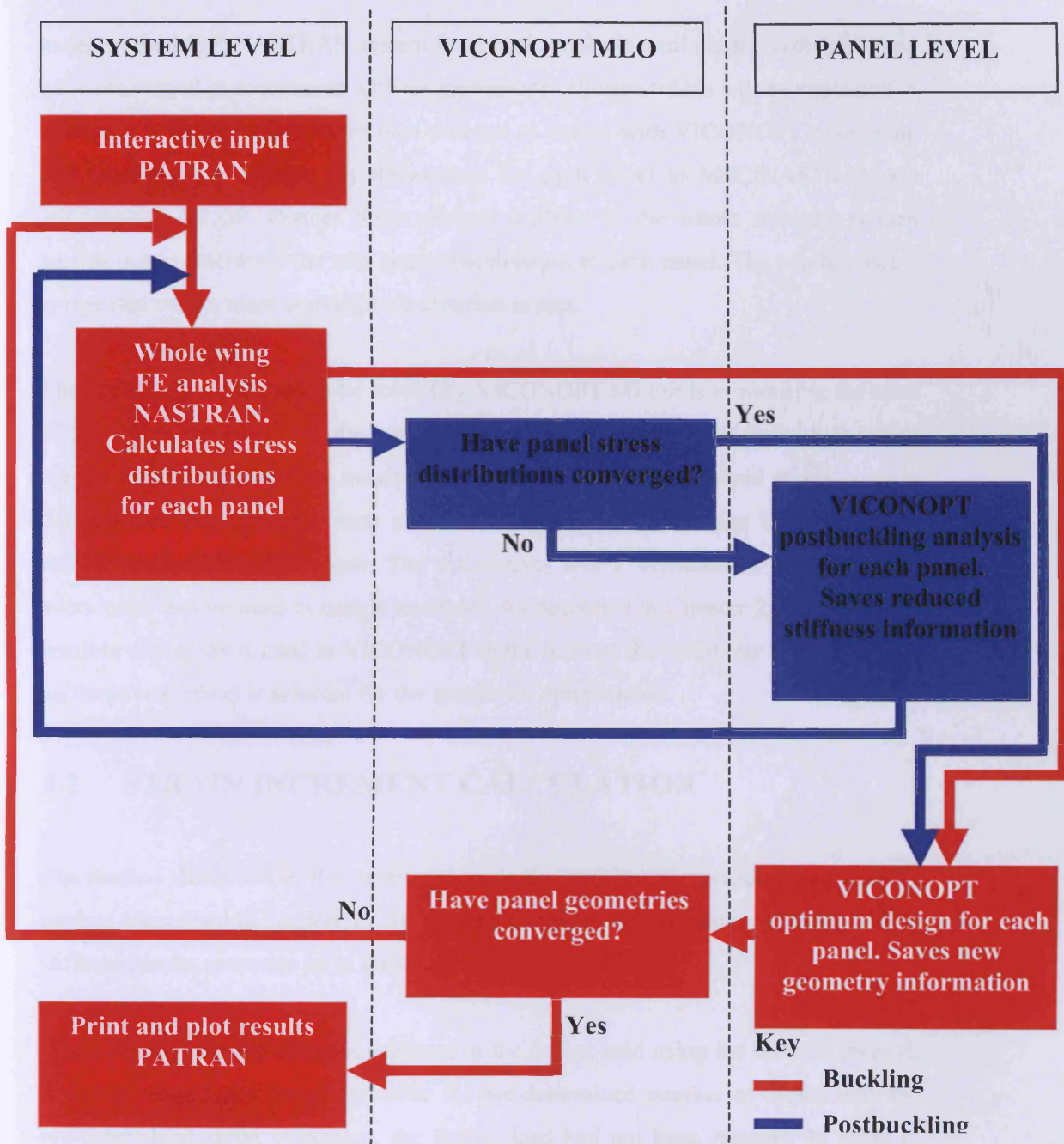


Figure 4.1 Multi-level framework for postbuckling design

Prior to each panel level optimisation step, a VICONOPT postbuckling analysis is performed on the panel to determine the postbuckling stress distribution and the reduced stiffness of each of its component plates. These values are then used during the optimisation step, but it is important to note that they also affect the load carrying capacity of the postbuckled panel relative to the other panels. It is therefore necessary

to repeat the MSC/NASTRAN system level static analysis until the stress distributions have converged in accordance with an appropriate criterion which will be explained in Section 4.3. Panel optimisations then proceed as before with VICONOPT calculating and returning the updated ply thicknesses for each panel to MSC/NASTRAN via VICONOPT MLOP. Further finite element analysis of the whole structure is then carried out to determine the new stress distributions in each panel. The whole process is repeated until a mass convergence criterion is met.

The optimisation problem to be solved by VICONOPT MLOP is minimising the mass of the whole structure, i.e. the sum of the masses of each of the individual panels subject to constraints on the maximum stresses that can be developed at any point in the structure and allowing each panel to buckle below the design load and hence exhibit postbuckling behaviour. The thicknesses and/or orientations of each ply of every plate can be used as design variables. As described in Chapter 2, the method of feasible directions is used in VICONOPT in the form of the optimizer CONMIN, and an iterative method is selected for the multilevel optimisation.

4.2 STRAIN INCREMENT CALCULATION

The method described in this section extends the VICONOPT postbuckling analysis method (described in Section 3.2.3), in order to ensure the calculation of postbuckling stiffness results proceeds up to the design load.

When determining the effective stiffness at the design load using the Newton method, it was in some cases found that after the pre-determined number of cycles with the pre-determined strain increment, the design load had not been reached. In order to correct this, a new strategy has been developed to adjust the strain increment ε_{inc} in each cycle to an appropriate value. The pre-determined strain increment is only used after the first cycle, to calculate the new strain ε_2 for the second cycle. Thereafter, the strain increment is calculated after each cycle by

$$\varepsilon_{inc} = \frac{\varepsilon_{design} - \varepsilon_i}{n - i} \quad (4.1)$$

where ϵ_{design} is the strain at design load, ϵ_i is the strain at cycle i and n is the pre-determined number of cycles. Ideally the strain at the last cycle ϵ_n is slightly above ϵ_{design} , to ensure the value of ϵ_{design} is reached during the analysis (Figure 4.2).

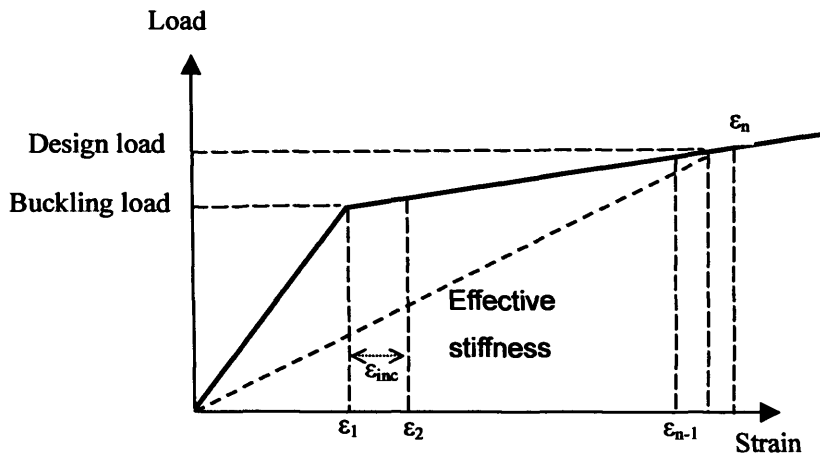


Figure 4.2 Calculation of strain increment.

4.3 REDUCED STIFFNESS RATIO

The reduced stiffnesses of each panel's component plates are calculated by multiplying the original stiffnesses by reduction factors called reduced stiffness ratios.

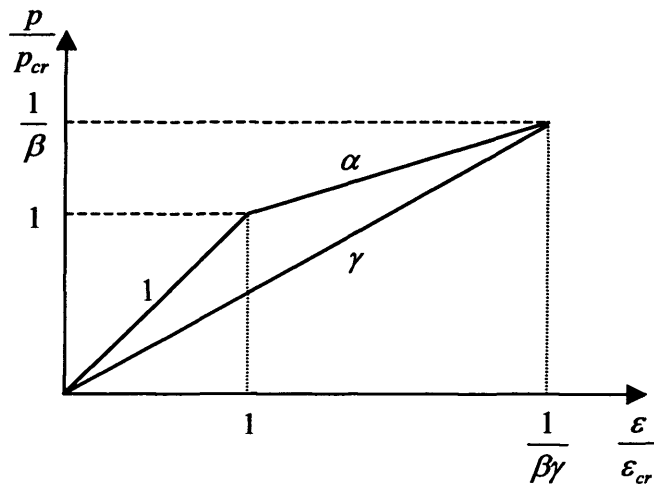


Figure 4.3 Plot of load against end shortening for a panel

The calculation of the reduced stiffness ratio for each plate is carried out by VICONOPT MLOP based on information passed from the VICONOPT postbuckling analysis, which includes: β , the value of the panel's critical buckling load relative to the design load; α , the average postbuckling to prebuckling stiffness ratio for the panel; γ , the overall reduced stiffness ratio for the panel (estimated at the design load) and α_x , the postbuckling to prebuckling stiffness ratio for plate x .

Figure 4.3 shows the load versus end shortening plot for a panel during both prebuckling and postbuckling, where ε is the end shortening strain due to the applied design load p and ε_{cr} is the end shortening strain at the critical buckling load p_{cr} .

At the design load, it can be seen that:

$$\frac{\varepsilon}{\varepsilon_{cr}} = \frac{1}{\beta\gamma} \quad (4.2)$$

As shown in Figure 4.4, for plate x , the ratio of the applied design load p_x to the critical buckling load p_{crx} is given by

$$\frac{p_x}{p_{crx}} = \frac{\varepsilon \cdot \gamma_x}{\varepsilon_{cr}} = \frac{\gamma_x}{\beta\gamma} \quad (4.3)$$

Also from Figure 4.4, the postbuckling to prebuckling stiffness ratio α_x can be written as

$$\alpha_x = \frac{\frac{\gamma_x}{\beta\gamma} - 1}{\frac{1}{\beta\gamma} - 1} = \frac{\gamma_x - \beta\gamma}{1 - \beta\gamma} \quad (4.4)$$

Solving for γ_x ,

$$\gamma_x = \alpha_x + (1 - \alpha_x) \cdot \beta \cdot \gamma \quad (4.5)$$

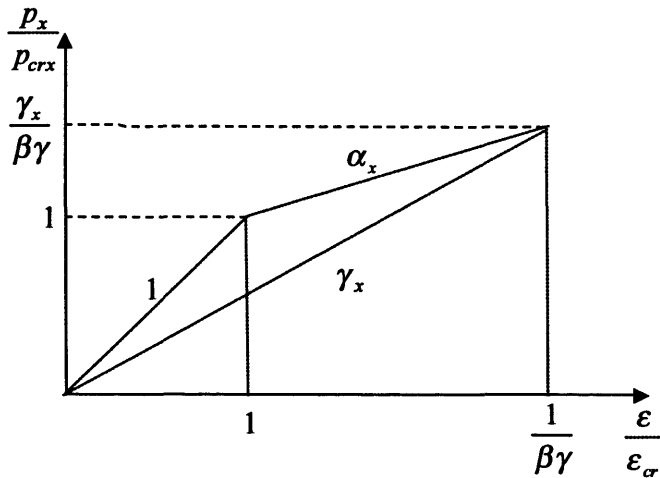


Figure 4.4 Plot of load against end shortening for a plate

For the plates which do not buckle, e.g. those loaded in tension, α_x is equal to 1. Equation 4.5 then gives $\gamma_x = 1$.

In real life problems, the prebuckling stiffness ratios are usually non-uniform and less than 1, due to imperfections, and the postbuckling to prebuckling tangent stiffness ratios α_x are non-uniform. However, in the research presented here, the design calculations merely require the secant stiffness ratios γ_x at the design load (which is determined separately by MSC/NASTRAN). Details of the path taken to reach the design load are not taken into account in the optimisation, and so the results obtained by the approach described here is considered as accurate and safe to be used in practice.

4.4 PLATES WITH NEGATIVE REDUCED STIFFNESS

During a postbuckling analysis, some panels contain plates which experience tension, due to large out-of-plane deflection. These plates will have negative reduced stiffness ratios γ_x as shown in Figure 4.5, which are not recognised by MSC/NASTRAN.

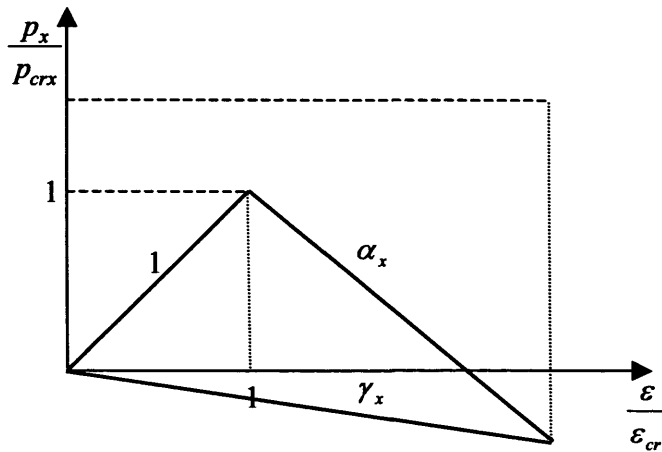


Figure 4.5 Load against end shortening for a plate with negative stiffness ratio.

In these cases, the value of design loading $p_{designx}$ for each plate x is assumed to comprise a compressive element plus a tensile one as shown in Figure 4.6, which is expressed by the formula

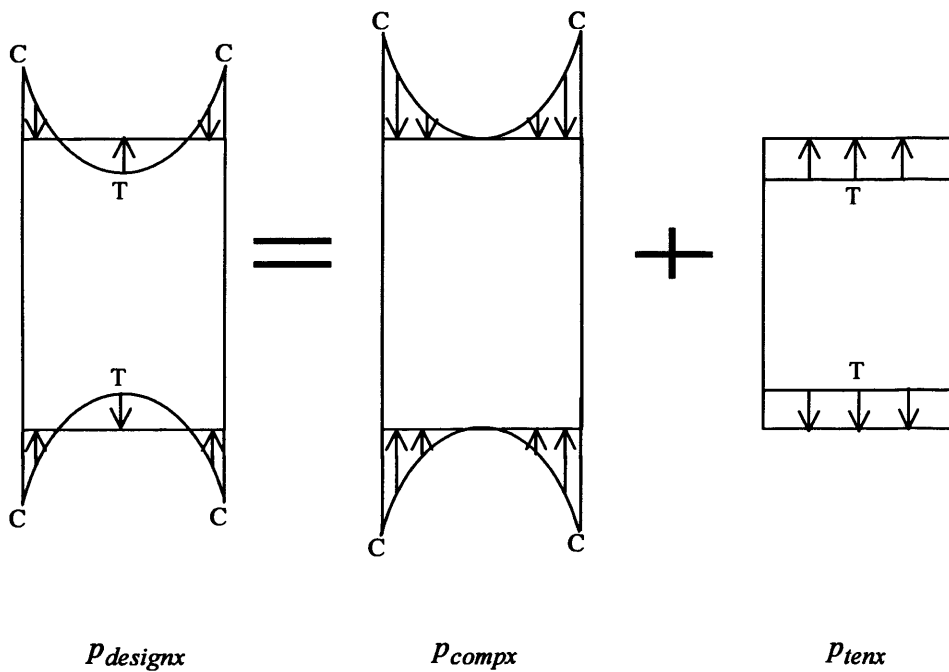


Figure 4.6 Schematic load distributions across a panel.

$$P_{designx} = P_{comp} + P_{tenx} \quad (4.6)$$

where P_{comp} is the assumed compressive load and P_{tenx} is the assumed tensile load.

Theoretically, an extra pre-buckling stiffness δ^* is first applied to all plates to ensure they are under compression as shown in Figure 4.7, i.e. point Q replaces point R after postbuckling.

Therefore, in Figure 4.7, \overline{OP} denotes the prebuckling path, \overline{PQ} denotes the postbuckling path and \overline{QR} denotes the necessary adjustment under tensile loading, which is made separately. This gives

$$\frac{P_{comp}}{P_{crx}} = \frac{\gamma_x}{\beta\gamma} + \delta^* \geq 0 \quad (4.7)$$

and theoretically always has

$$\frac{P_{designx}}{P_{crx}} = \frac{\gamma_x}{\beta\gamma} \quad (4.8)$$

In order to meet the condition of Equation 4.7 for all plates, the most negative reduced stiffness ratio $\gamma^* = \min_x \gamma_x$ for the whole wing is used to select δ^* , giving

$$\delta^* = -\frac{\gamma^*}{\beta\gamma} \quad (\geq 0) \quad (4.9)$$

The effective non-negative reduced stiffness ratios γ_{comp} for each plate is then given by

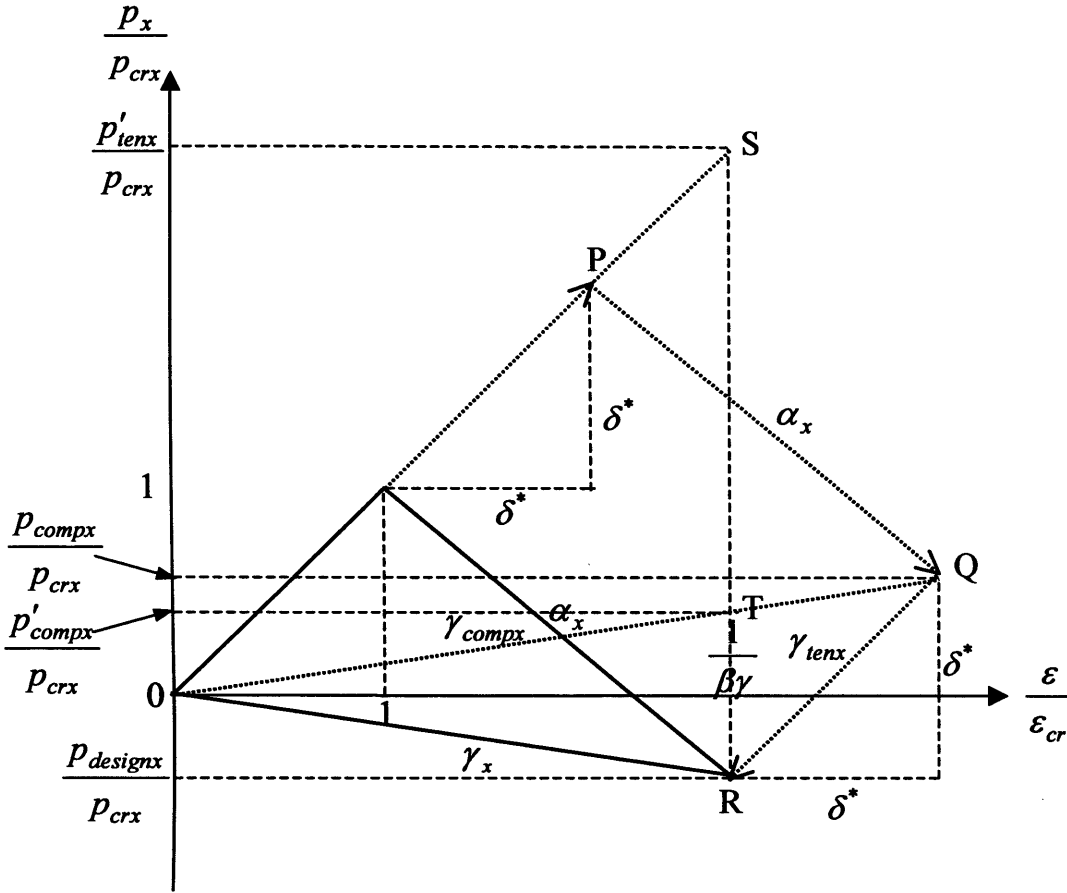


Figure 4.7 Theoretical calculation for a plate with negative stiffness ratio.

$$\gamma_{comp} = \frac{\frac{p_{comp}}{p_{crx}}}{\frac{\varepsilon}{\varepsilon_{cr}} + \delta^*} = \frac{\gamma_x + \left(\frac{-\gamma^*}{\beta\gamma}\right)}{\frac{1}{\beta\gamma} + \left(\frac{-\gamma^*}{\beta\gamma}\right)} = \frac{\gamma_x - \gamma^*}{1 - \gamma^*} \quad (4.10)$$

Substituting Equation 4.9 into Equation 4.7 gives

$$\frac{p_{comp}}{p_{crx}} = \frac{\gamma_x}{\beta\gamma} - \frac{\gamma^*}{\beta\gamma} \quad (4.11)$$

which using Equation 4.8, gives

$$p_{comp} = p_{design} \left(1 - \frac{\gamma^*}{\gamma_x}\right) \quad (4.12)$$

When superposing the assumed tension, the effective stiffness ratio used is

$$\gamma_{tenx} = 1 \quad (4.13)$$

The assumed tension p_{tenx} is applied, in order to remove the extra stiffnesses, resulting in

$$\frac{p_{tenx}}{p_{crx}} = -\delta^* = \frac{\gamma^*}{\beta\gamma} \quad (4.18)$$

which using Equation 4.8, gives

$$p_{tenx} = p_{designx} \left(\frac{\gamma^*}{\gamma_x} \right) \quad (4.19)$$

MSC/NASTRAN is called twice to find the true design load $p_{designx}$ for VICONOPT, once for compression and once for tension.

The first time MSC/NASTRAN is called, the most negative reduced stiffness ratio for the whole wing $\gamma^* = \min_x \gamma_x$ is determined and the MSC/NASTRAN input file is created using the effective non-negative reduced stiffness ratios γ_{comp} for each plate, given by Equation 4.10. The applied compressive load p'_{comp} calculated by MSC/NASTRAN is given by the point T in Figure 4.7, which corresponds to a normalised strain of $\frac{1}{\beta\gamma}$ and reduced stiffness ratio γ_{comp} . This is expressed by

$$\frac{p'_{comp}}{p_{crx}} = \frac{\gamma_{comp}}{\beta\gamma} = \frac{\gamma_x - \gamma^*}{1 - \gamma^*} \quad (4.20)$$

Substituting Equation 4.8 into Equation 4.20 gives

$$p'_{comp} = p_{design} \frac{\gamma_x - \gamma^*}{(1 - \gamma^*)\gamma_x} \quad (4.21)$$

Then, from Equations 4.12 and 4.21, it can be seen that

$$p_{comp} = p'_{comp}(1 - \gamma^*) \quad (4.22)$$

i.e. the requirement that the compressive loads p'_{comp} calculated by MSC/NASTRAN are all multiplied by the positive factor $(1 - \gamma^*)$.

MSC/NASTRAN is now called for a second time, with effective reduced stiffness ratios for each plate given by $\gamma_{ten} = 1$, giving an applied tensile load p'_{ten} as shown by the point S in Figure 4.7, which also corresponds to a normalised strain of $\frac{1}{\beta\gamma}$.

This is expressed by

$$\frac{p'_{ten}}{p_{cr}} = \frac{\gamma_{ten}}{\beta\gamma} = \frac{1}{\beta\gamma} \quad (4.23)$$

Substituting Equation 4.8 into Equation 4.23 gives

$$p'_{ten} = \frac{p_{design}}{\gamma_x} \quad (4.24)$$

Then, from Equations 4.19 and 4.24, it can be seen that

$$p_{ten} = p'_{ten}\gamma^* \quad (4.25)$$

i.e. the compressive loads p'_{ten} calculated by MSC/NASTRAN are all scaled by the negative factor γ^* to give tensile loads.

Finally, the load calculations from Equations 4.22 and 4.25 are substituted into Equation 4.6 to determine the real applied design load $p_{designx}$ for VICONOPT. VICONOPT MLOP carries out this whole process automatically if any negative stiffnesses are found.

In practical terms, MSC/NASTRAN not only has difficulty in considering negative stiffnesses, but also zero stiffnesses. In order to avoid zero stiffnesses, values of δ^* are always taken to be slightly larger than those calculated from Equation 4.9.

In order to prove the accuracy of the method described above, an example of a simple panel is given. The panel contains three plates of uniform thickness which have the known variables as shown in Table 4.1. The panel has critical buckling load p_{cr} and overall reduced stiffness ratio γ .

Plate number	1	2	3
Reduced stiffness ratio	-0.4	-0.1	0.8
Width	1	3	2

Table 4.1 The variables of a simple panel.

From the given variables, it is easy to calculate the total design load of the panel by hand, which is

$$p_{design} = ((-0.4 \times 1) + ((-0.1) \times 3) + (0.8 \times 2))X = 0.9X \quad (4.26)$$

where $X = \frac{p_{cr}}{\beta\gamma}$.

Then, calculating the total design load using the method described above, Table 4.1 gives

$$\gamma^* = -0.4 \quad (4.27)$$

By applying Equation 4.10, the effective non-negative reduced stiffness ratios are given by

$$\left. \begin{aligned} \gamma_{comp1} &= \frac{-0.4 - (-0.4)}{1 - (-0.4)} = 0 \\ \gamma_{comp2} &= \frac{-0.1 - (-0.4)}{1 - (-0.4)} = \frac{3}{14} \\ \gamma_{comp3} &= \frac{0.8 - (-0.4)}{1 - (-0.4)} = \frac{6}{7} \end{aligned} \right\} \quad (4.28)$$

Therefore, the applied compressive loads are

$$\left. \begin{aligned} p'_{comp1} &= (0 \times 1)X = 0X \\ p'_{comp2} &= \left(\frac{3}{14} \times 3\right)X = \frac{9}{14}X \\ p'_{comp3} &= \left(\frac{6}{7} \times 2\right)X = \frac{12}{7}X \end{aligned} \right\} \quad (4.29)$$

Substituting Equation 4.29 into Equation 4.22 gives

$$\left. \begin{aligned} p_{comp1} &= (1 - (-0.4)) \times 0X = 0X \\ p_{comp2} &= (1 - (-0.4)) \times \frac{9}{14}X = 0.9X \\ p_{comp3} &= (1 - (-0.4)) \times \frac{12}{7}X = 2.4X \end{aligned} \right\} \quad (4.30)$$

The total assumed compressive load of the panel is then

$$p_{comp} = 0X + 0.9X + 2.4X = 3.3X \quad (4.31)$$

Because the assumed tension stiffness ratios are all equal to 1, the applied tensile loads are

$$\left. \begin{aligned} p'_{ten1} &= (1 \times 1)X = X \\ p'_{ten2} &= (1 \times 3)X = 3X \\ p'_{ten3} &= (1 \times 2)X = 2X \end{aligned} \right\} \quad (4.32)$$

Substituting Equation 4.32 into Equation 4.25 gives

$$\left. \begin{aligned} p_{ten1} &= (-0.4) \times X = -0.4X \\ p_{ten2} &= (-0.4) \times 3X = -1.2X \\ p_{ten3} &= (-0.4) \times 2X = -0.8X \end{aligned} \right\} \quad (4.33)$$

Then, the total assumed tensile load of the panel is

$$p_{ten} = -0.4X - 1.2X - 0.8X = -2.4X \quad (4.34)$$

The total design load of the panel calculated by adding Equations 4.31 and 4.34 together is

$$p_{design} = 3.3X - 2.4X = 0.9X \quad (4.35)$$

The result calculated by applying the method described above (Equation 4.35) is the same as the results calculated by hand (Equation 4.26). It is thus shown that this method as used in VICONOPT MLOP is accurate.

4.5 LOAD CONVERGENCE

For each analysis cycle in a design cycle after the first one, the VICONOPT postbuckling analysis is followed by a load convergence check.

For panel s in analysis cycle a , the load in a particular panel is $p_{s,a}^*$. The largest initial panel load within the current design cycle will be recorded as $p_{s,0}^*$. The load in the whole model will be considered as converged, only if the load in each single panel meets the criterion

$$\left| \frac{p_{s,a}^* - p_{s,a-1}^*}{p_{s,0}^*} \right| \leq \eta \quad (4.36)$$

where η is the convergence criterion. The number of analysis cycles performed is strongly affected by the convergence criterion η . In VICONOPT MLOP, η is either defined by the user or a default value 0.01 is used; more information on η will be given in Chapter 5. For the case study described in Chapter 6, the convergence criterion η takes the default value 0.01.

In a multilevel postbuckling optimisation problem, each panel may take more than one type of loading, e.g. axial load, bending moment, shear load, etc. Each of these will have their own largest initial panel load $p_{s,0}^*$. The load of the panel will be considered as converged, only if each type of load in this panel meets the criterion.

Once the load changes between two subsequent analysis cycles satisfy the convergence criterion, the postbuckling analysis process for the current design cycle is complete.

4.6 MASS CONVERGENCE

In contrast to the load convergence, a mass convergence check is carried out for each VICONOPT design run even if it is the first one. This is because the panel mass will change after every VICONOPT design run. The values of initial and final mass of each panel for the current completed design cycle can be easily found in the VICONOPT results files which will be described in Chapter 5.

Two different mass convergence checks have been implemented in the new version of VICONOPT MLOP, a total mass convergence check and an individual mass convergence check. The individual mass convergence check is the default method, however, the user is able to switch to the total mass convergence check method if required. This will be covered in Chapter 5.

Assume the initial total mass of the whole structure is M_0 . In any design cycle d , the total mass of the structure is M_d , and the mass of panel s is $m_{s,d}$.

For the total mass convergence check, the mass will be considered as converged if

$$\left| \frac{M_d - M_{d-1}}{M_0} \right| \leq \eta \quad (4.37)$$

where η is the convergence criterion, which is described in Chapter 4.3, and for the case study described in Chapter 6 takes the value 0.01.

For the individual mass convergence check, the initial mass of panel s will be recorded as $m_{s,0}$. The mass of the structure will be considered as converged, only if the mass of each single panel meets the criterion

$$\left| \frac{m_{s,d} - m_{s,d-1}}{m_{s,0}} \right| \leq \eta \quad (4.38)$$

Once the mass savings between two subsequent design cycles meet the convergence criterion, the whole multilevel postbuckling optimisation process is completed, and a final MSC/NASTRAN analysis is carried out in order to generate the final results files to be displayed in MSC/PATRAN. Otherwise, VICONOPT MLOP will start a new analysis cycle in a new design cycle with all the updated panel geometries from the VICONOPT design results, beginning with a new MSC/NASTRAN static analysis.

4.7 CONVERGENCE ACCELERATION

In order to increase efficiency and reduce computational cost in VICONOPT MLOP, the loads calculated by MSC/NASTRAN are not used directly in VICONOPT. Instead load convergence acceleration takes place to calculate the loads to be used in the VICONOPT input files.

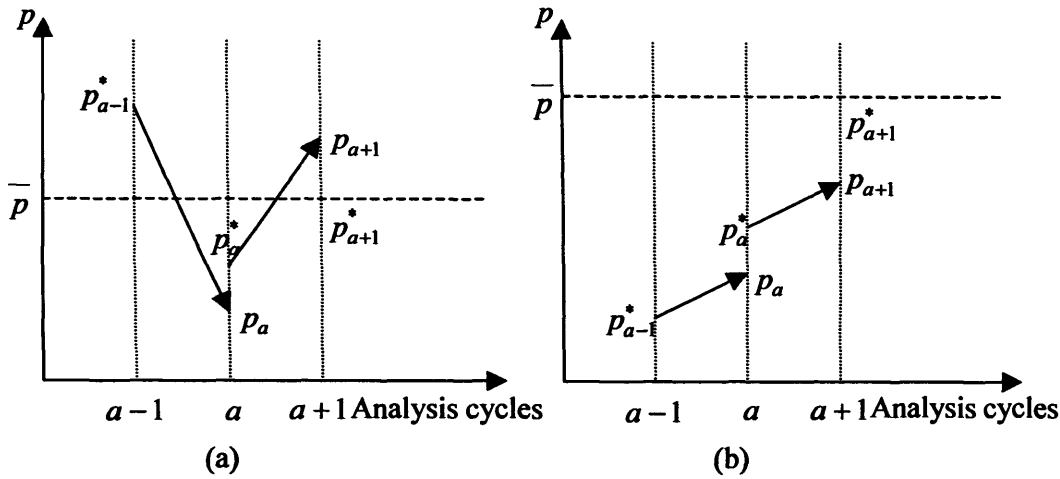


Figure 4.8 Load convergence acceleration, (a) oscillating convergence ($0 < \kappa < 1$) and (b) one-sided convergence ($\kappa > 1$).

Figure 4.8 shows two scenarios of oscillating and one-sided convergence. Suppose the load in a particular panel is p . In any analysis cycle a the starting load is p_{a-1}^* and the predicted load is p_a . The expected converged result is \bar{p} which is as yet unknown. Because the value of p_a will never be equal to \bar{p} , the analysis cycles still need to converge. Therefore, the value of p_a is used to estimate the value of \bar{p} at the end of the analysis cycle, as follows. Assume

$$\left(\bar{p} - p_{a-1}^* \right) = \kappa (p_a - p_{a-1}^*) \quad (4.39)$$

where κ is the ratio between the required step and the predicted step. For oscillating convergence $0 < \kappa < 1$ and for one-sided convergence $\kappa > 1$. It is assumed that κ will take the same value in the next cycle, so that

$$\left(\bar{p} - p_a^*\right) = \kappa(p_{a+1} - p_a^*) \quad (4.40)$$

Eliminating \bar{p} to solve for κ gives

$$\kappa = \frac{p_a^* - p_{a-1}^*}{p_a + p_a^* - p_{a-1}^* - p_{a+1}} \quad (4.41)$$

Then the prediction p_{a+1} is replaced by p_{a+1}^* , given by

$$p_{a+1}^* = p_a^* + \kappa(p_{a+1} - p_a^*) \quad (4.42)$$

In order to avoid numerical difficulties, if κ is less than 0.01 it is adjusted to 0.01; if κ is greater than 2 it is adjusted to 2.

This acceleration can only be used after two analysis cycles of each design cycle, because the calculation of κ requires two previous results. In other words, if the previous run is a design run, this acceleration will not be carried out.

Chapter 5

Multilevel Optimisation Procedure of VICONOPT MLOP

5.1 INTRODUCTION

This chapter describes in detail the operation of the interface program VICONOPT MLOP, and the data input required to generate VICONOPT models for each of the panels. A number of improvements to the process used in VICONOPT MLO have been made to increase usability, e.g. the use of defaults and the ability to save models during input. The procedures presented in this chapter are mainly based on the current development and the new software VICONOPT MLOP. However, a brief introduction is given on the previous functions where applicable, in order to integrate the procedures. More detailed information about the previous functions of VICONOPT MLO is given by Fischer (2002).

In order to speed up the data input process for a large model, such as a whole aircraft wing containing a large number of component panels, each of which requires input data such as postbuckling analysis parameters, stress and strain constraints and design variables, the Windows-based interface program VICONOPT MLOP incorporates a series of flash input buttons. These buttons, known as ‘Default Values’ buttons, have been developed to enable such data to be saved and reused for similar panels, thereby simplifying the manual input procedure.

A typical window of VICONOPT MLOP, containing these ‘Default Values’ buttons, is shown in Figure 5.1. Following specification of the model parameters for one of the panels, the user can save the input data for later use by clicking the ‘Set Default Values’ button (Figure 5.1[1]). When the same parameters are required for another panel, the user can easily import them by clicking the ‘Use Default Values’ button (Figure 5.1[2]).

It should be noted that each time the user clicks the ‘Set Default Values’ button, the previously saved default values will be replaced. It is therefore convenient to specify the panels which require the same parameters consecutively, in order to minimize the manual input.

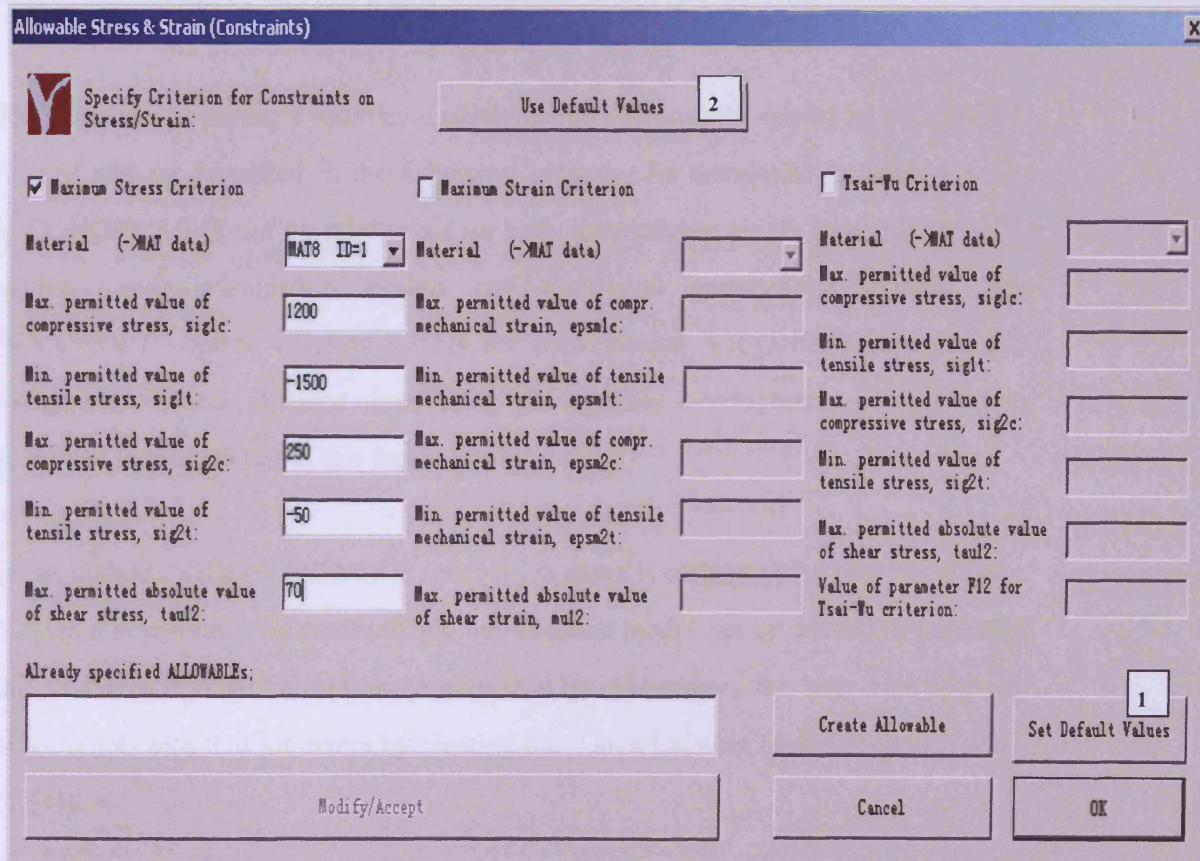


Figure 5.1 A typical window with ‘Default Values’ options.

Finally, in both academic and industrial situations, it may be necessary to optimise several times either with or without changes to the data. Allowing users to save their work and return to it at any time is therefore desirable. VICONOPT MLOP allows users to save their work at any stage of the design process to .MLO1 and .MLO2 files. The .MLO1 file stores information relating to the job in text format and the .MLO2 file is a binary system file. The user can access previous jobs by reloading these two files. More detailed information on the saving function in VICONOPT MLO will be given in Section 5.2.10.

5.2 POSTBUCKLING MODEL BUILDING PROCESS

5.2.1 General

The process of creating a multilevel postbuckling optimisation model in VICONOPT MLOP will be described in the following sections. As mentioned in Section 3.3.1, VICONOPT MLO can be used to set up both conventional single level VICONOPT analysis and optimisation models and multilevel optimisation models. The ‘VICONOPT’ option (Figure 5.2[2]) for conventional VICONOPT analysis and design has not been changed significantly during these developments, so will not be presented in great detail in this thesis.

In the updated VICONOPT MLOP, once a job name is defined in the text box (Figure 5.2[1]), a new multilevel postbuckling optimisation model can be created by selecting the ‘VICONOPT MLO’ option (Figure 5.2[3]). Otherwise, the user can open an existing job with that job name by clicking the ‘Open Existing Model’ button (Figure 5.2[4]).

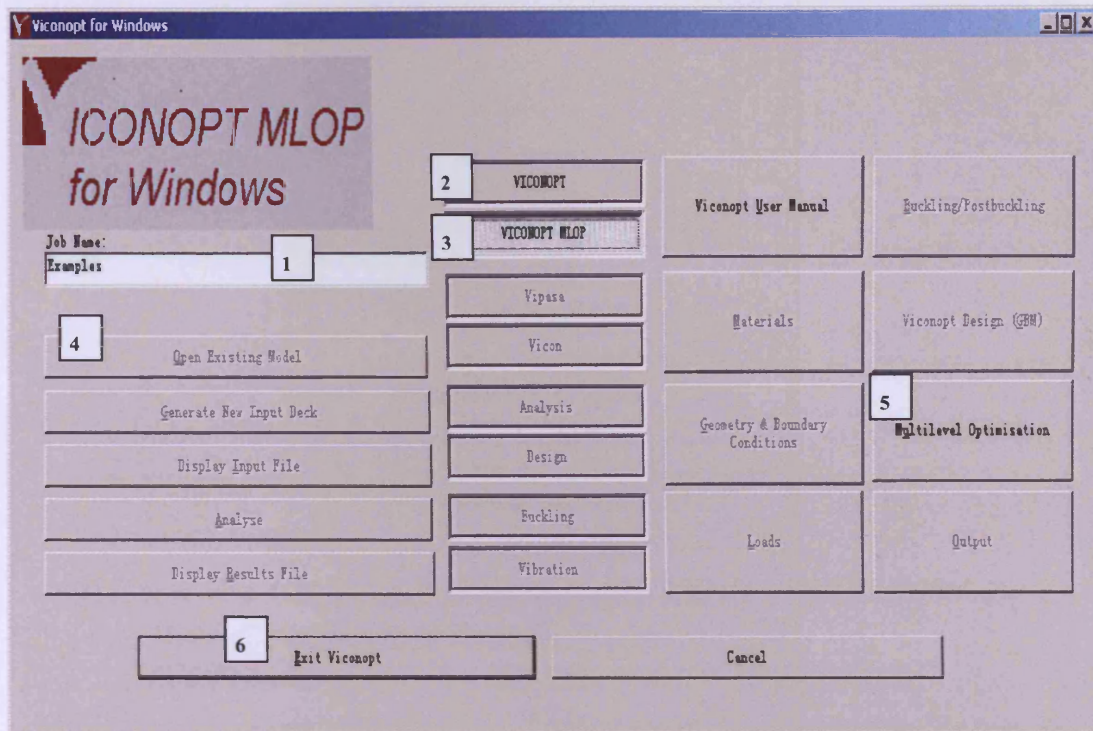


Figure 5.2 VICONOPT MLOP main window.

5.2.2 MSC/NASTRAN Model Translation

After selecting the ‘Multilevel Optimisation’ option in the VICONOPT MLOP main window (Figure 5.2[3]), the ‘MLO Process & Procedure’ window shown in Figure 5.3 will appear. The user can then specify the MSC/NASTRAN model by providing the name and location of the relevant .bdf file which is the input file for the MSC/NASTRAN analysis, or by using a previously saved default path (Figure 5.3[1]). The users can click the ‘Display NASTRAN File’ button (Figure 5.3[2]) to see the .bdf file in WordPad format or transfer all the relevant geometric and material information from the finite element model which is described in Section 3.3.2 to VICONOPT MLOP by selecting the ‘Translate NASTRAN File’ option (Figure 5.3[3]). VICONOPT MLOP then carries out this translation automatically.

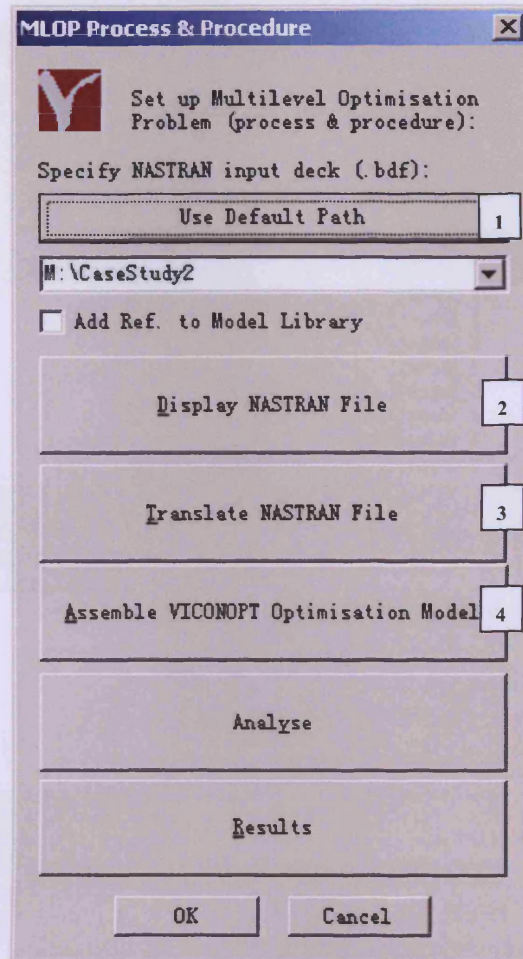


Figure 5.3 VICONOPT MLOP—MLOP Process & Procedure.

5.2.3 Assembly of Geometric Models

After the model properties have been translated successfully, the VICONOPT optimisation models can be assembled. Figure 5.4 shows the ‘Assemble VICONOPT Optimisation Model’ window (Figure 5.3[4]).

All the available MSC/NASTRAN groups are shown in the list box (Figure 5.4[1]). The user first needs to name the panel which will be assembled. This name will also be used as the name of the initial VICONOPT input and results files for this panel.

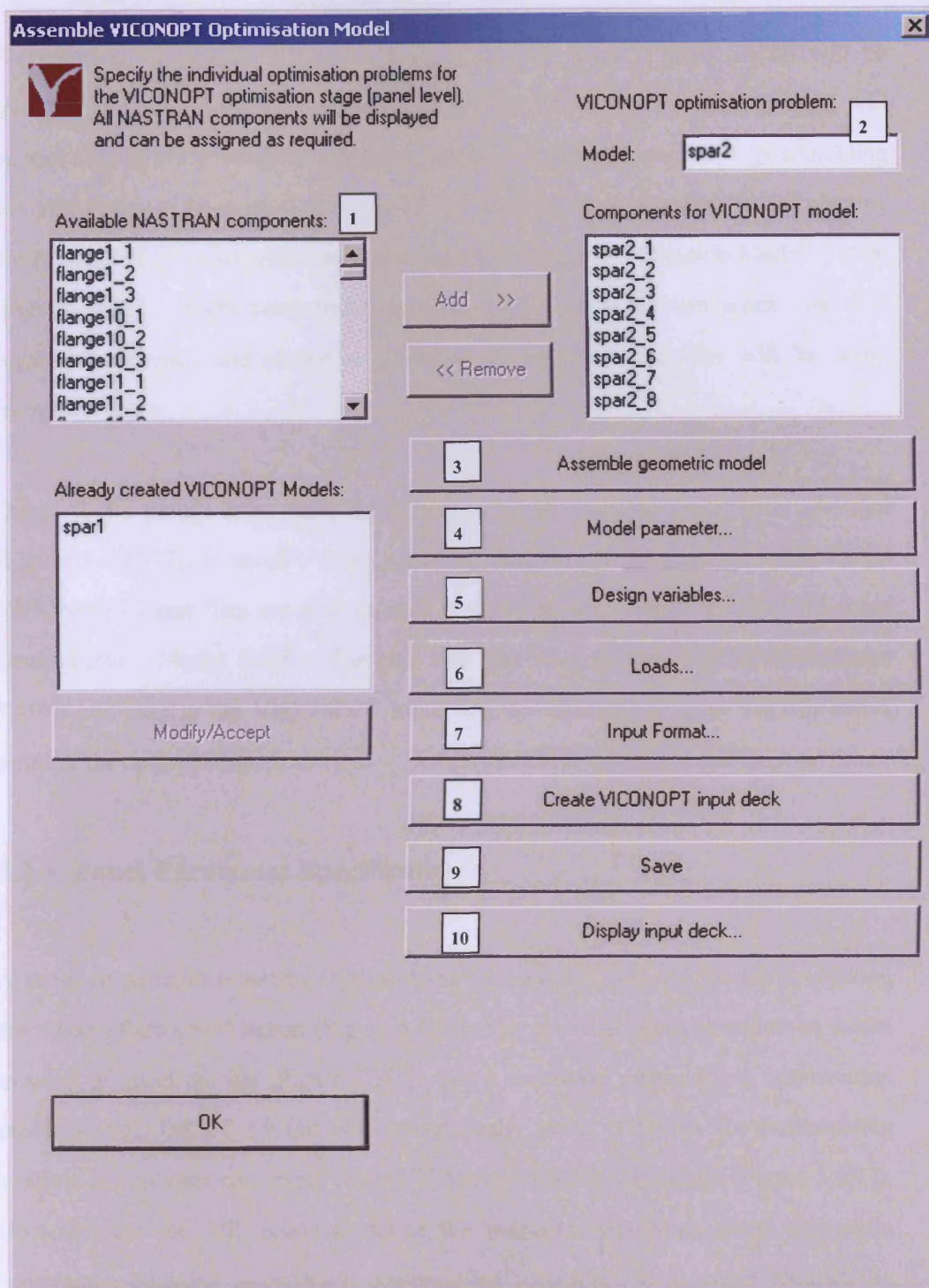


Figure 5.4 ‘Assemble VICONOPT Optimisation Model’ window

For example, the initial VICONOPT input file for spar2 (Figure 5.4[2]) will be spar2.dat and the results files produced by the VICONOPT analysis/design runs will be spar2.res (general results), spar2.u11 (design results) and spar2.u14 (postbuckling analysis results). After naming the panel, the user can then assemble it by selecting the relevant component plates and pressing the ‘Assemble Geometric Model’ button (Figure 5.4[3]). If the component elements of the finite element model are well organised, grouped and named as explained in Section 3.3.2, they will be easily recognised here.

Once all the panels have been assembled, the user can use the options provided (Figure 5.4[4]-[7]) to modify these panels as described in Section 5.2.4. The initial VICONOPT input files are then created by clicking the ‘Create VICONOPT Input Deck’ button (Figure 5.4[8]). The user can also save all the work to date (Figure 5.4[9]) and display the VICONOPT input files for checking (Figure 5.4[10]) before running the optimisation.

5.2.4 Panel Parameter Specification

A series of parameters need to be specified for each VICONOPT model by clicking the ‘Model Parameter’ button (Figure 5.4[4]). The user first needs to select the model to work on from the list (Figure 5.5[1]). For a multilevel postbuckling optimisation problem, VICONOPT MLOP will automatically select VIPASA for postbuckling analysis but the user can select either VIPASA or VICON for design (Figure 5.5[2]). However, the user still needs to define the boundary conditions, stress and strain constraints, buckling parameters, postbuckling parameters and output requests by pressing the buttons provided (Figure 5.5[3]-[7]).

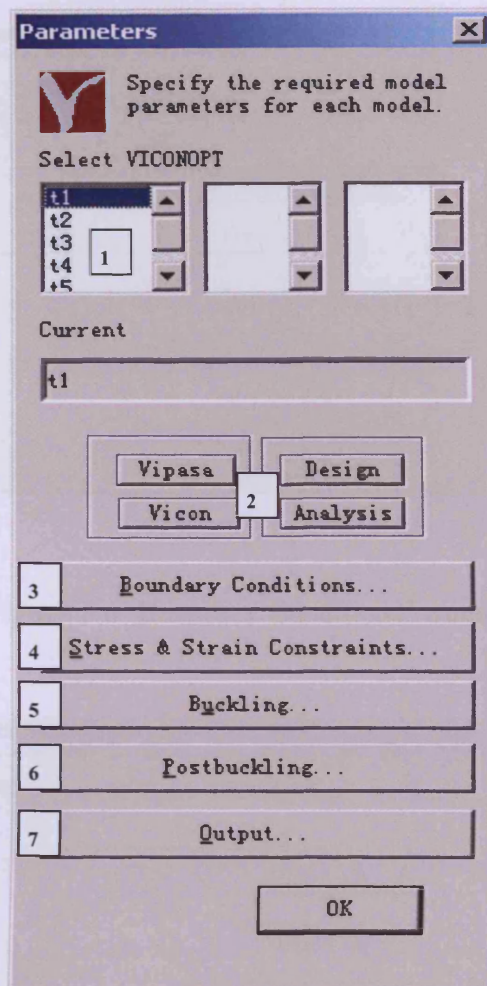


Figure 5.5 'Parameters' window.

5.2.4.1 Boundary Conditions

Several different types of boundary conditions are available in VICONOPT, e.g. longitudinal line supports, point supports, elastic Winkler foundations, and connections to supporting structures. However, in VICONOPT MLOP, the user can only use longitudinal line supports (Figure 5.6[1]) and point supports (Figure 5.6[2]), which are described in detail in the VICONOPT Users Manual (Williams *et al.*, 1996).

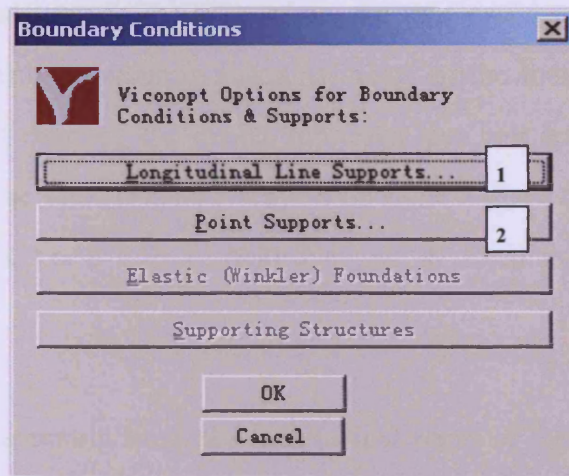


Figure 5.6 'Boundary Conditions' window.

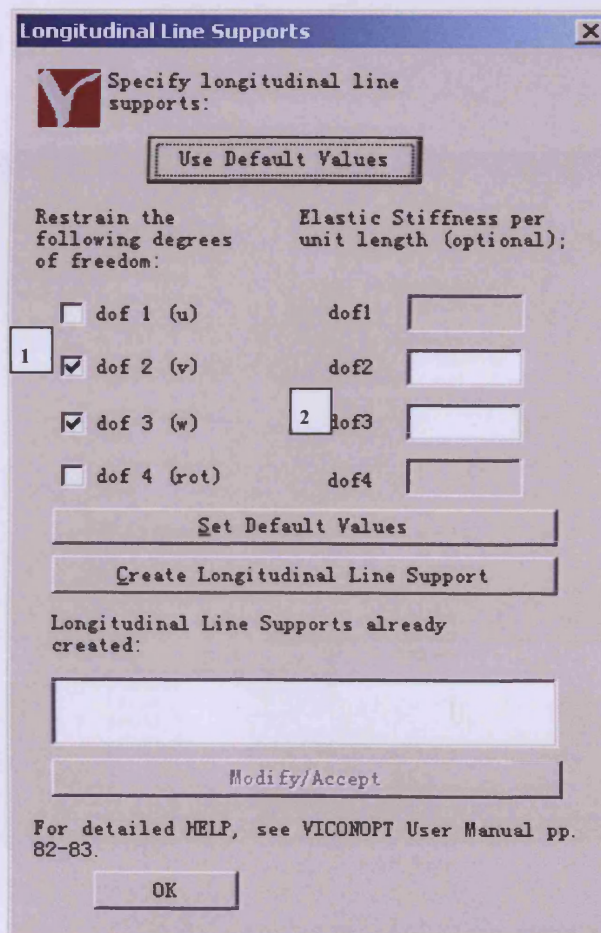


Figure 5.7 'Longitudinal Line Supports' window.

In the 'Longitudinal Line Supports' window, the user can restrain the longitudinal edges of each panel by combining restraints in any of the four degrees of freedom (Figure 5.7[1]) and defining the elastic stiffnesses per unit length for each of the degrees of freedom selected (Figure 5.7[2]). If no value is given for an elastic stiffness, an infinite stiffness, i.e. a fully restrained degree of freedom, will be applied by default.

In addition to line supports along the longitudinal edges of the panels, the user can also specify point supports at the ends of each plate (or elsewhere) by restraining any of the translational and rotational degrees of freedom and defining the elastic stiffnesses per unit length for each of the degrees of freedom selected (Figure 5.8[1]). In the same way as for the longitudinal line supports, a default of full restraint will be used if no value is given for an elastic stiffness.

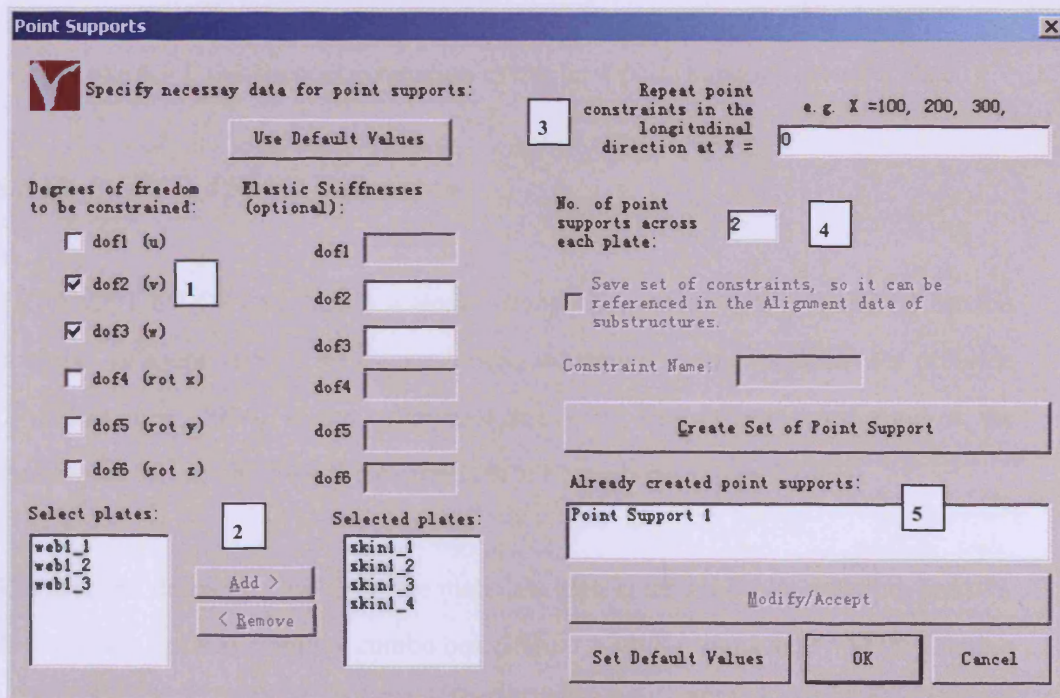


Figure 5.8 'Point Supports' window.

Each time a point support is created, the user needs to select those plates to which the supports are to be applied (Figure 5.8[2]) and define the repeat intervals along the longitudinal length (Figure 5.8[3]) which affect the panel in the way described in Section 3.2.1.2, as well as the number of point supports desired across each plate (Figure 5.8[4]) which will generate nodes automatically in the way shown in Figure 5.9.

Point supports will be shown in the ‘Already created point supports’ list box (Figure 5.8[5]) after creation.

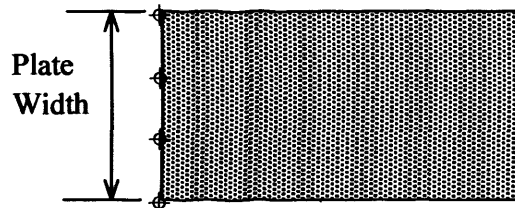


Figure 5.9 Point support generation example: 4-point supports across a plate.

5.2.4.2 Stress and Strain Constraints

VICONOPT MLOP can specify material strength constraints for VICONOPT models in three different forms; maximum stress, maximum strain, or Tsai-Wu criterion (Williams *et al.*, 1996). In the ‘Allowable Stress and Strain Constraints’ window, the user can select which of the three criteria is to be applied (Figure 5.10[1]).

The user can define the limits for the materials used in the model by selecting one of the available options from the combo box (Figure 5.10[2]), and specifying the limiting values of the stresses or strains. Stress/strain constraints will be shown in the ‘Already specified ALLOWABLES’ list box (Figure 5.10[3]) after creation.

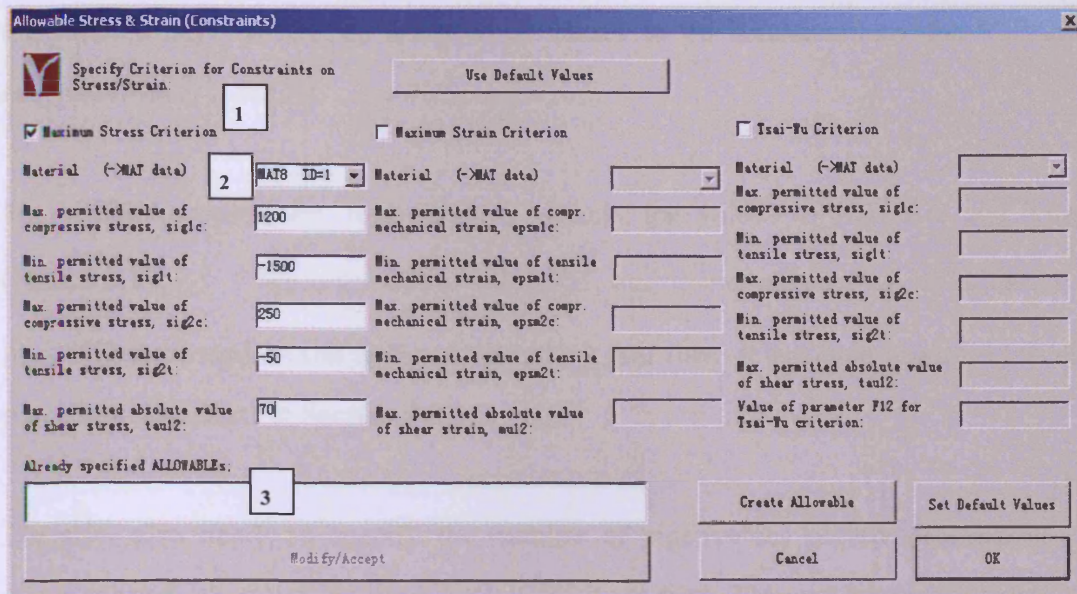


Figure 5.10 ‘Allowable Stress & Strain’ window.

5.2.4.3 Buckling Parameters

For multilevel postbuckling optimisation, the buckling parameters described in Section 3.2.1.2 for both VIPASA and VICON models have to be specified, since VICONOPT MLOP uses VIPASA for postbuckling analysis and VICON for design.

For VIPASA models, the axial half-wavelengths λ must be chosen by the user. There are three different input methods which can be used. The j -specification method (Figure 5.11[1]) defines a series of λ 's in terms of $\ell/j_1, \ell/j_2, \dots, \ell/j_n$, where ℓ is the overall length of the panel, and j_1 is the initial value of j , which is gradually incremented by j_{inc} until j_n is passed. j_1 , j_n and j_{inc} need to be specified by the user. The constant ratio method (Figure 5.11[2]) can be used to define the values of λ where successive values of λ are obtained by multiplying by the ratio r until the limit λ_2 has been passed, where λ_1 is the initial value of λ . Finally, the list method allows

the users simply to specify a list of λ values to be considered by the VIPASA analysis (Figure 5.11[3]).

For VICON models, the user needs to specify the values of ξ_1 , ξ_2 and ξ_{inc} (Figure 5.11[4]). ξ takes the initial value ξ_1 , and is incremented by ξ_{inc} until the limit ξ_2 is passed. Axial half-wavelengths λ are then determined according to the procedure described in Section 3.2.1.2.

The user also needs to specify the number of eigenvalues required (normally 1), which is used when writing the VICONOPT input files. This can be done by clicking on the appropriate number provided at the bottom of the ‘Buckling Parameters’ window (Figure 5.11 [5]).

Buckling Parameters

Specify wavelength data Use Default Values

VIPASA

J-Specification: Lambda & const. Ratio: List of lambda val

1 J1= 1 2 lambda1=

Jn= 10 lambda2= 3 3

Jinc= 1 r=

FAST 1

FAST 2 6

FAST 3

PFAST 1

PFAST 2 7

PFAST 3

Geometry

For detailed HELP, see pp.38-42 in VICONOPT USER MANUAL.

VICON 4

ξ_1 = 0 ξ_2 = 1 ξ_{inc} = 0.25

Specify number of eigenvalues required: 5

1 2 3 4 5 6

For detailed HELP, see pp.36 in VICONOPT USER MANUAL.

Create Wavelength Card Set Default Values

OK

Figure 5.11 ‘Buckling Parameters’ window.

If one of the ‘FAST’ options (Figure 5.11[6]) has been selected, a single line of input will be displayed in each of the VICONOPT input files to reduce the length of the overall computation. By selecting the ‘FAST 1’ option, VICONOPT will find the lowest eigenvalue for each value of λ in a VIPASA analysis, and for each value of ξ in a VICON analysis. By selecting the ‘FAST 2’ option, VICONOPT will find the lowest eigenvalue for each change set in the problem. By selecting the ‘FAST 3’ option, VICONOPT will find the lowest eigenvalue for the whole problem, i.e. the lowest over all the change sets. In a multilevel postbuckling optimisation, change sets are not used, so selection of either option ‘FAST 2’ or ‘FAST 3’ will have the same effect in VICONOPT. It is necessary to be aware that, in VICONOPT design problems, the ‘FAST’ options only affect the initial and final analyses, and have no effect on the intermediate eigenvalue calculations during the sizing process defined in Section 3.2.2.1.

In a similar way to the ‘FAST’ options, once any of the ‘PFAST’ options (Figure 5.11[7]) has been selected, a single line of input will be displayed in each of the VICONOPT input files to reduce the amount of printed and graphical output. By selecting the ‘PFAST 1’ option, VICONOPT will obtain and print or plot the mode of the lowest eigenvalue found for each value of λ in a VIPASA analysis, and for each value of ξ in a VICON analysis. By selecting the ‘PFAST 2’ option, VICONOPT will obtain and print or plot the mode of the lowest eigenvalue for each change set. By selecting the ‘PFAST 3’ option, VICONOPT will obtain and print or plot the mode of the lowest eigenvalue for the whole problem, i.e. the lowest for any change set. Both ‘PFAST 2’ and ‘PFAST 3’ options will have the same effect in multilevel postbuckling optimisation, because no change sets will be considered. It is also necessary to be aware that, in design problems, the ‘PFAST’ options only affect the final analysis, and have no effect on the initial analysis and intermediate eigenvalue calculations during the sizing process.

5.2.4.4 Postbuckling Parameters

For historical reasons, there are three different postbuckling analysis methods available for the user to choose, denoted the SMP method, the Newton method (Mel) and the Newton method (latest). The user can choose one of these methods by clicking on the relevant button provided in the ‘Postbuckling Methods’ window (Figure 5.12). The present work uses only the Newton method (latest), and so detailed descriptions of the other options have been omitted but details are given in Powell *et al.* (1998) and Anderson and Kennedy (2008).

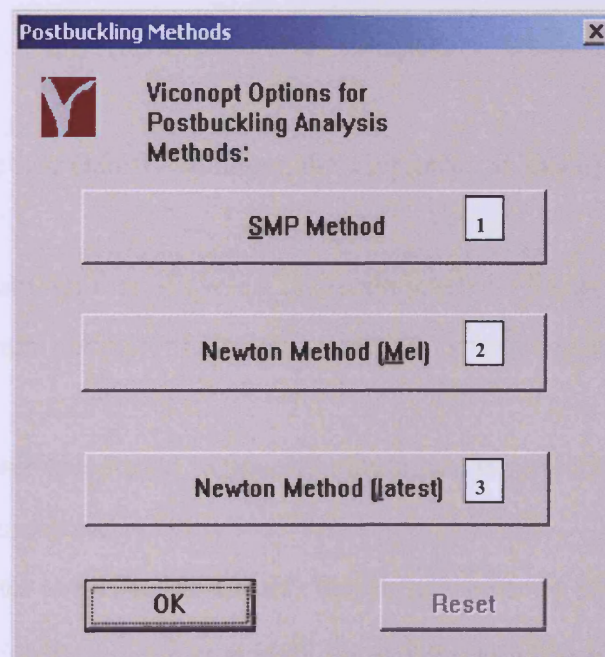


Figure 5.12 ‘Postbuckling Methods’ window.

Newton Method (latest)

Specify necessary data for postbuckling analysis:

Use Default Values

Maximum No. of cycles	20	Convergence tolerance for each cycle	0.001
Maximum No. of iterations	20	Boundary conditions parameter on the longitudinal edges	1
Maximum imperfection amplitude parameter	0	Transverse tension parameter	0
The strain level parameter to be used in the first cycle	1.005	Number of cycles between two plots of the postbuckling mode	10
The strain increment parameter from one cycle to the next	-0.005	A integer of up to 5 digits, controlling the volume of printed results	1

Create/Accept Set Default Values Create Postbuckling Card OK Cancel

Figure 5.13 'Latest Newton Method' window.

In the 'Newton Method (latest)' window, the user needs to specify (Figure 5.13).

- (i) the maximum number of cycles, i.e. strain levels, to be used in the analysis;
- (ii) the maximum number of iterations permitted for convergence at each strain level;
- (iii) the parameter to be used to specify maximum imperfection amplitude (this is ignored at present);
- (iv) the parameter to be used to specify the strain level to be used in the first cycle;
- (v) the parameter to be used to specify the strain increment from one cycle to the next;
- (vi) the convergence tolerance for each cycle for which the recommended value is around 10^{-3} ;
- (vii) the parameter to be used to specify boundary conditions on the longitudinal edges (which currently needs be set to 1, indicating free edges);

- (viii) the parameter to be used to specify transverse tension (this is ignored at present);
- (ix) the frequency, i.e. number of cycles, at which postbuckling results will be printed and modes will be plotted;
- (x) the control factor for the volume of printed results, which allows an integer of up to 5 digits (if digit 1 is present, it prints the postbuckling stiffnesses of each plate; if digit 2 is present, it prints the stress resultants in each plate strip; if digit 3 is present, it prints the postbuckling mode in tabular form; if digit 4 is present, it prints the strains in each plate strip; if digit 5 is present, it prints the end moments for each plate).

As described in Section 4.2, there is an alternative method to calculate the strain increment in the Latest Newton method, which is denoted by a negative sign in front of the increment parameter. VICONOPT MLOP users need to type this negative sign if they want to use the relevant method.

5.2.4.5 VICONOPT Output Requests

The ‘Output Request’ window contains a detailed overview of the available options and their implications. The user can control the VICONOPT results output, e.g. the number of results files, the amount of detail given in the results files and the type of graphical results generated, by selecting the provided options. The VICONOPT User Manual (Williams *et al.*, 1996) gives more information about the output controls.

In multilevel postbuckling optimisation, it is essential that some of these options are selected, and these are those selected automatically by VICONOPT MLOP. These are the last option of the ‘PRINT’ group (Figure 5.14[1]), the fourth option of the ‘PLOT’ group (Figure 5.14[2]) and the first and the fourth options in the ‘FILE’ group (Figure 5.14[3]-[4]).

The last of option of the ‘PRINT’ group results in the mass of each configuration and the values of the design variables being printed at the end of each sizing cycle during a design cycle. This is necessary since these are used for mass convergence checking after the design cycle. The fourth option of the ‘PLOT’ group allows the mode shapes to be calculated and plotted as solid lines.

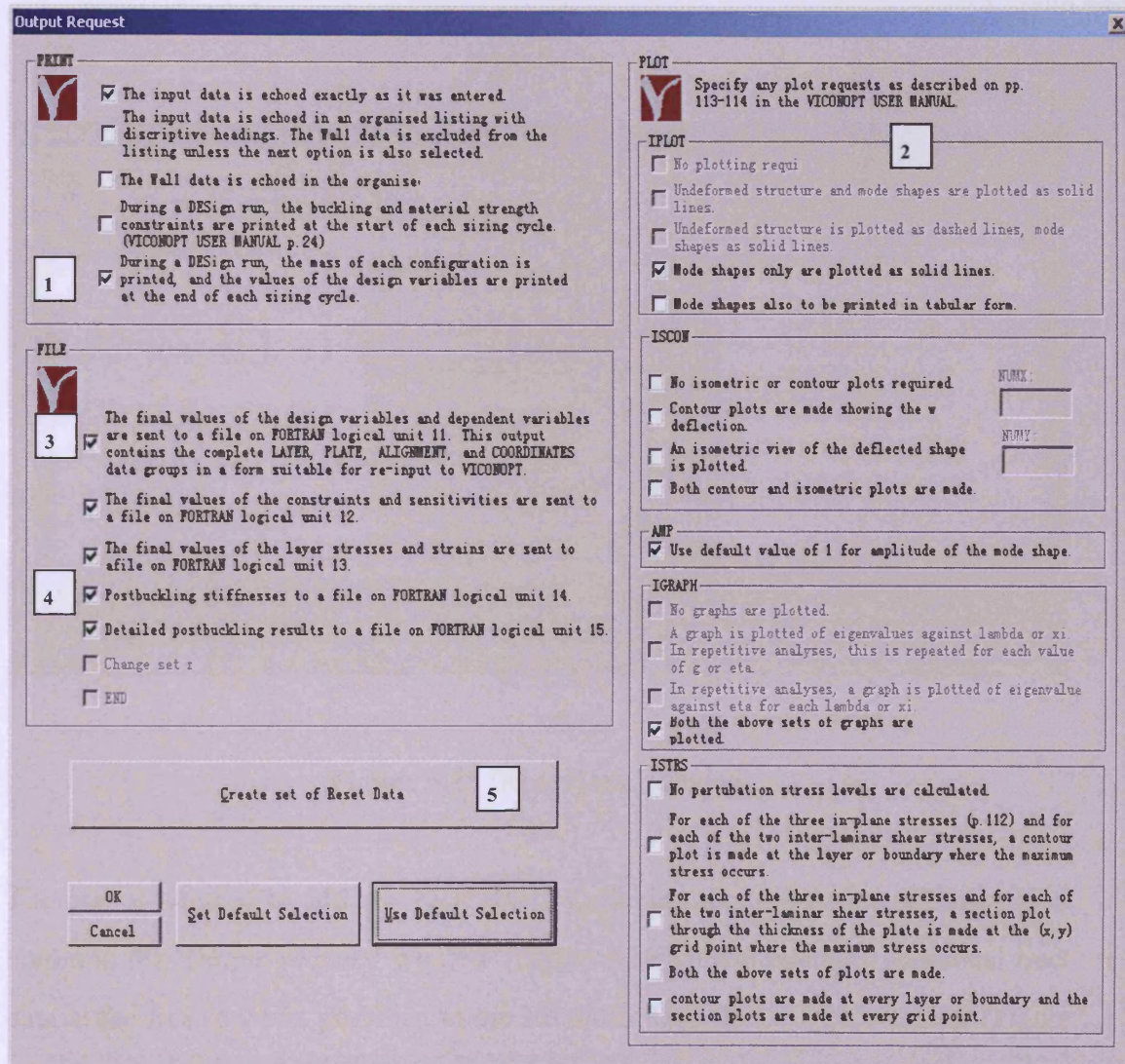


Figure 5.14 ‘Output Request’ window.

The first option in the 'FILE' group results in the (.u11) file which contains all the geometrical results from the VICONOPT design being created, which is required when generating new MSC/NASTRAN input files for postbuckling analysis after every design run. The fourth option of the 'FILE' group results in the (.u14) file being created, which is required when calculating the material cards for the new MSC/NASTRAN input files and generating new VICONOPT input files for design runs after the loads have converged.

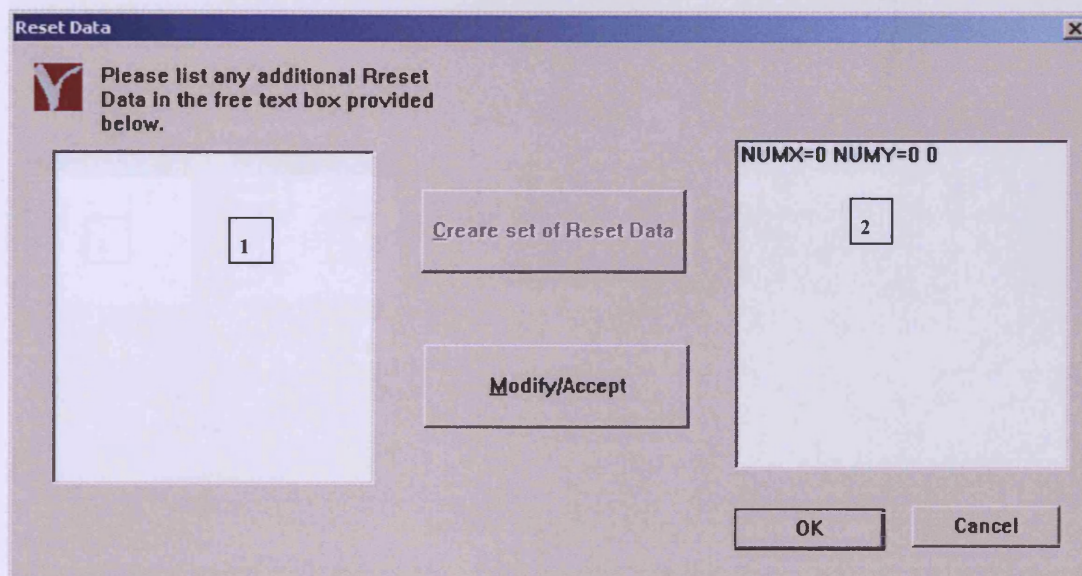


Figure 5.15 'Reset Data' window.

The user is allowed to add any reset data by clicking the 'Create set of Reset Data' button in the 'Output request' window (Figure 5.14[5]) and inputting additional reset data in the free text box provided in the left side of the 'Reset Data' window (Figure 5.15[1]). All the reset data information, which already exists, will be shown in the text box in the right side of the window (Figure 5.15[2]).

5.2.5 Design Variables

Only continuous design variables can be defined for the VICONOPT models in VICONOPT MLOP for multilevel postbuckling optimisation. Users can specify design variables for both ply thicknesses and orientations. In the case study to be presented in Chapter 6, only ply thicknesses will be considered as design variables.

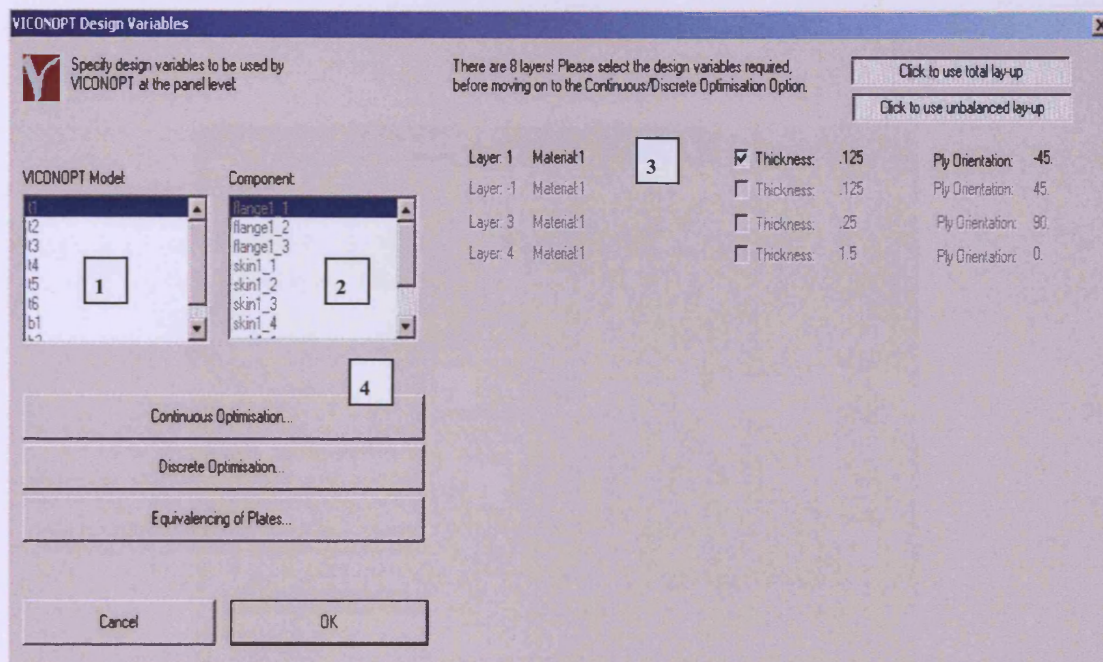


Figure 5.16 'VICONOPT Design Variables' window.

In the 'Design Variables' window, the user can select from a list of the VICONOPT models previously created (Figure 5.16[1]). The component plates of that model will then be displayed in the adjacent component list box (Figure 5.16[2]). When clicking on any of the component plates, its lay-up information will be shown in the right of the window, and the design variables can be defined (Figure 5.16[3]) by clicking the 'Continuous Optimisation' button (Figure 5.16[4]).

5.2.5.1 Continuous Design Variables

The ‘Continuous Optimisation’ window will display after clicking the ‘Continuous Optimisation’ button in the ‘Design Variables’ window. At the top of the ‘Continuous Optimisation’ window the current plate and layer numbers are displayed for the layer selected (Figure 5.17[1]). The current ply thickness (Figure 5.17[2]) and orientation (Figure 5.17[3]) are also shown in this window.

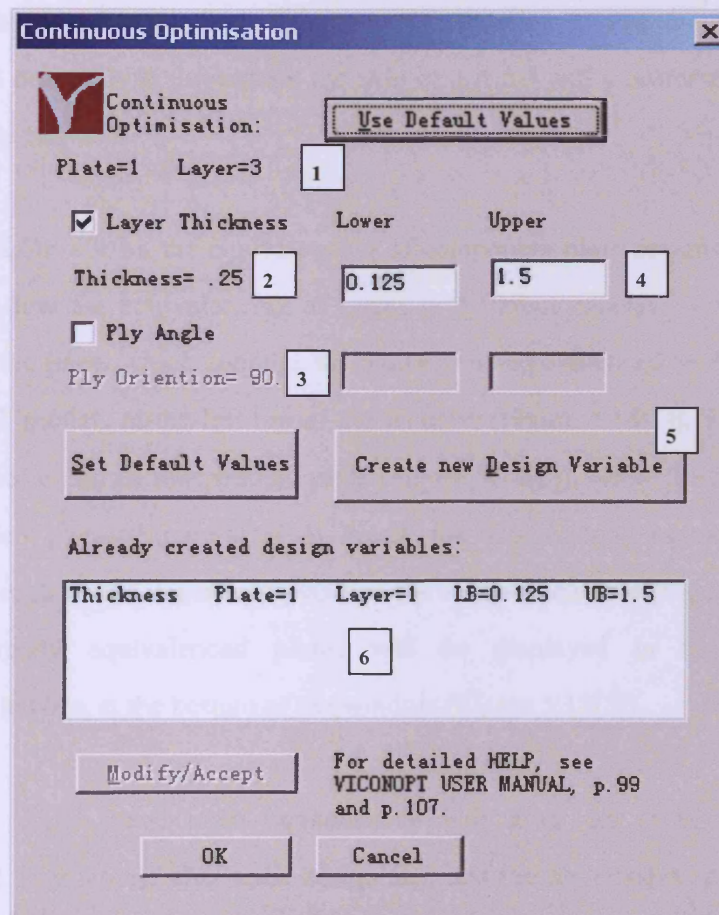


Figure 5.17 ‘Continuous Optimisation’ window.

The user needs to choose the type of design variables by selecting either the ‘Layer Thickness’ or the ‘Ply Angle’ radio button, and giving values for lower and upper bounds (Figure 5.17[4]). The design variable can then be specified by clicking the ‘Create new Design Variable’ button (Figure 5.17[5]). Design variables which have already been created are displayed in a list box at the bottom of the window (Figure 5.17[6]).

5.2.5.2 Equivalencing of Plates in VICONOPT MLOP

Due to manufacturing constraints, it is common practice to use the same layer thicknesses and orientations throughout the skin of a panel and a uniform design for the stringers of a panel.

VICONOPT MLOP allows the equivalencing of component plate designs in a panel (but does not allow the equivalencing of plates in different panels). The user first needs to select the panel which contains the plates to be equivalenced from the list of the VICONOPT models at the left top of the window (Figure 5.18[1]). Then one of the plates is selected as an independent plate (Figure 5.18[2]), while the other plates become dependent plates (Figure 5.18[3]). Finally the ‘Equivalence’ button is pressed to equivalence each of the dependent plates to the independent one (Figure 5.18[4]), Details of already equivalenced plates will be displayed in the ‘Existing Dependencies’ list box at the bottom of the window (Figure 5.18[5]).

All the plates which have been equivalenced will have the same final layer thicknesses and orientations after each design run, and the optimisation process will take into account the differing load distributions within all of the related component plates.

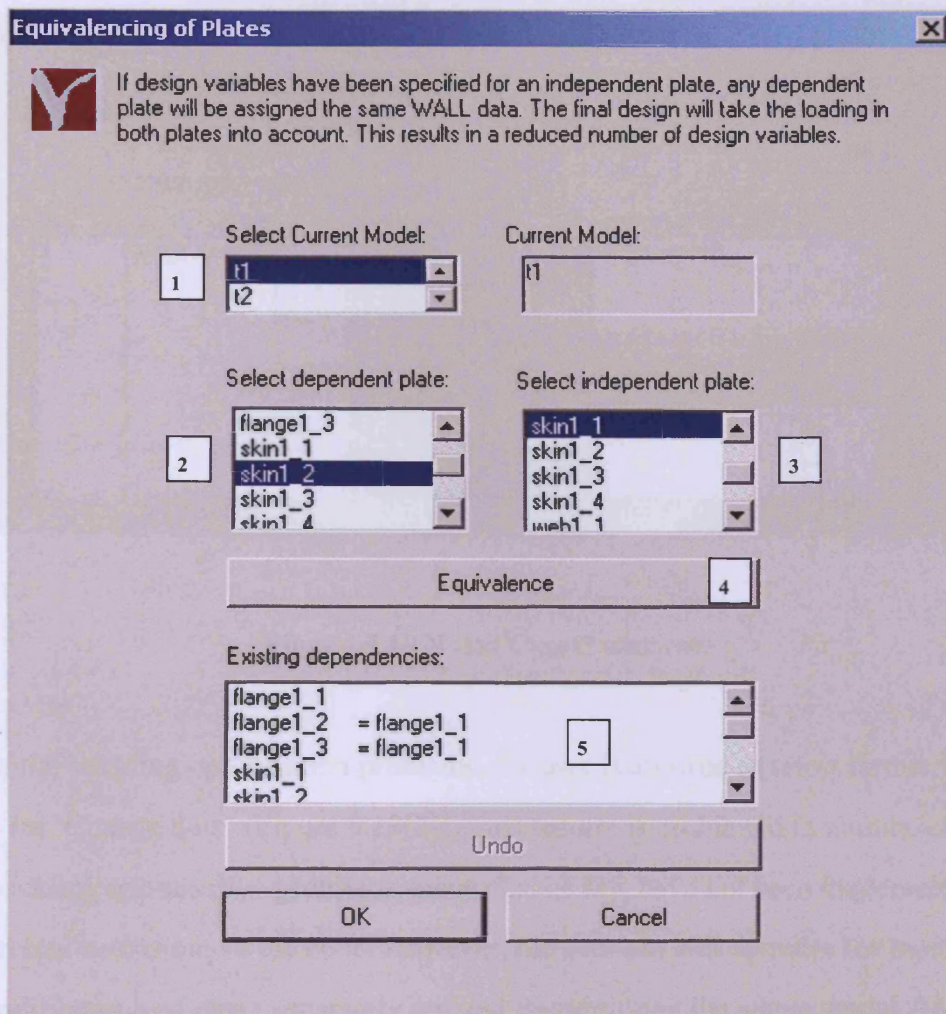


Figure 5.18 'Equivalencing of Plates' window.

5.2.6 Assigning Load Cases in VICONOPT MLOP

VICONOPT MLOP can automatically identify different load cases from the MSC/NASTRAN model and list them in the list box in the 'Load Cases' window (Figure 5.19[1]). The user can then simply specify the load case which will be used for the VICONOPT models by selecting its name from the list box and clicking the 'add' button (Figure 5.19[2]).

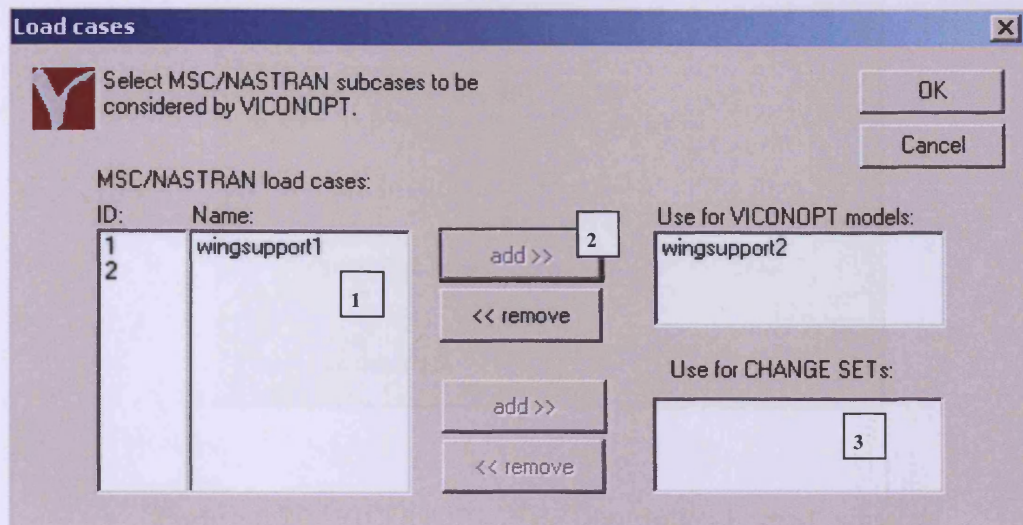


Figure 5.19 'Load Cases' window.

For initial buckling optimisation problems, the user is allowed to select further load cases for 'Change Sets' (Figure 5.19[3]). This feature is prohibited in multilevel postbuckling optimisation problems, since change sets have not been implemented in the present extensions to the code. However, the user can still optimise the model under different load cases separately without re-specifying the whole model. This can be done by saving and reloading the current model. The user then just needs to change the load case that has been selected.

5.2.7 Format of VICONOPT Plate Description

MSC/NASTRAN stores information regarding the geometry of the structure in the form of nodes with coordinates. After transferring data from the finite element model, VICONOPT MLOP allows the user to choose an approach which assembles the plates in their correct positions in the VICONOPT input file, by either entering node coordinates, or entering the plate breadths, orientation and connectivity (Williams *et al.*, 1996). Figure 5.20 shows the available options in VICONOPT MLOP for the user to choose.

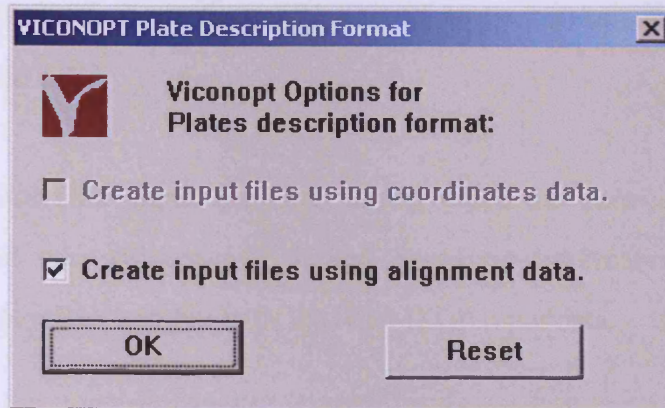


Figure 5.20 ‘VICONOPT Plate Description Format’ window.

By selecting the ‘Create input file using coordinate data’ option, VICONOPT MLOP will create VICONOPT input files including the COORDINATES data group to assemble the structure. The breadths and orientations of the plates occurring in the structure will be calculated automatically by VICONOPT.

By selecting the ‘Create input file using alignment data’ option, VICONOPT MLOP will calculate the breadths and orientations of the plates, and define the PLATE data group and a series of ALIGNMENT data groups. The CONNECTION data groups are also created once the alignment option has been selected, to assemble each panel for VICONOPT input. The VICONOPT User Manual (Williams *et al.*, 1996) gives more information about these.

5.2.8 Generation of VICONOPT Input Files

After the user has specified everything described above for the whole finite element model, the initial VICONOPT input files can be generated by clicking the ‘Create VICONOPT input deck’ button (Figure 5.4[8]). This process will take a few seconds, due to the number of procedures, i.e. the load transfer between MSC/NASTRAN and VICONOPT, the re-numbering of nodes within the plate assembly, and the creation of

the initial VICONOPT input files, which need to be carried out as described in Sections 3.3.2 and 3.3.3.

The initial VICONOPT input files are named using the panel name which was specified by the user (Figure 5.4[2]) and based on information from both the MSC/NASTRAN model and the VICONOPT MLOP input data.

5.2.9 Viewing VICONOPT Input Files

VICONOPT MLOP allows the user to view the VICONOPT input files by clicking the 'Display input deck' button (Figure 5.4[10]) in the 'Assemble VICONOPT Optimisation Model' window and selecting the file from the displayed list box (Figure 5.21).

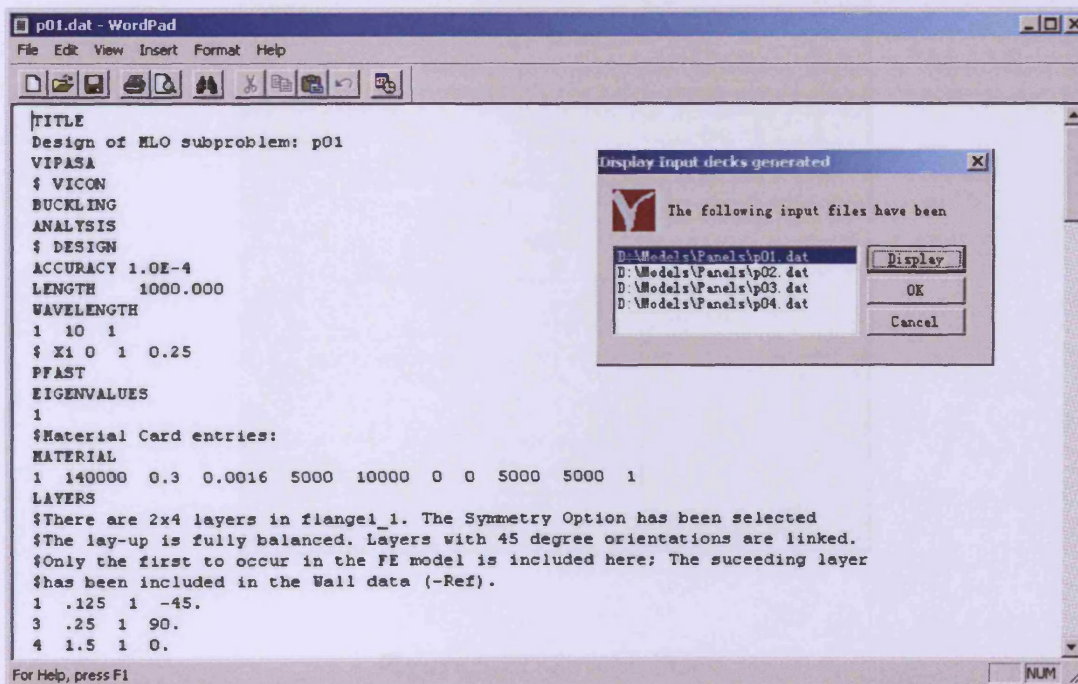


Figure 5.21 Display the VICONOPT input files.

Once the file is opened, the user can modify it manually if necessary. Since VICONOPT MLOP is still under development and does not yet cover all of the VICONOPT and MSC/NASTRAN features, this option gives the user more flexibility and controllability when any additional feature is required.

5.2.10 Save Optimisation

VICONOPT MLOP allows users to save their work at any stage during the model building process by clicking the ‘Save’ button (Figure 5.4[9]) in the ‘Assemble VICONOPT Optimisation Model’ window, or when exiting VICONOPT MLO (Figure 5.2[5]). The job will be saved in to two files, .MLO1 and .MLO2, once the user clicks the ‘Save’ button in the ‘Save’ window (Figure 5.22).

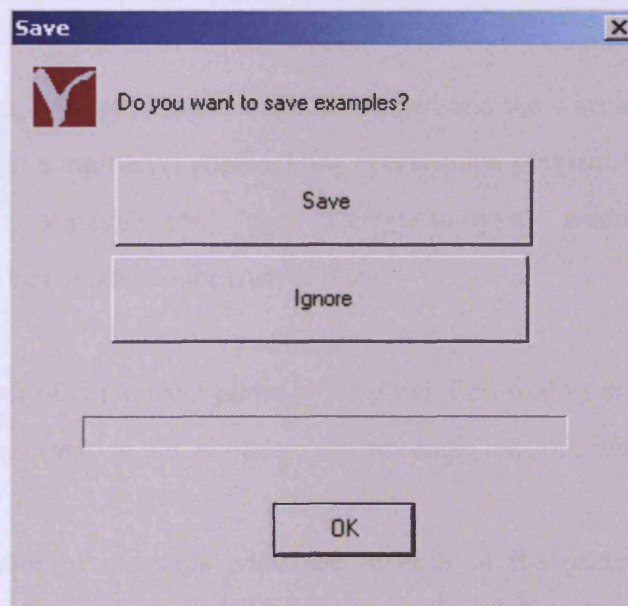


Figure 5.22 ‘Save’ window.

Figure 5.23 shows an example of an .MLO1 file which contains all the following information:

- 1) The location of the initial finite element model, the location of the 'Input.dat' file which is used to run VICONOPT automatically, and the ID number and name of the material card for the model in the MSC/NASTRAN input file. In this example, there is only one set of material cards recorded, but more may be recorded for different examples or for different stages of the optimisation.
- 2) A number corresponding to the criterion used in the stress and strain constraints, which is selected as described in the Section 5.2.4.2, and the details of this constraint.
- 3) The total number of component panels contained in the model.
- 4) The panel name, the optimisation method selected and the wavelength specified for each panel. In a multilevel postbuckling optimisation problem, the .MLO1 file contains both 'Vipasa/Vicon' and 'Design/Analysis' methods, and the wavelengths to be considered for each of them.
- 5) The total number of component plates in the panel, followed by the name and the detailed layer information, i.e. ply thickness, ply angle, etc, of each of the plates.
- 6) The total number of elements contained in each of the plates, followed by information on their locations.
- 7) The stress distribution in each of the plates in the panel.
- 8) The total number and details of the design variables including the type of variable and the lower and upper bounds.

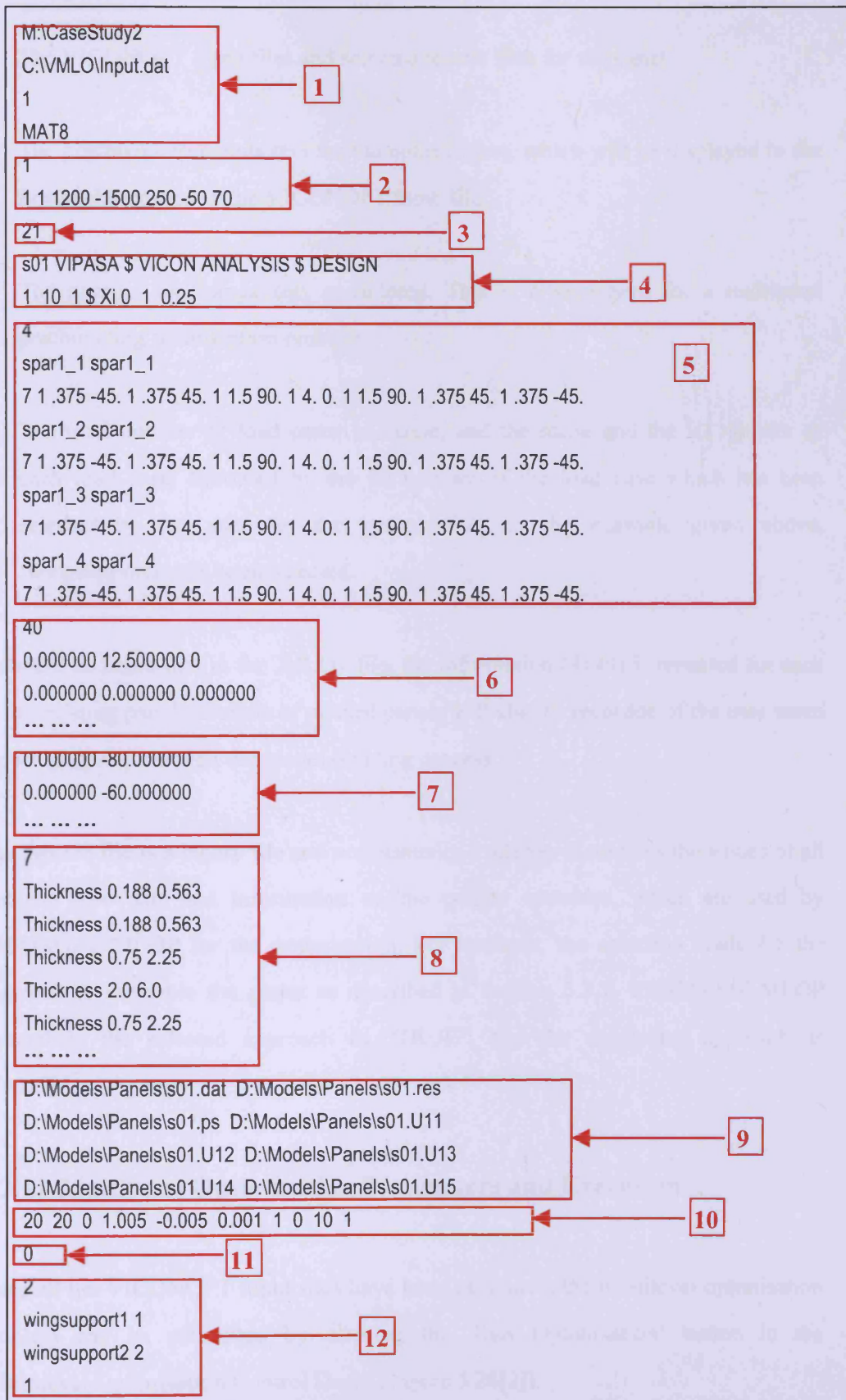


Figure 5.23 VICONOPT MLO Save File: .MLO1

- 9) The VICONOPT input files and selected results files for the panel.
- 10) The postbuckling parameters for the optimisation, which will be displayed in the Postbuckling card in the VICONOPT input file.
- 11) The number of change sets considered. This is always zero for a multilevel postbuckling optimisation problem.
- 12) The total number of load cases available, and the name and the ID number of each load case, followed by the ID number of the load case which has been selected by the user for the optimisation. In the example given above, ‘wingsupport2’ has been selected.

It should be noted that in the .MLO1 file, the information (4)-(9) is repeated for each of the existing panels. Details of unused panels will also be recorded, if the user saves the job part way through the model building process.

The .MLO2 file is a binary file and not manually readable. It contains the values of all Boolean type data and information on the pointer variables, which are used by VICONOPT MLOP for the optimisation. For example, the selection made for the approach to assemble the plates as described in Section 5.2.7, VICONOPT MLOP remembers the selected approach as “TRUE”, and the unselected approach as “FALSE”.

5.2.11 Multilevel Optimisation Parameters and Execution

Once all the VICONOPT input files have been generated, the multilevel optimisation problem can be submitted by clicking the ‘Run Optimisation’ button in the ‘Multilevel Optimisation Control Deck’ (Figure 5.24[2]).

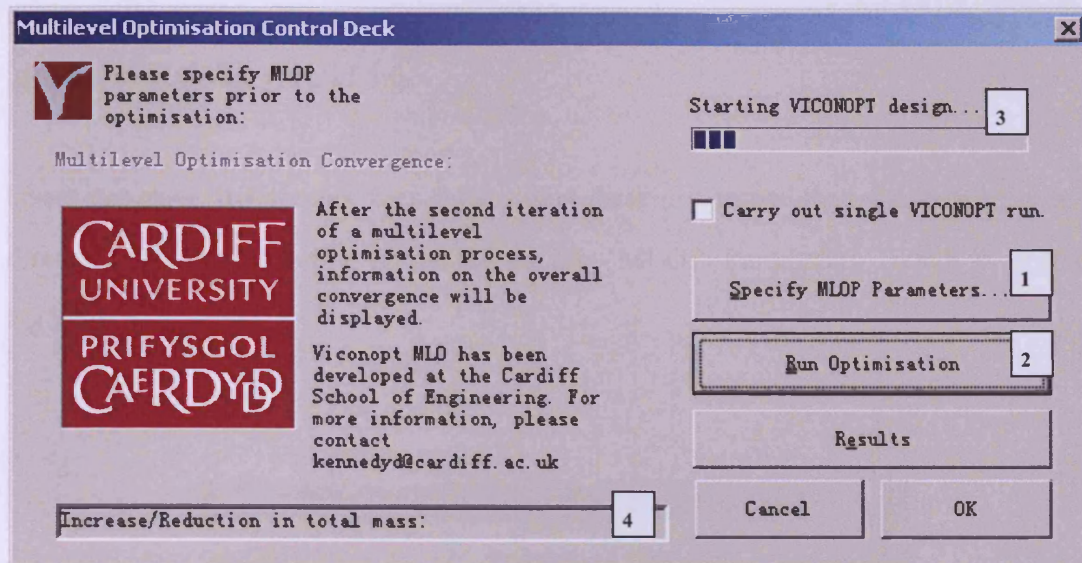


Figure 5.24 ‘Multilevel Optimisation Control Deck’ window.

However, before this, the user may wish to specify a number of control parameters to manage the multilevel optimisation process by clicking the ‘Specify MLOP parameters’ button (Figure 5.24[1]) and filling in the necessary information in the ‘MLOP Parameters’ window (Figure 5.25).

The user can control the number of analysis/design cycles by specifying either the convergence criteria or a maximum number of iterations (Figure 5.25[1]). If no parameters are specified for either of these, a default value of 1% will be used for the convergence criteria.

VICONOPT MLOP provides two methods for the mass convergence check. One checks convergence on the total mass of the structure, and the other checks convergence based on individual panel mass. The default method is the individual panel mass convergence check, but the user can switch to the total mass convergence check by selecting the ‘Check total mass convergence only’ option (Figure 5.25[2]). By doing this, less accurate results are obtained, but the number of analysis/design

cycles will be reduced, i.e. saving time. More detail regarding the convergence checks is given in Sections 4.5 and 4.6.

Users can save the results files into a new directory rather than the default output directory by specifying a pathname in the ‘MLOP Parameters’ window (Figure 5.25[3]).

MLOP Parameters

Please specify any required parameters for the multilevel optimisation process:

Convergence level: 1

Max. number of iterations:

Check total mass convergence only 2

Output directory other than default: 3

Delete following files from intermediate analyses at system level:

.bdf .MASTER 4

.f06 DBALL

.f04

Specify any additional MSC/NASTRAN keywords+values (e.g. "out=D:\\Models dbs=D:\\Models"):

OK Cancel

Figure 5.25 ‘MLO Parameters’ window.

During the optimisation, VICONOPT MLOP only requires the finite element model (.bdf) and the numerical results file (.f06) to update the models at panel level. Therefore, some of the result files from the finite element analysis can be deleted to reduce storage requirements. This is done by selecting the unwanted files in the ‘MLOP Parameters’ window (Figure 5.25[4]).

Finally, users can specify any additional parameters required in the free text box provided in the ‘MLOP Parameters’ window (Figure 5.25[5]). These must be written in the format specified in the MSC/NASTRAN Version 70.5 Quick Reference Guide (MSC/NASTRAN, 1998).

During optimisation, information regarding the state of the analysis will be displayed in the ‘Multilevel Optimisation Control Deck’ window (Figure 5.24[3]). The current total increase/reduction in mass of the overall structure will also be displayed in this window (Figure 5.24[4]) after each design cycle.

5.3 MULTILEVEL POSTBUCKLING OPTIMISATION PROCESS

5.3.1 General

Development of the optimisation process to include postbuckling effects has required significant changes to the existing code in order to ensure convergence and deal with issues such as tension fields in postbuckled panels. Figure 5.26 shows the multilevel optimisation process as coded in VICONOPT MLOP; the design cycle is marked in red and the analysis cycle is marked in blue. In comparison with the previous procedure shown in Figure 3.9, it is clear that many more VICONOPT features have had to be incorporated into the optimisation process. In the following sections, this process will be described in detail.

During each analysis cycle, VICONOPT MLOP generates a VICONOPT input file for each of the panels and a MSC/NASTRAN file for the whole finite element model. Each of these files will lead to a set of VICONOPT result files. A good file naming procedure is required to avoid files being overwritten and to enable them to be recognised easily.

The results file from the initial finite element analysis carried out by MSC/NASTRAN has the same name as the initial finite element model file which the user entered into the window shown in Figure 5.4 but with a different file extension.

Once the optimisation has started, VICONOPT analysis input files are named in the format 'Panelname_d_a' and design input files are named in the format 'Panelname_d', where 'Panelname' is the name chosen by the user when assembling the panel (Figure 5.4[2]), 'd' is the number of the current design cycle and 'a' is the current analysis cycle in that design cycle. All of these VICONOPT input files have the extension '.dat'. For example, the name and extension of the analysis input file for panel 'Spar3', in the third analysis cycle of the second design cycle, is 'Spar3_2_3.dat'. VICONOPT results files have the same name as each of their input files but with different extensions, i.e. .res, .u11, .u12 and etc. MSC/NASTRAN input files (.bdf) and their results files (.f04, .f06, .op2 and etc) are named in the format 'Modelname_d_a(n)' and 'Modelname_d(n)' for analysis or design respectively, where 'd' and 'a' are the same as for the VICONOPT files, 'Modelname' is the name of the initial finite element model file, and 'n' is a number which is normally equal to 0, except when some plates have negative stiffnesses as described in Section 4.4, in which case a pair of MSC/NASTRAN input files is required, one of which will be named with 'n' equal to 1.

5.3.2 VICONOPT Postbuckling Analysis

After the VICONOPT MLOP model has first been generated, and after each design run has been completed, VICONOPT will start the postbuckling analysis which will be repeated until the loads in each panel are converged, i.e. the start of a new analysis cycle of the optimisation.

5.3.2.1 VICONOPT process control file

Since VICONOPT can only analyse one panel at a time here, a process control file, which is named 'Input' with a .dat extension, is generated by VICONOPT MLOP to ensure VICONOPT analyses all the panels consecutively.

```

2111111
D:\Models\Panels\p12_2_1.dat
D:\Models\Panels\p12_2_1.res
D:\Models\Panels\p12_2_1.ps
D:\Models\Panels\p12_2_1.u11
D:\Models\Panels\p12_2_1.u12
D:\Models\Panels\p12_2_1.u13
D:\Models\Panels\p12_2_1.u14
D:\Models\Panels\p12_2_1.u15
000000
END

```

Figure 5.27 VICONOPT Process Control File: Input.dat

Figure 5.27 is a typical process control file. The file starts with the current panel ID number which is defined by VICONOPT MLOP, followed by five numbers which can each take a value of either 1 or 0 depending on whether the results files .u11, .u12, .u13, .u14 and .u15 are required in Figure 5.14. In this example, all five of these files are to be generated. As described in Section 5.2.4.5, .res, .u11,

and .u14 files are the default files selected for all multilevel postbuckling optimisation problems, and the .ps file, which contains the graphic results, is also generated for all such problems by default. Then the full pathnames of the input and results files are printed in the process control file to ensure VICONOPT can find and generate them in the correct locations. Finally, six zeros are printed out to set the six numbers, which are printed on the first line of the file, back to their initial conditions.

It should be noted that only one 'Input.dat' file is created during the whole optimisation, and that VICONOPT MLOP replaces this file automatically for different panels. The response from VICONOPT to the VICONOPT process control file is shown in Figure 5.28.

```

1
***          V I C O N O P T          ***
***  VERSION NUMBER 1.41   RELEASED DECEMBER 2008  ***
***  THIS EXECUTION WAS ON THE W32 COMPUTER.      ***

INPUT DEVICE NUMBER = 5   OUTPUT DEVICE NUMBER = 6

Analysis and design of panel                21
Data will be read from file                D:\Models\Panels\p12_2_1.dat

Results will be written to file            D:\Models\Panels\p12_2_1.res

Graphics will be written to file          D:\Models\Panels\p12_2_1.ps

Optimum design geometry to file           D:\Models\Panels\p12_2_1.u11

Constraint information to file             D:\Models\Panels\p12_2_1.u12

Buckling stresses to file                 D:\Models\Panels\p12_2_1.u13

Postbuckling stiffnesses to file          D:\Models\Panels\p12_2_1.u14

Postbuckling stress resultants to file    D:\Models\Panels\p12_2_1.u15

```

Figure 5.28 VICONOPT analysis/design window

5.3.2.2 VICONOPT postbuckling analysis results file

Although .u11 and .u14 files are generated for each VICONOPT run, nothing is printed into the .u11 file after the postbuckling analysis is completed. Only the .u14 file, which contains the reduced stiffnesses information, contains data. An example of a .u14 file is given in Figure 5.29.

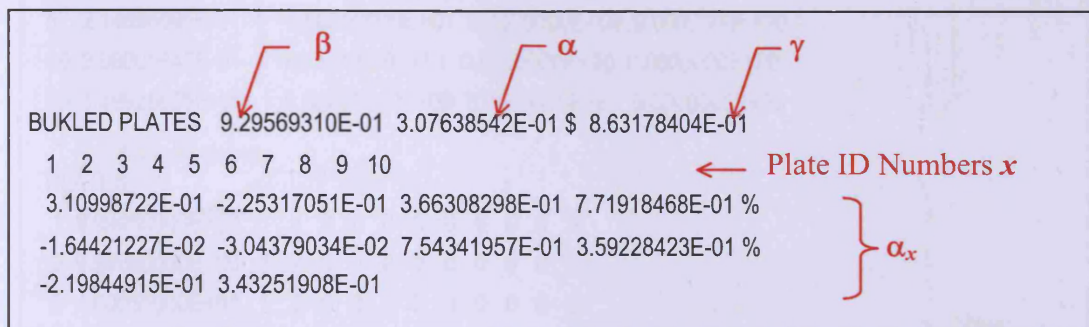


Figure 5.29 VICONOPT Postbuckling Analysis Results File: .u14

The information contained in the .u14 file is also known as BUKLED PLATES data, and will be a part of the VICONOPT design input file, if the load convergence test is passed in the next stage. Otherwise, it will be used to calculate the reduced stiffness ratio for each plate as described in Section 4.3. The overall reduced stiffness ratio γ for the panel is presented in the .u14 file only for the calculation of reduced stiffness ratio but is not used in the VICONOPT design.

5.3.3 VICONOPT Design

Once all the panels have met their load convergence criteria, VICONOPT MLOP will generate VICONOPT design input files based on the current loading information and the VICONOPT design run will be carried out, which marks the end of the current design cycle and the beginning of a new one.

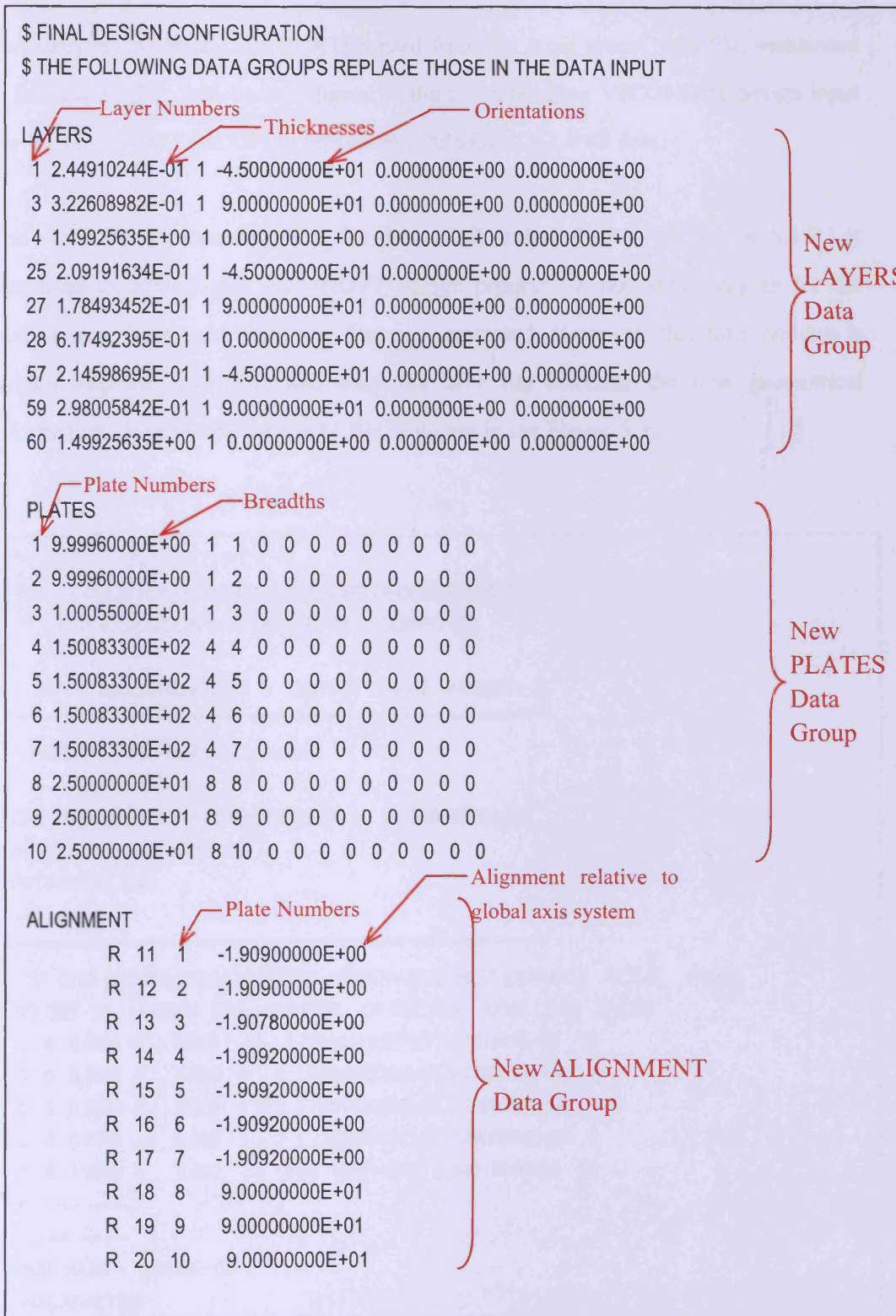


Figure 5.30 VICONOPT design Results File: .u11

Furthermore, the BUKLED PLATES card from the most recent .u14 file, mentioned in Section 5.3.2.2, will be transferred to the corresponding VICONOPT design input file by VICONOPT MLOP, to replace the POSTBUCKLING data.

The VICONOPT process control file 'Input.dat' as described in the Section 5.3.2.1 is also used to control the VICONOPT design process. In the same way as for the analysis run, both .u11 and .u14 files are generated. However, this time nothing is written into the .u14 file, and only the .u11 file contains the new geometrical information. An example of a .u11 file is shown in the Figure 5.30.

```

**          V I C O N O P T          **
**  VERSION NUMBER 1.41  RELEASED DECEMBER 2008  **
**  THIS EXECUTION WAS ON THE  W32  COMPUTER.    **

INPUT DEVICE NUMBER = 5  OUTPUT DEVICE NUMBER = 6
*****
RESULTS FOR PROBLEM NUMBER  1
-----
CPU TIME USED FOR PREPROCESSING =  0.0310 SECONDS
INITIAL MASS =  3.5536E+03
INITIAL ANALYSIS
-----
*****
ST  CHA (VICON) (VIPASA) (REPET.) EIGENVALUE BEST ESTIMATE  TOTAL  ITERS.
NO SET XI  LAMBDA ETA  NUMBER  OF FACTOR  AXIAL LOAD TAKEN
0  0  0.0000 -  0.000  1  1.776444156E+00  2.7381841E+05  14
0  0  0.2500 -  0.000  1 - 2  1.776560220E+00  2.7383630E+05  14
0  0  0.5000 -  0.000  1 - 2  1.769142047E+00  2.7269287E+05  14
0  0  0.7500 -  0.000  1 - 2  1.226202662E+00  1.8900502E+05  9
0  0  1.0000 -  0.000  1  1.001168814E+00  1.5431864E+05  11
-----
FINAL MASS =  3.0892E+03
FINAL ANALYSIS
-----

```

Figure 5.31 VICONOPT .res file.

As described in Section 4.4, the values of initial and final mass of each panel for the current completed design cycle can be found in its .res files after the run has completed as shown in Figure 5.31.

5.3.4 MSC/NASTRAN Model Updating

On the basis of the VICONOPT results, the MSC/NASTRAN finite element model is subsequently updated and re-analysed.

If the load has converged and a design run has been carried out, the MSC/NASTRAN Property Card will be replaced as described in Section 3.3.2. Otherwise, the previous Property Card from the last design run will remain.

```

$ Referenced Material Records
$ Material Record: HighStrengthCarbonEpoxy
$ Description of Material: Date: 04-Aug-01 Time: 16:17:02
MAT8 1 140000. 10000. .3 5000. 5000. 5000. .0016

```

Figure 5.32 Typical MSC/NASTRAN Material Card

The MSC/NASTRAN Material Card has to be changed every time the model is updated. A typical MSC/NASTRAN Material Card is shown in Figure 5.32. After the material name and ID which are used to identify the material, there are another 7 parameters, which are Longitudinal Young's Modulus E_1 , Transverse Young's Modulus E_2 , Major Poisson's Ratio ν_{12} , Shear Moduli G_{12} G_{13} and G_{23} and Density ρ . Following each analysis cycle MSC/NASTRAN takes the reduced stiffness information as described in Section 4.2 and multiplies each plate's Young's Modulus and Shear Moduli by the related reduced stiffness ratio, to calculate the loads for the next analysis cycle.

Once the new load distribution has been calculated by MSC/NASTRAN, VICONOPT MLOP transfers this load distribution to each panel and creates a set of VICONOPT postbuckling analysis input files for the new analysis cycle. Details of how load is transferred between MSC/NASTRAN and VICONOPT have been given in Section 3.3.3 and Section 4.6, and so no more description will be given here.

5.3.5 VICONOPT MLOP Output File

In addition to the VICONOPT and MSC/NASTRAN results files, VICONOPT MLOP also generates its own output file to record all the convergence information. This file has the same name as the initial finite element model and the extension .clog. An example of a .clog file is shown in Figure 5.33. The file begins with some general information regarding the job, e.g. the name of the initial finite element model (Figure 5.33[1]). Then all the convergence results are printed twice in two different formats; in the first format the information is grouped by design cycles (Figure 5.33[2]); in the second format it is grouped by panels (Figure 5.33[3]). The user can choose either to make post-processing easier.

The data shown in the example are:

- (1) P.N., Panel Name;
- (2) InM, Initial Mass;
- (3) CuM, Current Mass;
- (4) PD, Mass saving relative to Previous Design;
- (5) TM, Total relative Mass Saving so far;
- (6) InAL, Initial Axial Load;
- (7) CuAL, Current Axial Load;
- (8) TAL, Total relative Axial Load Change so far;;
- (9) Convergence, Convergence Criteria so far;
- (10) D.C., Design Cycle;

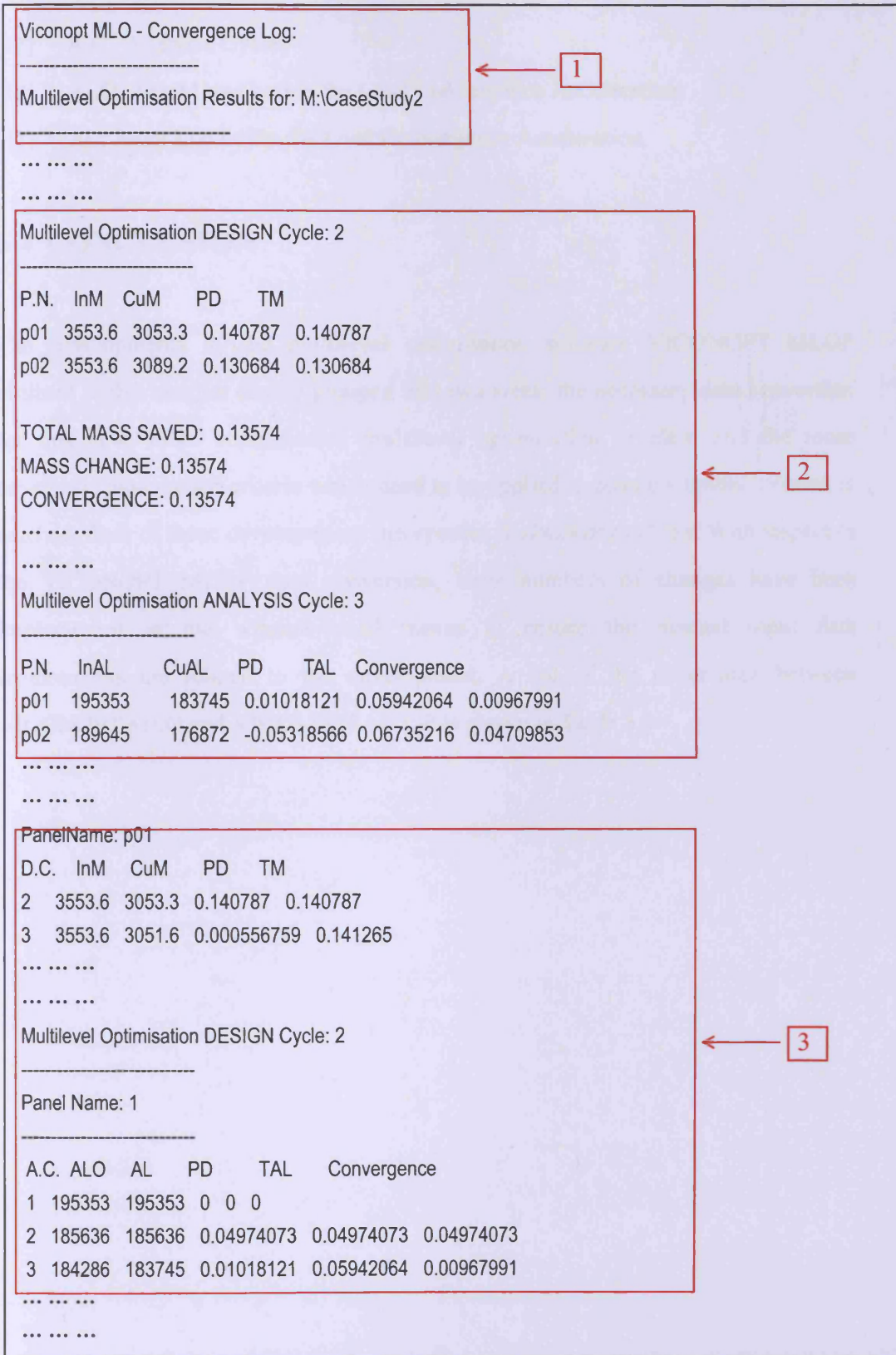


Figure 5.33 VICONOPT MLO Output File: .clog

- (11) A.C., Analysis Cycle;
- (12) ALO, Axial Load before the Load Convergence Acceleration;
- (13) AL, Axial Load after the Load Convergence Acceleration.

5.4 CONCLUSION

The developments to the multilevel optimisation software VICONOPT MLOP outlined in this chapter can be grouped into two areas: the necessary data conversion for this new, more sophisticated multilevel optimisation problem and the more advanced convergence criteria which need to be applied to ensure a timely solution is reached. Both of these developments incorporate postbuckling effects. With respect to the VICONOPT MLOP data conversion, large numbers of changes have been implemented in the window-based menus to ensure the manual input data requirements are related to the development. A list of the differences between VICONOPT MLO and VICONOPT MLOP is shown in Table 5.1.

Features	VICONOPT MLO	VICONOPT MLOP
<u>Data Converter</u>		
VICONOPT process control file	Contains the directories of the VICONOPT input and results files.	These file names have been brought up to date.
VICONOPT input file	VICONOPT MLO only generates the initial buckling design input files.	Both postbuckling analysis input files and initial buckling design input files are generated with Bukled Plates card.
VICONOPT results files	VICONOPT MLO reads the data in .res and .u11 files.	VICONOPT MLOP reads the data in .res and .u11 files after each design run, and the data in .u14 files after each analysis run.
MSC/NASTRAN input file	Updates the property card with the new geometrical information, e.g. ply thicknesses.	Updates the property card after each design run, and updates the material card after each analysis run with the new reduced stiffness ratio.
MSC/NASTRAN results file	VICONOPT MLO reads the new loading data from the .f06 file.	No difference.
VICONOPT MLO output file	Contains the mass convergence information.	Contains information about mass convergence, load convergence and load convergence acceleration.
VICONOPT MLO saving file	Exists but does not work properly.	Works properly and is up to date.
<u>Convergence Checking System</u>		
Mass convergence check	Based on the overall mass of the structure.	Two methods are available: overall mass check and individual mass check which is based on the mass of each panel.
Load convergence check	Not applicable	Based on the load of each panel.
Convergence acceleration	Not applicable	Carried out after two analysis cycles in each design cycle.

Table 5.1 Differences between VICONOPT MLO and VICONOPT MLOP.

Chapter 6

Multilevel Optimisation of a Composite Aircraft Wing Incorporating Postbuckling Effects

6.1 INTRODUCTION AND PROBLEM DESCRIPTION

A case study was conducted into the optimisation of the schematic composite aircraft wing, which was created based on the GARTEUR benchmark mentioned in Chapter 1, shown in Figure 6.1, in order to demonstrate the capabilities of VICONOPT MLOP. The wing contains twelve skin panels, six at the top (T1 – T6) and six at the bottom (B1 – B6), nine spar panels (S1 – S9) and four ribs (see Figures 6.1 and 6.2). The objective was to optimise the ply thicknesses in each of the skin and spar panels. No attempt was made to optimise the ribs, which were included in the model to provide simply supported edge conditions for the skin and spars.

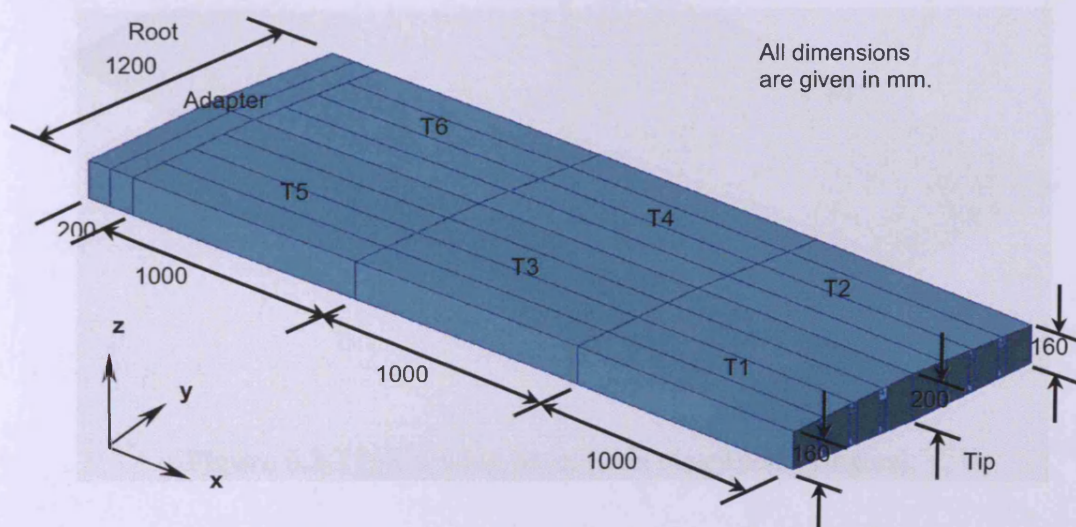


Figure 6.1 Panels T1 to T6 on the top of the wing and adapter.

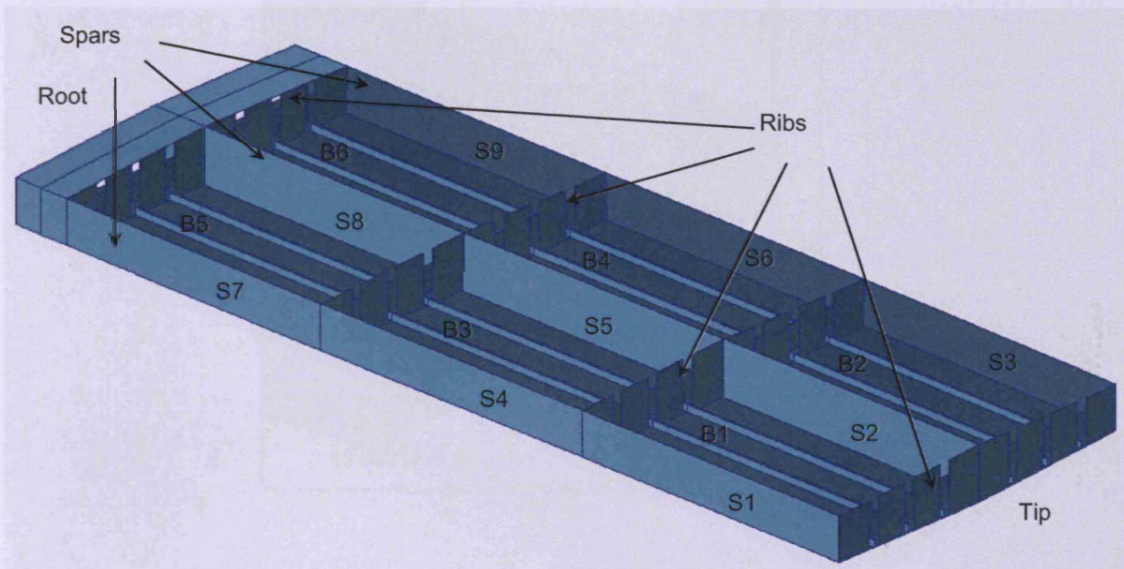


Figure 6.2 Panels B1 to B6 at the bottom of the wing, spars and ribs.

For each skin panel, three L-shaped stringers provided increased longitudinal stiffness resulting in a total of ten plates to be defined: four skin plates, three webs and three flanges (Figure 6.3).

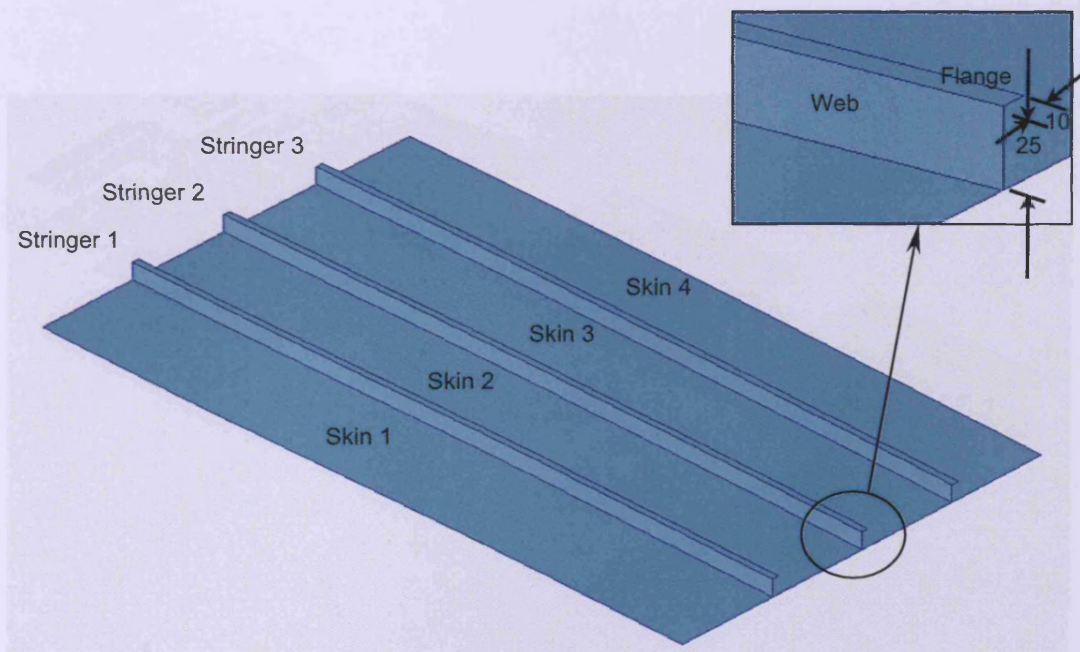


Figure 6.3 Typical wing panel (skin plates and stringers).

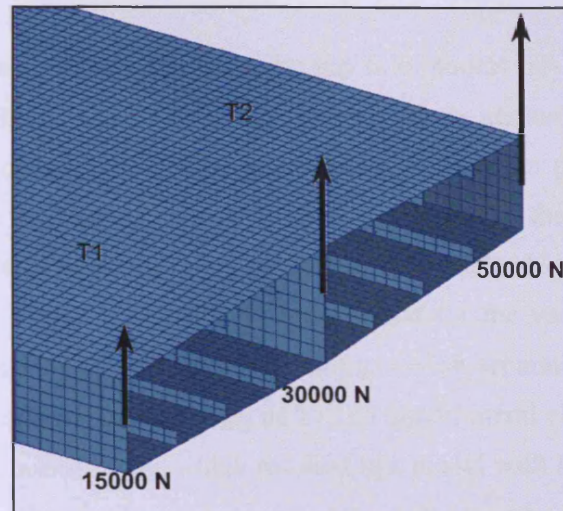


Figure 6.4 Load case: Twist.

The root of the wing was attached to a steel adapter, which was fully clamped at its free end, to model realistic boundary conditions. Two load cases from a previous study (Fischer *et al.*, 2002a,b) were considered and the more critical one (Figure 6.4) which results in torsion about the wings was selected for the present case study.

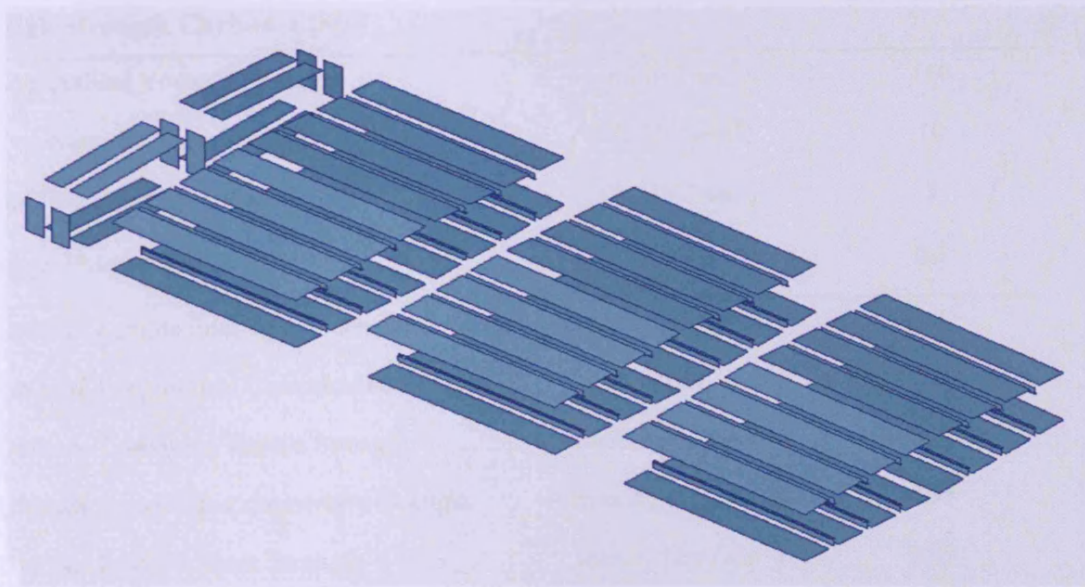


Figure 6.5 Component plates of the wing (excluding spar and rib plates).

The optimisation covered panels T1-T6 on the top skin, panels B1-B6 on the bottom skin and panels S1-S9 on the three spars. The ribs were assumed to be of fixed dimensions and sufficient to provide simple support to the skin panels. Figure 6.3 shows details of the skin/stringer configuration for each of the 12 skin panels. Individual property cards were specified in the MSC/NASTRAN model for each of the component plates (Figure 6.5), in order to account for the variation of reduced postbuckling stiffness, and also to allow the user to define separate design variables for each plate. A uniform mesh consisting of 29,280 quadrilateral elements (QUAD4) was generated for the overall wing, which resulted in a model with 126,860 degrees of freedom.

6.2 INITIAL DESIGN

High strength carbon-epoxy was used as the material for the individual laminae of all component plates. Table 6.1 summarises the properties in the principal material directions, together with the material density and the ultimate material strengths, which were used as allowable limits in the optimisation.

High Strength Carbon-Epoxy		
Longitudinal Young's Modulus	$E_1(kN/mm^2)$	140
Transverse Young's Modulus	$E_2(kN/mm^2)$	10
In-Plane Shear Modulus	$G_{12}(kN/mm^2)$	5
Major Poisson's Ratio	ν	0.3
Ultimate Longitudinal Tensile Strength	$\max.\sigma_{1t}(kN/mm^2)$	1.5
Ultimate Longitudinal Compressive Strength	$\max.\sigma_{1c}(kN/mm^2)$	1.2
Ultimate Transverse Tensile Strength	$\max.\sigma_{2t}(kN/mm^2)$	0.05
Ultimate Transverse Compressive Strength	$\max.\sigma_{2c}(kN/mm^2)$	0.25
Ultimate In-Plane Shear Strength	$\max.\tau_{12}(kN/mm^2)$	0.07
Density	$\rho(g/mm^3)$	0.0016

Table 6.1 Material properties of high strength carbon-epoxy.

T1, T2, B1, B2 (Tip)		Initial Design	Lower Bound	Upper Bound
Skin	45° and -45° plies	0.250	0.125	1.500
	90° plies	0.500	0.125	1.500
	0° plies	0.500	0.125	1.500
Web	45° and -45° plies	0.125	0.125	1.500
	90° plies	0.250	0.125	1.500
	0° plies	1.500	0.125	1.500
Flange	45° and -45° plies	0.125	0.125	1.500
	90° plies	0.250	0.125	1.500
	0° plies	1.500	0.125	1.500
T3, T4, B3, B4 (Middle)		Initial Design	Lower Bound	Upper Bound
Skin	45° and -45° plies	0.375	0.125	1.500
	90° plies	0.625	0.125	1.500
	0° plies	1.000	0.125	1.500
Web	45° and -45° plies	0.250	0.125	1.500
	90° plies	1.250	0.125	1.500
	0° plies	2.000	0.125	2.000
Flange	45° and -45° plies	0.250	0.125	1.500
	90° plies	1.250	0.125	1.500
	0° plies	2.000	0.125	2.000
T5, T6, B5, B6 (Root)		Initial Design	Lower Bound	Upper Bound
Skin	45° and -45° plies	0.500	0.125	1.500
	90° plies	0.750	0.125	1.500
	0° plies	1.500	0.125	1.500
Web	45° and -45° plies	0.375	0.125	1.500
	90° plies	2.250	0.125	2.250
	0° plies	2.500	0.125	2.500
Flange	45° and -45° plies	0.375	0.125	1.500
	90° plies	2.250	0.125	2.250
	0° plies	2.500	0.125	2.500
Spars S1-S9		Initial Design	Lower Bound	Upper Bound
	45° and -45° plies	0.375	0.188	0.563
	90° plies	1.500	0.750	2.250
	0° plies	4.000	2.000	6.000

Table 6.2 Initial ply thicknesses, upper and lower bounds (all in *mm*).

Each plate had a symmetric balanced lay-up $[-45^\circ/45^\circ/90^\circ/0^\circ/90^\circ/45^\circ/-45^\circ]$ with different thicknesses for skin, web, flange and spar plates. The initial ply thicknesses and the design variables used in the VICONOPT models for each skin panel and for the spars are shown in Table 6.2. The plates of each skin panel were equivalenced in order to ensure uniform ply thicknesses across the skin. The web and flange plates were also equivalenced to ensure the three stringers of each panel were identical.

The panels were assumed simply supported along all four edges, so that out-of-plane and transverse in-plane displacements were fully constrained. Four point supports were specified at the end of each skin plate in the way described in Chapter 5, resulting in a total of thirteen point supports across each panel.

6.3 NUMERICAL RESULTS

An initial linear static finite element analysis was carried out for the overall wing using MSC/NASTRAN, following which VICONOPT models were generated for individual skin panels and spars using VICONOPT MLOP. A total of 135 design variables were specified for the ply thicknesses of their component plates.

VICONOPT MLOP carried out a total of nine multilevel optimisation cycles, before the strictest convergence criterion, i.e. 0.01 (1%), for the mass of each panel was met. Figure 6.6 shows the mass changes during the optimisation process. It can be seen that the total mass of the wing converged well on a value of approximately 50 kg, which represented a total saving of 44% over the initial design. All the panels experienced a decrease in mass, but the mass of the bottom skin panels reduced much more significantly than mass of the top panels, due to them being in tension.

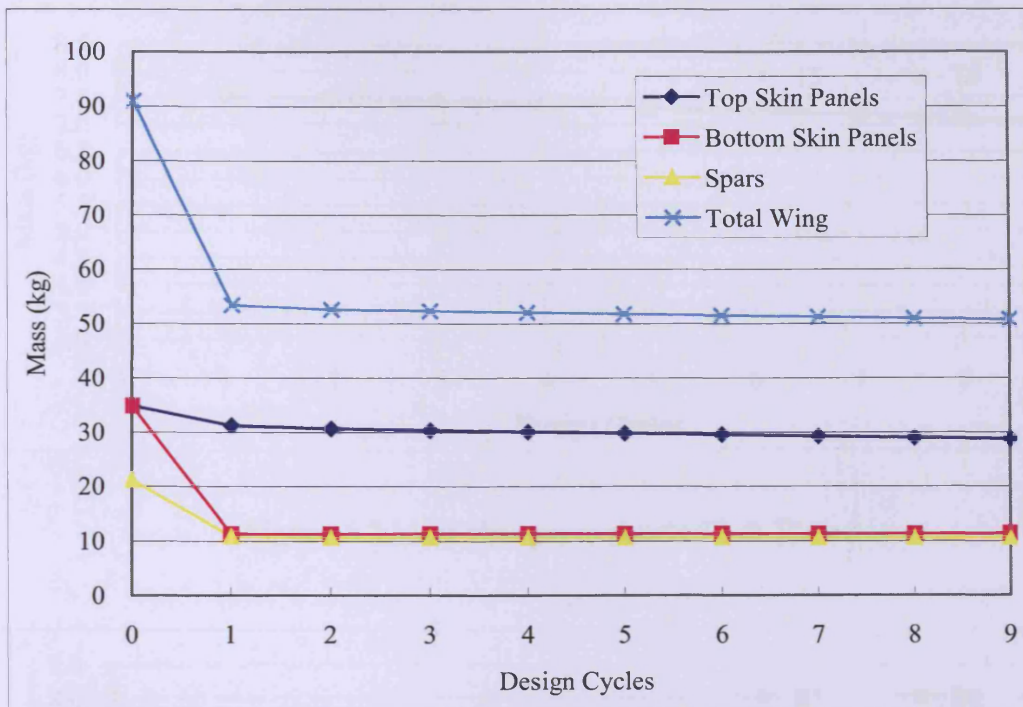


Figure 6.6 Total mass changes during the multilevel optimisation process.

The panels which are near the root are more sensitive to mass changes and more difficult to get to converge, since they carry most of the loading. As expected, the root panels which are required to carry higher loads (panels T5, T6, B5 and B6) have more material assigned to them than the tip panels (panels T1, T2, B1 and B2). Figures 6.7 and 6.8 show mass changes for the example of individual pairs of panels on the top (T5 and T6) and bottom (B5 and B6) skins. Complete results showing mass changes for every panel are given in Appendix A.

The mass of the spars reduces by 50% over the initial design, maintaining approximately the same percentage of wing mass and therefore avoiding attracting an artificially high percentage of the load. The middle spar is wider than the other spars, so the panels S2, S5 and S8 are always heavier than the other spar panels. An example showing the mass changes of spars S4, S5 and S6 is given in Figure 6.9.

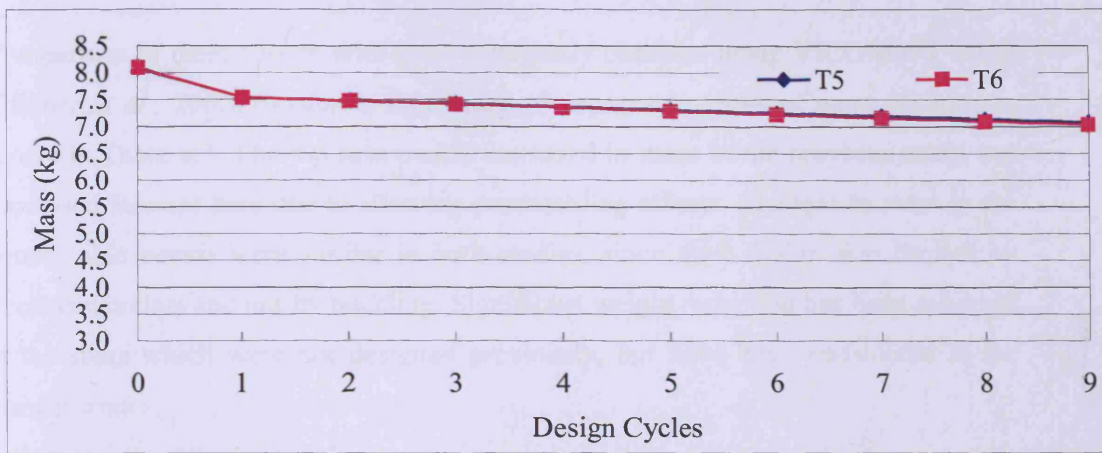


Figure 6.7 Mass changes in panels T5 & T6

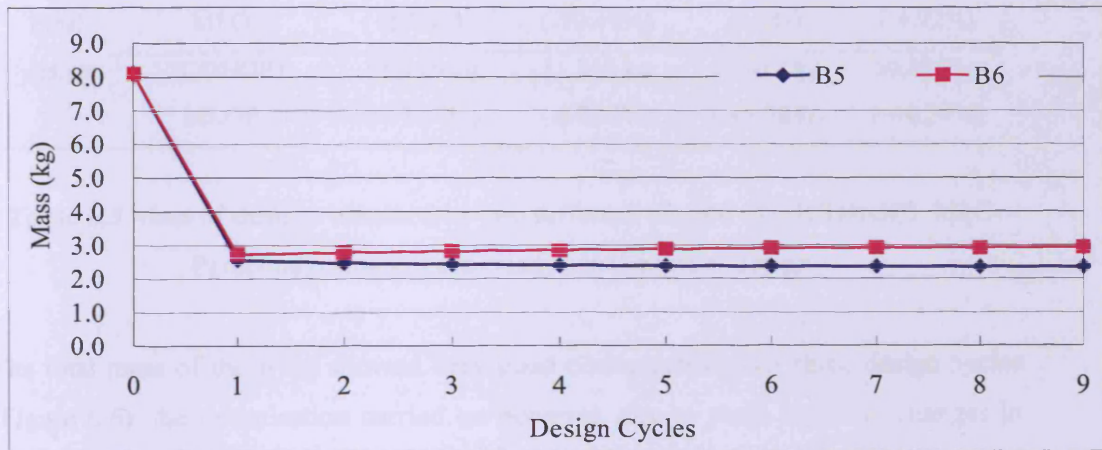


Figure 6.8 Mass changes in panels B5 & B6.

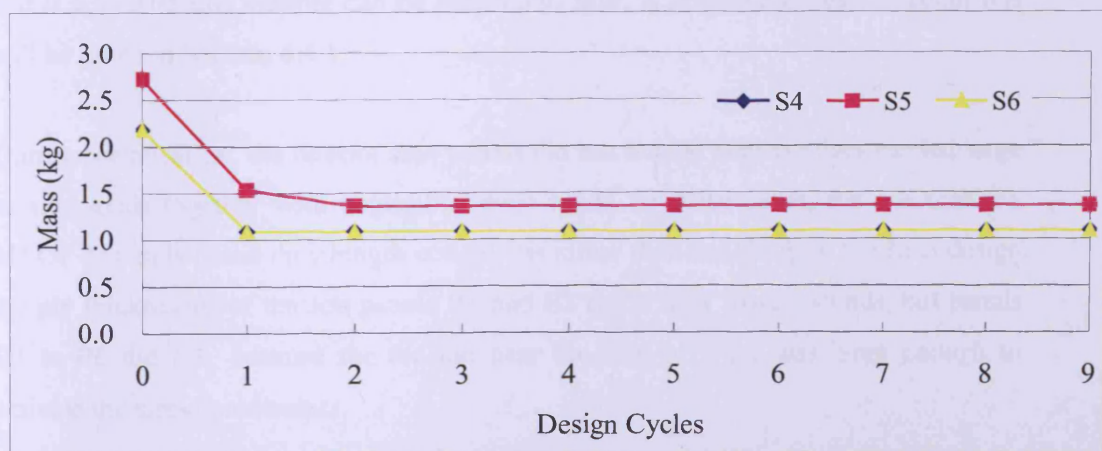


Figure 6.9 Mass changes in panels S4, S5 & S6.

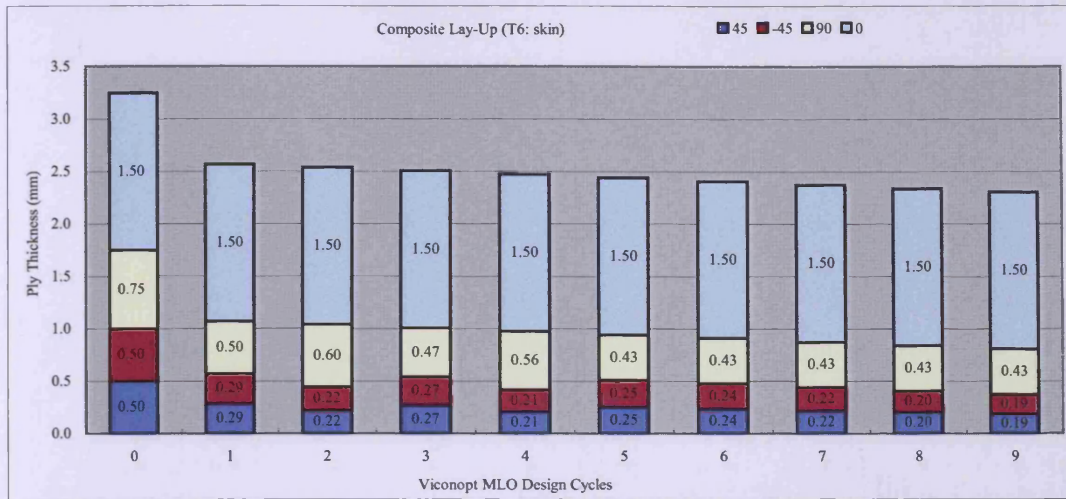
Comparison of these results with those previously obtained using VICONOPT MLO (Fischer *et al.*, 2002a,b), shows significant advantages in terms of mass savings, as shown in Table 6.3. The top skin panels increased in mass in the previous study, but decreased in mass here due to allowing postbuckling effects. Changes in mass in the bottom skin panels were similar in both studies, since their design was limited by stress constraints and not by buckling. Significant weight reduction has been achieved in the spars which were not designed previously, but have been considered in the present work.

		Top skin	Bottom skin	Spars	Total
	Initial design	34.935 kg	34.935 kg	21.216 kg	91.086 kg
	VICONOPT	55.081 kg	10.308 kg	21.216 kg	86.605 kg
Final	MLO	(+57.67%)	(-70.49%)	(±0%)	(-4.92%)
design	VICONOPT	28.796 kg	11.416 kg	10.612 kg	50.825 kg
	MLOP	(-17.57%)	(-67.32%)	(-49.98%)	(-44.20%)

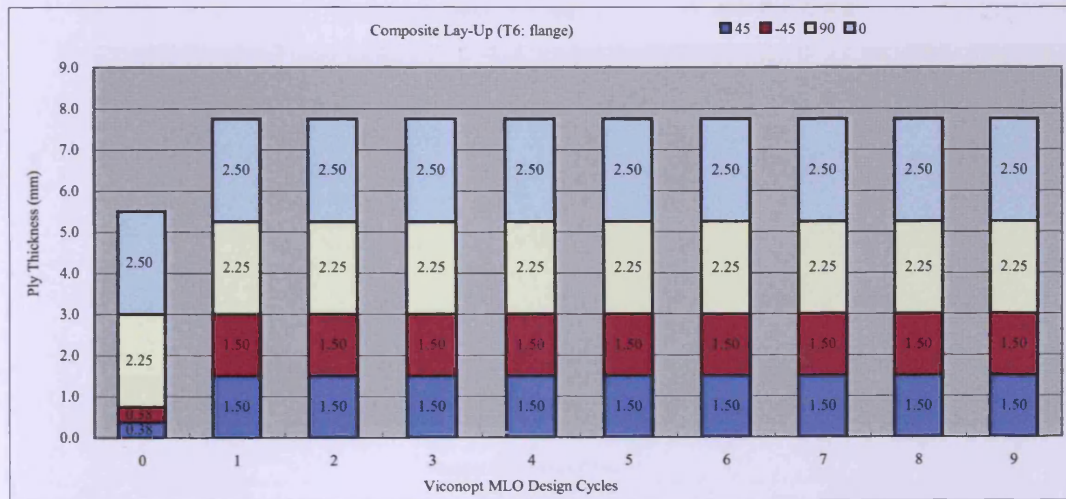
Table 6.3 Mass of designs obtained by two different version of VICONOPT MLO. Percentage changes are relative to the initial design.

The total mass of the wing showed very good convergence after three design cycles (Figure 6.6); the optimisation carried on however, due to mass and load changes in individual panels. The number of design cycles can be reduced by applying a looser convergence criterion ε instead of the 0.01 used during the optimisation. For example, if ε is set to 0.03, the number of design cycles can be reduced to approximately seven, and if ε is 0.05 this number can be reduced to four. A detailed discussion about this will be given in Section 6.4.1.

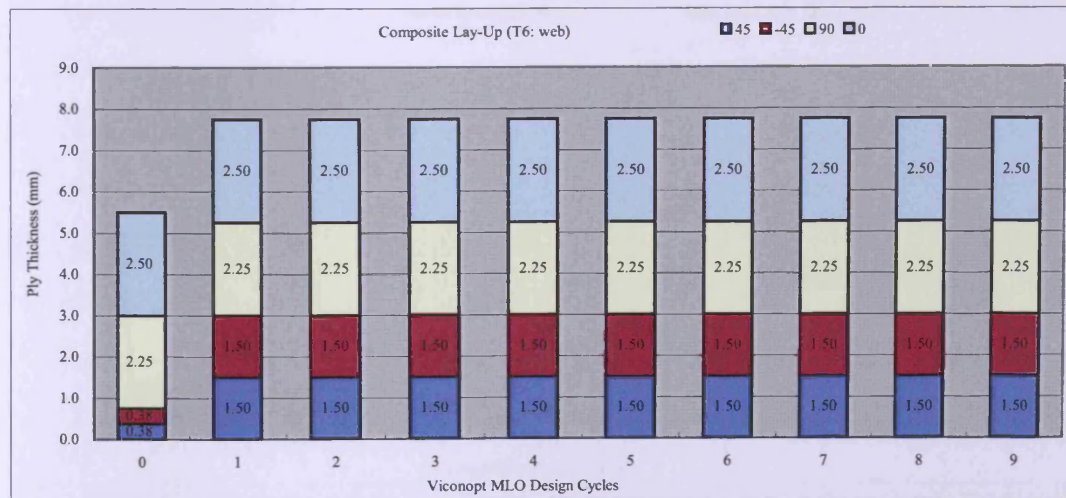
During optimisation, the bottom skin panels did not buckle because they carried large tension loads together with negligible shear loads. In these cases, the VICONOPT MLOP design is based on strength constraints rather than buckling. In the final design, the ply thicknesses of tension panels B1 and B2 reach their lower bounds, but panels B3 to B6 did not, because the tension near the root of wing was large enough to activate the stress constraints.



(a)

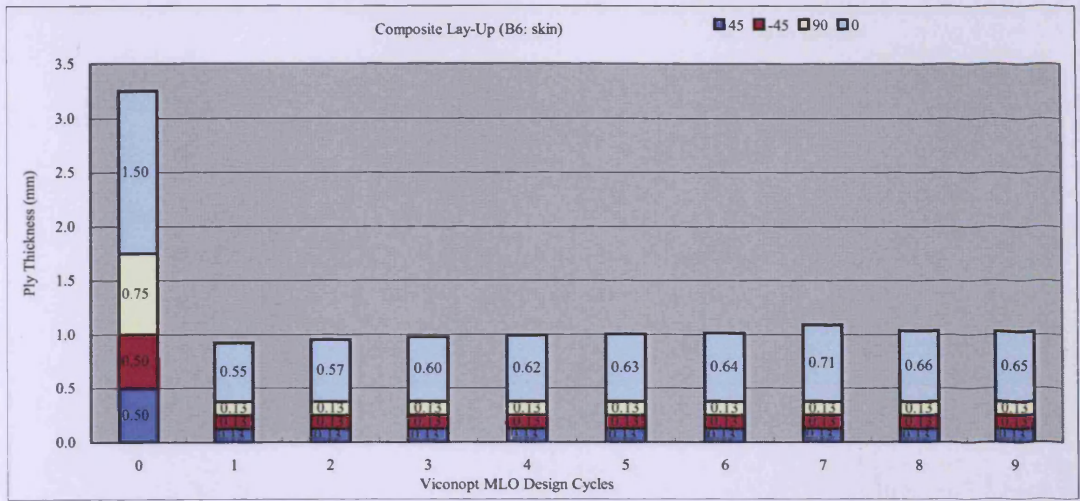


(b)

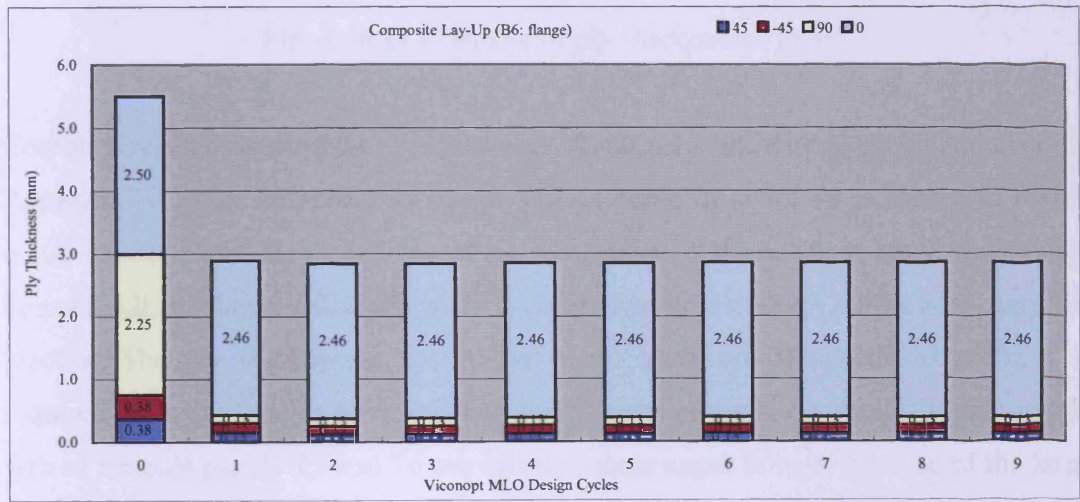


(c)

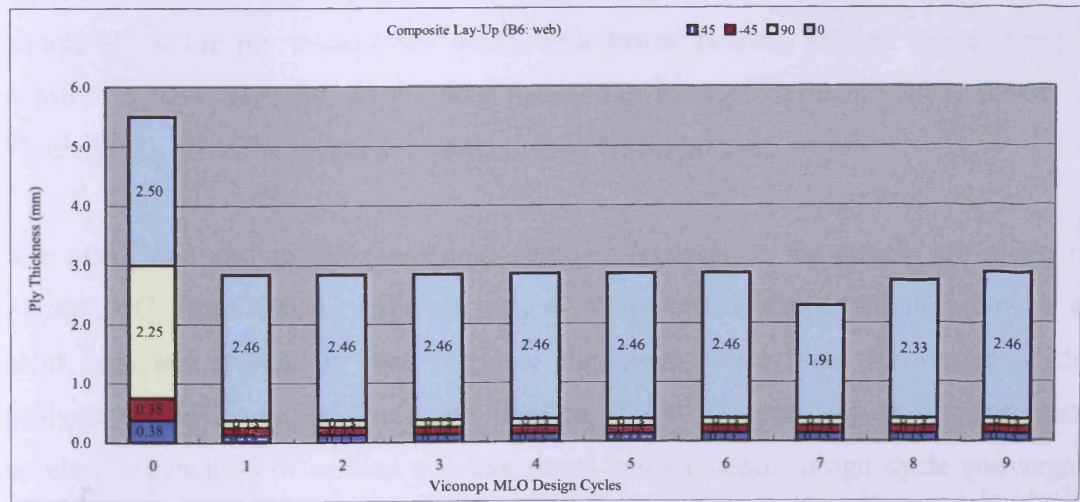
Figure 6.10 Changes of ply thicknesses (T6), (a) skin, (b) flange and (c) web.



(a)



(b)



(c)

Figure 6.11 Changes of ply thicknesses (B6), (a) skin, (b) flange and (c) web.

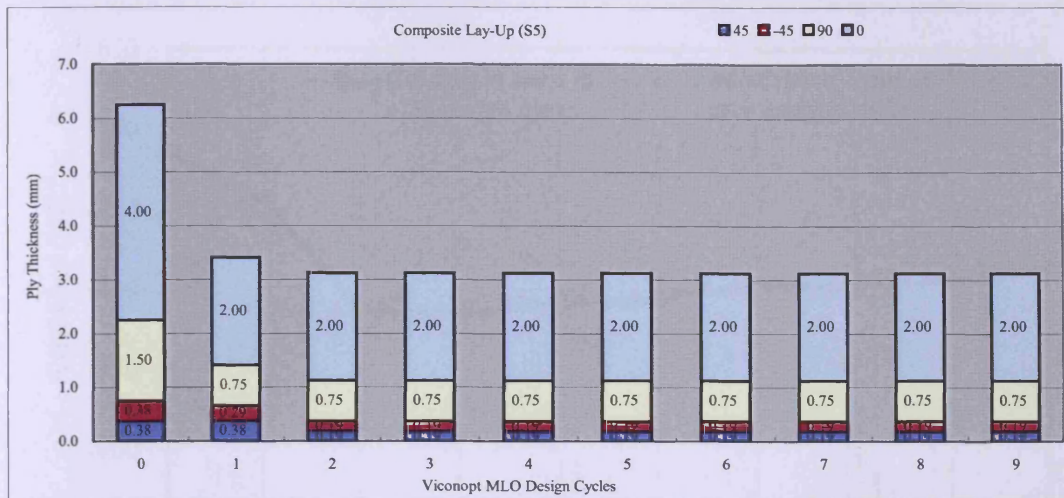
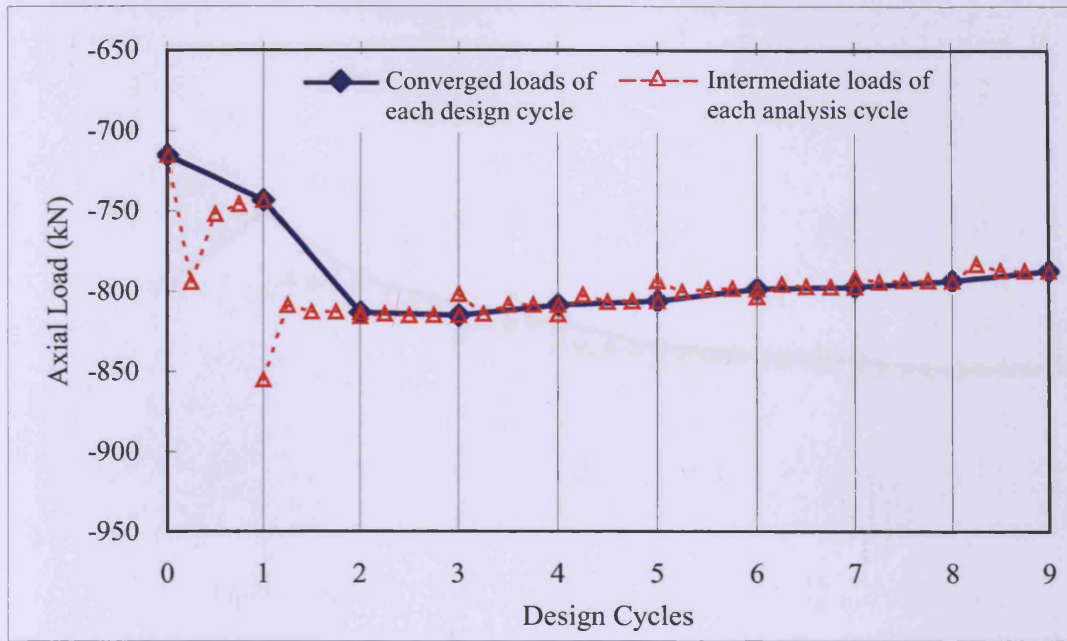


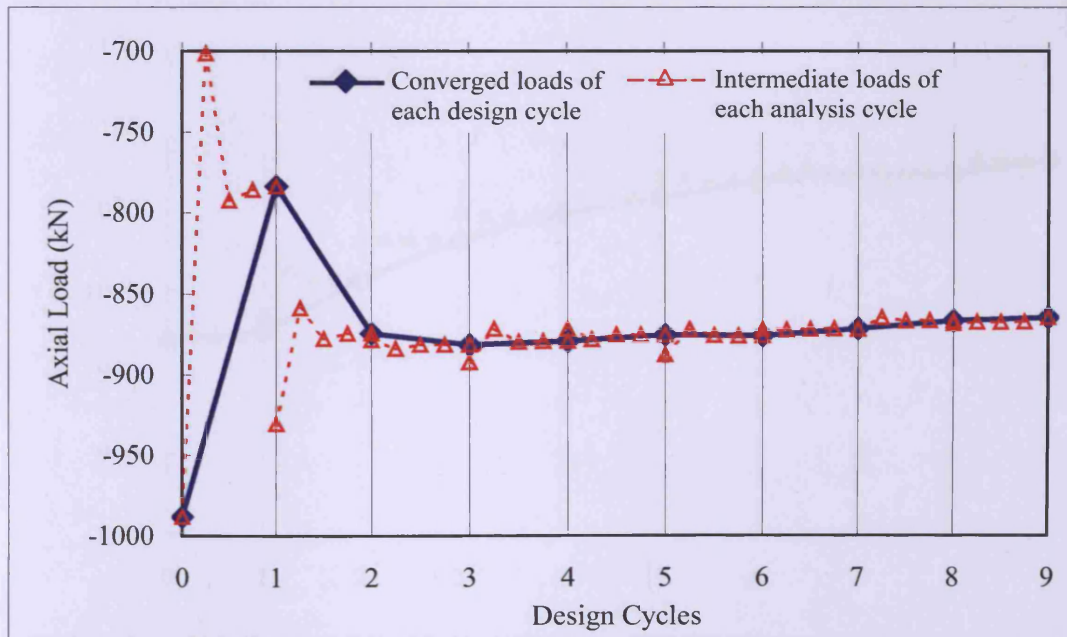
Figure 6.12 Changes of ply thicknesses (S5)

Complete results showing the ply thickness changes for individual panels are given in Appendix B. In the compression panels (an example of panel T6 is shown in Figure 6.10), almost all of the 0° layers, which take most of the loading, reach their upper bounds. All the flange thicknesses are increased to give enough stiffness to carry the loading. The ply thicknesses in the webs are increased if additional stiffness is required after the flanges have reached their upper bounds, e.g. both the flange and web of the root panels T5 and T6 are taken to their upper bounds because of the large compressive load. The thicknesses of some of the $\pm 45^\circ$ layers are increased to carry shear loads. In the tension panels (an example of panel B6 is shown in Figure 6.11), almost all of the ply thicknesses reach their lower bounds, except where strength constraints have been hit. In the spar panels (an example of panel S5 is shown in Figure 6.12), all of the layers are taken to their lower bound.

The axial load and bending moment changes in each of the panels are given in Appendix C. These figures show not only the converged loads of each design cycle in solid lines and marked in blue but also the intermediate loads from each of the analysis cycles in dashed lines and marked in red. By applying the convergence acceleration method of section 4.3, the panel loads in each design cycle converged well within four analysis cycles. However, within each design cycle the loads changed significantly, due to the changes in geometry and postbuckling stiffness.

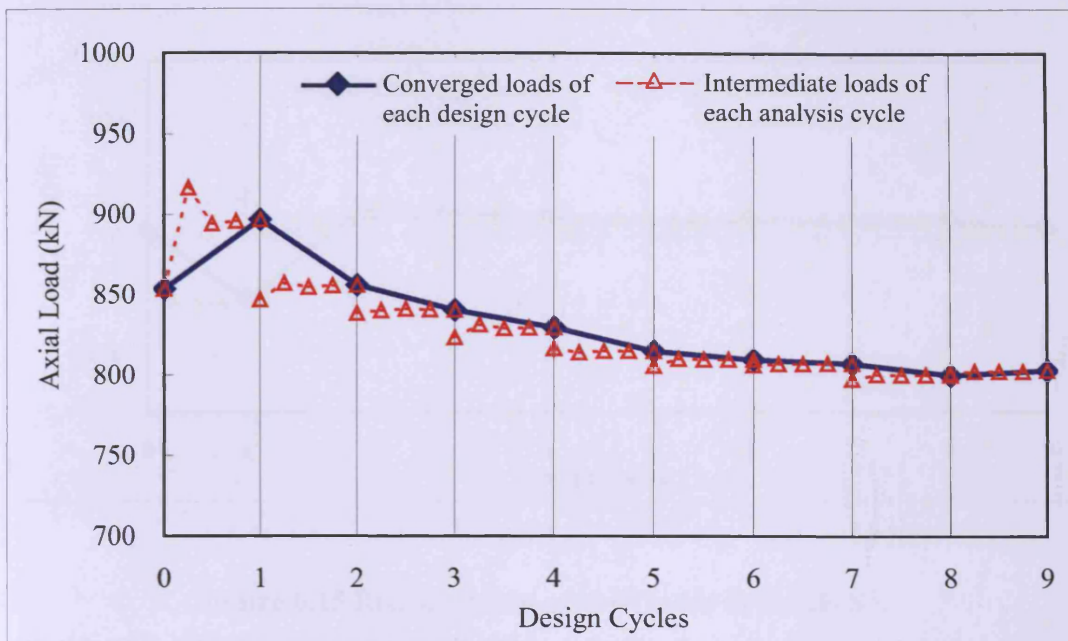


(a)

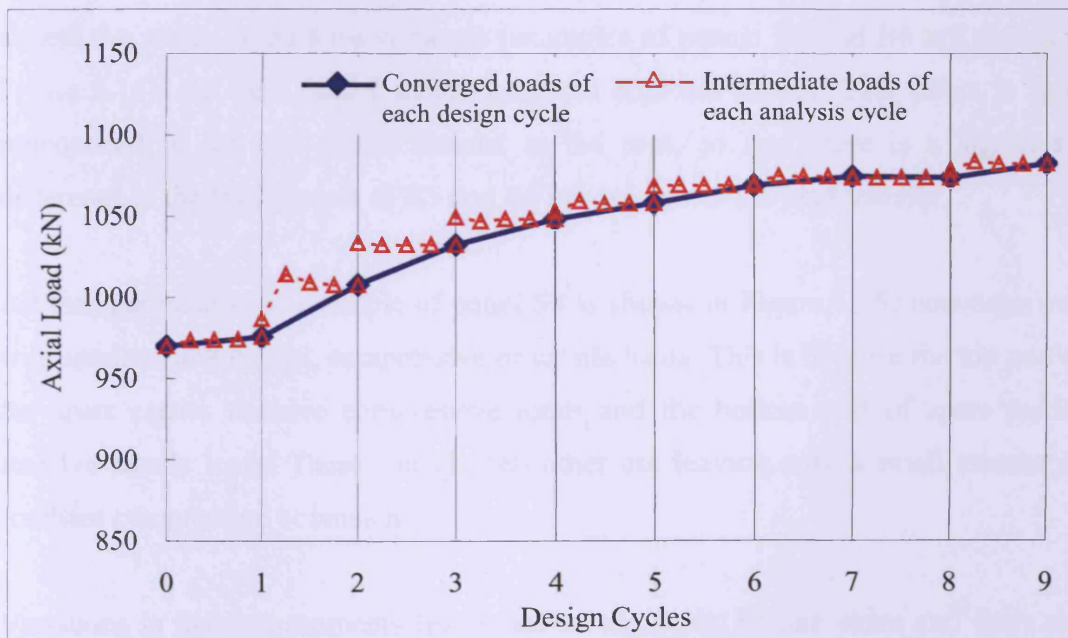


(b)

Figure 6.13 Redistribution of axial loads in panels (a) T5 and (b) T6.



(a)



(b)

Figure 6.14 Redistribution of axial loads in panels (a) B5 and (b) B6.

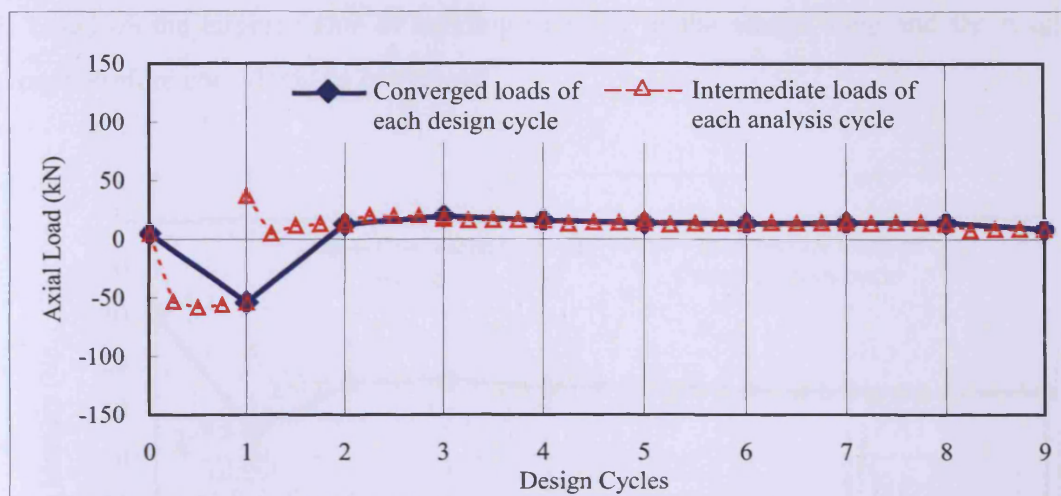


Figure 6.15 Redistribution of axial loads in panels S5.

In the compression panels (examples of panels T5 and T6 are shown in Figure 6.13), the axial load in panels T2, T4 and T6 increases whilst in the adjacent panels T1, T3 and T5 it decreases, so that the final axial compressive loads in adjacent panels are almost the same. In the tension panels (examples of panels B5 and B6 are shown in Figure 6.14), the axial load transfers between adjacent panels. This effect is most pronounced in the two panels nearest to the root, so that there is a significant difference in the final masses of B5 and B6 in response to the load transfer.

All the spar panels (an example of panel S5 is shown in Figure 6.15) converge well with small resultant axial, compressive or tensile loads. This is because the top part of the spars carries massive compressive loads and the bottom part of spars carries massive tensile loads. These cancel each other out leaving only a small amount of resultant compression or tension.

Variations in bending moments (examples of top skins, bottom skins and spars are given in Figures 6.16, 6.17 and 6.18, respectively) are negligible in comparison to the axial loads, and therefore have a much smaller effect. Although the bending moments appear to have converged very well, some of them may still vary by a large percentage of their own initial values. Figure 6.19 shows the same bending moment redistribution as Figure 6.18 using a larger scale related to the panel's own initial values, which appears to give unstable convergence. However, the convergence check

is based on the largest value of bending moment in the whole wing and the results were therefore considered as converged.

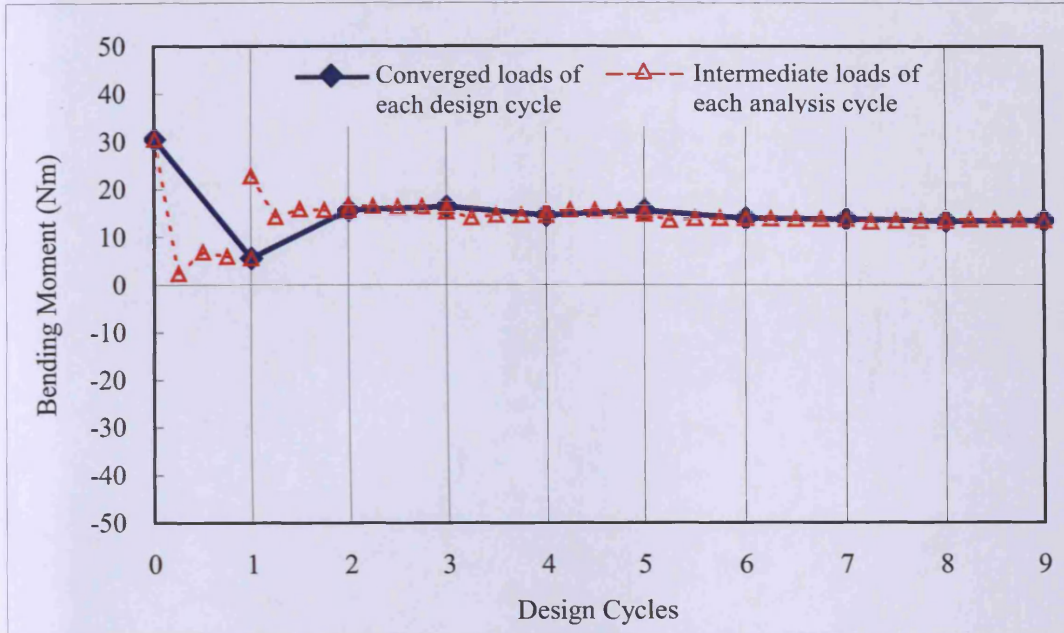


Figure 6.16 Redistribuition of bending moments in panel T6.

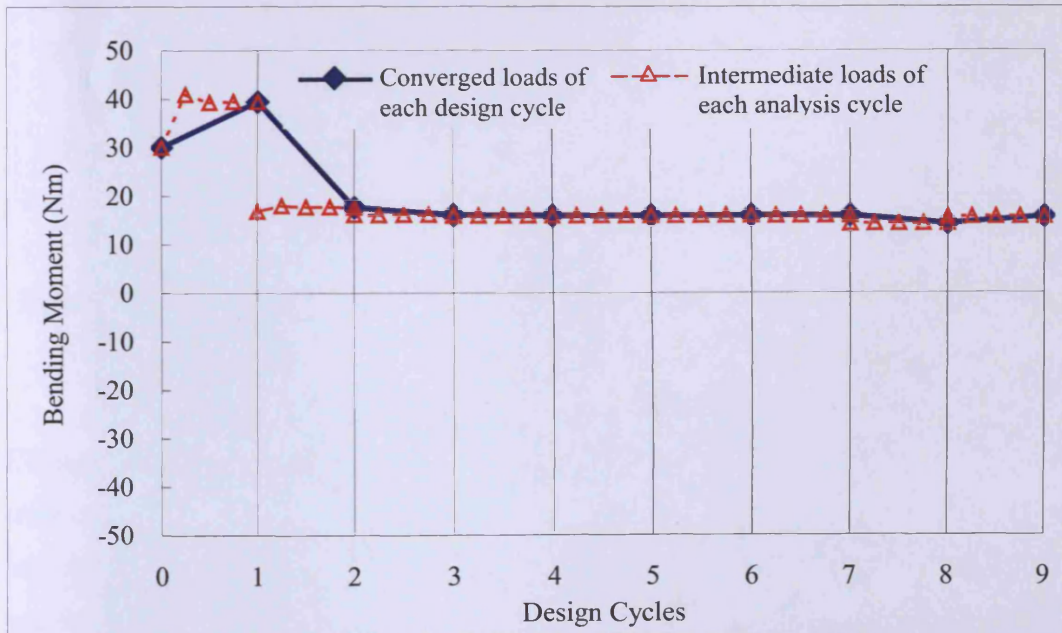


Figure 6.17 Redistribuition of bending moments in panel B6.

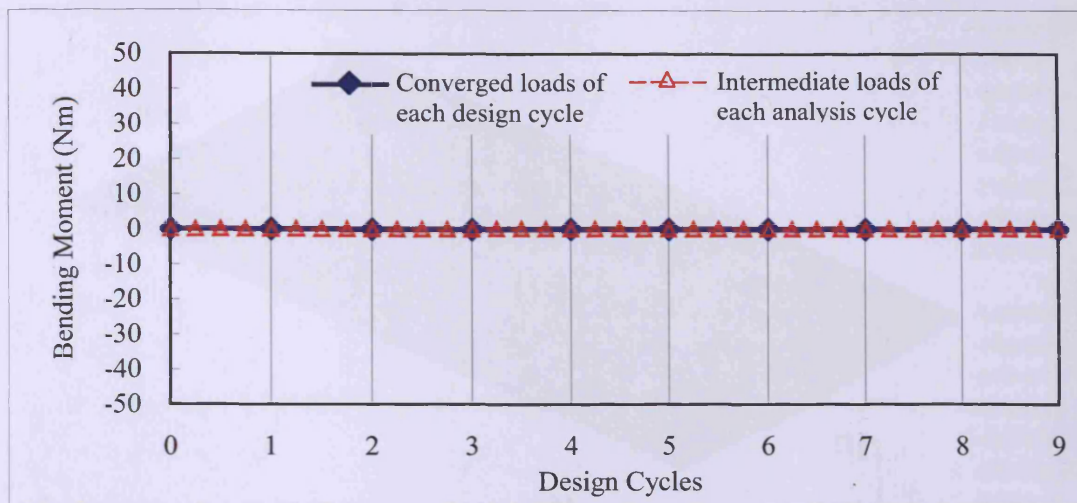


Figure 6.18 Redistribution of bending moments in panel S5.

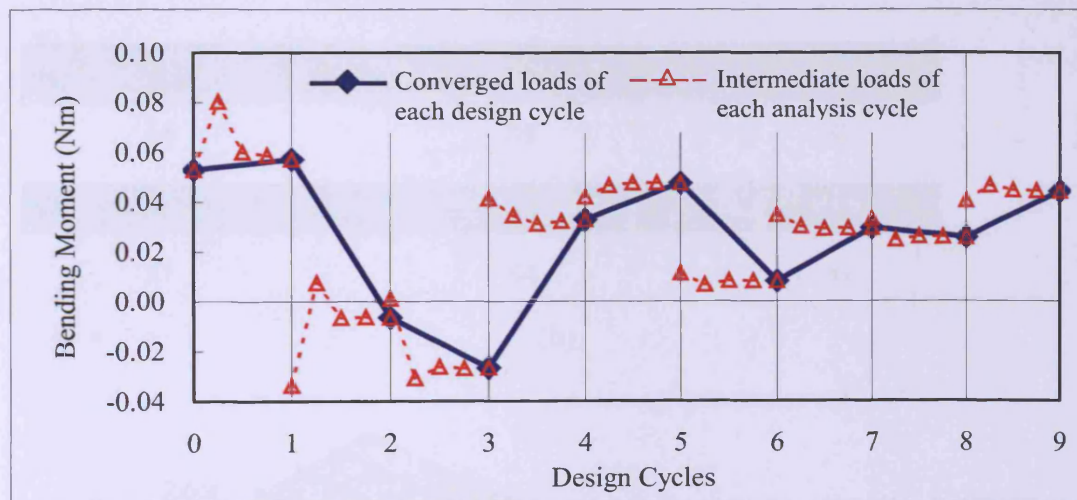


Figure 6.19 Redistribution of bending moments in panel S5 (using different scale of Figure 6.18).

Contours of longitudinal stress for the initial and final designs from NASTRAN are shown in Figures 6.20 and 6.21. Figure 6.21 shows that, at the final design stage, the top skin panels suffer a huge amount of compression and were analysed in the postbuckling region. However, the bottom skin panels carry tension only. Due to the variation in loads applied to the wing, the stresses in the panels on the side where the larger uplift is applied (T2, T4, T6, B2, B4 and B6) are slightly higher as would be expected.

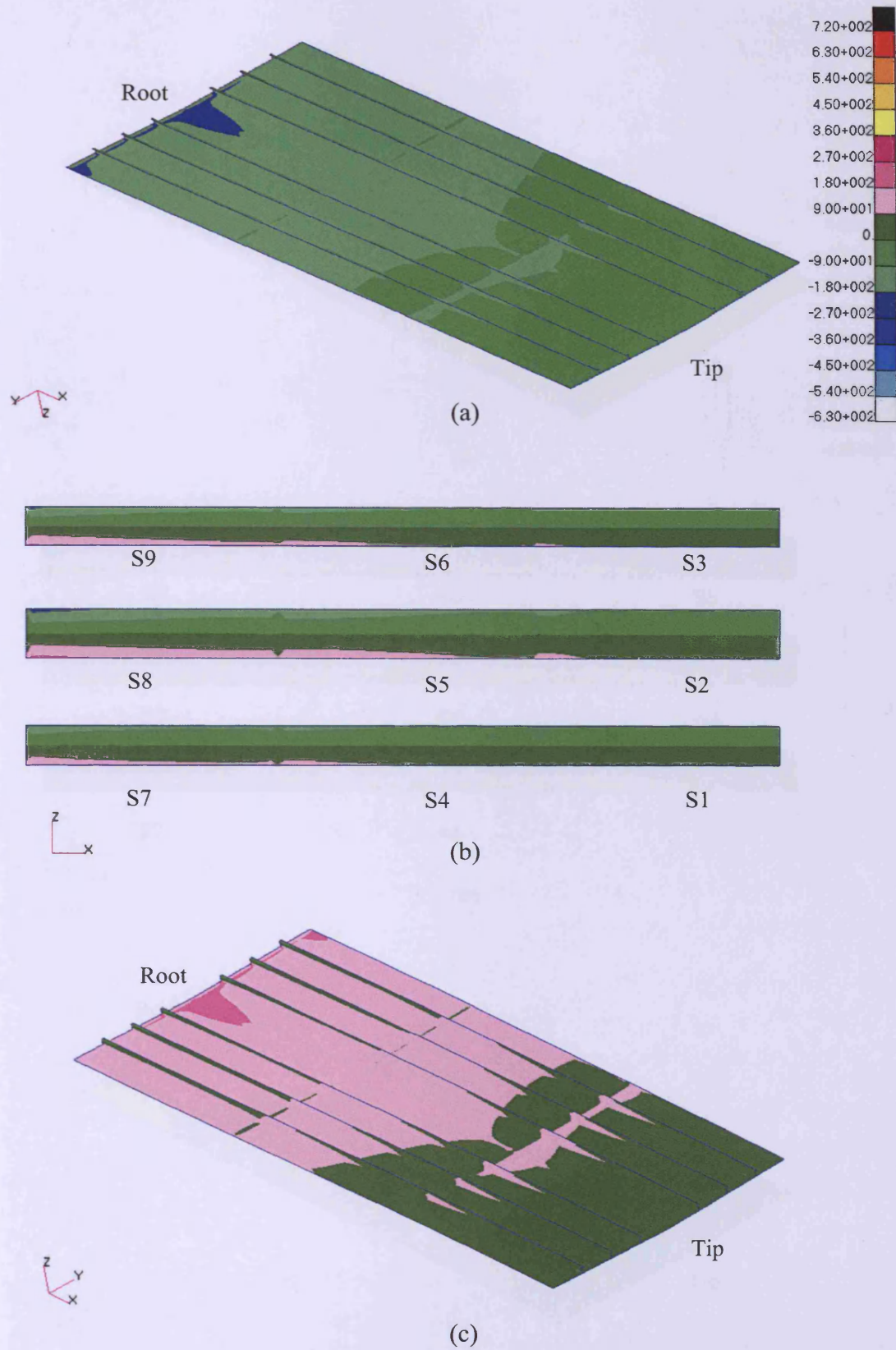


Figure 6.20 Longitudinal stress contours for the initial designs, (a) top skin (b) spars (c) bottom skin (N/mm^2)

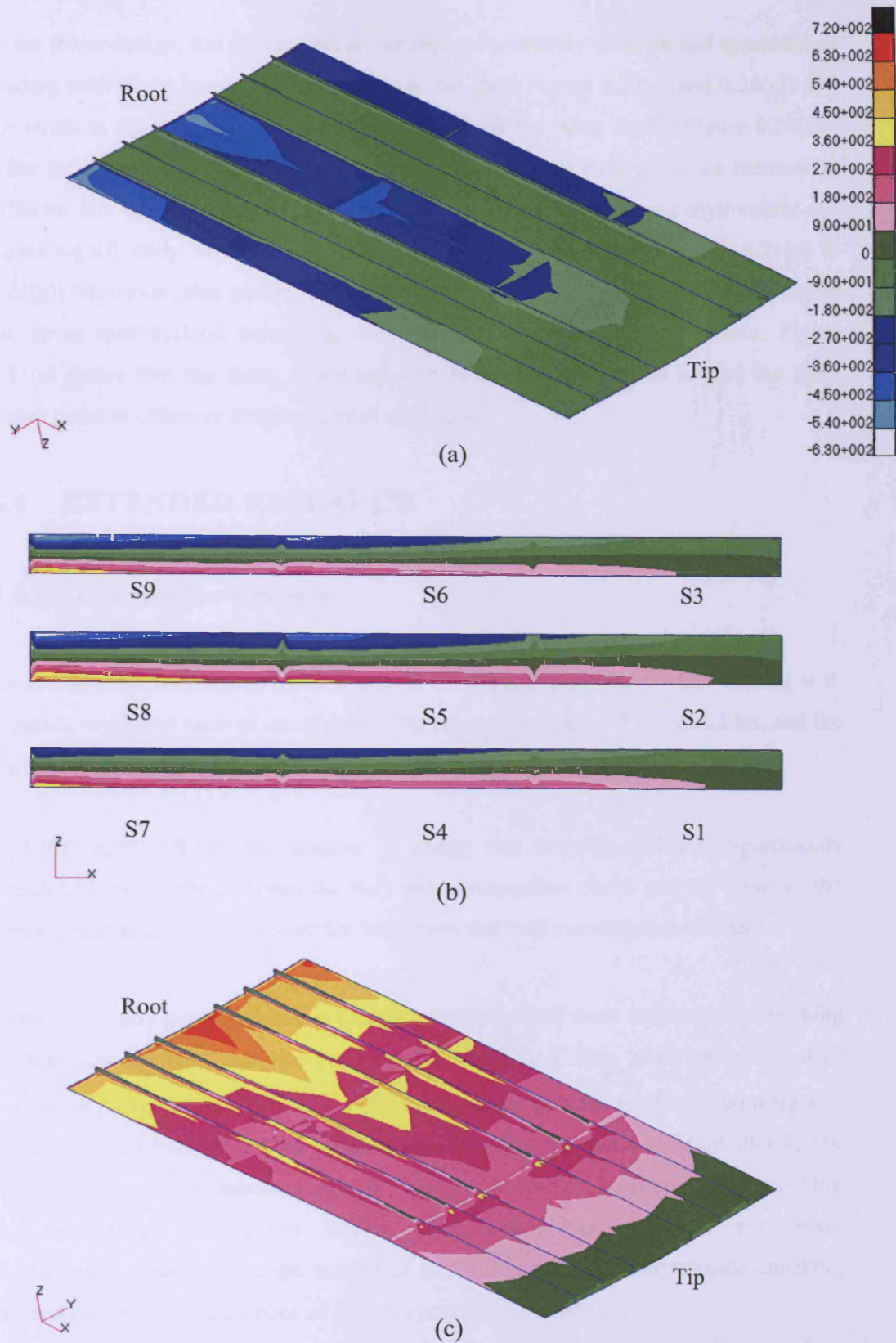


Figure 6.21 Longitudinal stress contours for the final designs, (a) top skin (b) spars and (c) bottom skin (N/mm^2)

In the initial design, the skin panels are under approximately uniform and symmetrical loading with slight increases from the tip to the root (Figure 6.20(a) and 6.20(c)) and the stress in the spar panels varies linearly through the wing depth (Figure 6.20(b)). After the optimisation, since the overall ply thicknesses of each panel are reduced by different amounts in adjacent panels, the stress distribution becomes asymmetric and varies significantly through the length and depth of the wing (Figures 6.21(a) to 6.21(c)). However, this action also balanced out the effect of twisting loads to avoid the stress distributions becoming very different between adjacent panels. Figure 6.21(a) shows that the stress in the top skin panels is concentrated around the spars which provide effective simple support to the skin.

6.4 EXTENDED RESEARCH

6.4.1 Convergence Criteria

As in many optimisation problems, one of the biggest challenges when dealing with complex structures such as an aircraft wing are convergence, which variables, and the multilevel aspect of the problem.

In VICONOPT MLOP, the number of design and analysis cycles is significantly affected by the method chosen for the mass convergence check and the value of the convergence criterion η defined for both mass and load convergence checks.

In the case study presented in this Chapter, the individual mass convergence checking method was selected and the convergence criterion η was taken as 0.01, which required 9 design cycles to satisfy. Figure 6.22 shows how the total mass convergence criterion varied through-out the optimisation. This criterion reached 0.009 after design cycle two, but the optimisation carried on due to some individual panels not reaching their individual convergence criteria. This proves that using the total mass convergence checking method instead of the individual mass convergence checking method can reduce the number of design cycles significantly.

The number of design and analysis cycles can also be reduced by increasing the value of the convergence criterion η . An example of the mass convergence checking from the case study is shown in Tables 6.4-6.6. All the panels converged to less than 2% of their individual mass after design cycle 3. The whole wing would be considered as converged on mass after design cycle 2 if the convergence criterion η was greater than 6.42%.

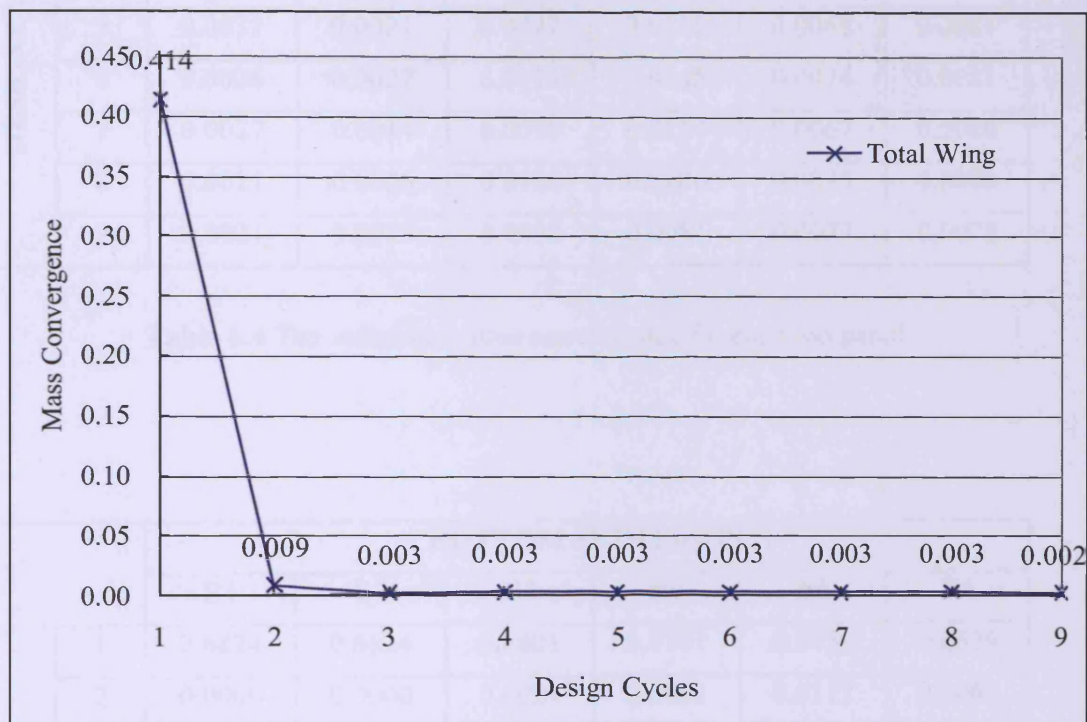


Figure 6.22 The total mass convergence through out the optimisation.

		TOP SKIN PANELS					
		T1	T2	T3	T4	T5	T6
DESIGN CYCLES	1	0.1408	0.1307	0.1527	0.1315	0.0682	0.0683
	2	0.0005	0.0116	0.0261	0.0416	0.0071	0.0070
	3	0.0025	0.0020	0.0101	0.0132	0.0067	0.0079
	4	0.0028	0.0033	0.0119	0.0101	0.0077	0.0075
	5	0.0031	0.0021	0.0092	0.0111	0.0068	0.0081
	6	0.0026	0.0027	0.0113	0.0145	0.0074	0.0081
	7	0.0027	0.0014	0.0095	0.0124	0.0067	0.0080
	8	0.0021	0.0026	0.0120	0.0100	0.0075	0.0078
	9	0.0021	0.0013	0.0098	0.0081	0.0077	0.0078

Table 6.4 The individual mass convergence for each top panel.

		BOTTOM SKIN PANELS					
		B1	B2	B3	B4	B5	B6
DESIGN CYCLES	1	0.6824	0.6824	0.6801	0.6701	0.6839	0.6629
	2	0.0000	0.0000	0.0021	0.0051	0.0117	0.0063
	3	0.0000	0.0000	0.0000	0.0037	0.0039	0.0060
	4	0.0000	0.0000	0.0011	0.0026	0.0028	0.0040
	5	0.0000	0.0000	0.0010	0.0002	0.0037	0.0025
	6	0.0000	0.0000	0.0004	0.0017	0.0014	0.0028
	7	0.0000	0.0000	0.0001	0.0010	0.0006	0.0014
	8	0.0000	0.0000	0.0001	0.0018	0.0018	0.0003
	9	0.0000	0.0000	0.0016	0.0025	0.0008	0.0023

Table 6.5 The individual mass convergence for each bottom panel.

		SPAR PANELS								
		S1	S2	S3	S4	S5	S6	S7	S8	S9
DESIGN CYCLES	1	0.4998	0.4998	0.4998	0.4998	0.4356	0.4998	0.4998	0.4998	0.4998
	2	0.0000	0.0000	0.0000	0.0000	0.0642	0.0000	0.0000	0.0000	0.0000
	3	0.0000	0.0000	0.0000	0.0000	0.0000	0.0000	0.0000	0.0000	0.0000
	4	0.0000	0.0000	0.0000	0.0000	0.0000	0.0000	0.0000	0.0000	0.0000
	5	0.0000	0.0000	0.0000	0.0000	0.0000	0.0000	0.0000	0.0000	0.0000
	6	0.0000	0.0000	0.0000	0.0000	0.0000	0.0000	0.0000	0.0000	0.0000
	7	0.0000	0.0000	0.0000	0.0000	0.0000	0.0000	0.0000	0.0000	0.0000
	8	0.0000	0.0000	0.0000	0.0000	0.0000	0.0000	0.0000	0.0000	0.0000
	9	0.0000	0.0000	0.0000	0.0000	0.0000	0.0000	0.0000	0.0000	0.0000

Table 6.6 The individual mass convergence for each spar panel.

6.4.2 Convergence Acceleration

As described in Section 4.3, load convergence acceleration is performed to calculate the loads for the VICONOPT input files after two analysis cycles in each design cycle.

Figure 6.23 illustrates the benefits achieved by applying the convergence acceleration method. It shows the load acting on panel T4 on the top surface within the first design cycle. Without applying the convergence acceleration method, it takes 16 analysis cycles to get the load to converge, but only 4 analysis cycles are required when this is applied. This proves the capability of the method in increasing efficiency and reducing computational cost.

Furthermore, the values of the load at the convergence point have less than 1% variation, which proves the accuracy of the method.

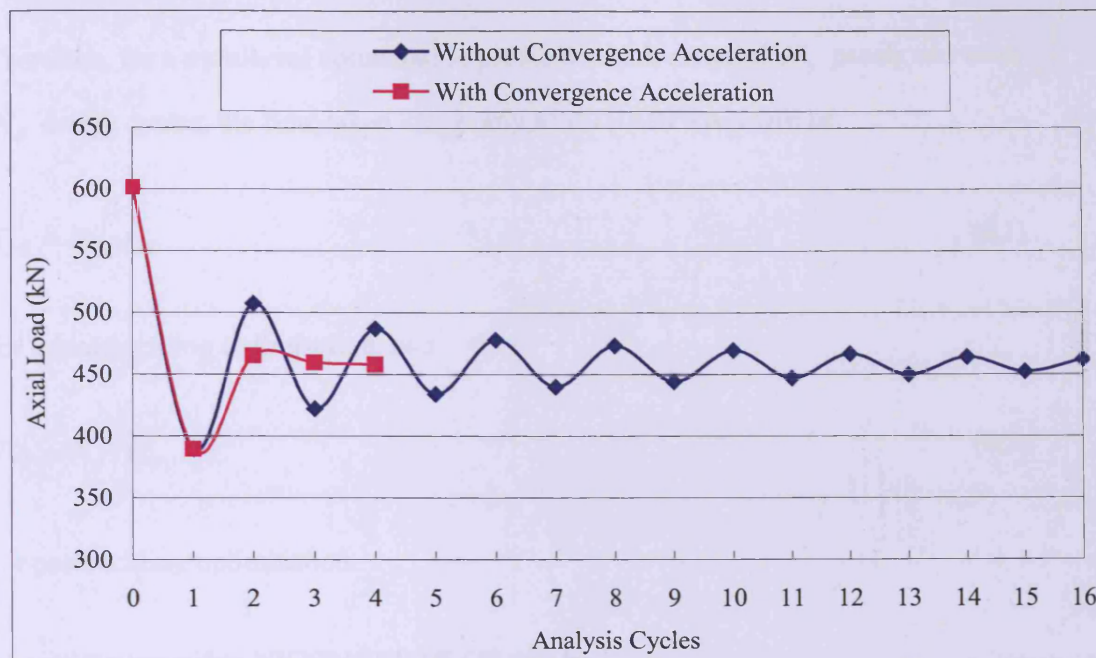


Figure 6.23 Load convergence with and without convergence acceleration.

6.4.3 Computational Efficiency

VICONOPT MLO was developed to be a computationally efficient program. To compare with optimisation using only finite element software, such as MSC/NASTRAN, the time saved on any multilevel optimisation problem by using VICONOPT MLOP can be estimated using the following method.

Using MSC/NASTRAN, the time taken to complete a static analysis, a finite element buckling analysis and a finite element postbuckling analysis are t_{Ms} , t_{Mb} and t_{Mp} respectively.

Using VICONOPT, analysis of each panel takes t_{Vd} and t_{Va} for a buckling design and a postbuckling analysis respectively.

The time required for all the VICONOPT MLOP processes in each design/analysis cycle, i.e. data conversion and convergence checking, is φ .

Therefore, for a multilevel optimisation problem which contains N_p panels and takes N_d design cycles, the time taken using only MSC/NASTRAN will be

$$T_{FE} = N_d \cdot t_{Mb} \quad (6.1)$$

for initial buckling optimisation, and

$$T'_{FE} = N_d \cdot t_{Mp} \quad (6.2)$$

for postbuckling optimisation.

The time taken using VICONOPT MLOP will be

$$T_{MLO} = N_d(t_{Ms} + \varphi + N_p \cdot t_{Vd}) \quad (6.3)$$

for initial buckling optimisation, and

$$T'_{MLO} = N_d(N_a(t_{Ms} + \varphi + N_p \cdot t_{Vd}) + t_{Ms} + \varphi + N_p \cdot t_{Vd}) \quad (6.4)$$

for postbuckling optimisation, where N_a is the number of analysis cycles within each design cycle.

Taking the case study which is presented in this Chapter as an example, Table 6.7 gives the time parameters for different software and the number of design and analysis cycles involved.

Note the values shown in Table 6.7 are average values through out the optimisation, and were measured on a Core™ 2 Duo, 2GHz, 1.96GB RAM computer.

Parameters for VICONOPT MLOP	N_p	21
	N_d	9
	N_a	4
	φ	240 seconds
Parameters for MSC/NASTRAN	t_{Ms}	54.6 seconds
	t_{Mb}	2302.4 seconds
	t_{Mp}	4709.8 seconds
Parameters for VICONOPT	t_{Vd}	2.0 seconds
	t_{Va}	0.2 seconds

Table 6.7 Parameters of the example for efficiency calculation.

The estimated time taken for optimising the example model using the two different optimisation techniques is shown in Table 6.8. In comparison with the finite element software MSC/NASTRAN, VICONOPT MLOP has a significant advantage in term of time saving. In optimising the example model, VICONOPT MLOP takes less than 30% of the time used by MSC/NASTRAN.

Optimisation Techniques	Buckling Optimisation	Postbuckling Optimisation
MSC/NASTRAN	$T_{FE} = 20722$ seconds	$T'_{FE} = 42388$ seconds
VICONOPT MLOP	$T_{MLO} = 3029$ seconds	$T'_{MLO} = 11626$ seconds
% Reduction	85.4%	72.6%

Table 6.8 Time taken for different optimisation techniques.

6.5 CONCLUSION

A case study involving the design of a whole aircraft wing is presented in this chapter. This has enabled a more detailed insight into the multilevel optimisation process and postbuckling behaviour of a complex structure. The results of the study show the total mass of the wing is reduced by 44% through optimisation, with the skin panels being reduced by approximately 42%. This compares to the results from the previous version of VICONOPT MLO (Fischer *et al.*, 2002a,b), with a further 36% of total mass being saved.

The final design of the panels is based on thick flanges or webs and much thinner skins. This is because, without a strict bound, skin plates always try to transfer load into the stringers and spars, and compared to the spars, the initial thicknesses of the stringers are too small to carry the load.

The multilevel optimisation carried out proved to be very efficient and displayed good convergence. Although the finite element model at system level was very large and a lot of data had to be transferred between the different levels, due to the efficiency of VICONOPT MLOP, the multilevel optimisation process required only 5-7 minutes to complete an analysis cycle on a Core™ 2 Duo, 2GHz, 1.96GB RAM, and of the overall solution time, less than 10% was spent in VICONOPT, around 40% was spent in VICONOPT MLOP and 50% was spent in MSC/NASTRAN.

Chapter 7

Conclusion and Recommendations for Future Work

7.1 CONCLUSIONS

This thesis presents the research work carried out during the author's PhD study period. The main objective of this work was to develop the multilevel optimisation software VICONOPT MLO, in order to incorporate postbuckling effects in the optimisation, enabling small amounts of stable postbuckling to occur in the optimised structure, hence further reducing the structure's mass. This objective has been achieved by a continuous research process, which consisted of three major parts.

The first part involved the study of the theories of buckling and postbuckling, optimisation, multilevel optimisation and C++ computer programming, in order to become familiar with the computer software VICONOPT, MSC/NASTRAN and VICONOPT MLO. In this thesis, this part of the research is reported in Chapters 2 and 3.

The second part, which was the most major and complex part of the research, and which took the longest time was the development of the software VICONOPT MLOP. The objective of this part was to find a solution to the problem of incorporating postbuckling into the optimisation problem whilst maintaining appropriate convergence. The theories on which the software is based are reported in Chapter 4. After coding these theories into VICONOPT MLO, the size of the program almost tripled. The new software VICONOPT MLOP not only allows multilevel optimisation to be carried out incorporating postbuckling effects but also provides improved design convergence procedures and manual and computational input/output data systems. In

the same way as for VICONOPT MLO, the development of VICONOPT MLOP is based on widely accepted standards for good Windows software design and great care has been taken to ensure the software package is at least as user-friendly as before or even better. An introduction into the multilevel optimisation procedures of VICONOPT MLOP is given in Chapter 5, which gives an overall view of how the postbuckling behaviour has been set up in the model.

The last part of the work involved testing the software. The use of VICONOPT MLOP has been demonstrated for the multilevel optimisation of a composite aircraft wing with twelve longitudinally stiffened panels and nine spar panels as described in Chapter 6. The multilevel optimisation carried out proved to be very efficient, and displayed good convergence on both mass and load. A total of 9 design cycles were carried out before the mass of each individual panel had converged and 4 analysis cycles were required within each design cycle to achieve load convergence. The results show that the total mass of the whole wing reduced by 44% throughout the optimisation, and that of the skin panels reduced by approximately 42%. This compares with the results from VICONOPT MLO (Fischer *et al.*, 2002a), with a further of 36% of total mass saved.

The main objective of this design study was to gain a more detailed insight into the multilevel optimisation of complex structures. A number of extended research studies were therefore carried out to prove the accuracy of some of the methods used in the software, e.g. the convergence acceleration method.

The objective of the research work was therefore achieved successfully by completing the three continuous steps described above. Whilst the software VICONOPT MLOP requires further development to enable it to be used in a commercial situation, this development has enabled substantial improvement of the software and multilevel optimisation in the postbuckling region. In this way, mass, and therefore economic and environmental cost, are reduced. Due to the significant speed of VICONOPT's analysis and optimisation procedures, it is believed that the VICONOPT MLO suite of software will become one of the most competitive tools for multilevel optimisation after more valuable developments. Some possible further developments are recommended in the following sections.

7.2 FUTURE STUDY AND DEVELOPMENT

7.2.1 Further Research Area Expansion

Chapter 5 in this thesis can be used as a brief manual of VICONOPT MLO. However, a more formal user manual and/or online help information for the software is an important future requirement.

Further developments of the VICONOPT MLO suite of software should be carried out in order to achieve the following tasks:

Implementation of some of the remaining features of VICONOPT in VICONOPT MLO, including the use of discrete design variables for multilevel optimisation, both with and without a postbuckling design capability.

Allowing more types of design variables and constraints; for example, plate widths, material strength constraints, and the geometric dimensions of the overall structure. Some of these changes may require mesh regeneration of the finite element model, which may lead to the reconstruction of the VICONOPT MLO data converter.

Investigation of more realistic wing models which include more complicated structures, e.g. damaged panels, curved panels and non-rectangular panels. This will require an exploration of VICONOPT MLO's performance in the context of multilevel postbuckling optimisation.

Additional case studies on more civil engineering and architectural designs, e.g. modern vehicles, spacecraft, thin-shell structures, etc, which will require a multi-disciplinary development and might begin from the fuselage section of the aircraft and the whole aircraft.

Enabling more practical manufacturing requirements to be taken into consideration during the optimisation, e.g. ply drop-off construction requirements.

Considering the possibility of connecting VICONOPT MLO with other commonly used software, for example, AutoCAD (Autodesk, 2011) and ABAQUS (ABAQUS, 1998), to increase the versatility of VICONOPT MLO.

7.2.2 Further Manual Input Simplification

Currently, VICONOPT MLOP is a standalone version of VICONOPT MLO, specifically for postbuckling design. If users want to optimise an initial buckling problem, they need to run the original VICONOPT MLO. It would be a great advantage if the user were allowed to optimise a problem with or without postbuckling effects in one program. Input data could be transferred automatically from one analysis to the other. The user would then only need to input the specific data which is not common to both types of analysis.

In VICONOPT MLOP, a new feature using ‘default values’ during the manual input process was shown to reduce the manual workload. This is explained in Section 5.1. The case study proved that using these ‘default values’ could halve the time required for user input. However, the time spent on manual input for the case study is still about half an hour. Therefore, further manual input simplification is required for more complicated structures. Two possible developments can be carried out in the future to achieve this requirement.

A feature could be developed to allow the user to group the panels which require the same input parameters. The users then only need to modify these parameters once for the group rather than type them in many times for each panel. A good example taken from the finite element software MSC/PATRAN is shown in Figure 7.1. The user first selects all the components (Figure 7.1[1]) to create a set (Figure 7.1[2]), and then specifies input data for the whole set.

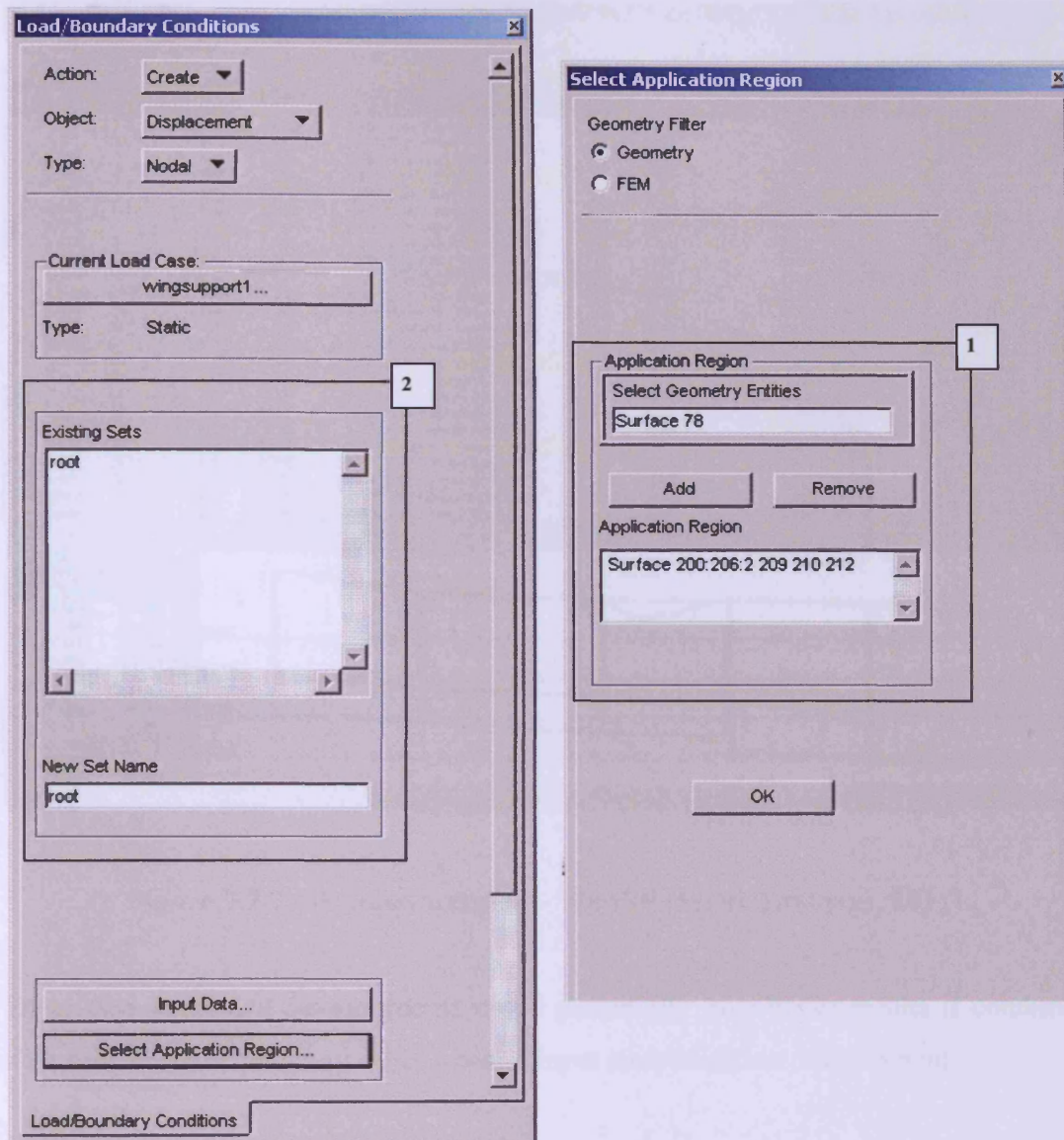


Figure 7.1 Group input — MSC/PATRAN.

Another development which would simplify the manual input procedure is the use of tabular input format. The example shown in Figure 7.2 is from the well-known drainage design suite WinDes (Micro Drainage, 2011). By displaying all the information in one table, the user can modify the parameters easily without entering individual windows, making it easier to notice and correct any mistakes and minimizing the risk of missing an entry.

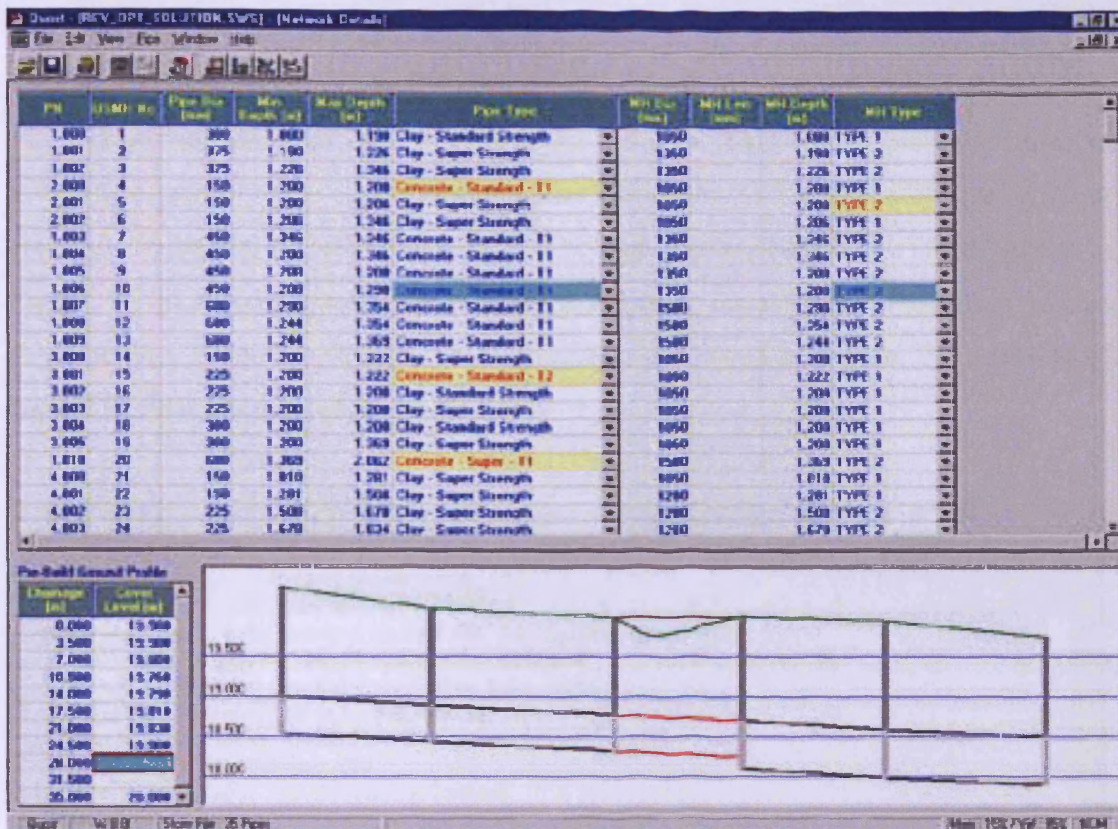


Figure 7.2 Table input format — WinDes (Micro Drainage, 2011).

These two suggested developments could potentially give better results if combined with each other or with any other manual input simplification development.

7.2.3 Further VICONOPT MLO Data File Development

As part of the development of VICONOPT MLOP, two text files are created during the optimisation process. One stores all the input data and the other one stores all the convergence information. Further developments could be made based on the suggestion given below.

Currently, VICONOPT MLOP input files known as ‘save files’ (Section 5.2.10) consist of one text file and one binary file. The user cannot modify the binary file directly, and is not able to edit the information in the text file easily without being familiar with VICONOPT MLOP’s background code, since no descriptions are included to explain the meaning of the data.

Further development might be made to combine these two input files into one big text file and provide detailed descriptions about the data. This would enable the user to generate or modify the optimisation model using any text editor software, without entering the data in VICONOPT MLOP. The input file for MSC/NASTRAN shown in Figure 7.3 is a very good example of text format input files. In addition to this development, a quick reference guide might be published to explain the meaning of each single data item used in the text file.

```

$ NASTRAN input file created by the MSC MSC.Nastran input file
$ translator ( MSC.Patran 13.1.089 ) on November 07, 2010 at 02:43:30.
$ Direct Text Input for Nastran System Cell Section
$ Direct Text Input for File Management Section
$ Implicit Nonlinear Analysis
SOL 600,NLSTATIC OUTF=op2,f06
$ Direct Text Input for Executive Control
CEND
SEALL = ALL
SUPER = ALL
IITLE = MSC.Nastran job created on 19-Feb-02 at 09:06:06
$ Direct Text Input for Global Case Control Data
SUBCASE 1
$ Subcase name : wingsupport2
SUBTITLE=wingsupport2
NLPARM = 1
SPC = 2
LOAD = 2
$ Direct Text Input for this Subcase
BEGIN BULK
PARAM POST -1
PARAM PRITMAXIM YES
PARAM LGDISP 1
PARAM MARCSLHT 5
MARCOUT E311 E321 E341 N1 N5 N34 N2
E301
NLPARM 1 20 ITER 1 20 P YES

```

Figure 7.3 Typical MSC/NASTRAN input file.

In comparison with the input files, the VICONOPT MLOP output file, which stores all the convergence information, is quite well formatted (Section 5.3.5). One feature which could be developed in the future, would be to give the capability to VICONOPT MLOP to display this data in the form of diagrams. An example from WinDes is shown in Figure 7.4. This would remove the need for the user to copy this

data into Excel and enable them to monitor the convergence for example during the optimisation process.

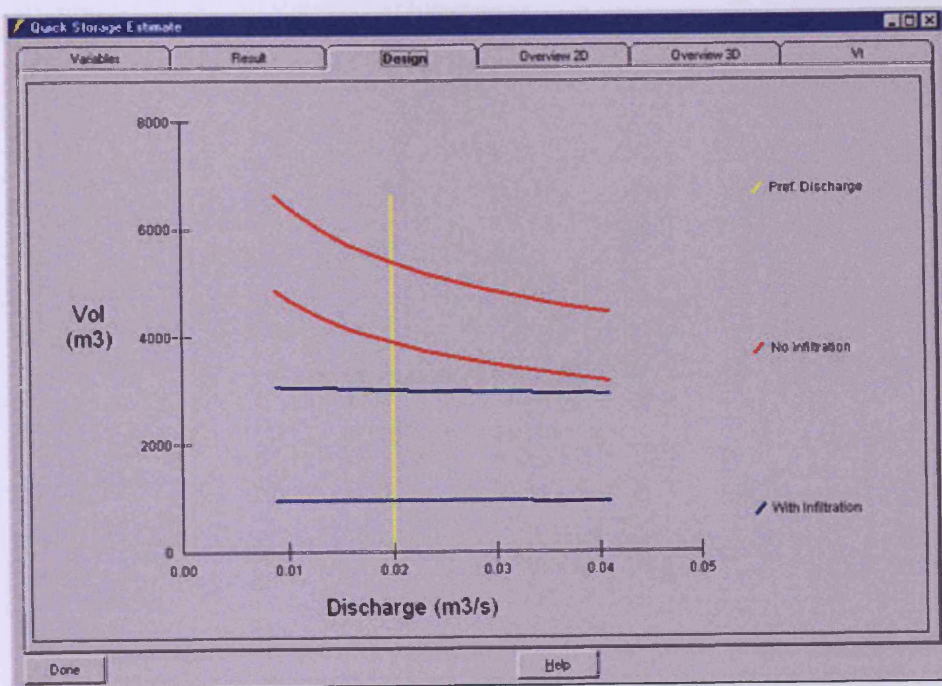


Figure 7.4 Results diagram — WinDes (Micro Drainage, 2011).

Appendix A

Mass changes in individual panels

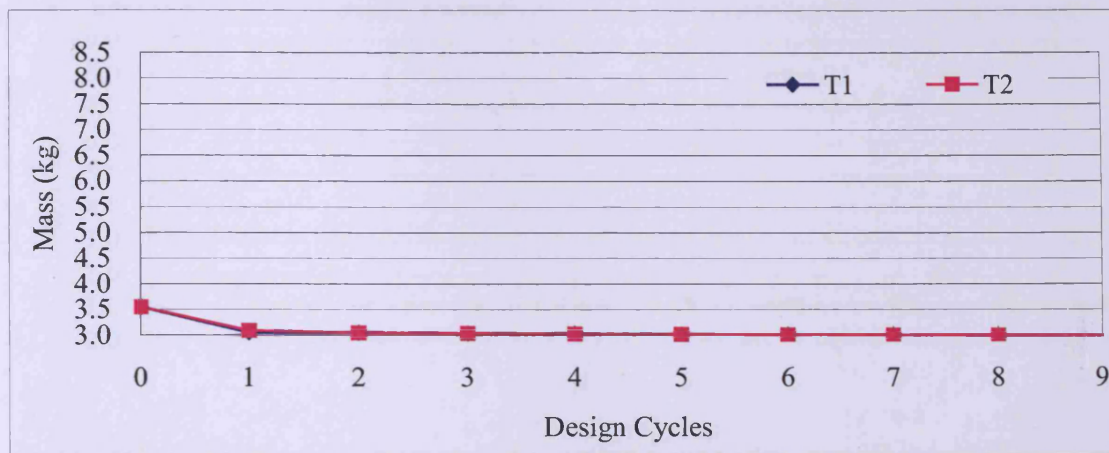


Figure A.1 Mass changes in panels T1 & T2.

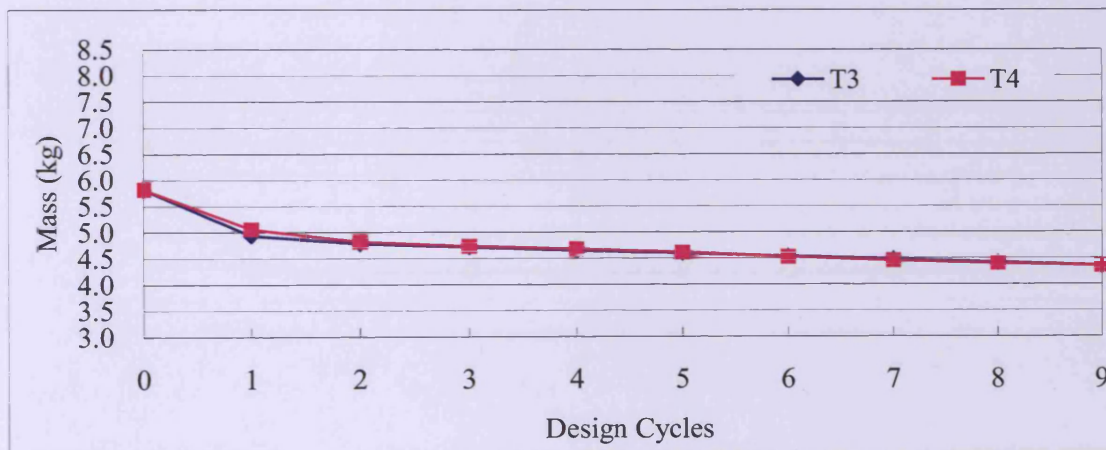


Figure A.2 Mass changes in panels T3 & T4.

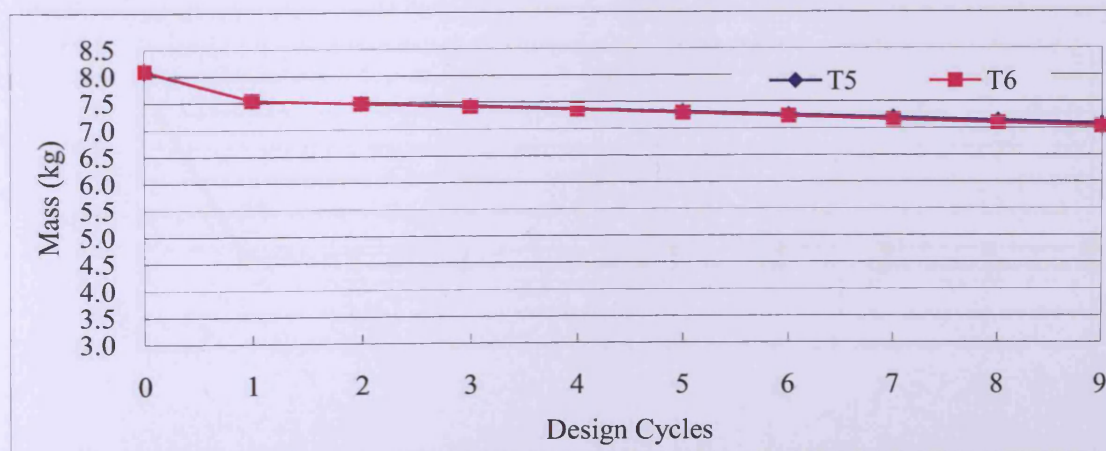


Figure A.3 Mass changes in panels T5 & T6

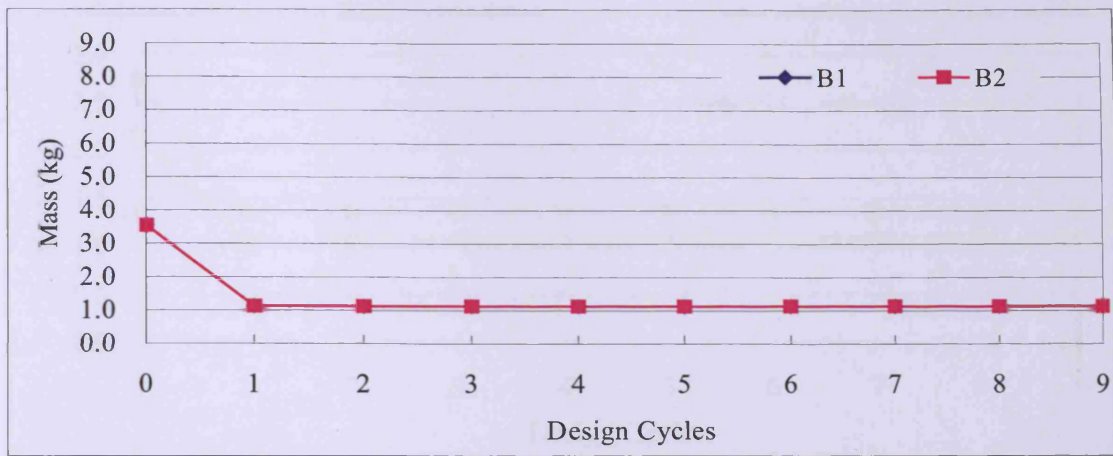


Figure A.4 Mass changes in panels B1 & B2.

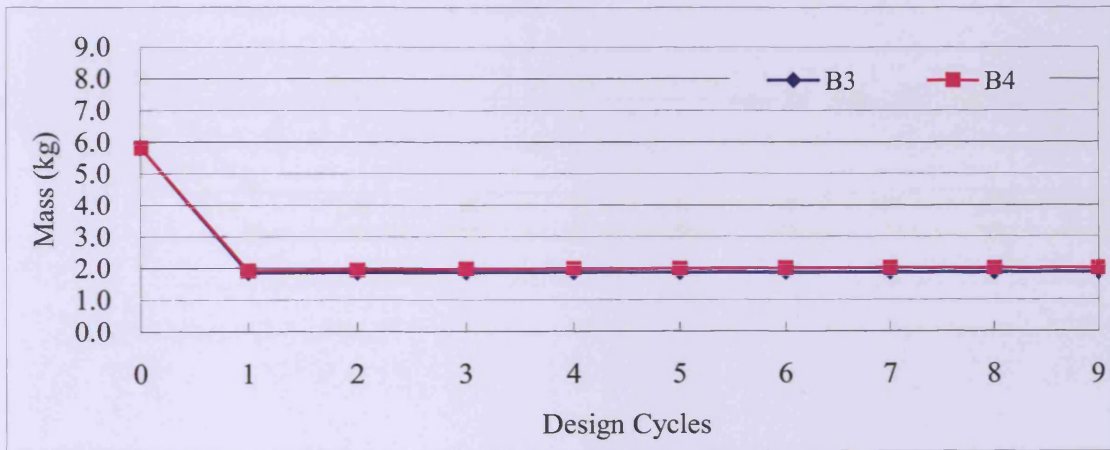


Figure A.5 Mass changes in panels B3 & B4.

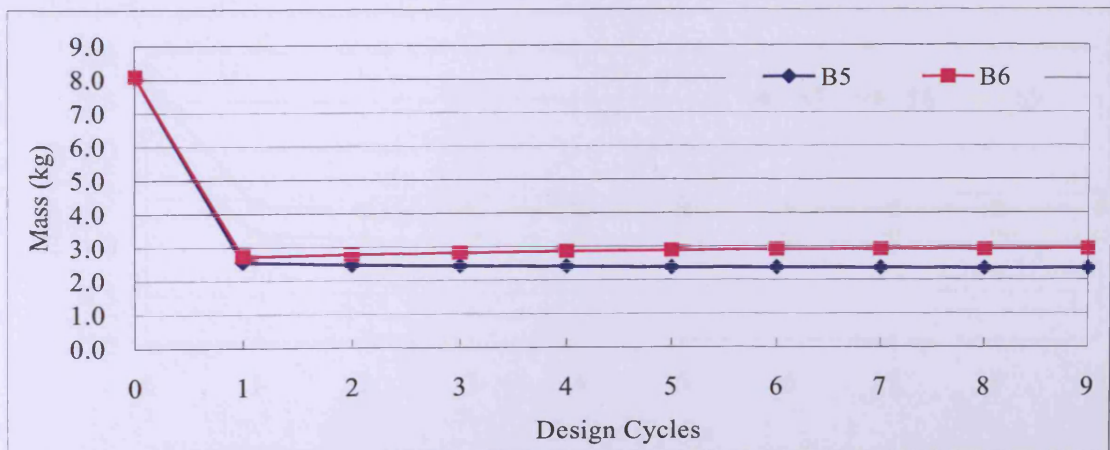


Figure A.6 Mass changes in panels B5 & B6.

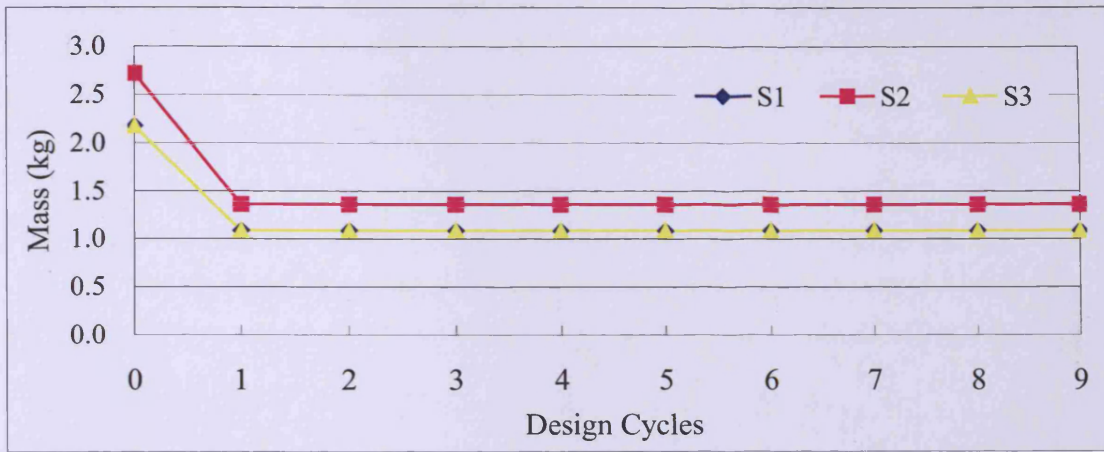


Figure A.7 Mass changes in panels S1, S2 & S3.

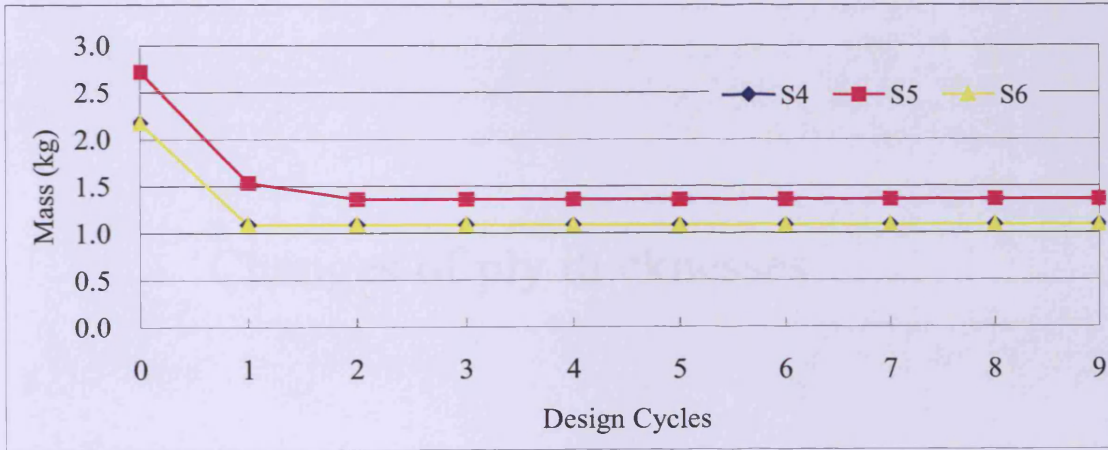


Figure A.8 Mass changes in panels S4, S5 & S6.

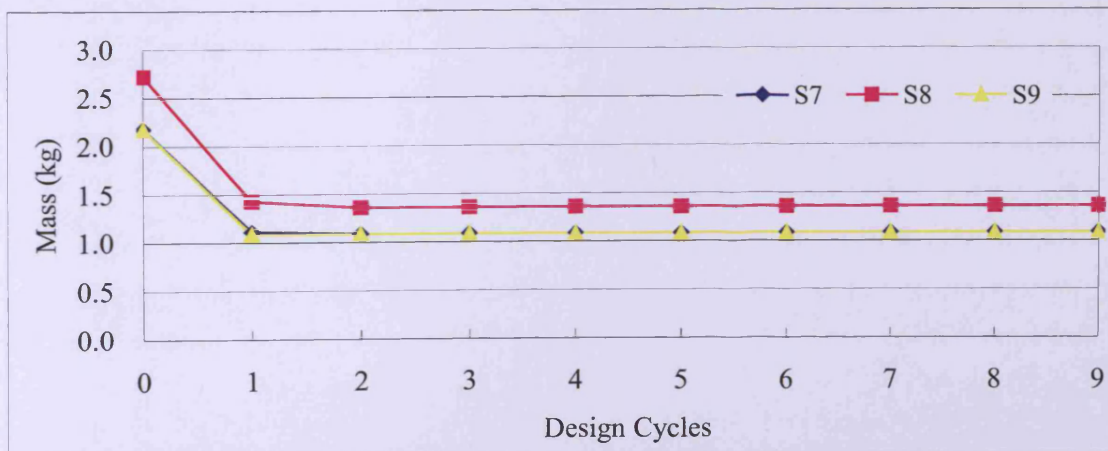
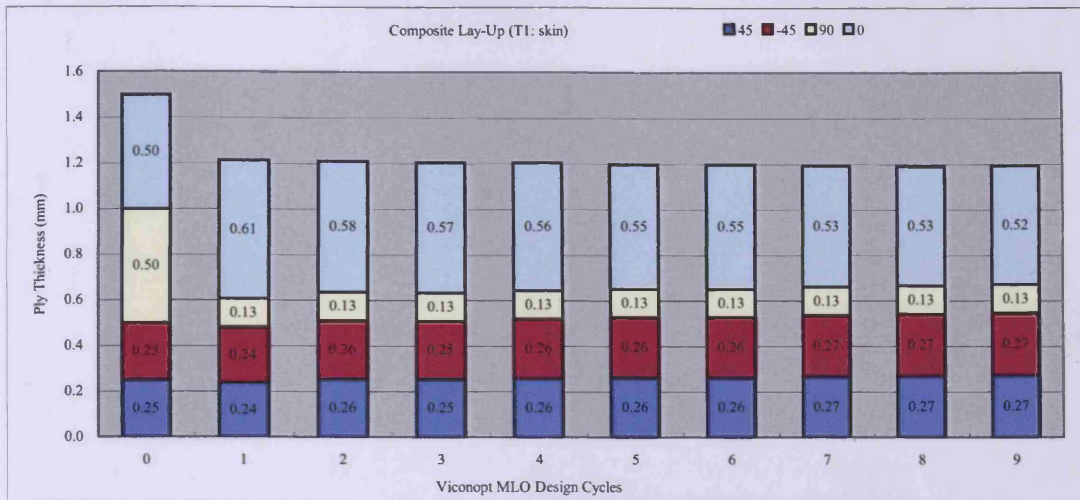


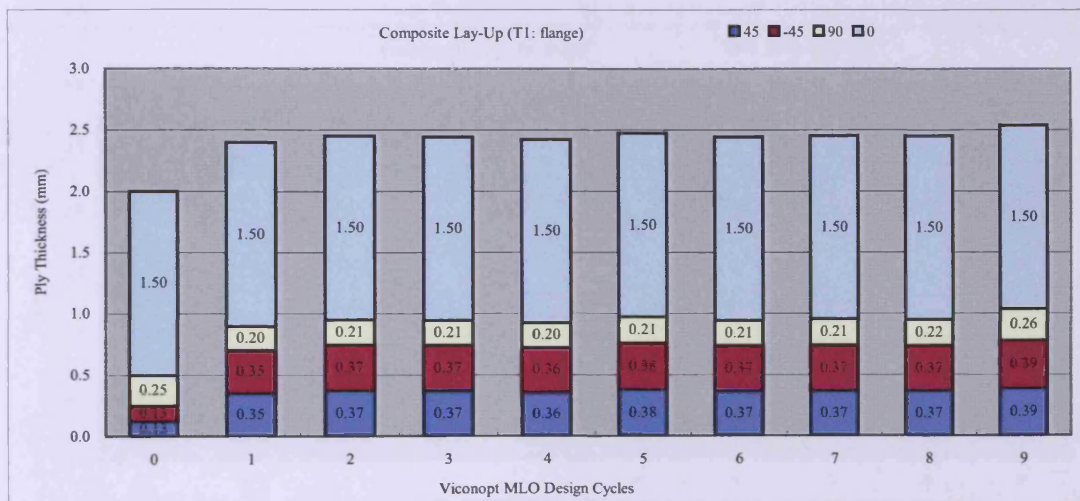
Figure A.9 Mass changes in panels S7, S8 & S9.

Appendix B

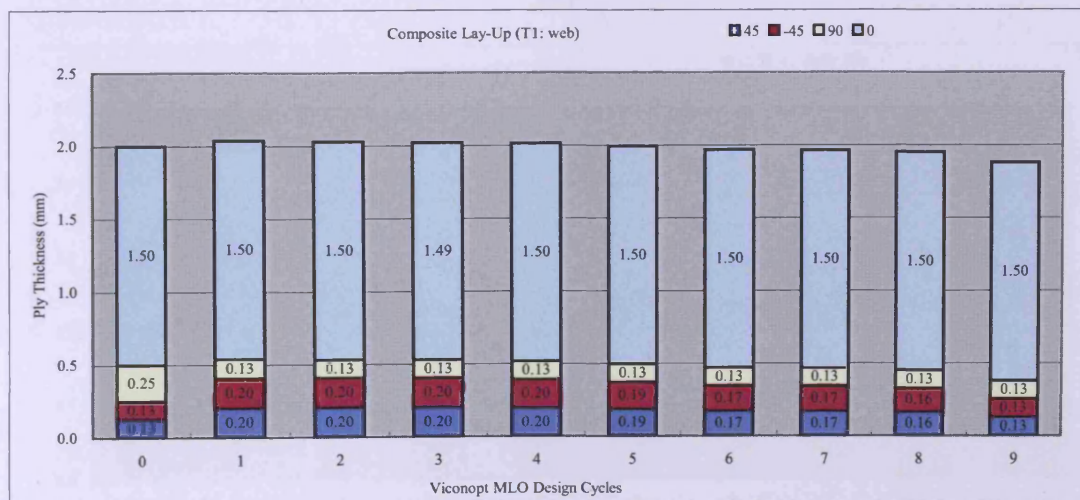
Changes of ply thicknesses



(a)

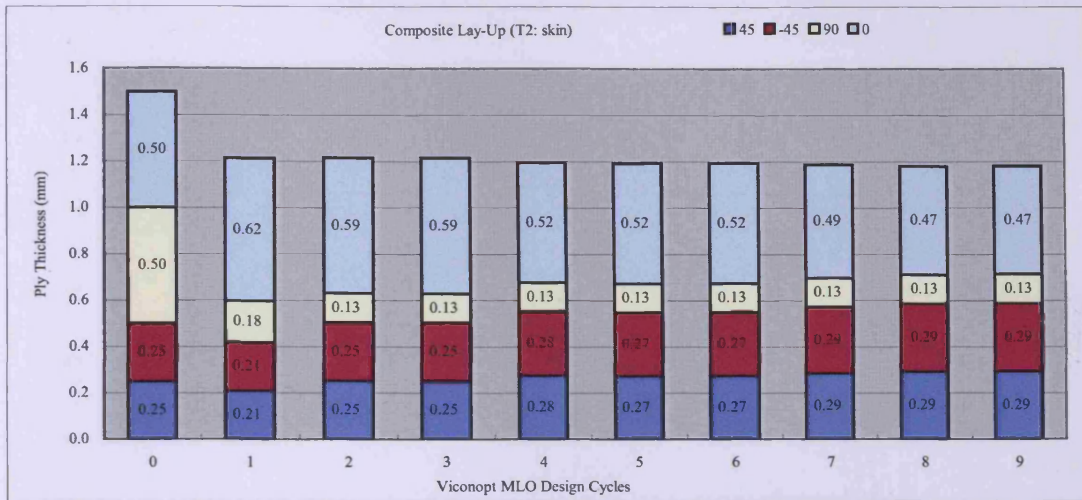


(b)

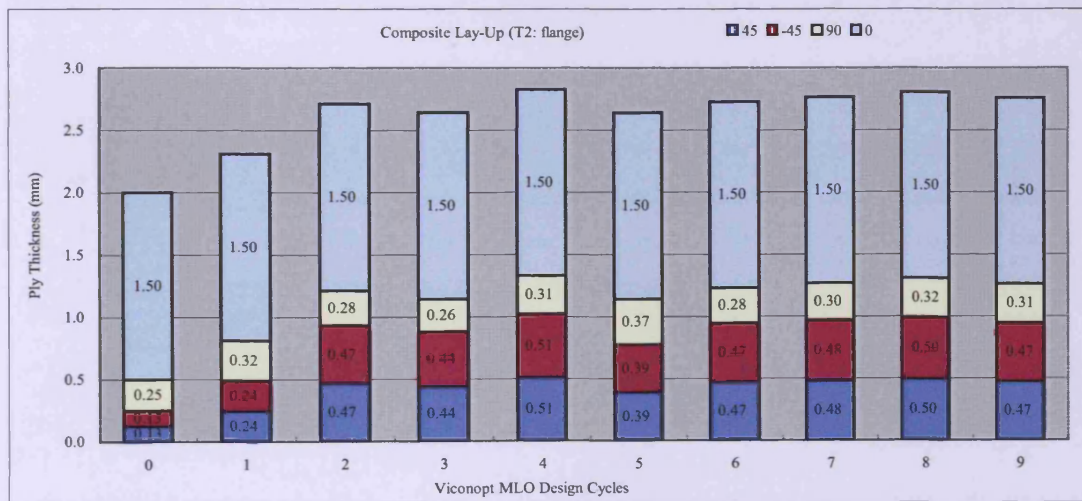


(c)

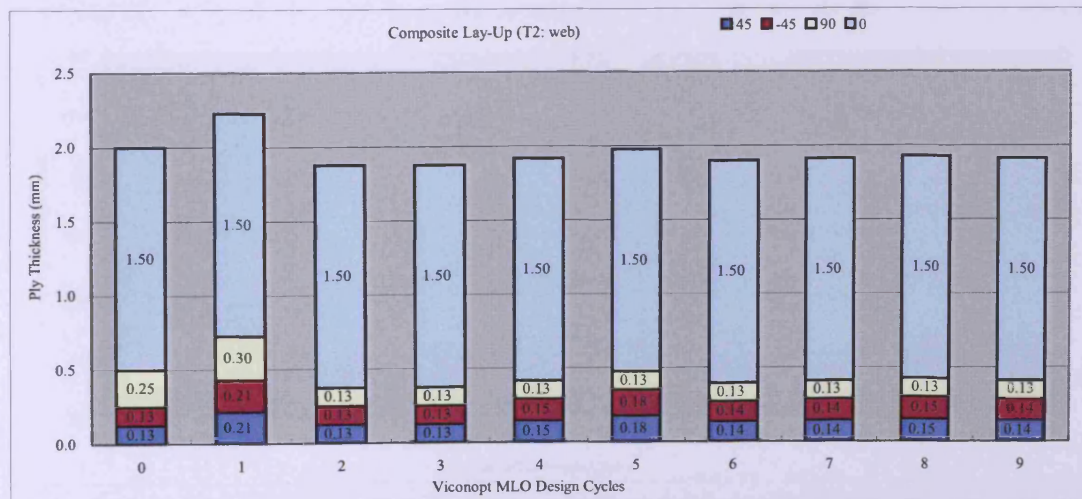
Figure B.1 Changes of ply thicknesses (T1), (a) skin, (b) flange and (c) web.



(a)

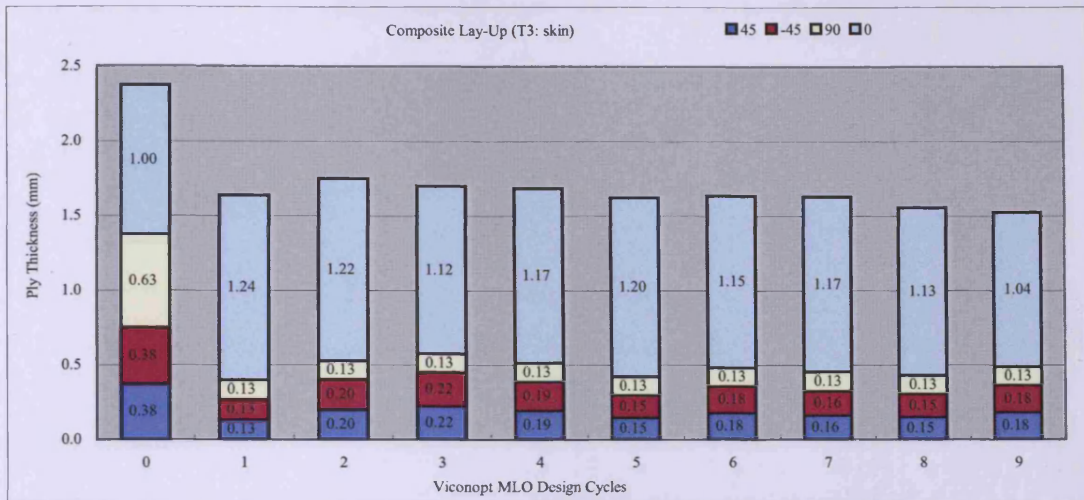


(b)

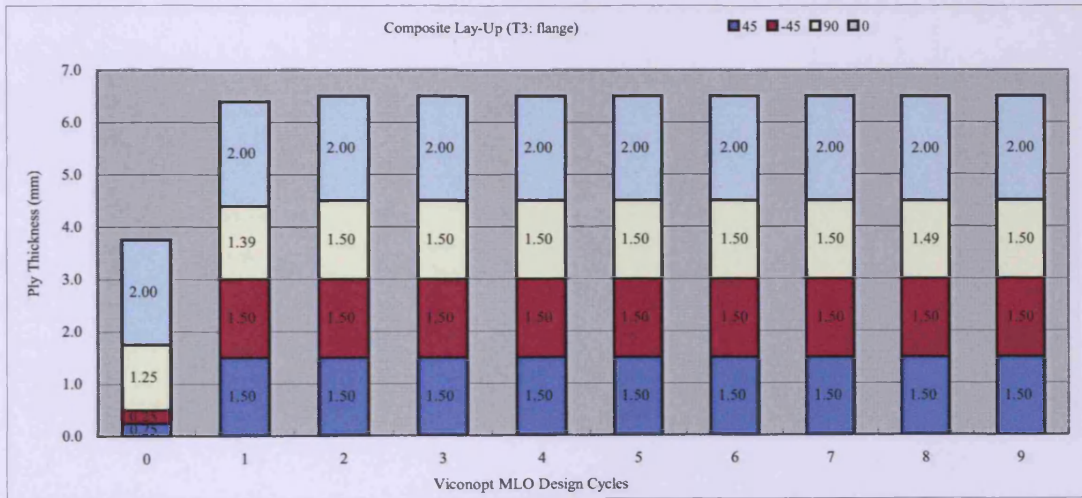


(c)

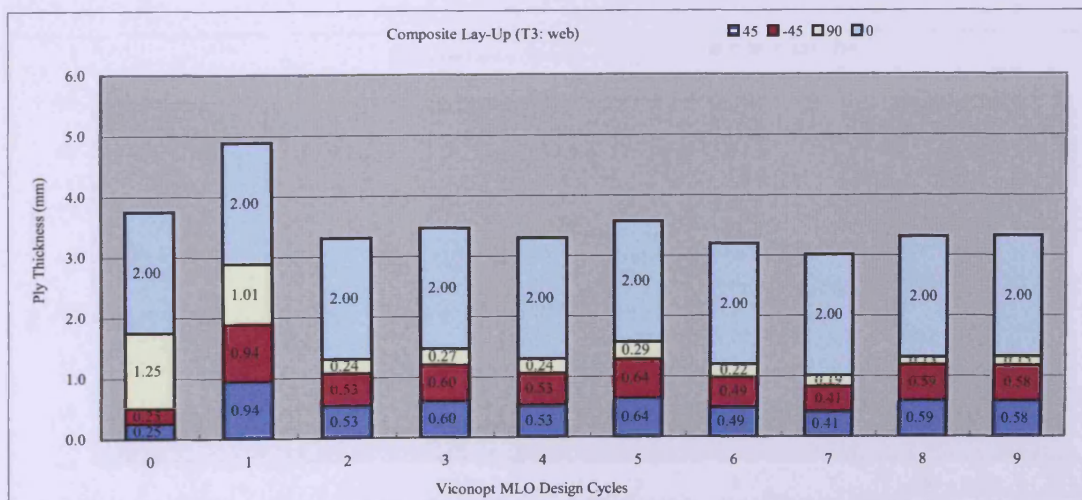
Figure B.2 Changes of ply thicknesses (T2), (a) skin, (b) flange and (c) web.



(a)

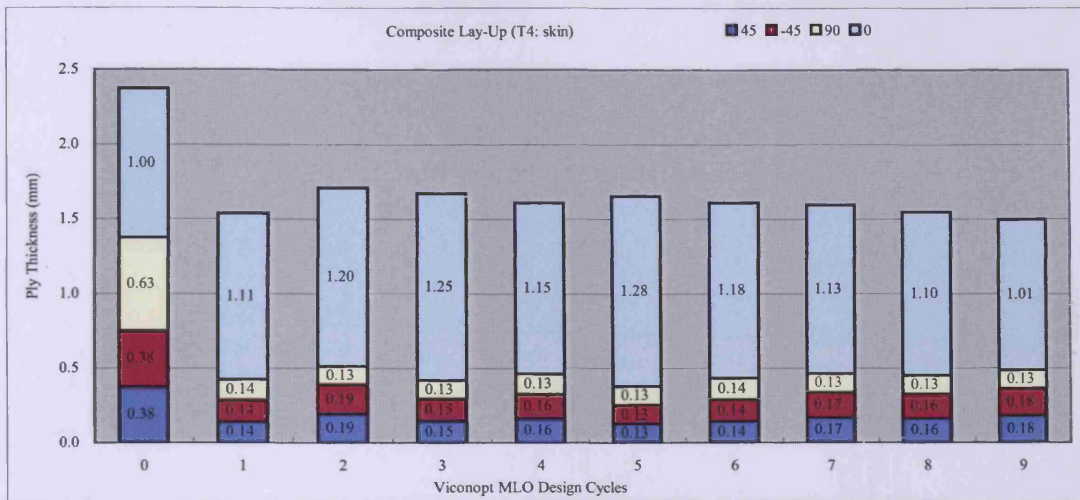


(b)

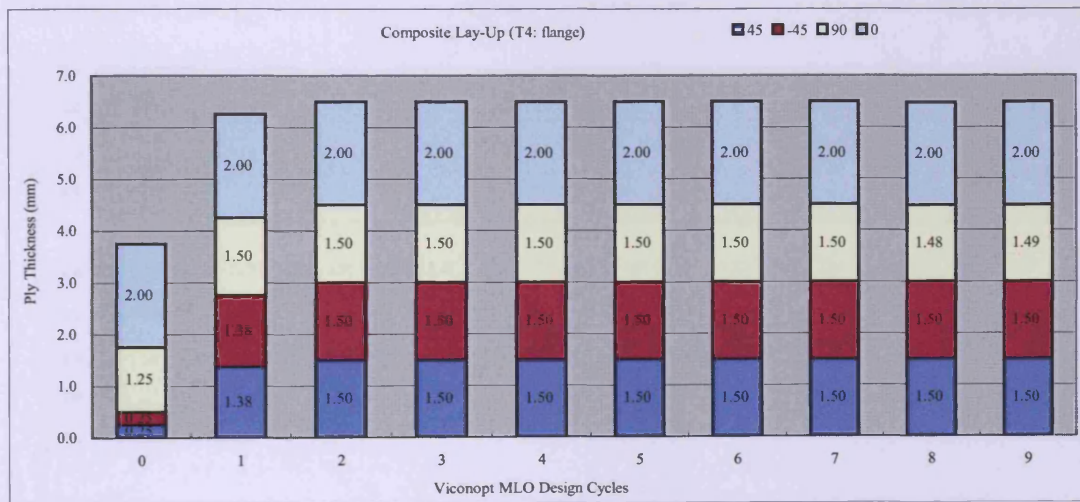


(c)

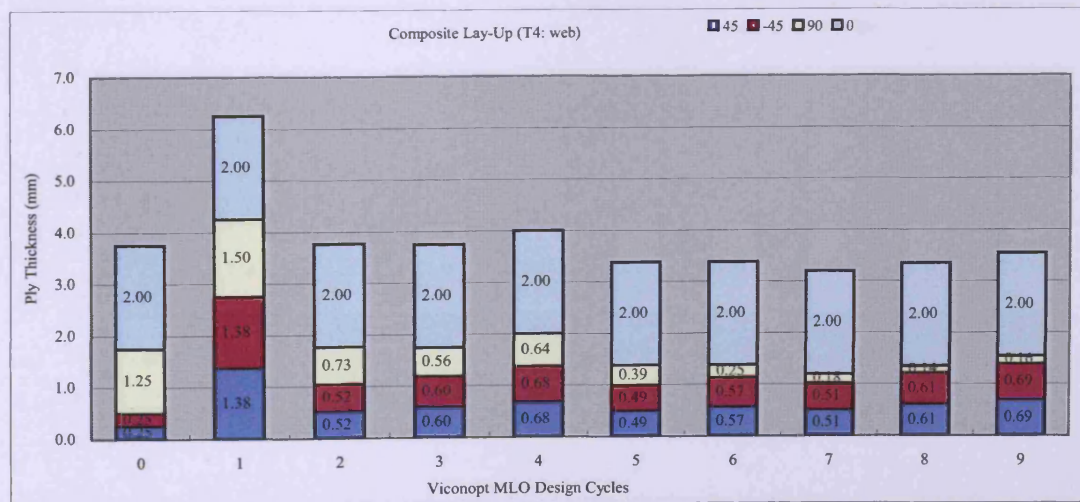
Figure B.3 Changes of ply thicknesses (T3), (a) skin, (b) flange and (c) web.



(a)

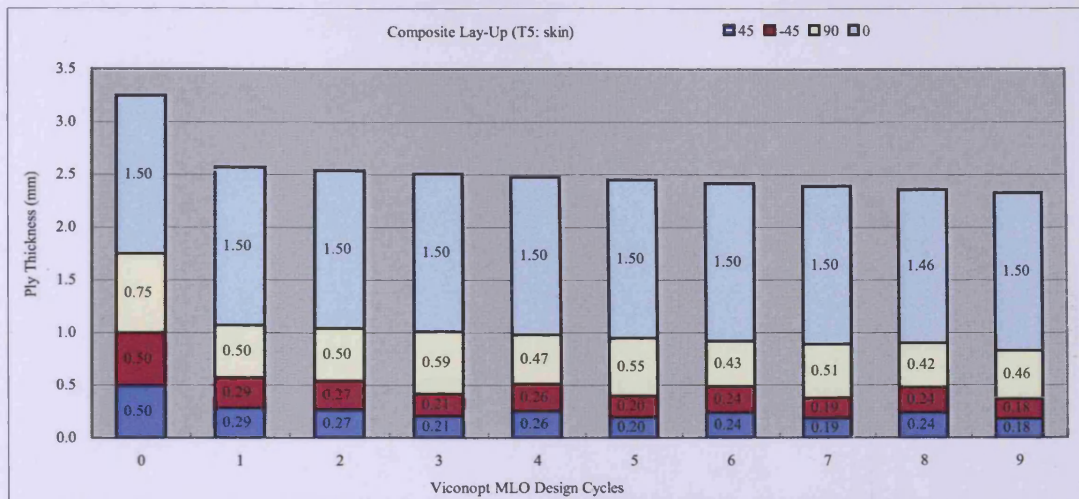


(b)

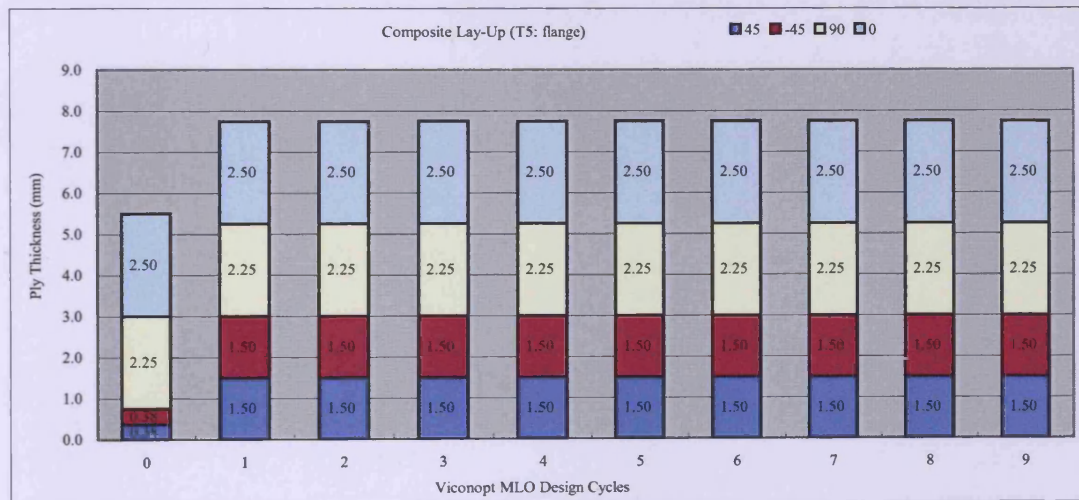


(c)

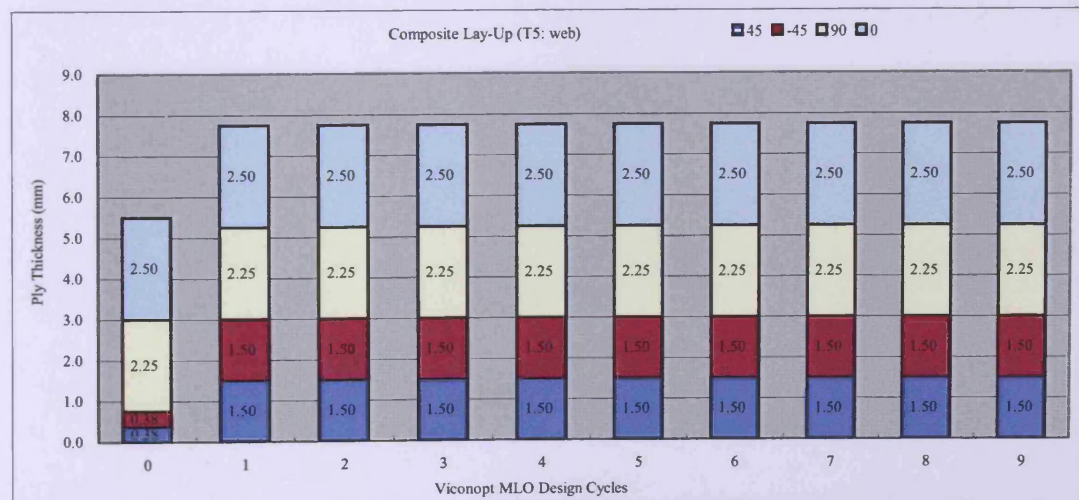
Figure B.4 Changes of ply thicknesses (T4), (a) skin, (b) flange and (c) web.



(a)

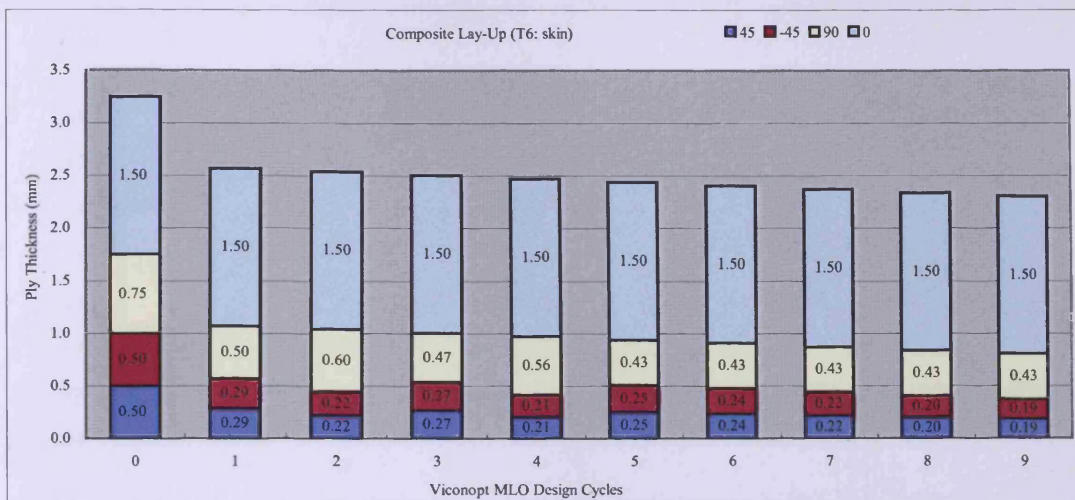


(b)

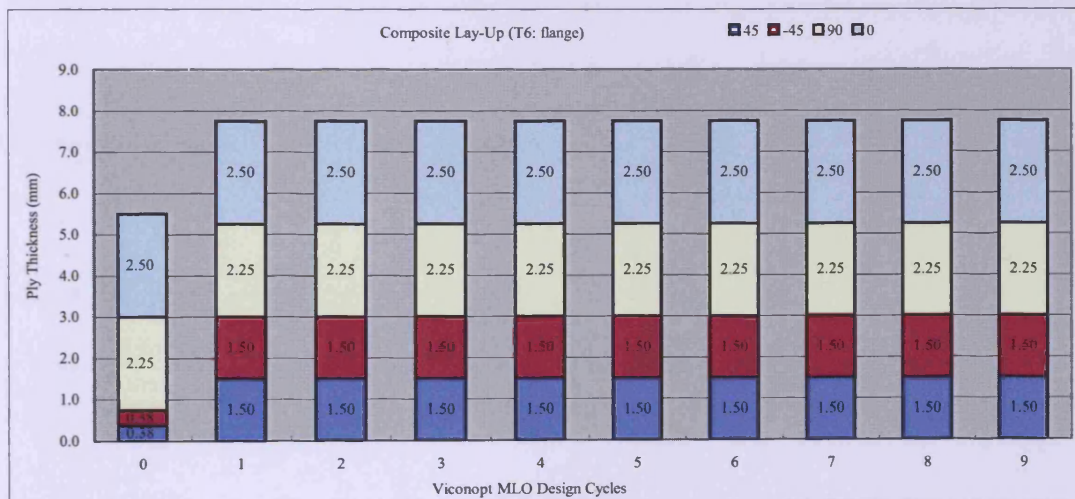


(c)

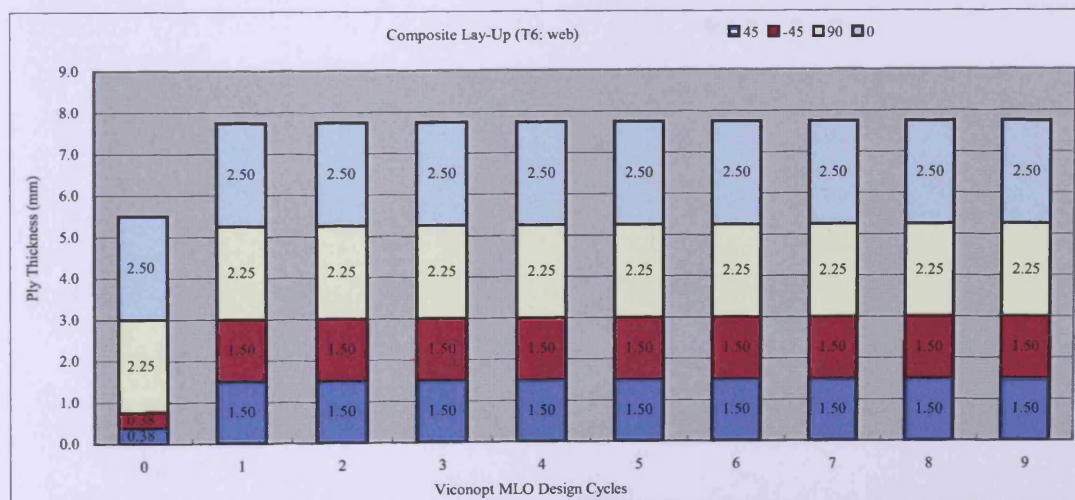
Figure B.5 Changes of ply thicknesses (T5), (a) skin, (b) flange and (c) web.



(a)

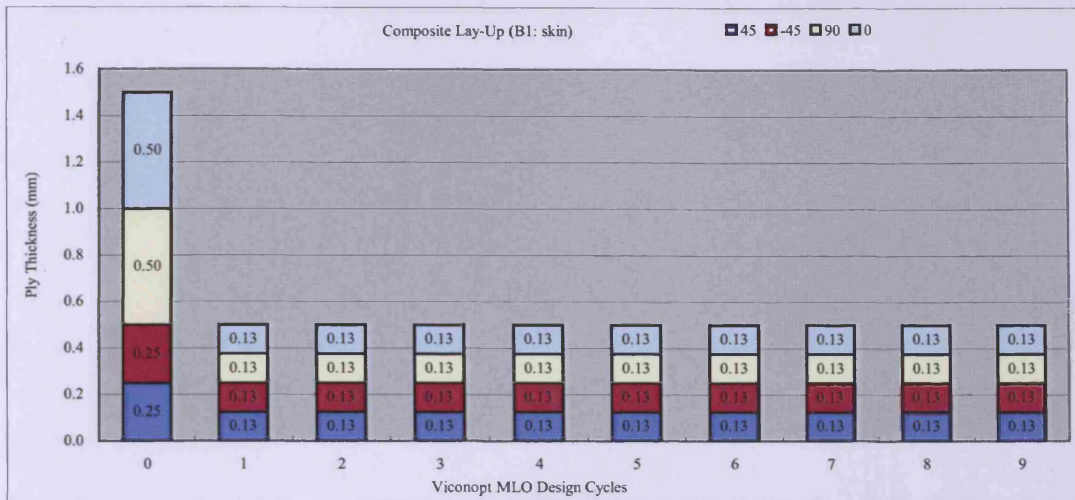


(b)

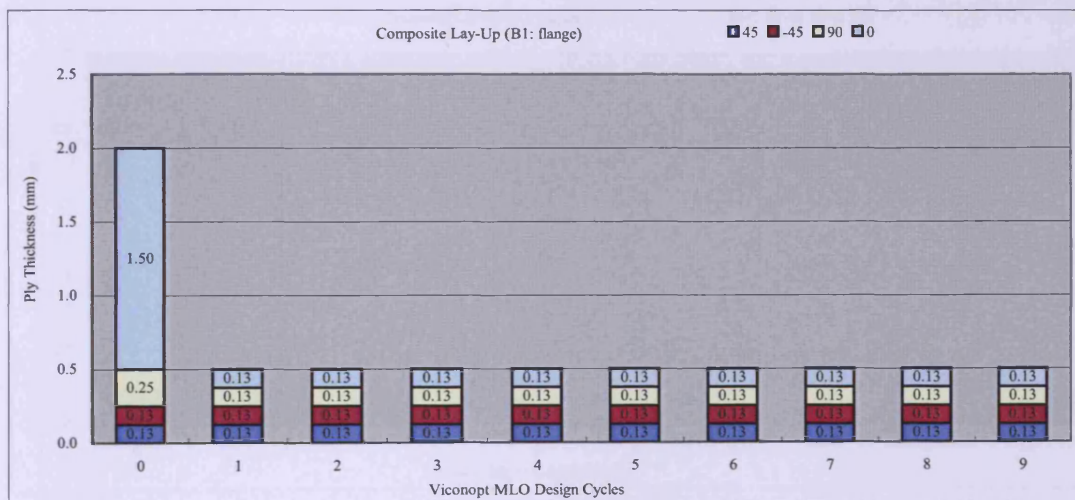


(c)

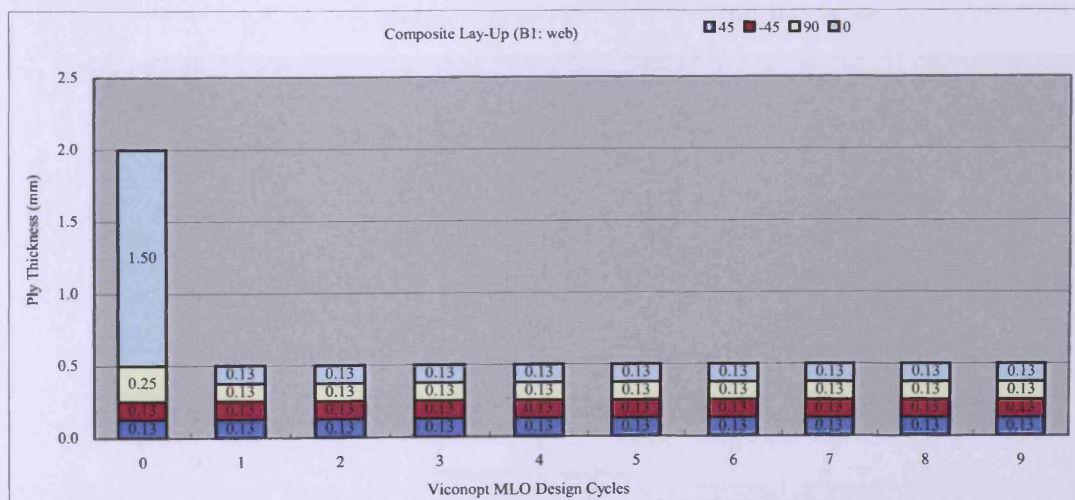
Figure B.6 Changes of ply thicknesses (T6), (a) skin, (b) flange and (c) web.



(a)

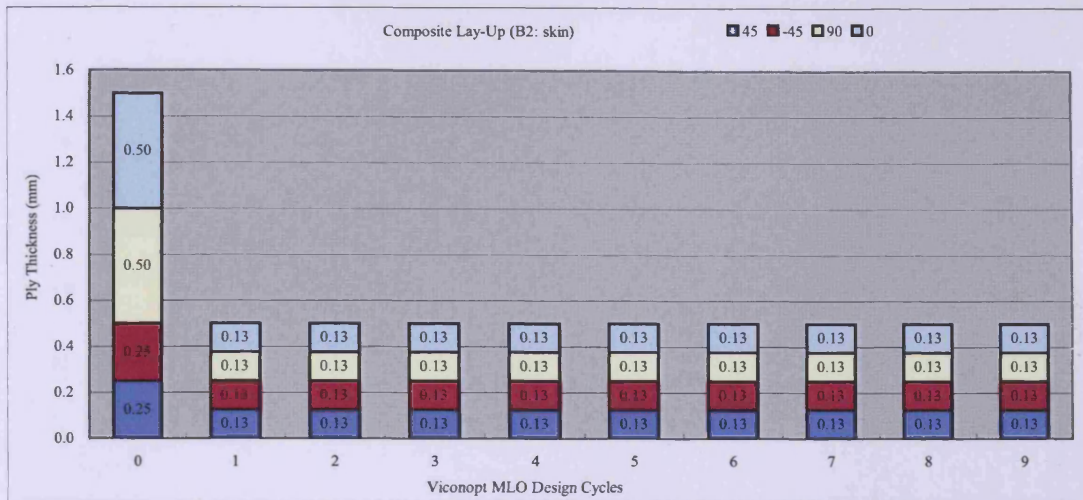


(b)

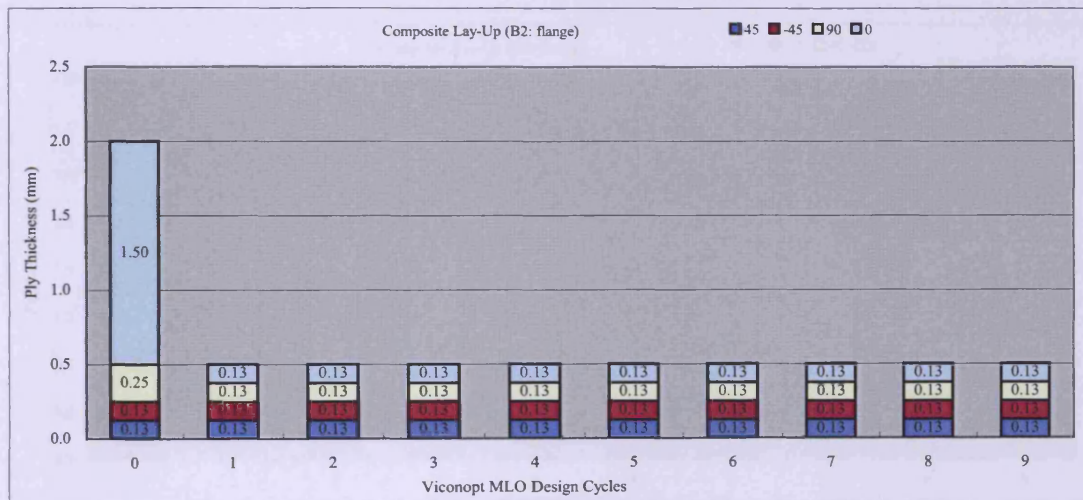


(c)

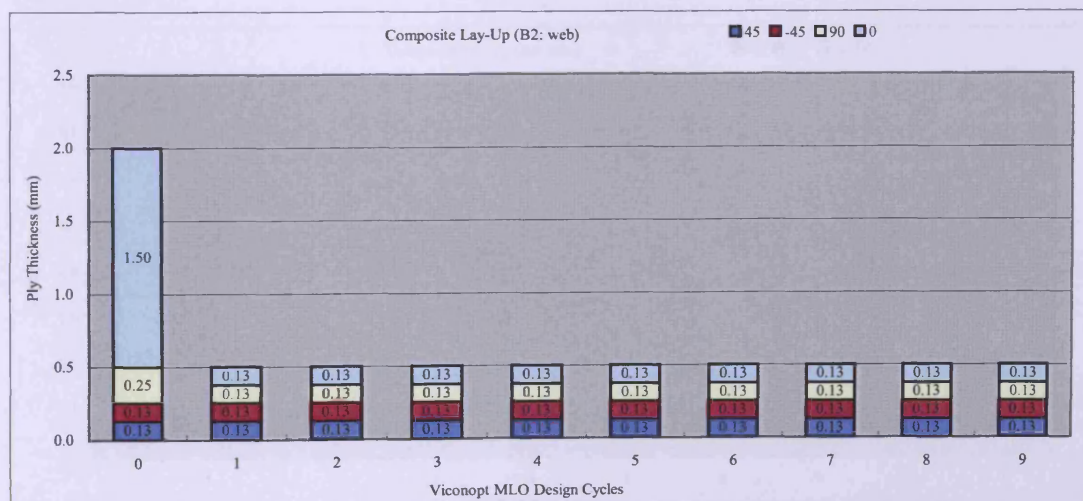
Figure B.7 Changes of ply thicknesses (B1), (a) skin, (b) flange and (c) web.



(a)

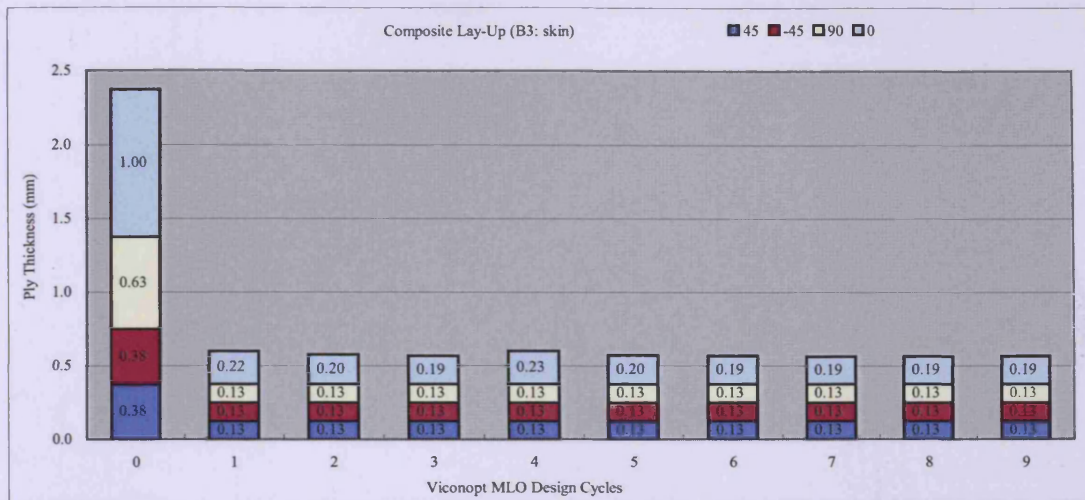


(b)

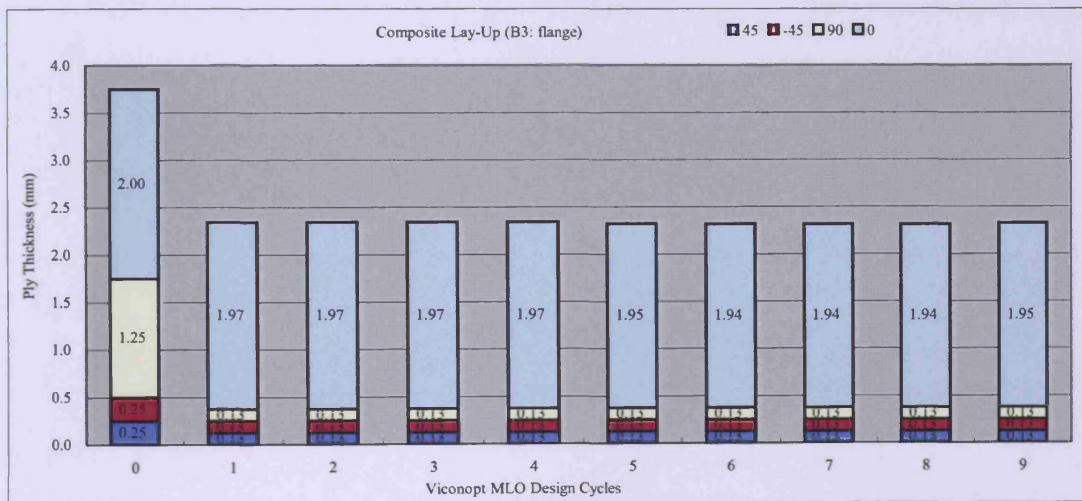


(c)

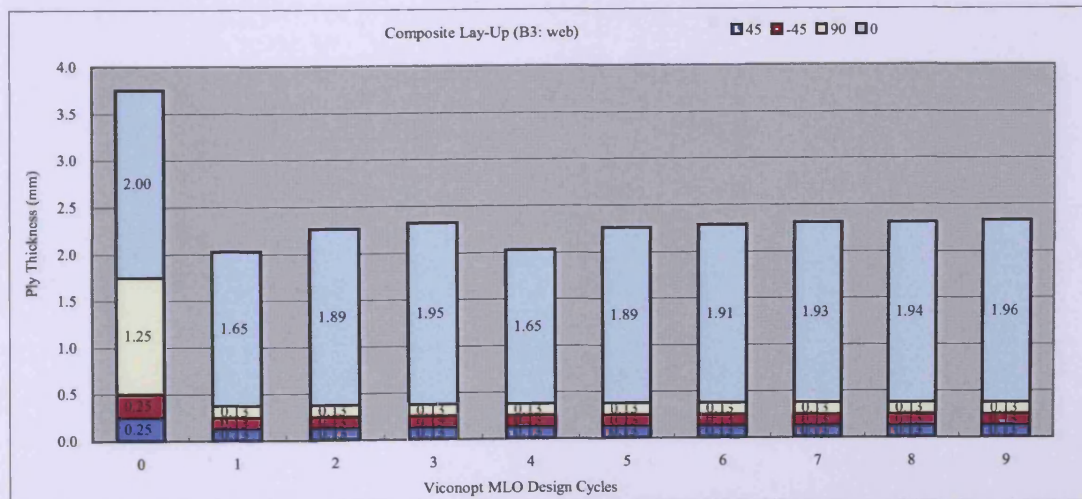
Figure B.8 Changes of ply thicknesses (B2), (a) skin, (b) flange and (c) web.



(a)

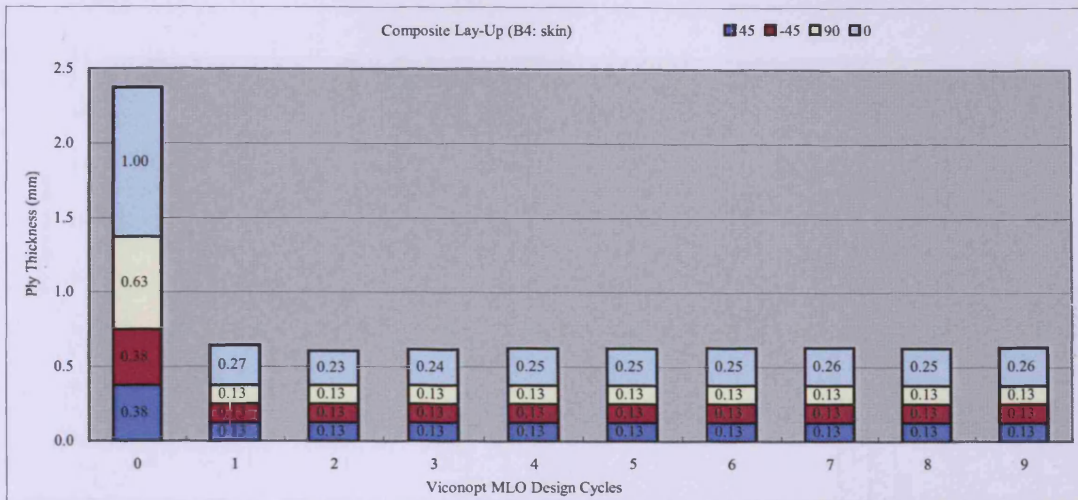


(b)

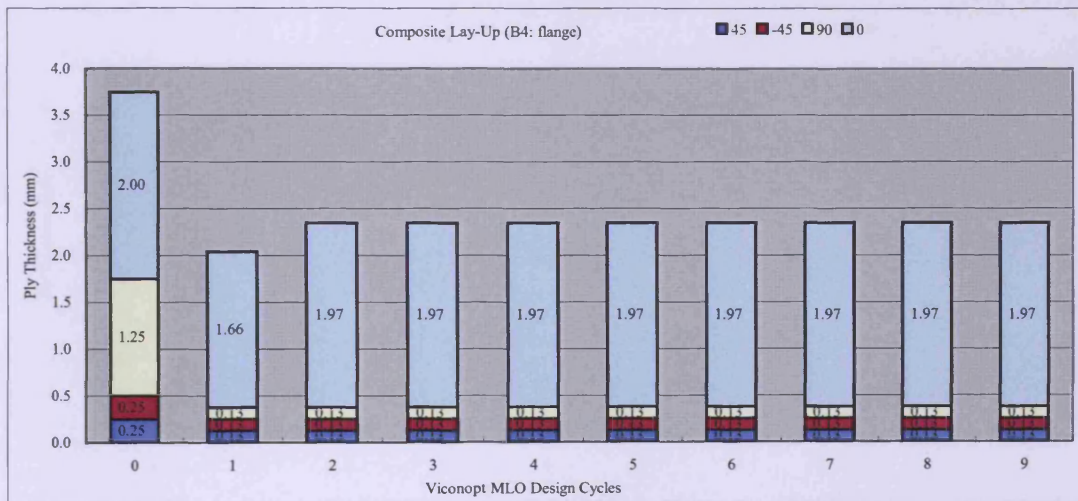


(c)

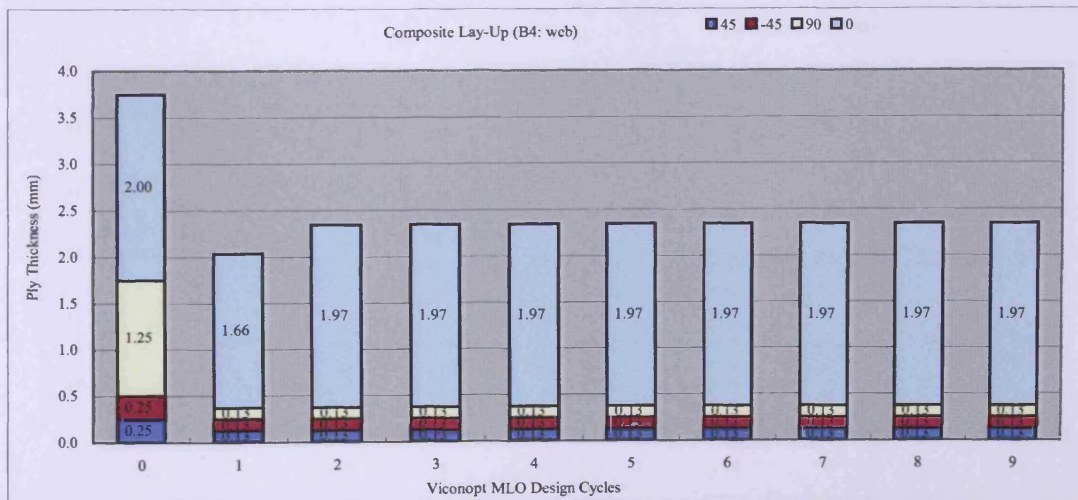
Figure B.9 Changes of ply thicknesses (B3), (a) skin, (b) flange and (c) web.



(a)

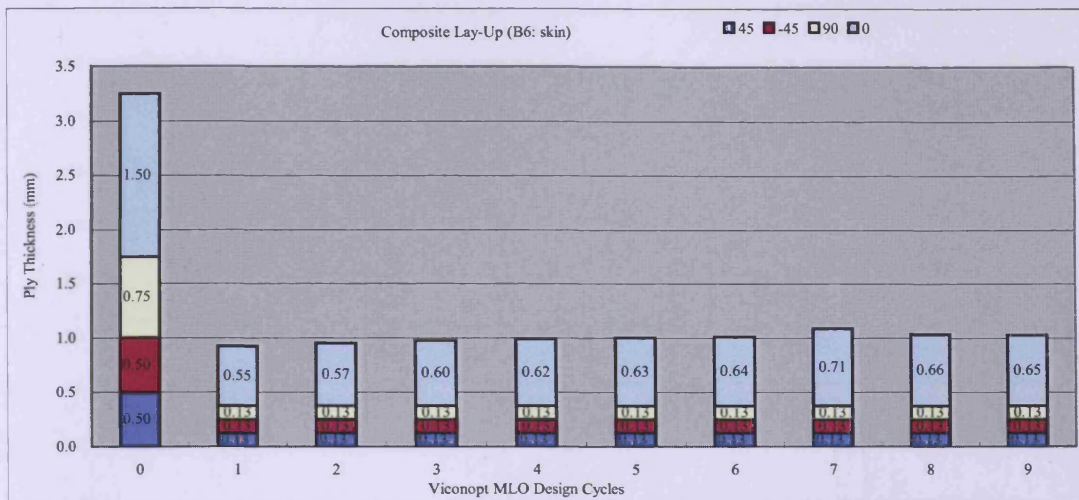


(b)

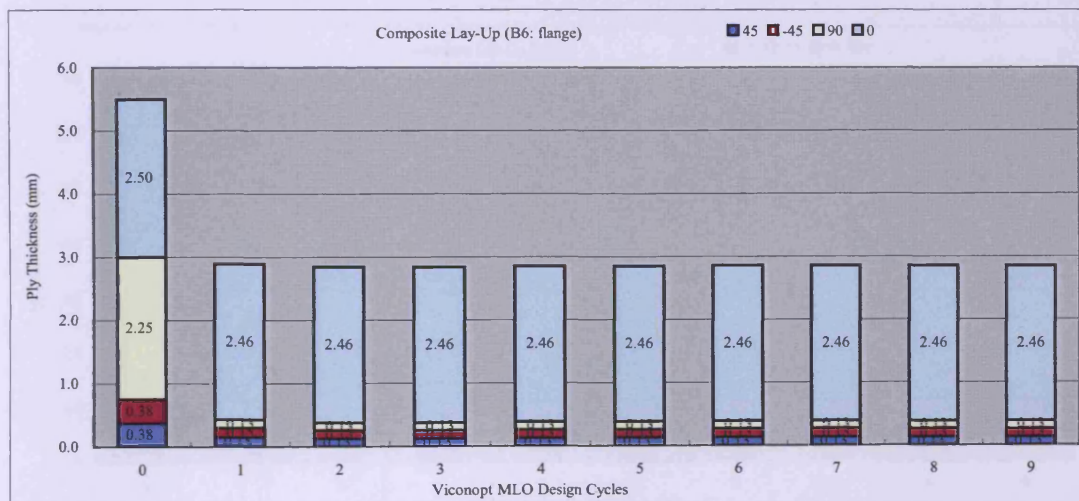


(c)

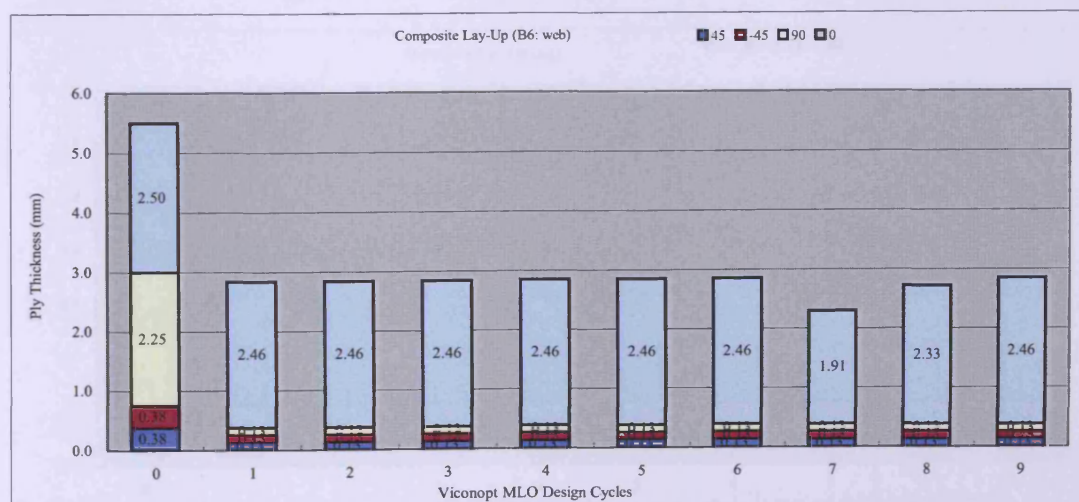
Figure B.10 Changes of ply thicknesses (B4), (a) skin, (b) flange and (c) web.



(a)



(b)



(c)

Figure B.12 Changes of ply thicknesses (B6), (a) skin, (b) flange and (c) web.

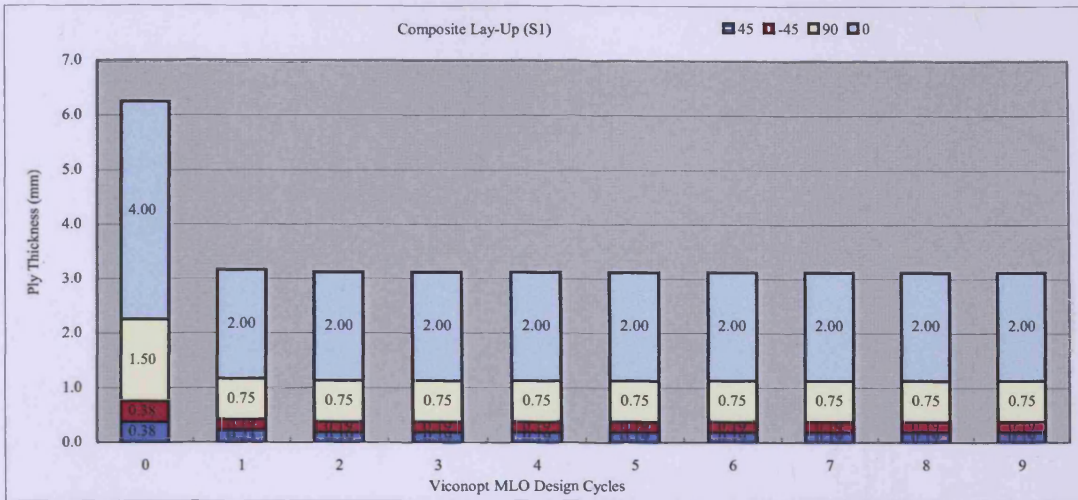


Figure B.13 Changes of ply thicknesses (S1)

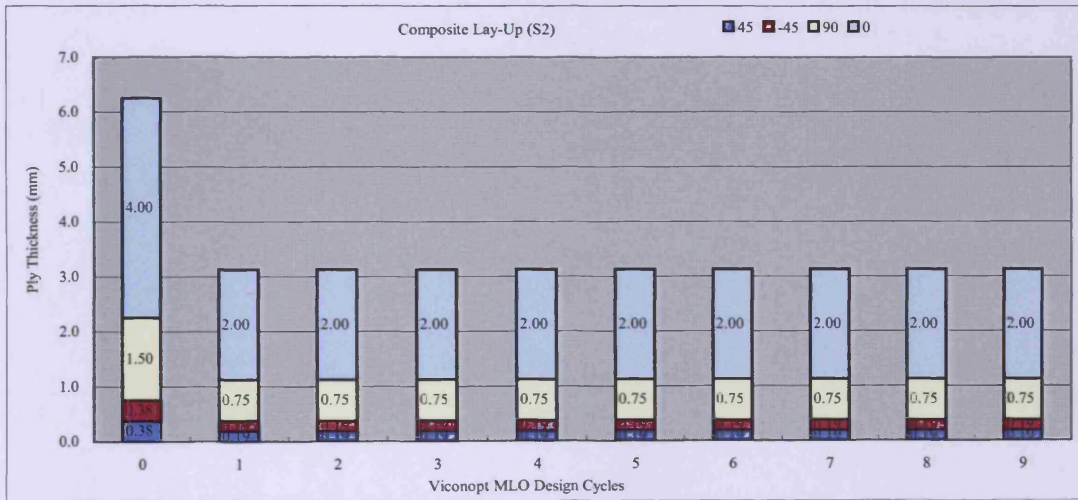


Figure B.14 Changes of ply thicknesses (S2)

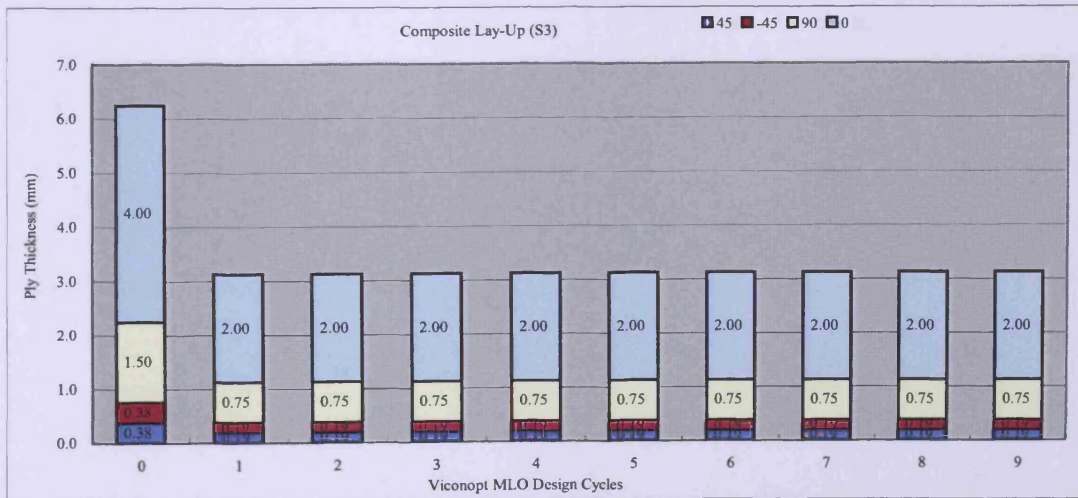


Figure B.15 Changes of ply thicknesses (S3)

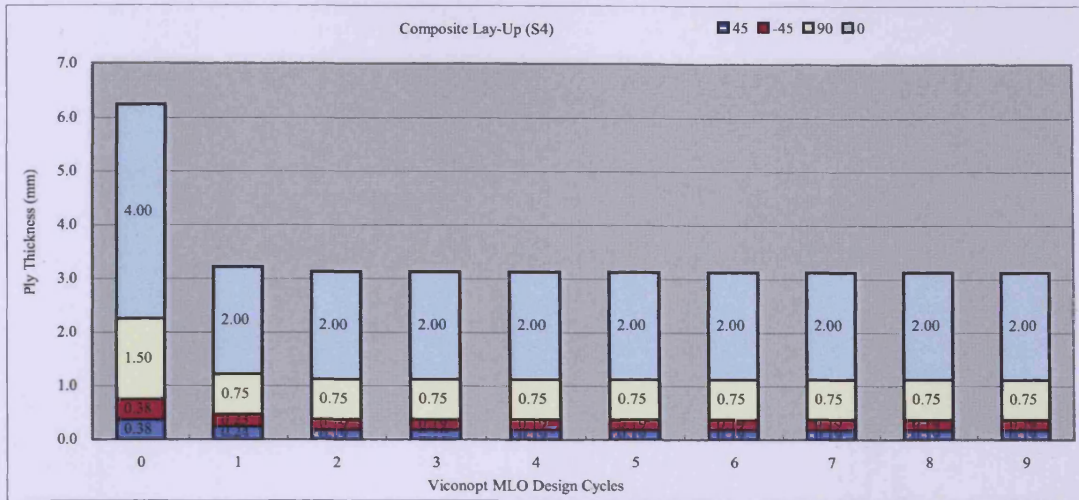


Figure B.16 Changes of ply thicknesses (S4)

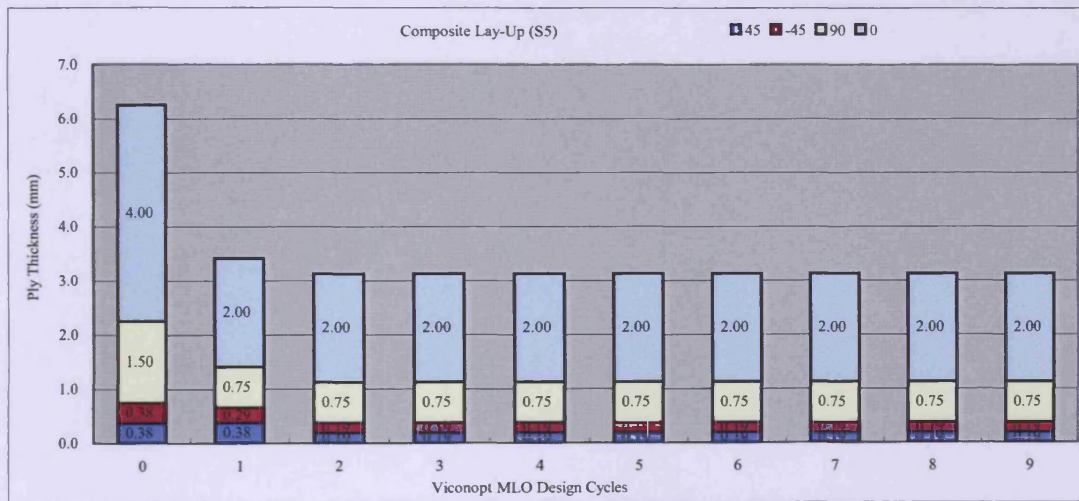


Figure B.17 Changes of ply thicknesses (S5)

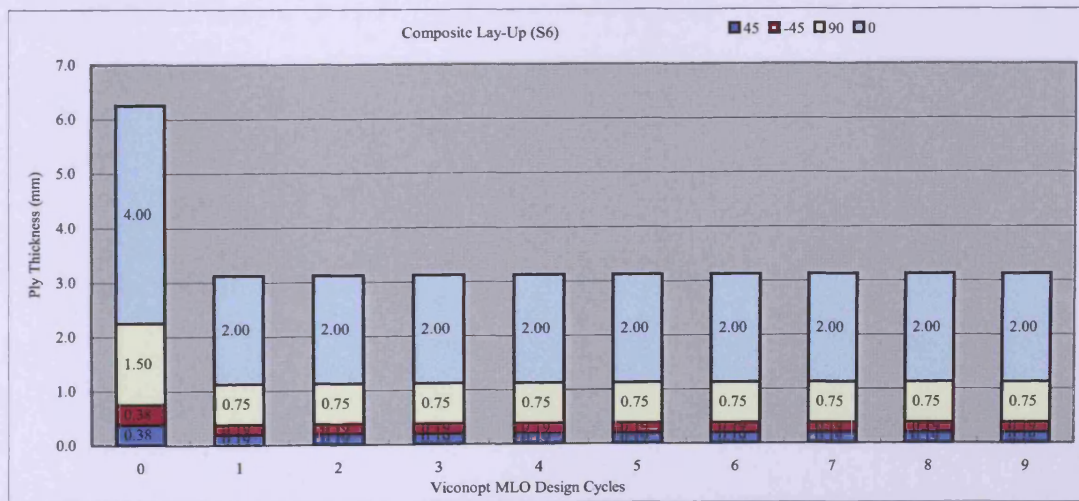


Figure B.18 Changes of ply thicknesses (S6)

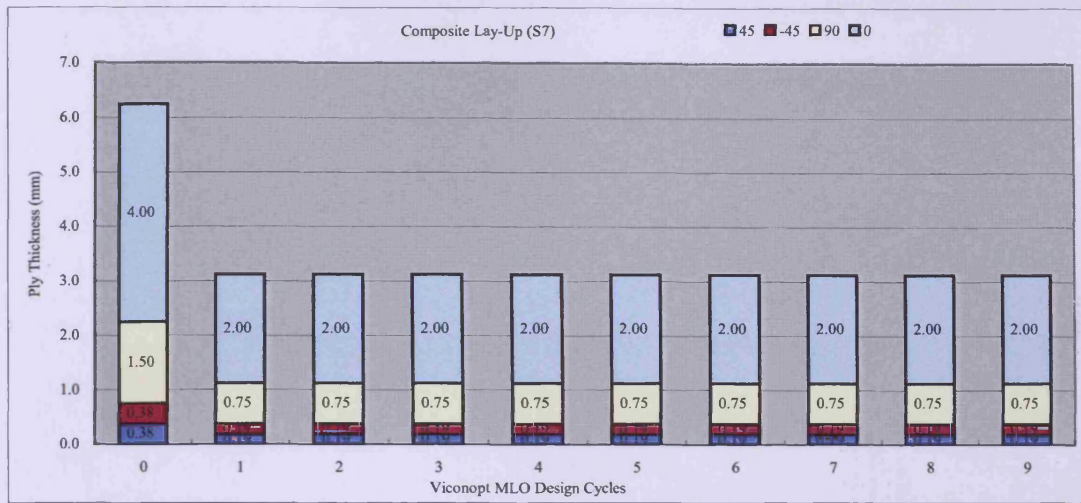


Figure B.19 Changes of ply thicknesses (S7)

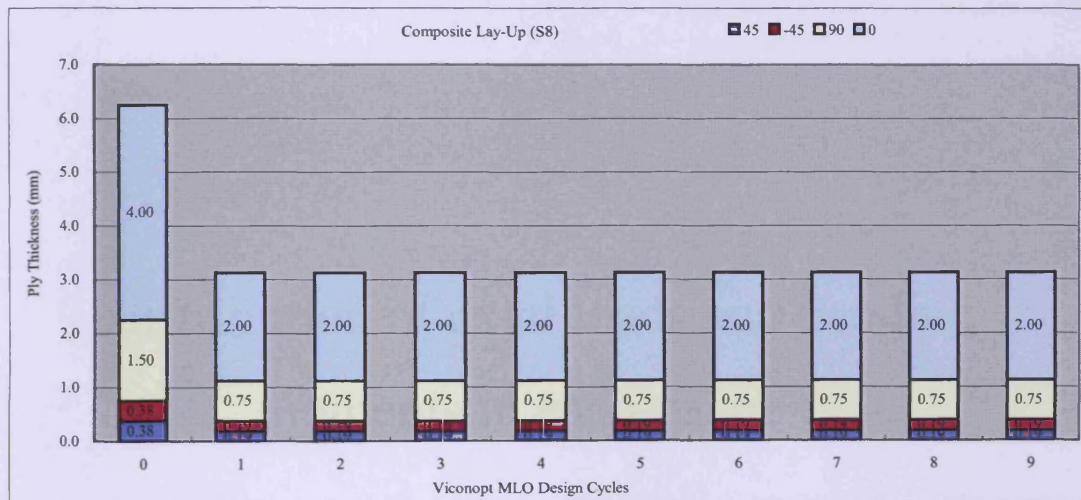


Figure B.20 Changes of ply thicknesses (S8)

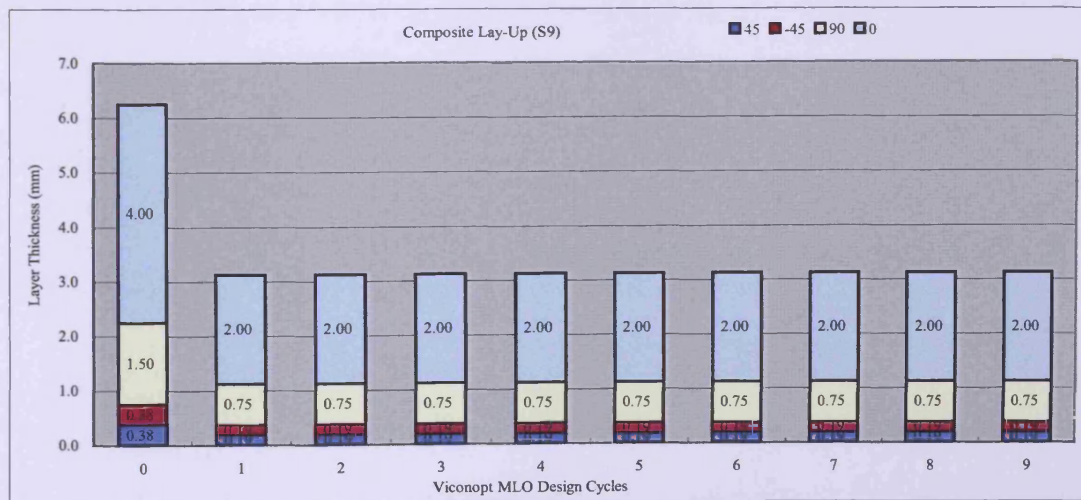
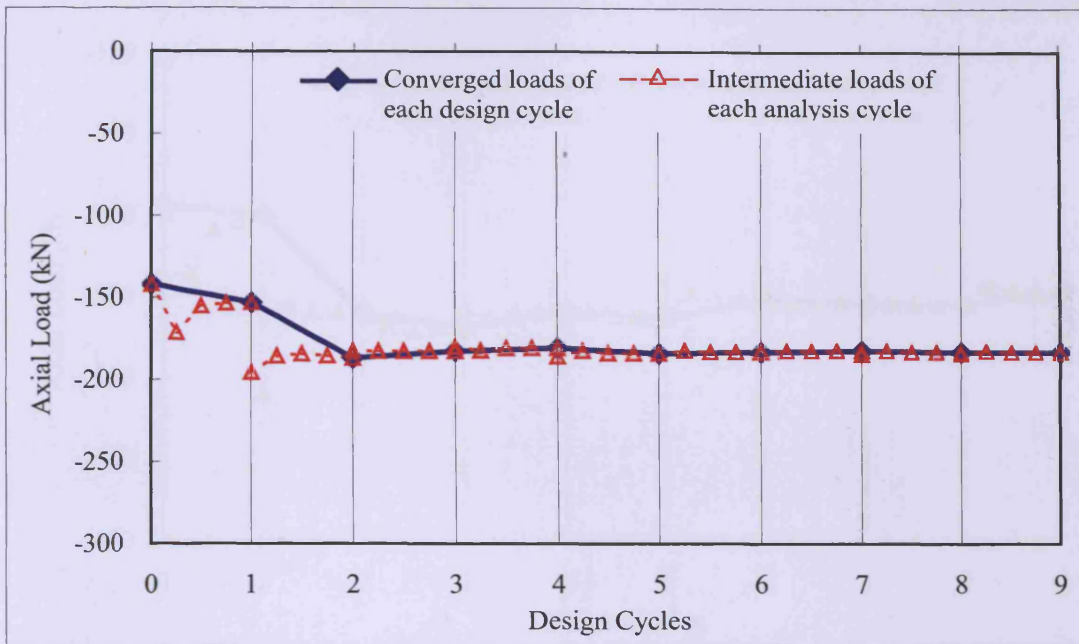


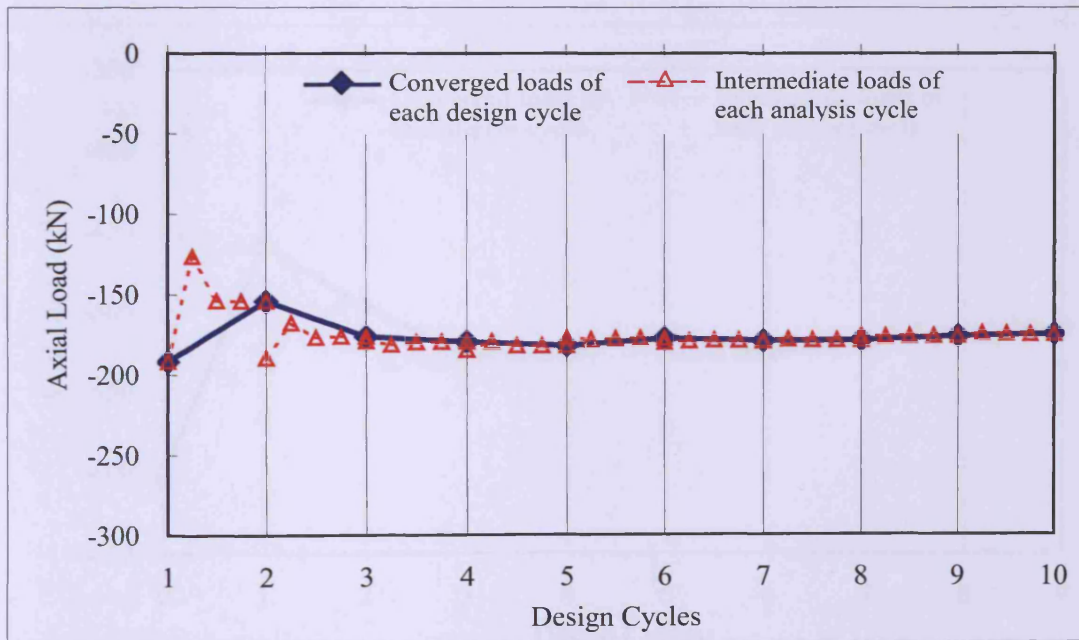
Figure B.21 Changes of ply thicknesses (S9)

Appendix C

Redistribution of axial loads and bending moments in each panel

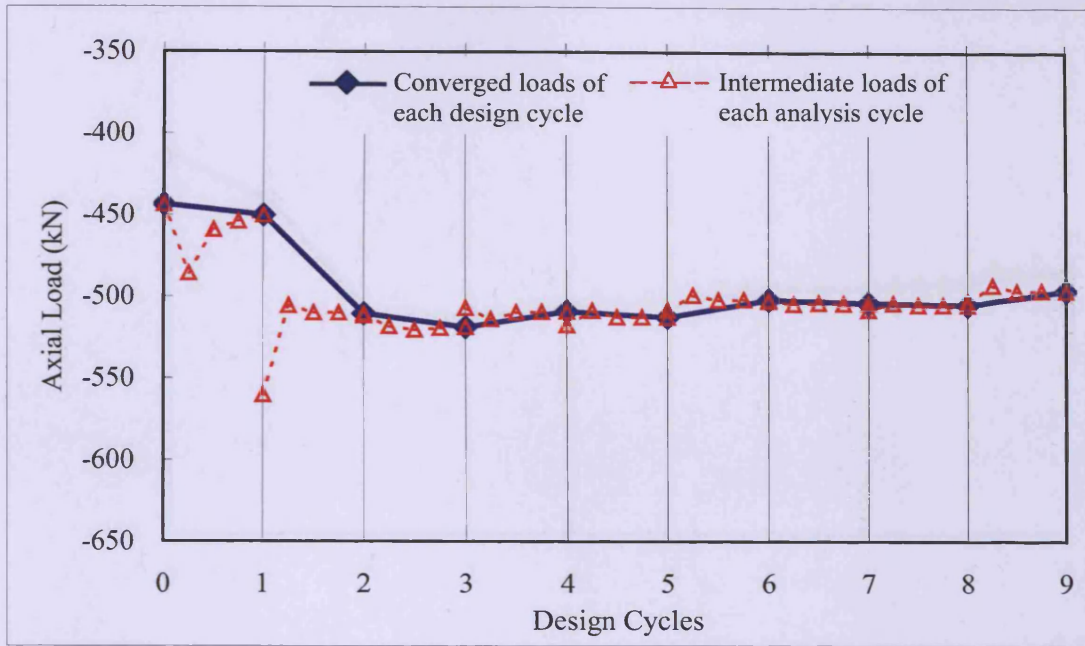


(a)

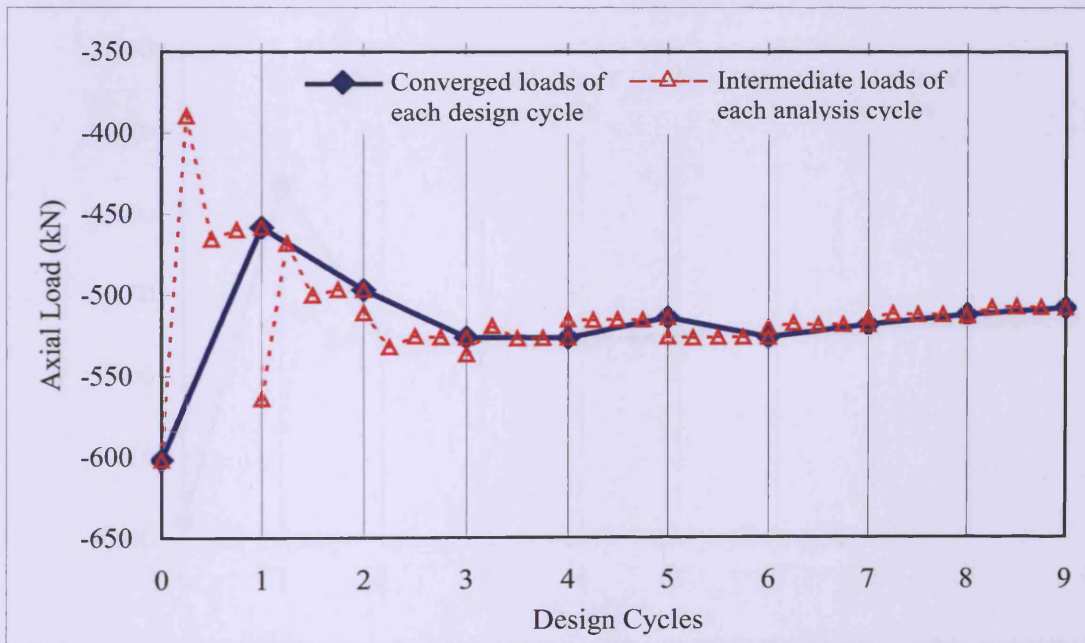


(b)

Figure C.1 Redistribution of axial loads in panels (a) T1 and (b) T2.

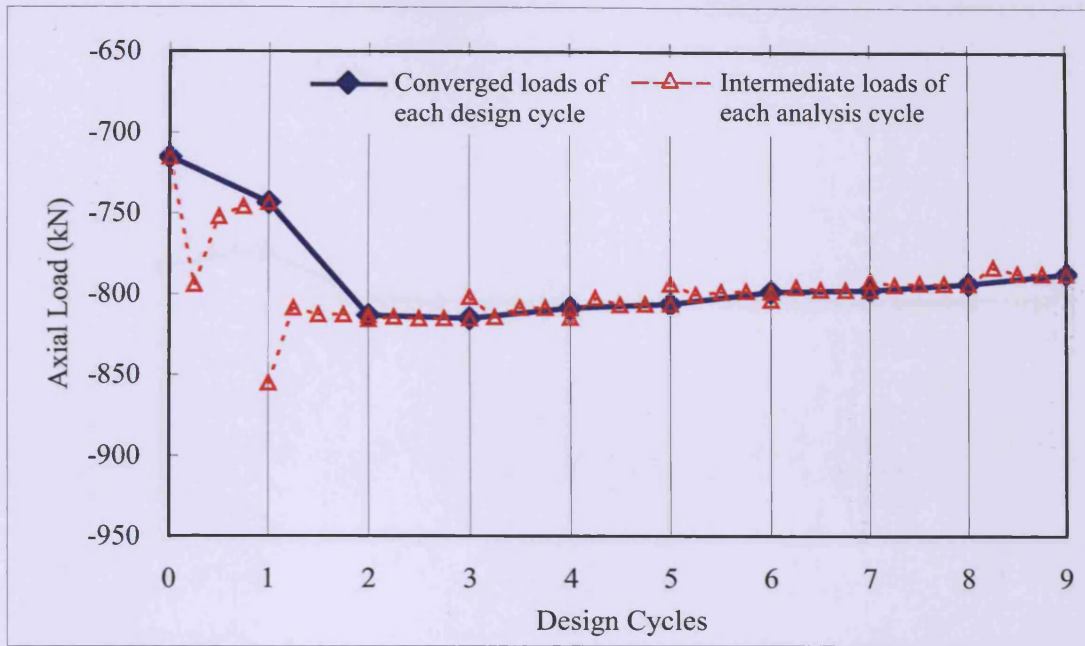


(a)

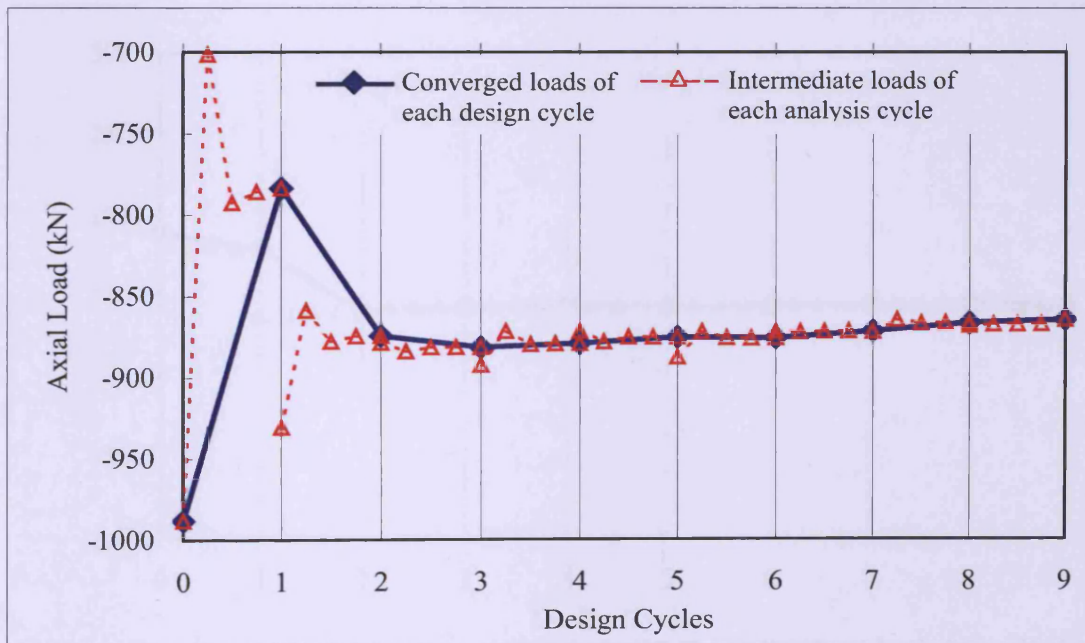


(b)

Figure C.2 Redistribution of axial loads in panels (a) T3 and (b) T4.

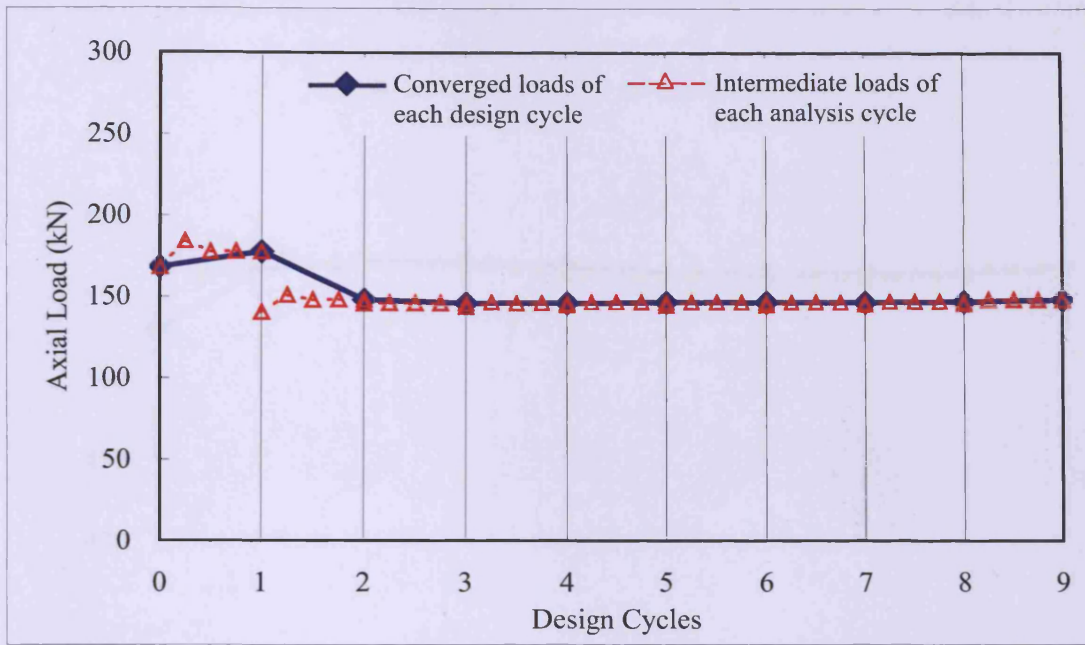


(a)

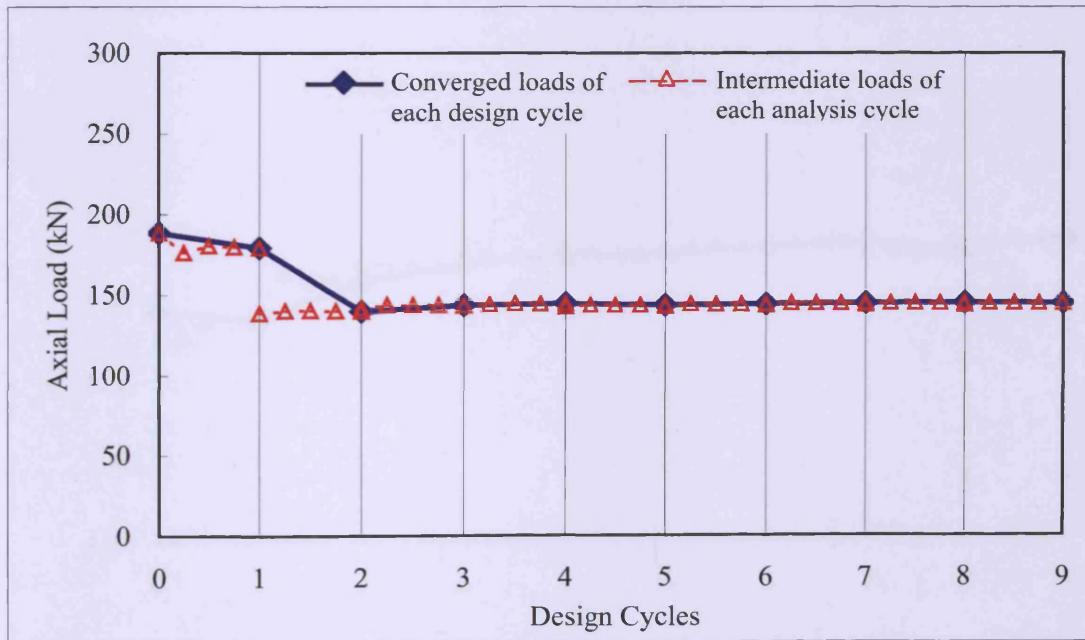


(b)

Figure C.3 Redistribution of axial loads in panels (a) T5 and (b) T6

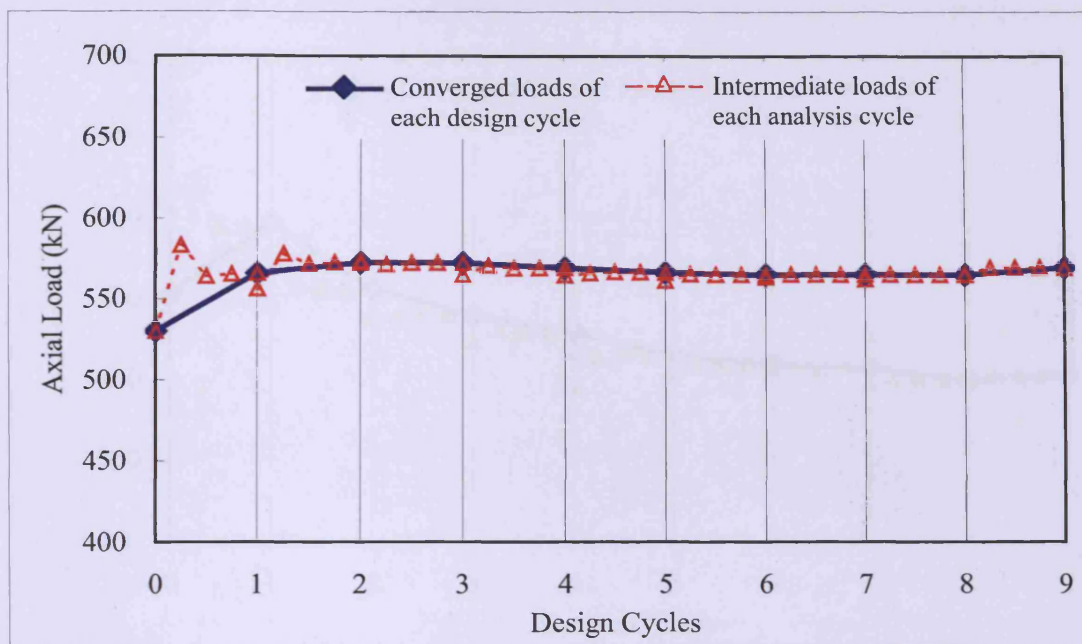


(a)

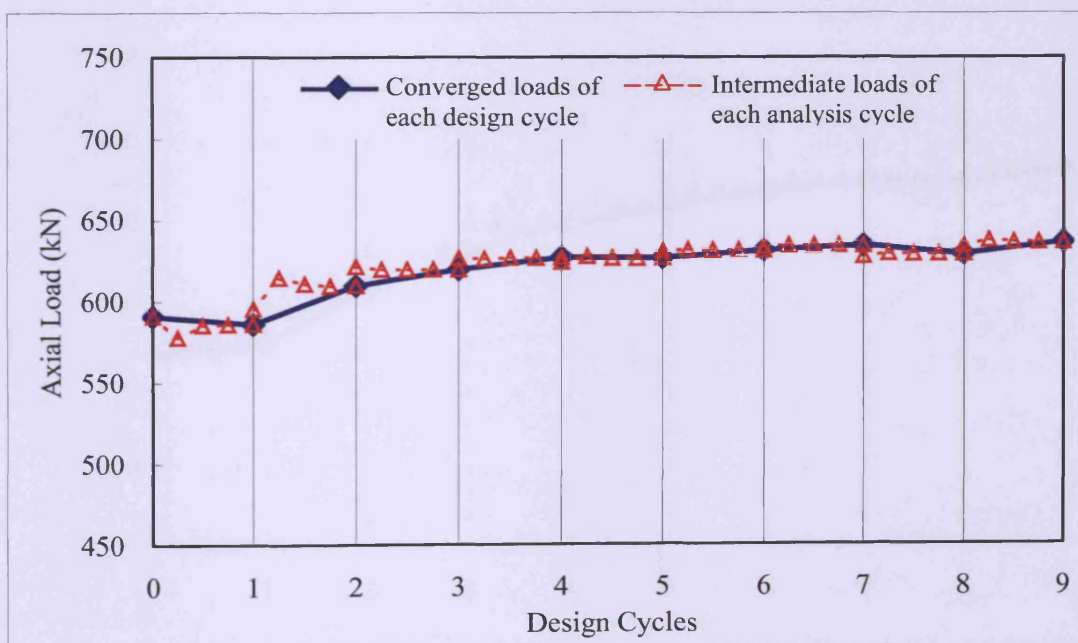


(b)

Figure C.4 Redistribution of axial loads in panels (a) B1 and (b) B2.

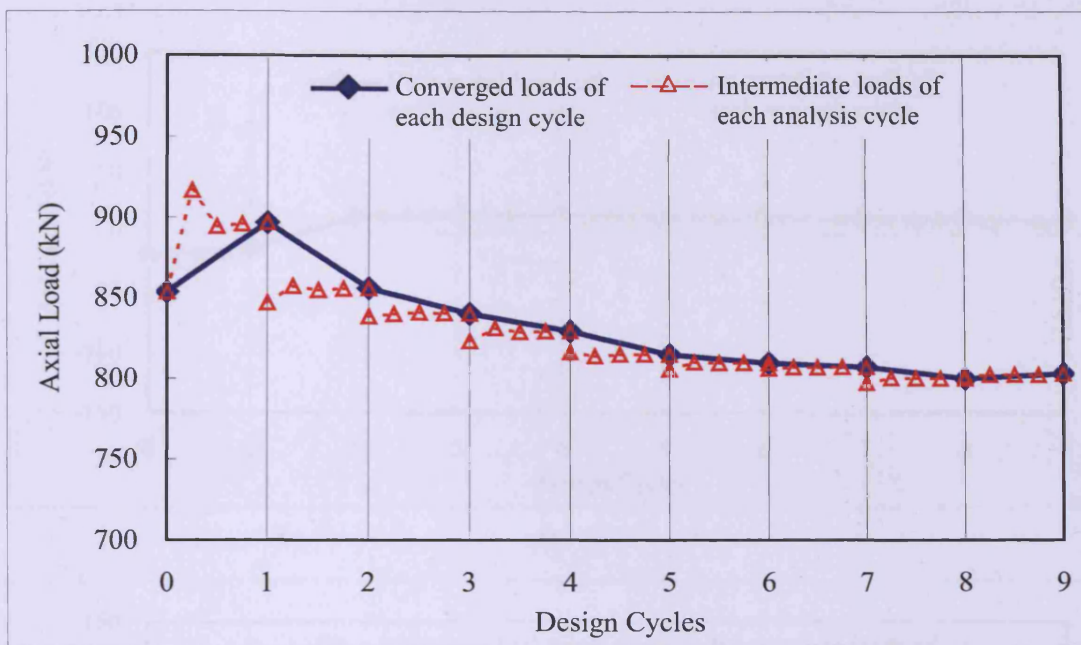


(a)

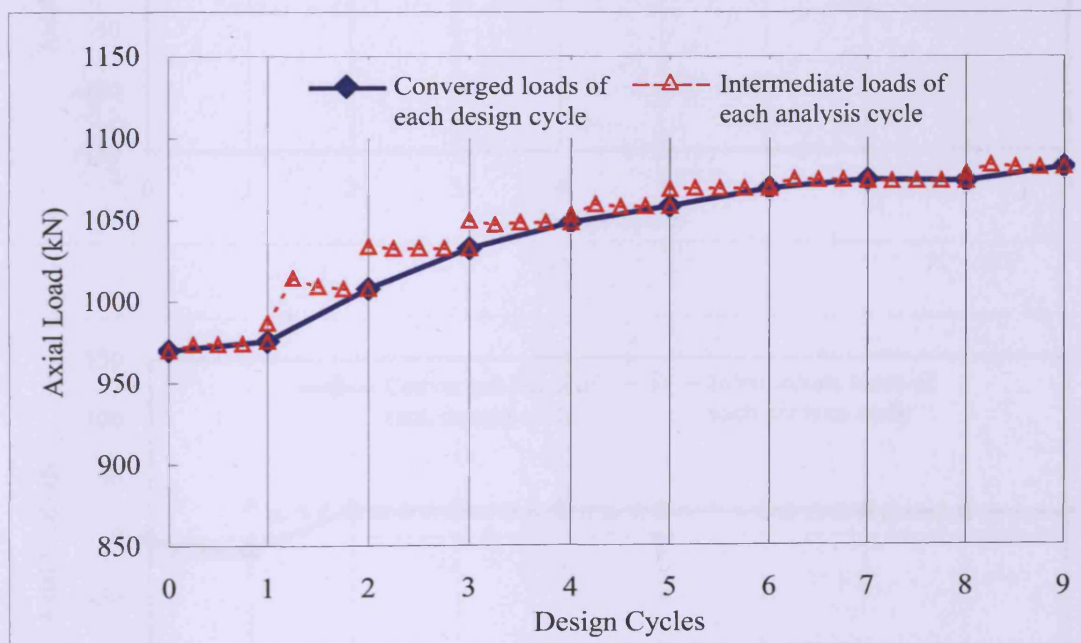


(b)

Figure C.5 Redistribution of axial loads in panels (a) B3 and (b) B4.

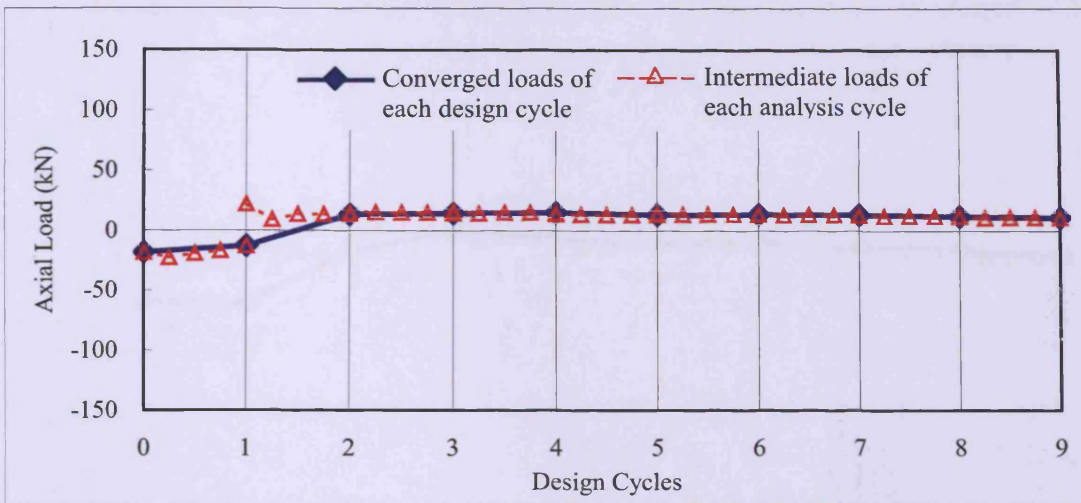


(a)

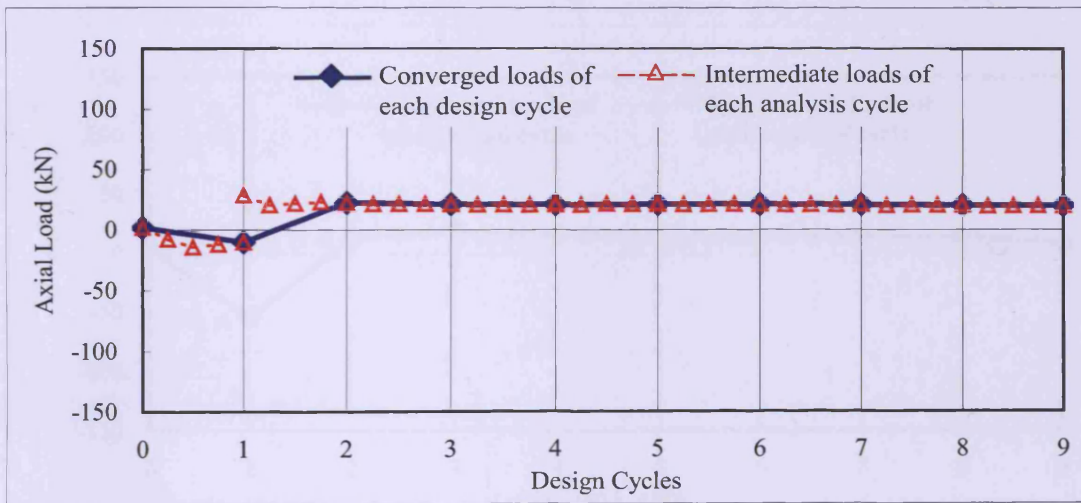


(b)

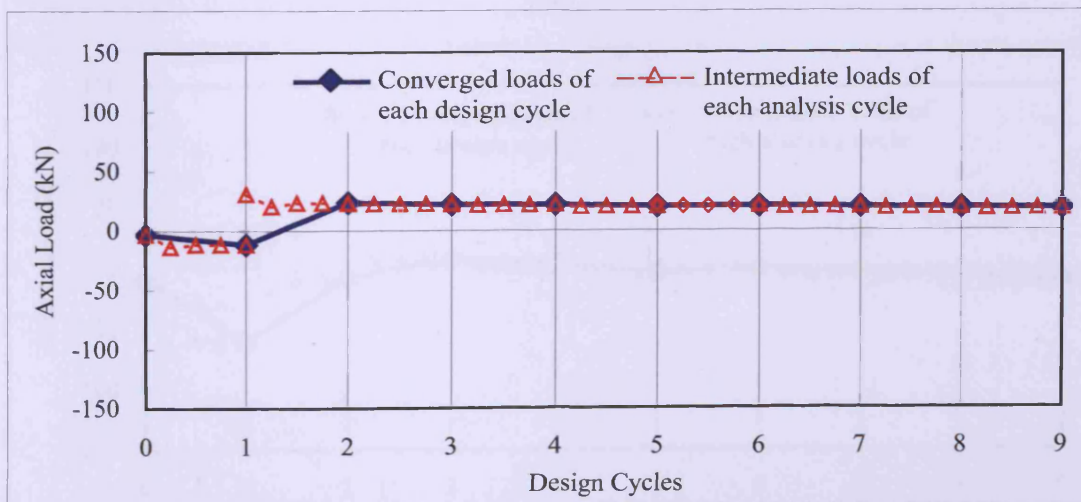
Figure C.6 Redistribution of axial loads in panels (a) B5 and (b) B6.



(a)

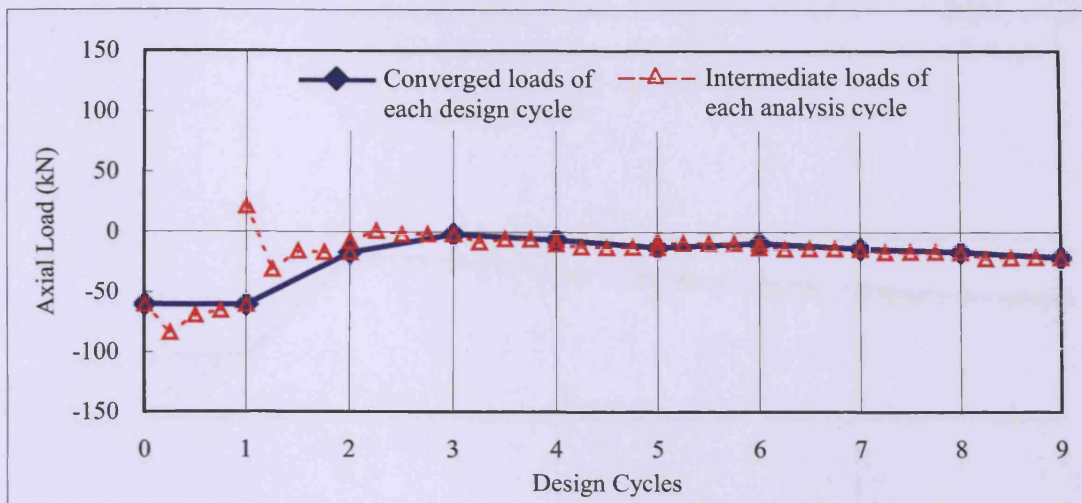


(b)

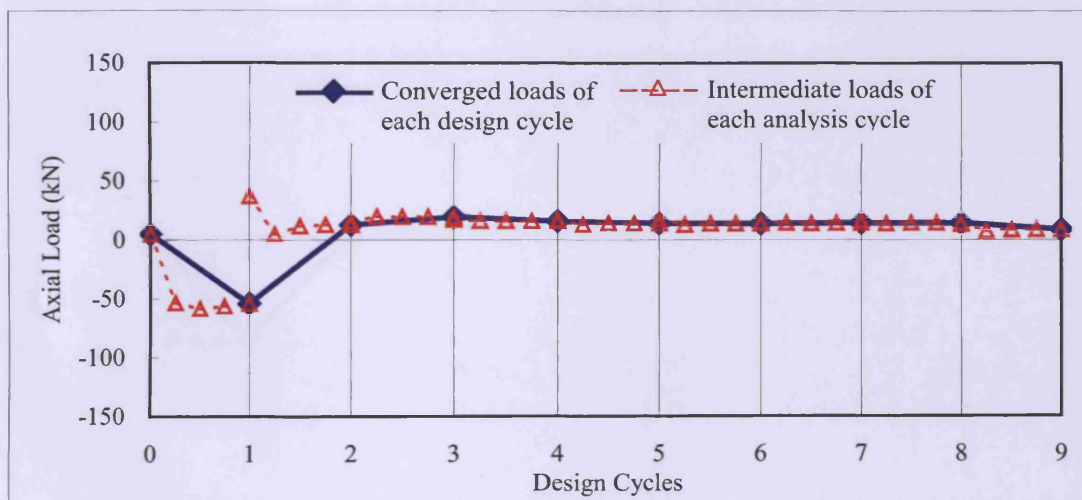


(c)

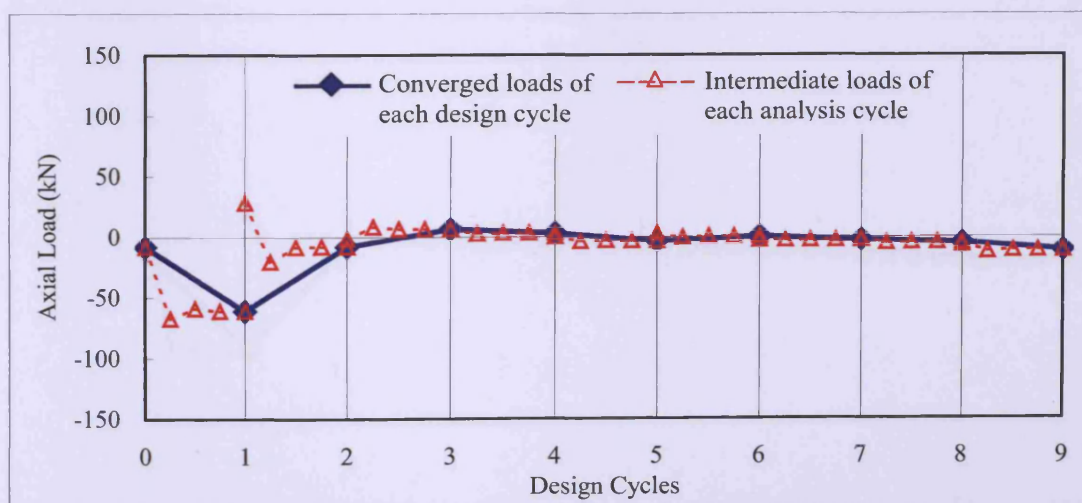
Figure C.7 Redistribution of axial loads in panels (a) S1, (b) S2 and (c) S3.



(a)

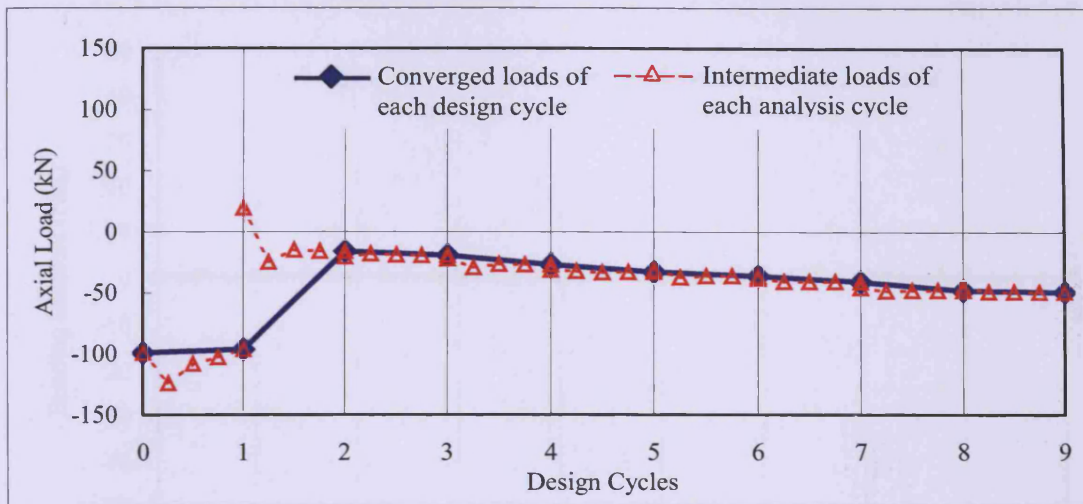


(b)

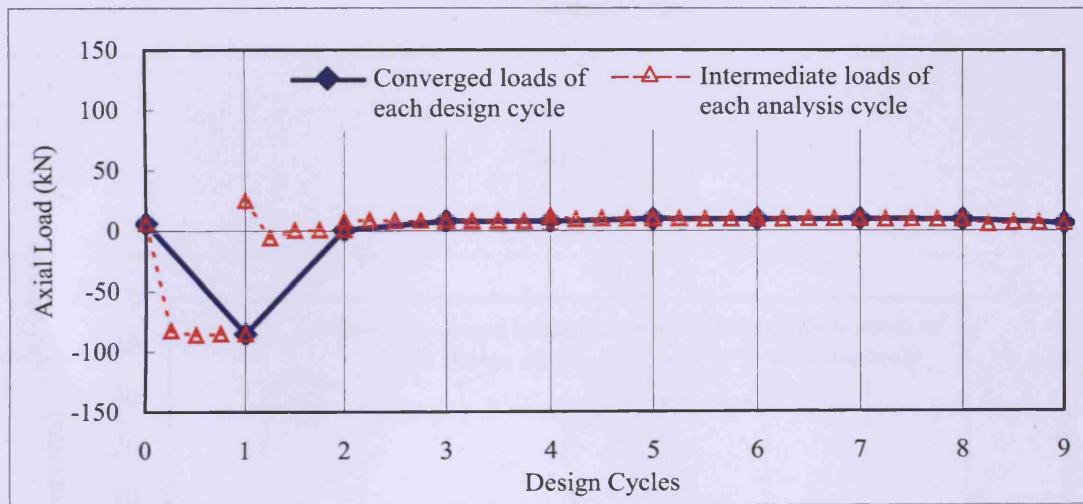


(c)

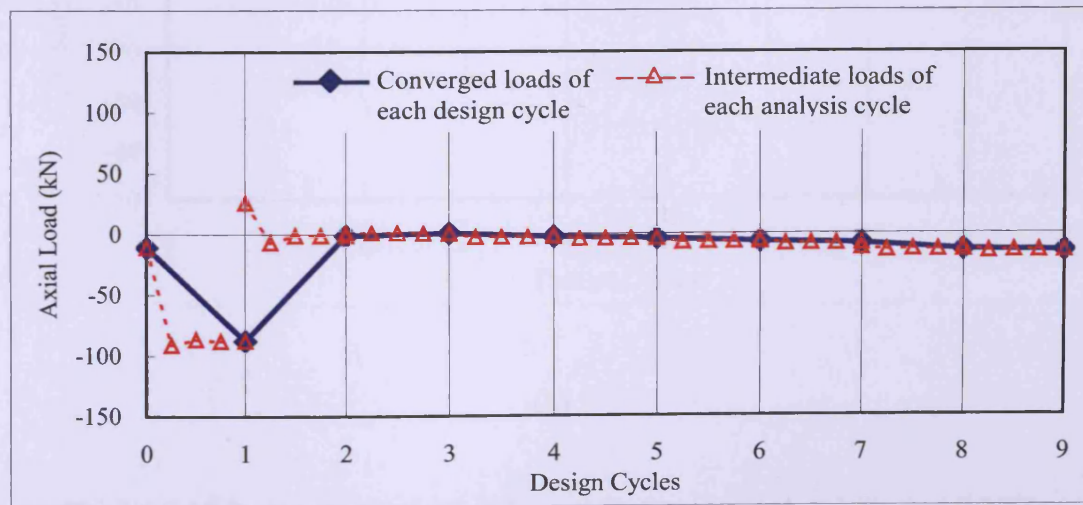
Figure C.8 Redistribution of axial loads in panels (a) S4, (b) S5 and (c) S6.



(a)

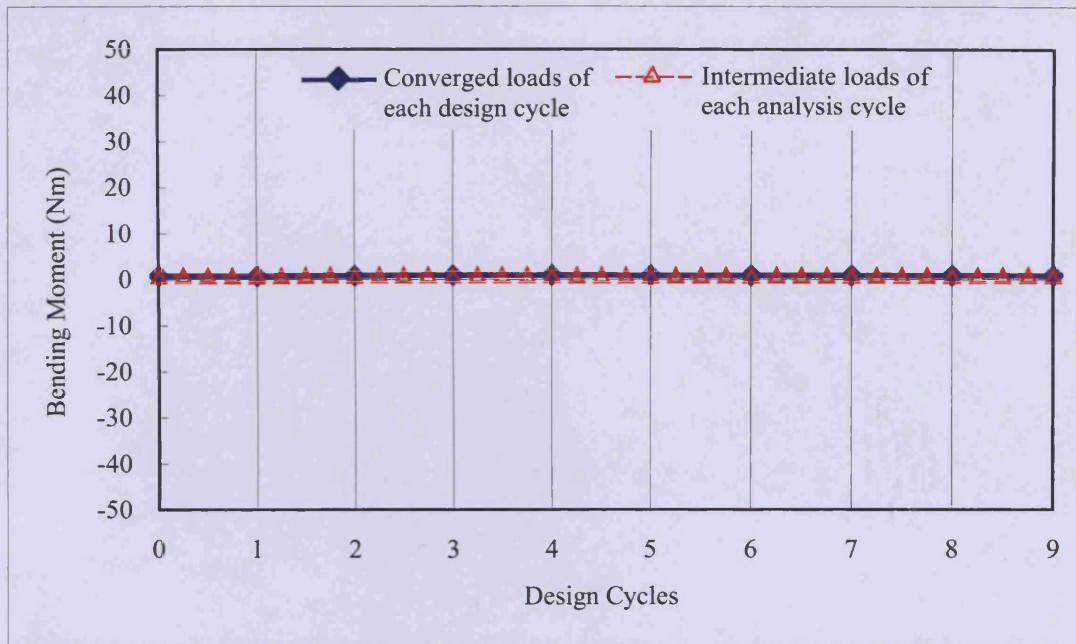


(b)

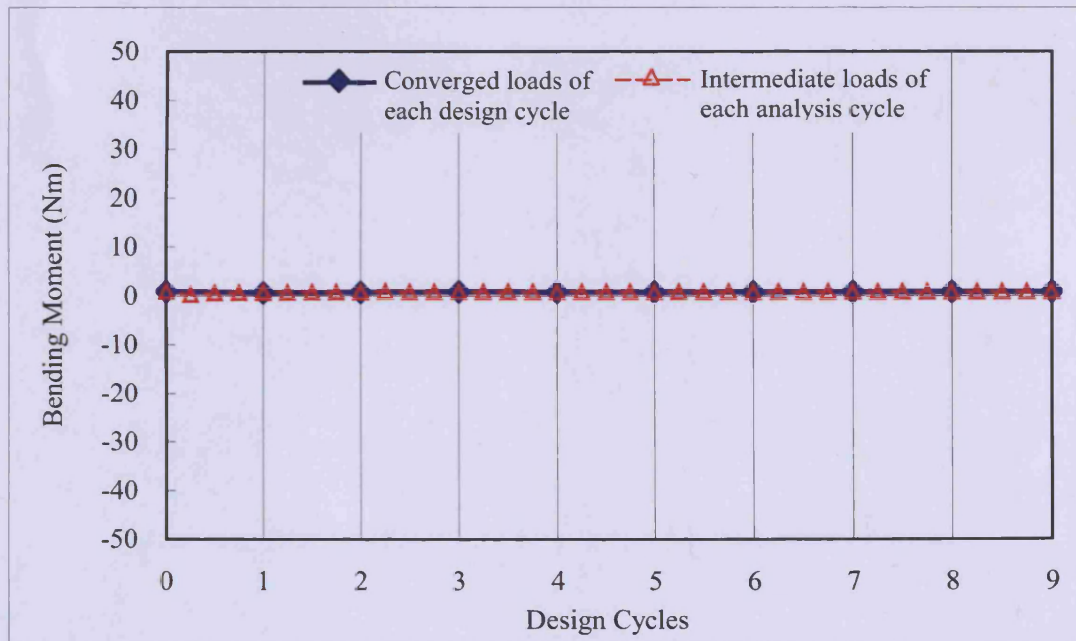


(c)

Figure C.9 Redistribution of axial loads in panels (a) S7, (b) S8 and (c) S9.

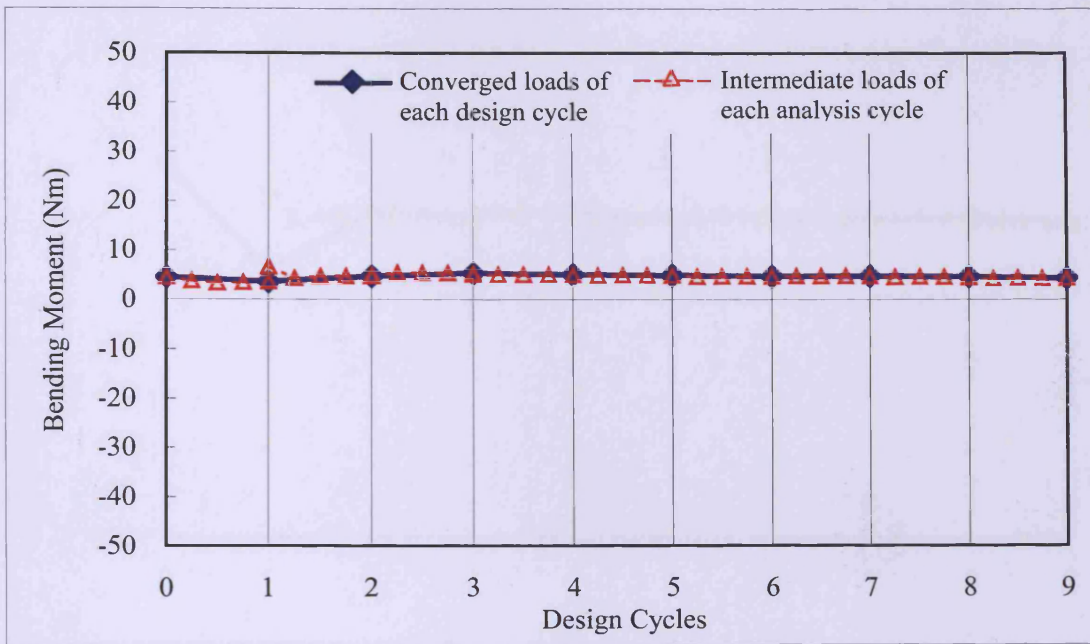


(a)

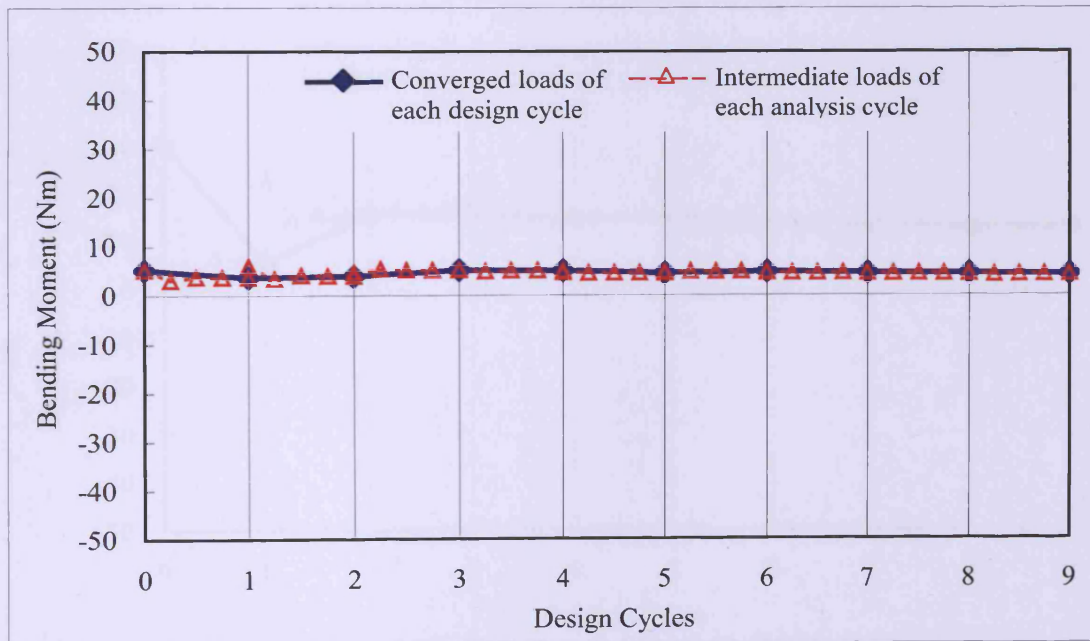


(b)

Figure C.10 Redistribution of bending moments in panels (a) T1 and (b) T2.

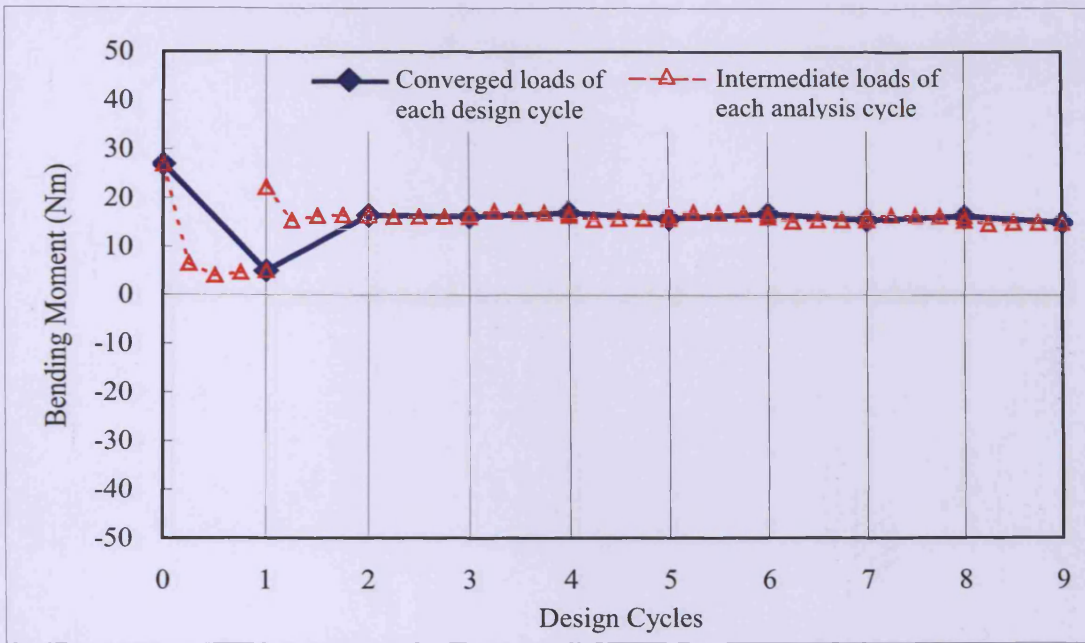


(a)

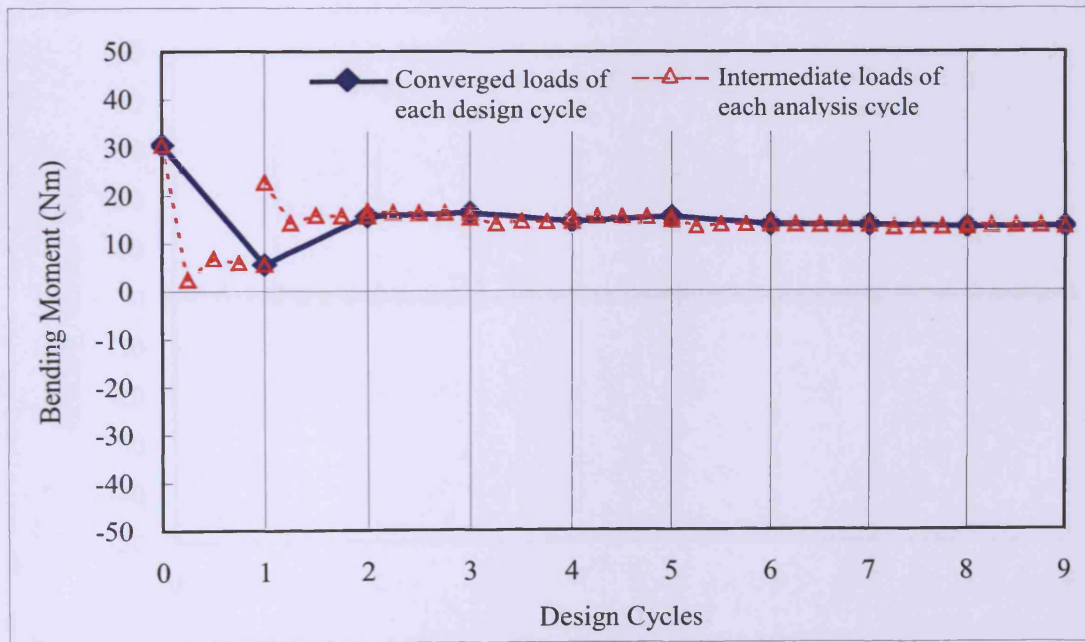


(b)

Figure C.11 Redistribution of bending moments in panels (a) T3 and (b) T4.

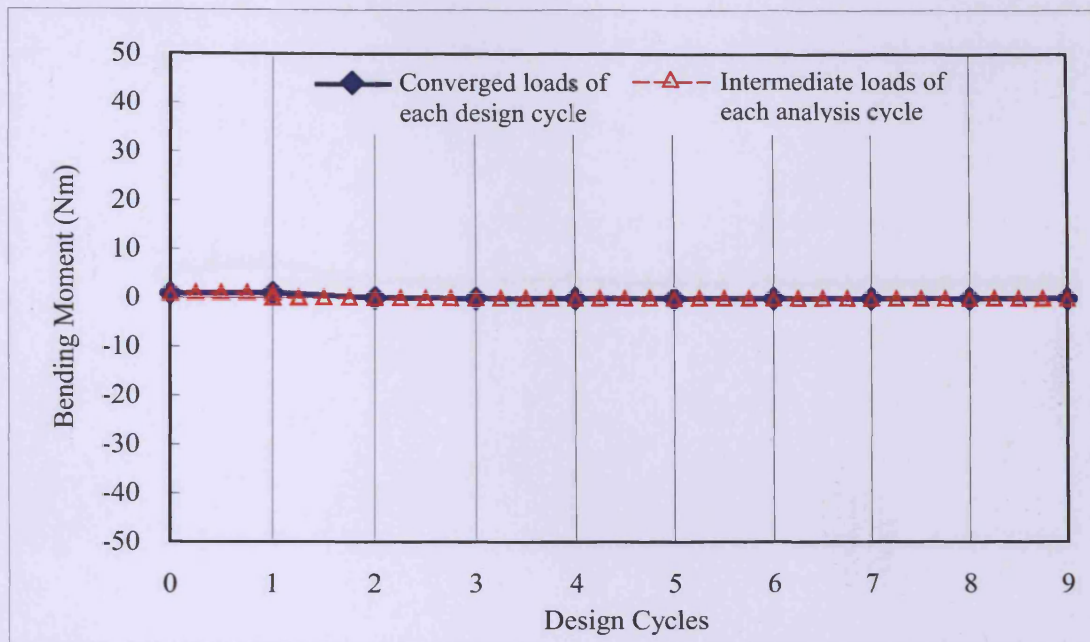


(a)

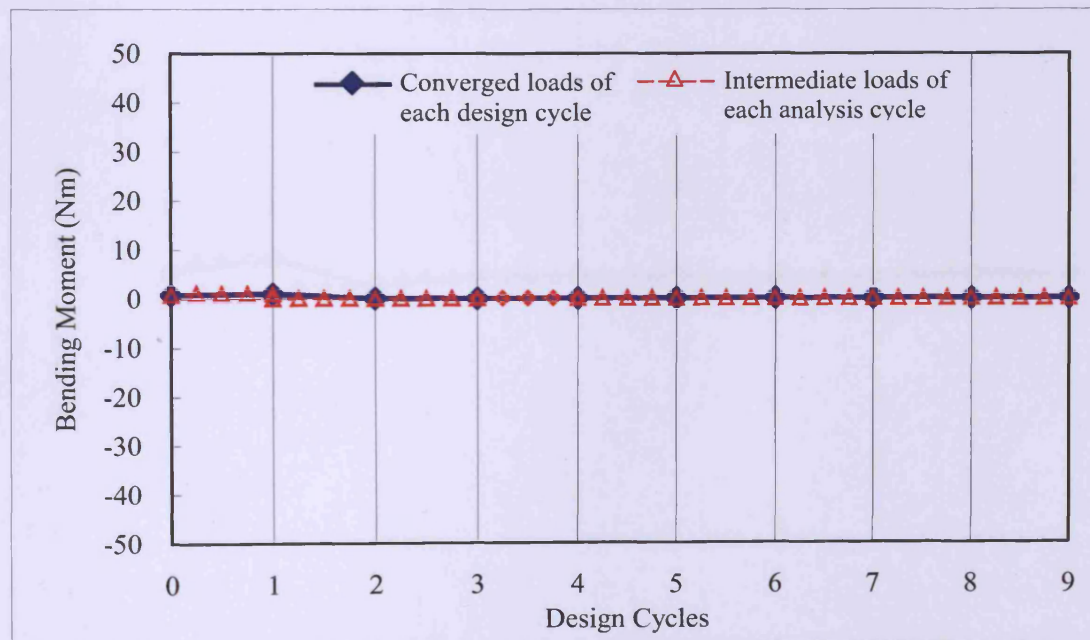


(b)

Figure C.12 Redistribution of bending moments in panels (a) T5 and (b) T6

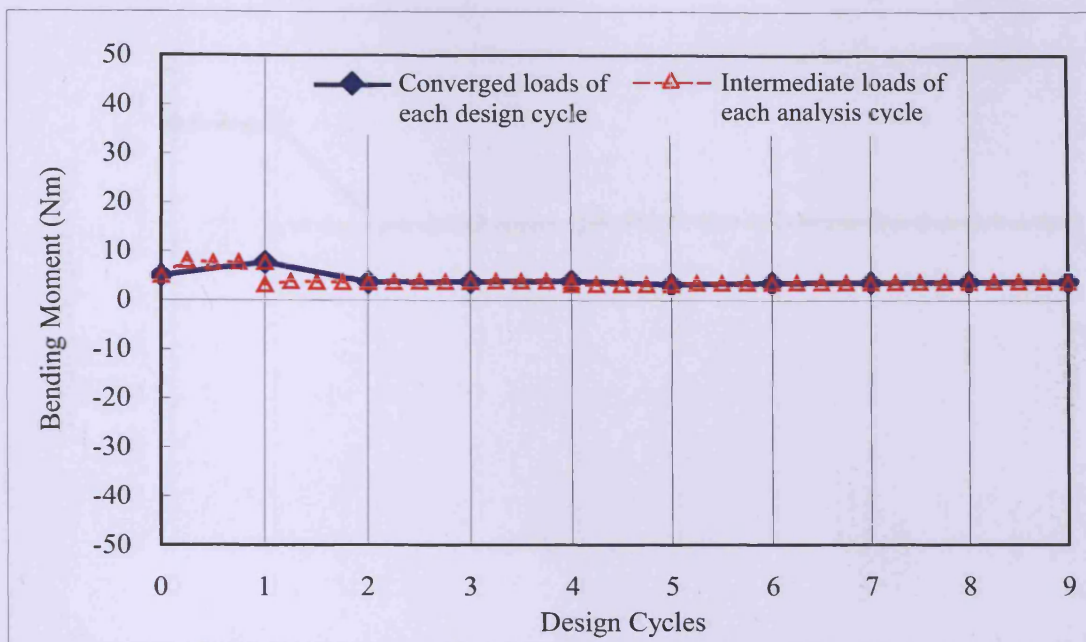


(a)

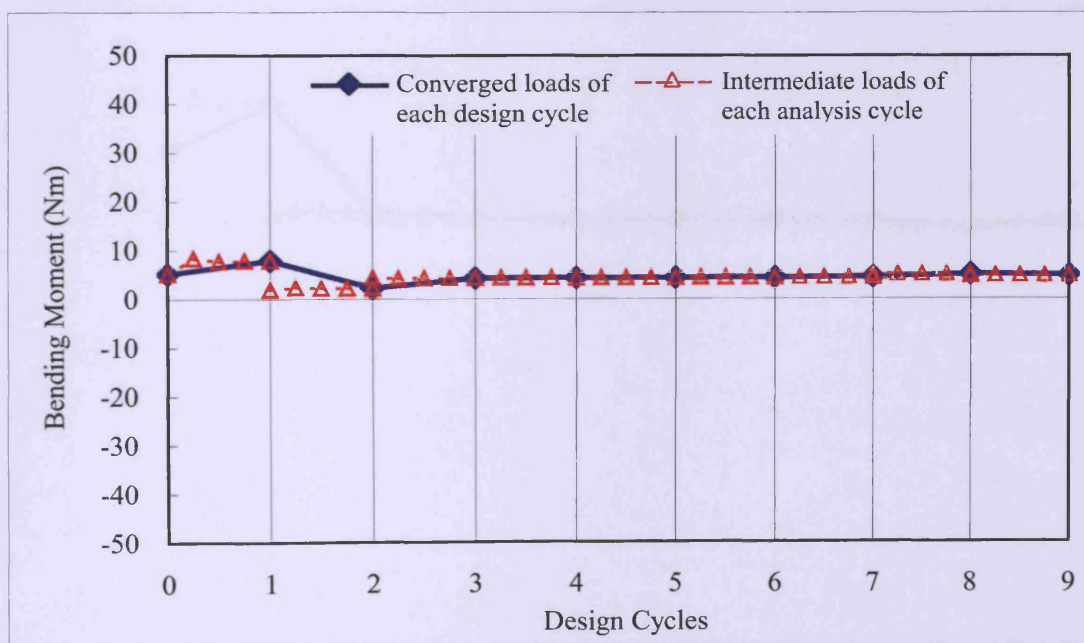


(b)

Figure C.13 Redistribution of bending moments in panels (a) B1 and (b) B2.

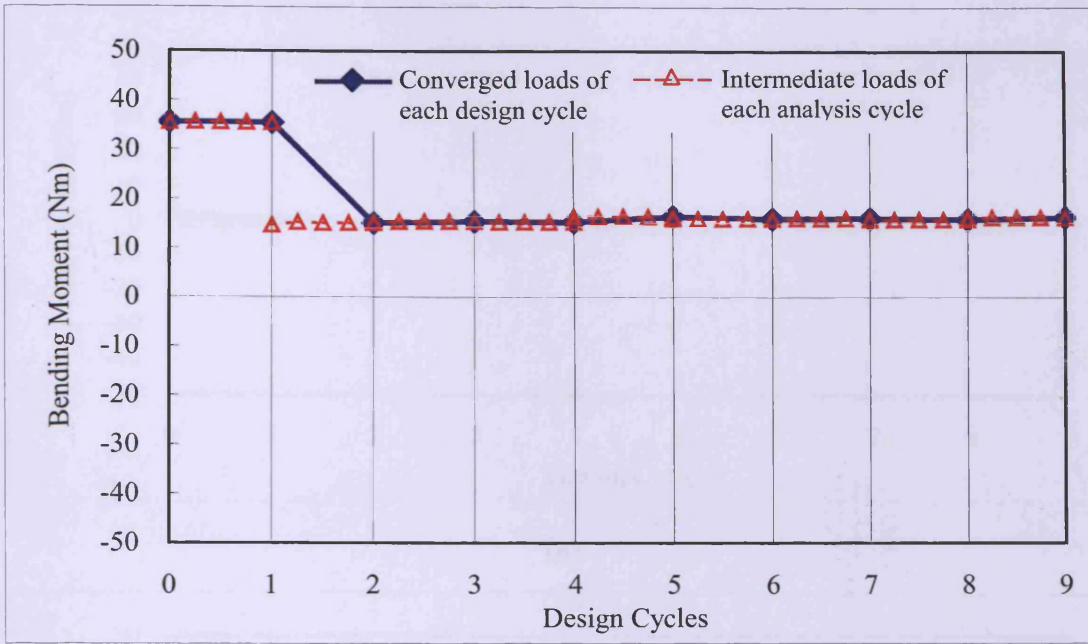


(a)

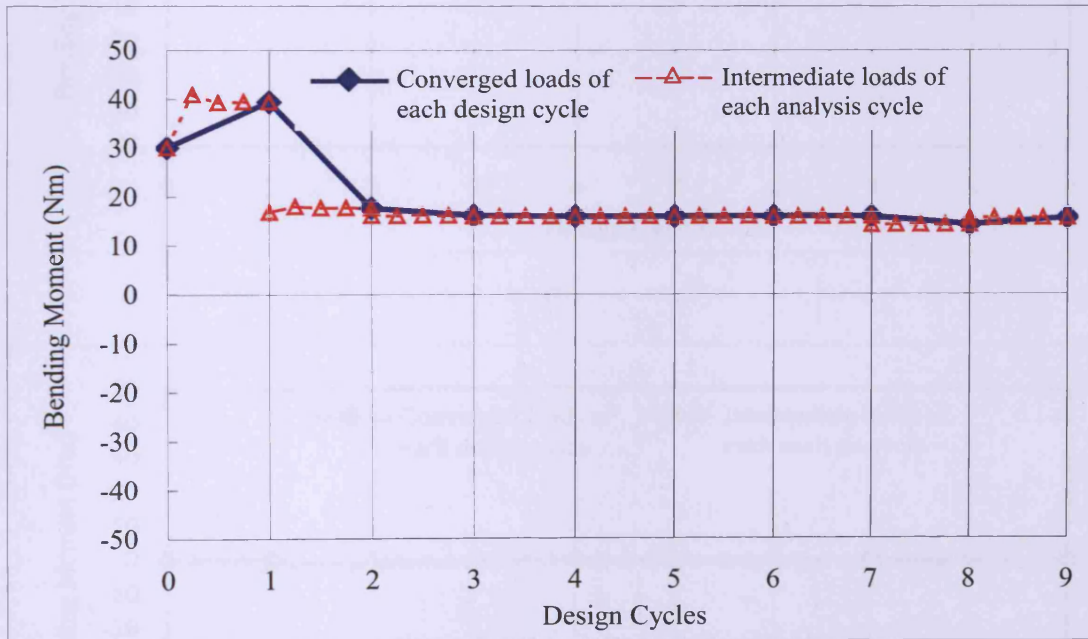


(b)

Figure C.14 Redistribution of bending moments in panels (a) B3 and (b) B4.

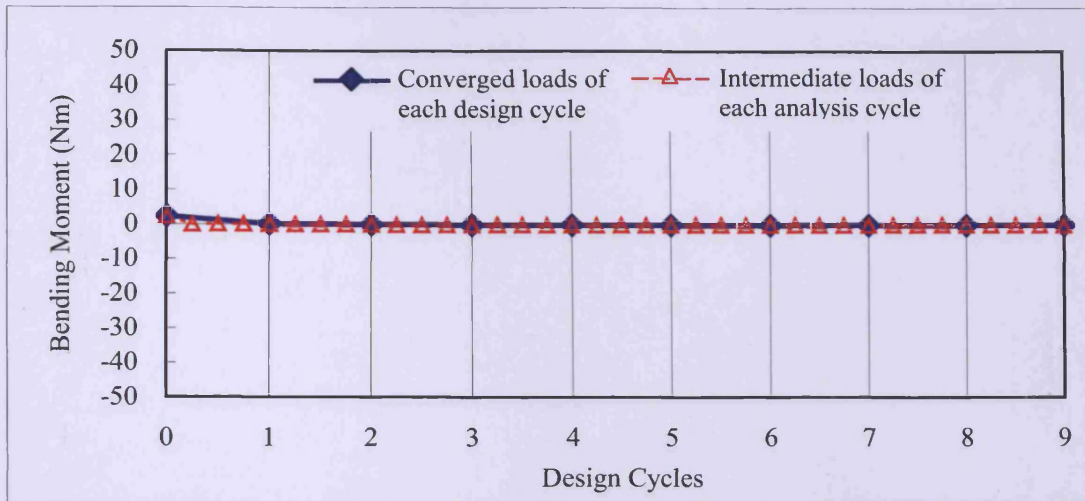


(a)

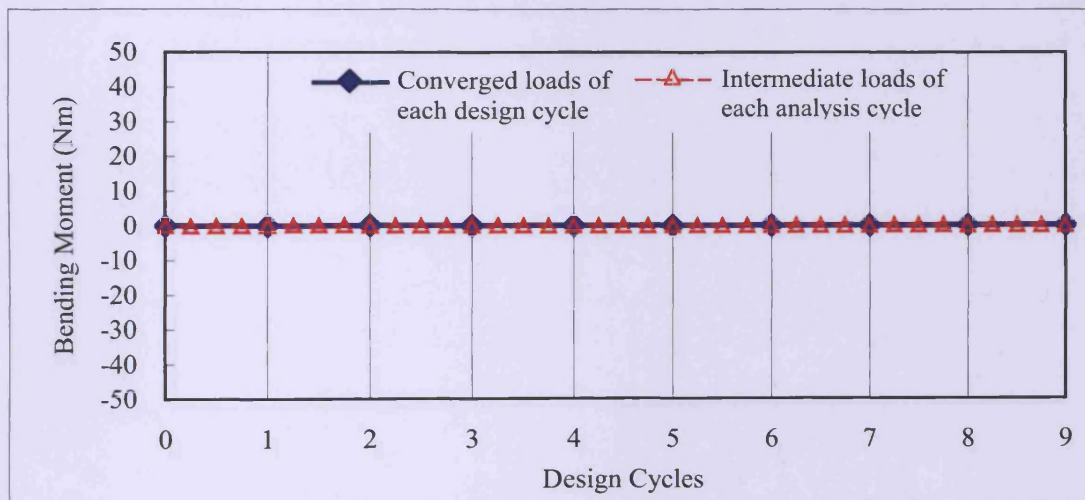


(b)

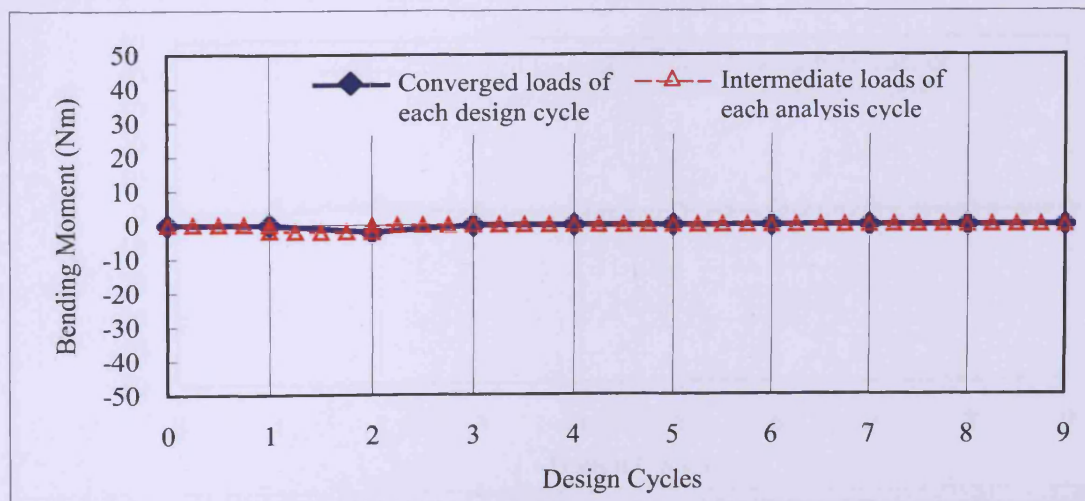
Figure C.15 Redistribution of bending moments in panels (a) B5 and (b) B6.



(a)

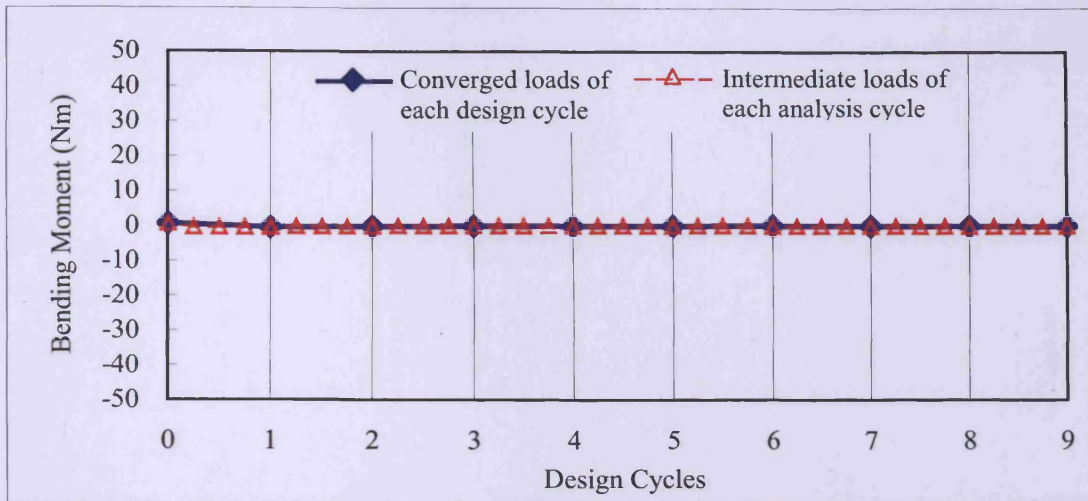


(b)

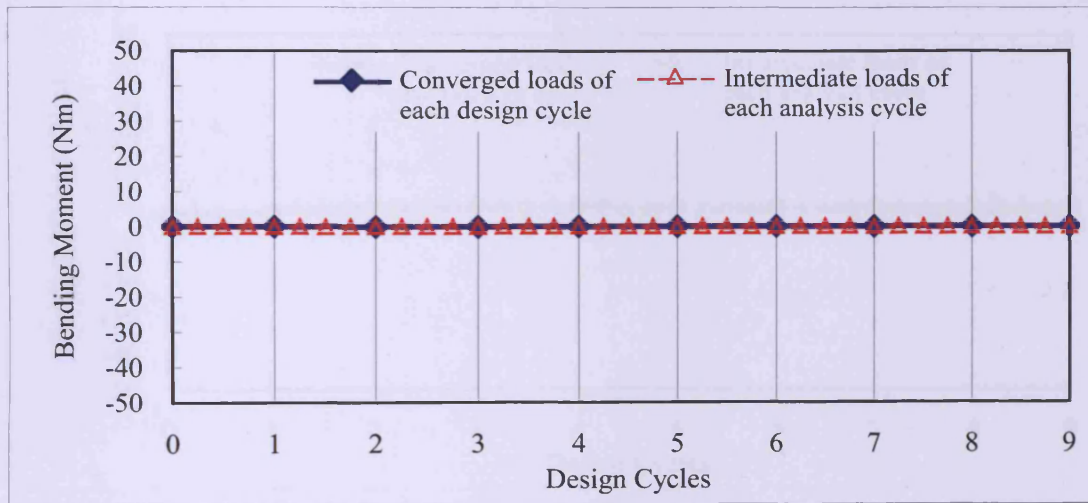


(c)

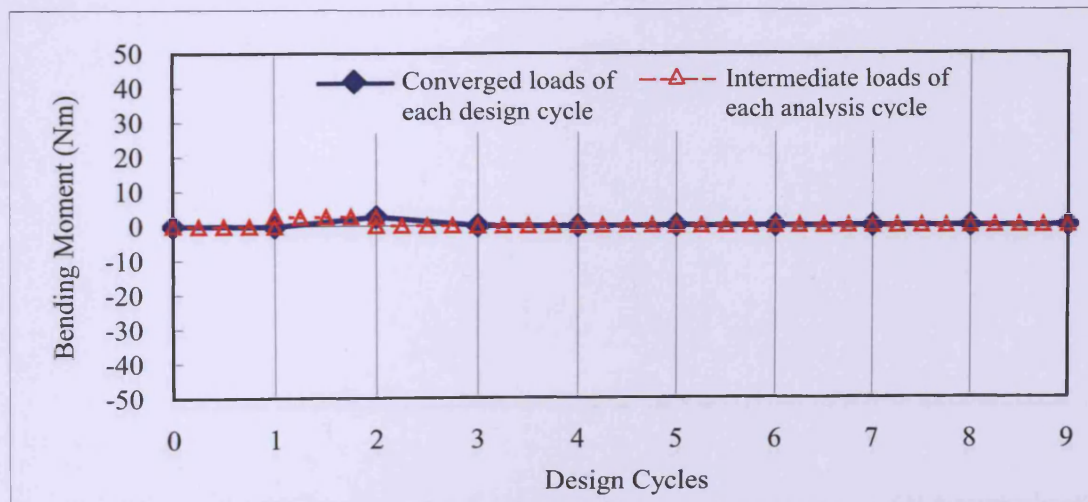
Figure C.16 Redistribution of bending moments in panels (a) S1, (b) S2 and (c) S3.



(a)

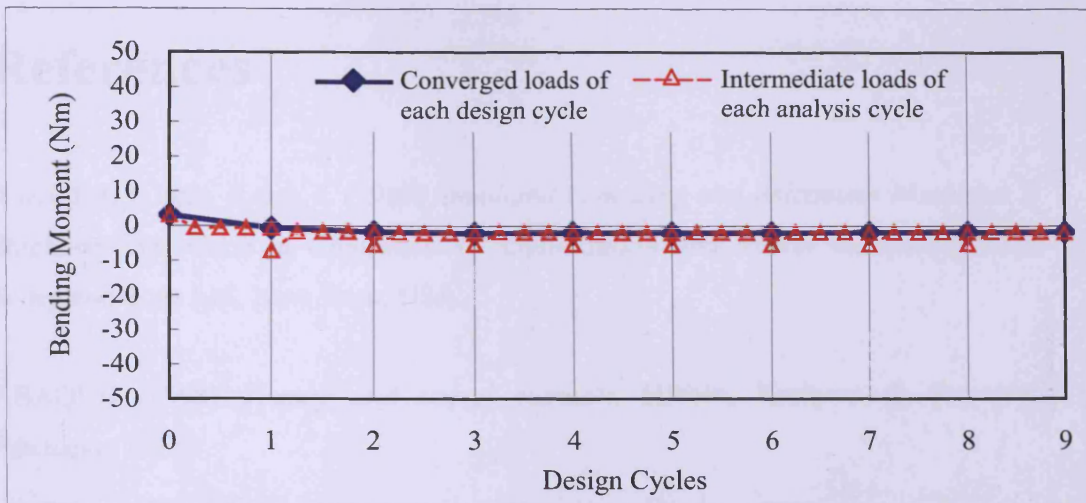


(b)

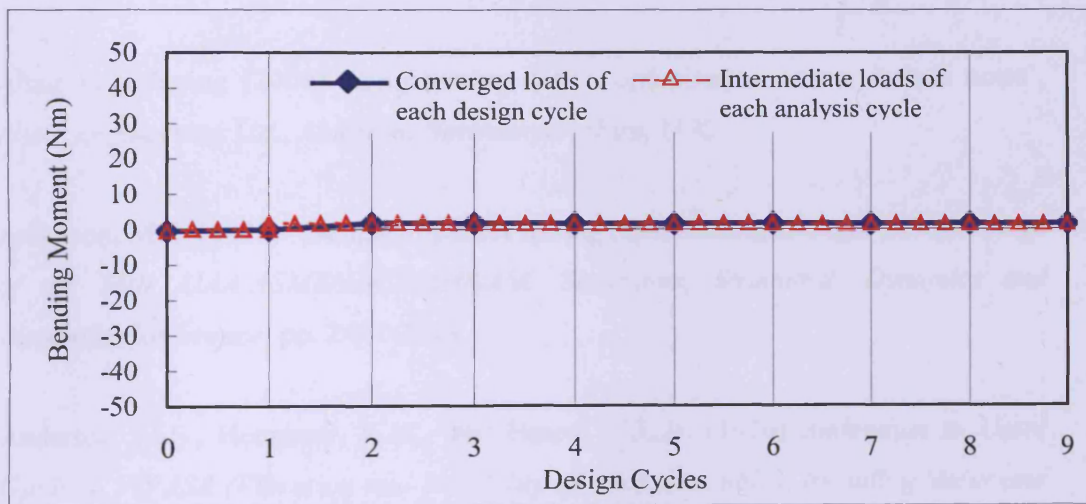


(c)

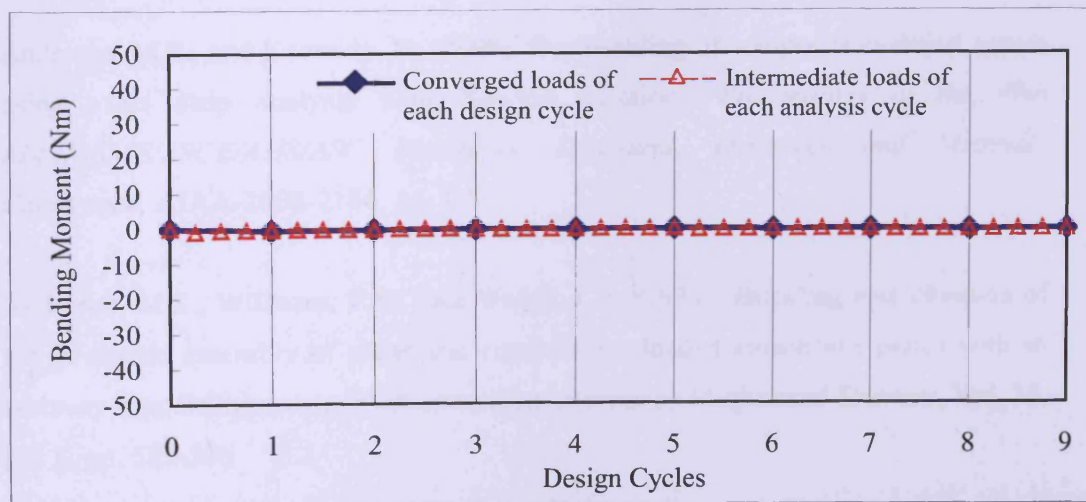
Figure C.17 Redistribution of bending moments in panels (a) S4, (b) S5 and (c) S6.



(a)



(b)



(c)

Figure C.18 Redistribution of bending moments in panels (a) S7, (b) S8 and (c) S9.

References

Aarts, E.H.L. and Korst, J. (1989) *Simulated Annealing and Boltzmann Machines: A Stochastic Approach to Combinatorial Optimisation and Neural Computing*, John Wiley and Sons Ltd, New York, USA.

ABAQUS (1998) *Theory and users' manuals*, Hibbitt, Karlsson & Sorensen, Pawtucket USA.

Almroth, B.O. and Brogan, F.A. (1978) *The STAGS computer code*, NASA CR-2950.

Altair Engineering (2000). 'Engineering design optimisation course lecture notes', *Altair Engineering Ltd., Alderton, Northamptonshire, U.K.*

Anderson, M.S. (1997) 'Design of panels having postbuckling strength', *Proceedings of the 38th AIAA/ASME/ASCE/AHS/ASC Structures, Structural, Dynamics and Materials Conference*, pp. 2407-2413.

Anderson, M.S., Hennessy, K.W., and Heard, W.L.Jr. (1976) *Addendum to Users Guide to VIPASA (Vibration and Instability of plate Assemblies including Shear and Anisotropy)*, NASA Technical Memorandum X-73914

Anderson, M.S., and Kennedy, D. (2008) 'Postbuckling of composite stiffened panels using exact strip analysis with Newton iteration', *Proceedings of the 49th AIAA/ASME/ASCE/AHS/ASC Structures, Structural, Dynamics and Materials Conference*, AIAA-2008-2184, pp. 1-8.

Anderson, M.S., Williams, F.W. and Wright, C.J. (1983) 'Buckling and vibration of any prismatic assembly of shear and compression loaded anisotropic plates with an arbitrary supporting structure', *International Journal of Mechanical Sciences*, Vol. 25, No. 8, pp. 585-596.

Arendsen, P. (2001) 'Final report of the GARTEUR Action Group (SM) AG-21 on multi disciplinary wing optimisation', NLR-TR-2001-557.

Arora, J.S. (1997) *Guide to structural optimisation*, ASCE manuals and reports on engineering practice NO. 90, ASCE Publication.

Autodesk [online] (Accessed 19 April 2011) available from <URL: <http://www.autodesk.co.uk>>.

Barrett, R., Berry, M., Chan, T.F., Demmel, J., Donato, J., Dongarra, J., Eijkhout, V., Pozo, R., Romine, C., and Van der Vorst, H. (1994) *Templates for the Solution of Linear Systems: Building Blocks for Iterative Methods*, 2nd Edition, SIAM, Philadelphia, PA.

Bisagni, C. and Lanzi, L. (2002) 'Post-buckling optimisation of composite stiffened panels using neural networks', *Composite Structures*, Vol. 58, pp. 237-247.

Butler, R. and Williams, F.W. (1990) 'Optimum design features of VICONOPT, an exact buckling program for prismatic assemblies of anisotropic plates', *Proceedings of the 31st AIAA/ASME/ASCE/AHS/ASC Structures, Structural Dynamics and Materials Conference*, Long Beach, CA, pp. 1289-1299.

Butler, R. and Williams, F.W. (1992) 'Optimum design using VICONOPT, a buckling and strength constraint program for prismatic assemblies of anisotropic plates', *Computers and Structures*, Vol. 43, No. 4, pp. 699-708.

Carroll, C.W., (1961) 'The created response surface technique for optimizing nonlinear restrained systems', *Operations Research*, Vol. 9, pp. 169-184.

Case, J., Chilver, L. and Ross, C.T.F. (1993) *Strength of materials and structures: with an introduction to finite element methods*, 3rd Rev. ed, Edward Arnold, London.

Che, B., Kennedy, D. and Featherston, C.A. (2010) 'Improved exact strip postbuckling analysis for anisotropic plates', Proceedings of 2nd Royal Aeronautical Society Conference on Aircraft Structural Design, London, Paper No. 37.

Cheung, Y.K. (1968) 'The finite strip method in the analysis of elastic plates with two opposite simply supported ends', *Proc. Inst. Civ. Eng.*, 40 (1), pp.1-7.

Cheung, Y.K. (1976) *Finite strip method in structural analysis*, Pergamon Press, Oxford, UK.

Cooper, L. and Steinberg, D. (1970) *Introduction to Methods of Optimisation*, W.B.Saunders Company.

Courant, R. (1943) 'Variational methods for the solution of problems of equilibrium and vibrations', *Bull. Am. Math. Soc.*, 49 (1), pp.1-23.

Dantzig, G.B. (1963) *Linear programming and its extensions*, Princeton University Press, Princeton, NJ.

Davidon, W.C. (1959) 'Variable metric method for minimisation', *SIAM Journal on Optimisation*, Vol. 1, pp. 1-17.

Dawe, D.J. (1977) 'Finite strip buckling analysis of curved plate assemblies under biaxial loading', *International Journal of Solids and Structures*, Vol. 13, pp. 1141-1155.

Dawe, D.J., Lam, S.S.E. and Azizian, Z.G. (1993) 'Finite strip post- local-buckling analysis of composite prismatic plate structures', *Computers & Structures*, Vol. 48, No. 6, pp. 1011-1023.

Day, A.S. (1965) 'An introduction to dynamic relaxation (Dynamic relaxation method for structural analysis, using computer to calculate internal forces following development from initially unloaded state)', *The Engineer*, Vol. 219, pp. 218-221.

Degenhardt, R., Rolfes, R., Zimmermann, R. and Rohwer, K. (2006) 'COCOMAT-improved material exploitation of composite airframe structures by accurate simulation of postbuckling and collapse', *Composite Structures*, Vol. 73, No. 2, pp. 175-178.

Diaconu, C.G. and Weaver, P.M. (2005) 'Approximate solution and optimum design for postbuckling of axially compressed laminated composite plates', *AIAA Journal*, Vol. 43, No. 4, pp. 906-914.

Faggioli, A. and Falzon, B.G. (2007) 'Optimisation strategy for minimizing damage in postbuckling stiffened panels', *AIAA Journal*, Vol. 45, No. 10, pp. 2520-2528.

Fares, M.E., Youssif, Y.G. and Elshoraky, A.E. (2006) 'Non-linear design and control optimisation of composite laminated plates with buckling and postbuckling objectives', *International Journal of Non-Linear Mechanics*, Vol. 41, pp. 807-824.

Fares, M.E., Youssif, Y.G. and Hafiz, M.A. (2005) 'Multiobjective design and control optimization for minimum thermal postbuckling dynamic response and maximum buckling temperature of composite laminates', *Structural and Multidisciplinary Optimization*, Vol. 30, No. 2, pp. 89-100.

Fiacco, A.V. and McCormick, G.P. (1968) *Nonlinear programming, sequential unconstrained minimization techniques*, John Wiley & Sons, New York.

Fischer, M. (2002) *Multilevel optimisation of aerospace and lightweight structures*, PhD Thesis, Cardiff University.

Fischer, M., Kennedy, D., and Featherston, C.A. (2002a) 'Multilevel optimisation of a composite aircraft wing using Viconopt MLO', *In Proceedings of the 9th AIAA/ISSMO Symposium on Multidisciplinary analysis and optimisation*, Atlanta, GA, Paper AIAA 2002-5511 (AIAA, Reston, VA).

Fischer, M., Kennedy, D., and Featherston, C.A. (2002b) 'Multilevel optimisation of aerospace and lightweight structures', *In Proceedings of the 23rd International*

Congress of Aeronautical Sciences, Toronto, pp. 344. 1-344.9 (Canadian Aeronautics and Space Institution, Ottawa).

Fletcher, R. and Powell, M.J.D. (1963) 'A rapidly convergent descent method for minimization', *Computer Journal*, Vol. 6, p.163.

Fletcher, R. and Reeves, C.M. (1964) 'Function minimisation by conjugate gradients', *Computer Journal*, Vol. 7, p.149.

Fogel, D.B. (1994) 'An introduction to simulated evolutionary optimization. IEEE Trans. on Neural Networks', *Special Issue on Evolutionary Computation*, Vol. 5, No. 1, pp. 3-14.

Fox, R.L. (1971) *Optimisation methods for engineering design*, Addison-Wesley, Mass.

GARTEUR (1997a) 'System level structural optimisation: A compendium of European aerospace programs. Final report of the GARTEUR Action Group on Structural Optimisation SM(AG13) [open literature]', Volume 1 of 3, *GARTEUR TP078*, DERA, Farnborough, UK.

GARTEUR (1997b) 'A compendium of European software facilities for stiffened plate design and multilevel optimisation. Final report of the GARTEUR Action Group on Structural Optimisation SM(AG13) [open literature]', Volume 2 of 3, *GARTEUR TP079*, DERA, Farnborough, UK.

GARTEUR (1997c) 'Assessment of benchmark problems on stiffened panel design and multilevel optimisation. Final report of the GARTEUR Action Group on Structural Optimisation SM(AG13) [limited literature]', Volume 3 of 3, *GARTEUR TP080*, DERA, Farnborough, UK.

Gass, S.I. (1969) *Linear Programming: Methods and Applications*, 3rd Edition, McGraw-Hill, New York.

- Giles, G.L. (1971) 'Procedure for automating aircraft wing structural design', *Journal of the Structural Division*, ASCE, Vol. 97, No. St1, pp. 99-113.
- Glover, F. (1989) 'Tabu search part I', *ORSA Journal on Computing*, Vol. 1, pp. 190-206.
- Glover, F. (1990) 'Tabu search part II', *ORSA Journal on Computing*, Vol. 2, pp. 4-32.
- Goldberg, D.E. (1989) *Genetic Algorithms in Search, Optimisation and Machine Learning*, Addison-Wesley Longman Publishing co., Inc, Boston, USA.
- Graves-Smith, T.R. and Sridharan, S. (1978) 'A finite strip method for the post-locally-buckled analysis of plate structures', *International Journal of Mechanical Sciences*, Vol. 20, pp. 833-842.
- Griffith, R.E., and Stewart, R.A. (1961) 'A nonlinear programming technique for the optimisation of continuous processing systems', *Management Science*, Vol. 7, No. 4 pp. 379-392.
- Groncu, V. (1994) 'General report: general theory of coupled instabilities', *Thin-walled structures*, Vol. 19, pp. 81-127.
- Gurney, K. (1997) *An Introduction to Neural Networks*. London, Routledge, ISBN 1-85728-673-1 (hardback) or ISBN 1-85728-503-4 (paperback).
- Hadley, G. (1962). *Linear Programming*, Addison-Wesley, Reading, Massachusetts.
- Hafka, R. T., and Gurdal, Z. (1991) *Elements of structural optimisation (3rd revised and expanded edition)*, Springer.
- Henwood D. and Bonet, J. (1996) *Finite Elements – A Gentle Introduction*, MacMillan Press Ltd, London.

- Hooke, R., and Jeeves, T. A. (1961) 'Direct search solution of numerical and statistical problems', *J. of Assn. Computing Machinery*, Vol. 8, pp. 212-229.
- Hutchinson, J.W. and Koiter, W.T. (1970) 'Postbuckling theory', *Applied Mechanics Review*, Vol. 23, pp. 1353-1366.
- Irisarri, F.X., Laurin, F., Leroy, H. and Maire, J.F. (2011) 'Computational strategy for multiobjective optimisation of composite stiffened panels', *Composite Structures*, Vol. 93, No. 3, pp. 1158-1167.
- Kalnins, K., Jekabsons, G. and Rikards, R. (2009) 'Metamodels for optimisation of post-buckling responses in full-scale composite structures', *8th World Congress on Structural and Multidisciplinary Optimisation*, Lisbon, Portugal.
- Kelley, C.T. (1999) *Iterative Methods for Optimisation*, the Society for Industrial and Applied Mathematics, Philadelphia.
- Kennedy, D. (2006a) 'Buckling of plates', *Lecture notes*, Cardiff University, Cardiff, UK.
- Kennedy, D. (2006b) 'Postbuckling of plates', *Lecture notes*, Cardiff University, Cardiff, UK.
- Kennedy, D., Featherston, C.A. (2010) 'Exact strip analysis and optimum design of aerospace structures', *The Aeronautical Journal*, Vol. 114, No. 1158, pp. 505-512.
- Kennedy, D., Fischer, M., and Featherston, C.A. (2007) 'Recent developments in exact strip analysis and optimum design of aerospace structures', *Proceedings of the Institution of Mechanical Engineers, Part C: Journal of Mechanical Engineering Science*, Vol. 221, No. 4, pp. 399-413.
- Kennedy, D., O'Leary, O.J. and Williams, F.W. (2005) 'Optimum design of prismatic plate assemblies with spectral gap constraints', *Proceedings of 5th International*

Symposium on Vibrations of Continuous Systems, Berchtesgaden, pp. 36-38 (Virginia Polytechnic Institute and State University, Blacksburg, VA).

Kennedy, D., Ong, T.J., O'Leary, O.J. and Williams, F.W. (1999) 'Practical optimisation of aerospace panels', *Proceedings of 1st ASMO UK/ISSMO Conference*, Ilkley, pp. 217-224 (MCB University Press, Bradford).

Kennedy, J. and Eberhart, R. (1995) 'Particle swarm optimisation', *Proceedings of IEEE International Conference on Neural Networks*, IV, pp. 1942-1948.

Kirsch, U. (1993) *Structural Optimisation – Fundamentals and Applications*, Springer Verlag, Berlin.

Koiter, W. T. (1967) *The stability of elastic equilibrium (Over de stabiliteit van het elastisch evenwicht)*, NASA TT F-10, 833, (Translated from thesis, Delft. University of Technology, 1945).

Lanzi, L. and Giavotto, V. (2006) 'Post-buckling optimisation of composite stiffened panels computations and experiments', *Composite Structures*, Vol. 73, No. 2, pp. 208-220.

Leunberger, D.G. (1984) *Introduction to linear and nonlinear programming*, Reading, Mass., Addison-Wesley.

Lillico, M., Butler, R., Hunt, G.W., Watson, A. Kennedy, D. and Williams, F.W. (2000) 'Optimum design and testing of a post-buckled stiffened panel'. *AIAA Journal*, Vol. 40, No. 5, pp. 996-1000.

Liu, W., Butler, R., Mileham, A.R. and Green, A.J. (2006) 'Bilevel optimisation and postbuckling of highly stiffened composite stiffened panels', *AIAA Journal*, Vol. 44, pp. 2562-2570.

Micro Drainage [online] (Accessed 19 April 2011) available from <URL: <http://www.microdrainage.co.uk>>.

Mohsin, R., Nasri, N.S., and Kefly, F. (2008) 'Structural analysis of NGVM pressure regulator via FEA'. *Journal of Chemical and Natural Resources Engineering*, Vol. 2 pp. 46-58. ISSN 1823-5255.

Moses, F. and Onoda, S. (1969) 'Minimum weight design of structures with application to elastic grillages', *International Journal for Numerical Methods in Engineering*, Vol.1, No. 4, pp. 311-331.

MSC/Software (1998) *MSC/NASTRAN Version 70.5 – Quick Reference Guide*, MSC, Los Angeles, USA.

MSC/Software (1999a) *MSC/NASTRAN version 70.7*, MSC, Los Angeles, USA.

MSC/Software (1999b), *MSC/PATRAN Version 9.0*, MSC, Los Angeles, USA.

Nelder, J.A. and Mead, R. (1965) 'A simplex method for function minimization', *The Computer Journal*, Vol. 7, pp. 308-313.

O'Leary, O.J. (2000) *Optimisation of prismatic plate structures with natural frequency constraints*, PhD thesis, University of Wales, Cardiff.

O'Leary, O.J., Williams, F.W. and Kennedy, D. (2001) 'Optimum stiffened panel design with fundamental frequency constraint', *Thin-Walled Structures*, Vol. 39, No. 7, pp. 555-569.

Parkinson, J.M. and Hutchinson, D. (1972) 'An investigation into the efficiency of variants on the simplex method', *In Numerical Methods for Non-linear Optimisation*, edited by Lootsma, F.A., Academic Press, New York, pp. 115-135.

Plank, R.J. and Wittrick, W.H. (1974) 'Buckling under combined loading of thin, flat-walled structures by a complex finite strip method', *International Journal for Numerical Methods in Engineering*, Vol. 8, No. 2, pp. 323-339.

Powell, S.M., (1997) *Buckling and postbuckling of prismatic plate assemblies using exact eigenvalue theory*. PhD Thesis, Cardiff University, Cardiff.

Powell, S.M., Williams, F.W., Askar, A.-S., and Kennedy, D. (1998) 'Local postbuckling analysis for perfect and imperfect longitudinally compressed plates and panels', *Proceedings of the 39th AIAA/ASME/ASCE/AHS/ASC Structures, Structural Dynamics and Materials Conference*, Long Beach, CA, pp. 595-603.

Qu, S., Kennedy, D., and Featherston, C.A. (2008) 'Multilevel postbuckling design of aerospace structures', *Proceedings of 8th World Congress on Computational Mechanics and 5th European Congress on Computational Methods in Applied Sciences and Engineering*, ISBN 978-84-96736-55-9.

Qu, S., Kennedy, D., Featherston C.A. (2009) 'Multilevel optimisation of an aircraft wing incorporating postbuckling effects', *Proceedings of CEAS European Air and Space Conference, Manchester, UK*, pp. 1-10, ISBN/ISSN: 1-85768-208-4.

Qu, S., Kennedy, D., Featherston C.A. (2010) 'Multilevel postbuckling design of aircraft wing using VICONOPT MLO', *The Third International Conference on Modeling, Simulation and Optimisation, Beijing, China*, pp. 111-114, ISBN/ISSN: 978-1-907801-09-9.

Qu, S., Kennedy, D., Featherston C.A. (2011) 'A multilevel framework for optimisation of an aircraft wing incorporating postbuckling effects', Paper accepted for publication in *Proceedings of the Institution of Mechanical Engineers, Part G, Journal of Aerospace Engineering, UK*, Ref: JAERO996.

Ragon, S.A., Gürdal, Z., Haftka, R.T. and Tzong, T.J. (1997) 'Global/local structural wing design using response surface techniques', *AIAA-97-1051, Proceedings of the 38th AIAA/ASME/ASCE/AHS/ASC Structures, Structural Dynamics and Material Conference*, Kissimmee, FL, Part 2, pp. 1204-1214.

Rao, S.S. (1984) *Optimization – Theory and Applications*, Wiley Eastern Ltd., New Delhi.

Rock, T.A., and Hinton, E. (1976) 'A finite element for the free vibration of plates allowing transverse shear deformation', *Computers & Structures*, Vol. 6, pp. 37-44.

Sigmund, O. (2000) 'Systematic design of mechanical systems using topology optimization', Keynote Paper, *Proceedings of the 2nd ASMO UK/ISSMO Conference*, Swansea, UK, pp. 5-12.

Sobieszczanski, J. and Leondorf, D. (1972) 'A mixed optimization method for automated design of the fuselage structures', *Journal of Aircraft*, Vol. 9, pp.805-822.

Sobieszczanski-Sobieski, J., James, B.B. and Riley, M.F. (1987) 'Structural sizing by generalised multi-level optimization', *AIAA Journal*, Vol. 25, pp.139-145.

Storn, R. and Price, K. (1997) 'Differential evolution – a simple and efficient heuristic for global optimisation over continuous spaces', *Journal of Global Optimisation*, Vol. 11, pp. 341-359.

Sun, W., Guo, L., Tong, M. and Dong, D. (2010) 'Post-buckling analysis and structure optimisation of integral fuselage panel subjected to axial compression load', *Transactions of Nanjing University of Aeronautics and Astronautics*, Vol. 27, No. 4, pp. 281-287.

Turvey, G. J. and Marshall, I. H. (1995) *Buckling and postbuckling of composite plates*, Chapman and Hall, London.

van Houten, M.H. and Zdunek, A. (2004) 'Post-buckling and collapse analysis, final technical report', GARTEUR SM(AG25) TP-149.

Vanderplaats, G.N. (1973) *CONMIN: A Fortran Program for Constrained Function Minimisation*, NASA Technical Memorandum, TMX-62282, Ames Research Center.

Vanderplaats, G.N. (1984) *Numerical Optimisation Techniques for Engineering Design*, McGraw-Hill, New York.

Vanderplaats, G.N. and Moses, F. (1973) 'Structural optimization by methods of feasible directions', *Computers & Structures*, Vol. 3, No. 4, pp. 739-755.

Von Karman, T. Sechler, E.E., and Donnell, L.H. (1932) 'The strength of thin plates in compssion', *Transactions of ASME*, Vol. 54, pp. 53-57.

Von Karman, T. and Tsien, H.S. (1941) 'The buckling of thin cylindrical shells under axial compression', *Journal of Aeronautical Science*, Vol. 8, pp. 303-312.

Wagner, H. (1931) 'Flat sheet metal girder with very thin metal web', *Tech Memo*, National Advisory Committee for Aeronautics, NACA TM 604-606.

Watson, A. and Kennedy, D. (2004) 'Mode jumping in post-buckled stiffened panels', *Proceedings of 4th International Conference on Thin-Walled Structures*, Institute of Physics, Bristol, pp. 573-580.

Williams, F.W. and Anderson, M.S. (1983) 'Incorporation of Lagrangian multipliers into an algorithm for finding exact natural frequencies or critical buckling loads', *International Journal of Mechanical Sciences*, Vol. 8, pp. 579-584.

Williams, F. W., Anderson, M. S., Kennedy, D., Buter, R., Aston G., and Hoh S. M. (1993) *User manual for VICONOPT: An exact analysis and optimum design program covering the buckling and vibration of prismatic assemblies of flat in-plane loaded, anisotropic plates, with approximations for curved and tapered plates, discrete supports and transverse stiffeners, Release 1.2*, School of Engineering, Cardiff University, UK.

Williams, F.W., Kennedy, D., and Anderson, M.S. (1990) 'Analysis features of VICONOPT, an exact buckling and vibration program for prismatic assemblies of anisotropic plates', *31st AIAA/ASME/ASCE/AHS/ASC Structure, Structural Dynamics and Materials Conference*, AIAA-90-0970, pp. 920-929.

Williams, F.W., Kennedy, D., Anderson, M.S. and Edwards, D.A. (1996) *User manual for VICONOPT; An exact analysis and optimum design program covering the buckling and vibration of prismatic assemblies of flat in-plane loaded, anisotropic plates, with approximations for curved and tapered plates, discrete supports and connections, version 1.3*, University of Wales Cardiff.

Williams, F.W., Kennedy, D., Butler R., and Anderson, M.S. (1991) 'VICONOPT: program for exact vibration and buckling analysis or design of prismatic plate assemblies', *AIAA Journal*, Vol. 29, 1927-1928.

Wittrick, W.H. and Williams, F.W. (1971) 'A general algorithm for computing natural frequencies of elastic structures', *Quarterly Journal of Mechanics and Applied Mathematics*, Vol. 24, No. 3, pp. 263-284.

Wittrick, W.H. and Williams, F.W. (1973) 'An algorithm for computing critical buckling loads of elastic structures', *Journal of Structural Mechanics*, Vol. 1, No. 4, pp. 497-518.

Wittrick, W.H. and Williams, F.W. (1974) 'Buckling and vibration of anisotropic or isotropic plate assemblies under combined loading', *International Journal of Mechanical Sciences*, Vol. 16, pp. 209-239.

Wu, H. Yan, Y., Yan, W. and Liao, B. (2010) 'Adaptive approximation-based optimisation of composite advanced grid-stiffened cylinder', *Chinese Journal of Aeronautics*, Vol. 23, No. 4, pp. 423-429.

Zienkiewicz, O.C., Taylor, R.L. (2000) *The finite element method*, 5th edition, Butterworth Heinemann, Oxford.

Zimmermann, R. and Rolfes, R. (2006) 'POSICOSS-improved postbuckling simulation for design of fibre composite stiffened fuselage structure', *Composite Structures*, Vol. 73, No. 2, pp.171-174.

